Quantitative scar assessment using cardiac magnetic resonance imaging to predict ventricular arrhythmia risk and cardiac resynchronisation response

Chen, Zhong

Awarding institution:
King's College London

Quantitative scar assessment using cardiac magnetic resonance imaging to predict ventricular arrhythmia risk and cardiac resynchronisation response

Zhong Chen

A dissertation submitted for the degree of

Doctor of Philosophy

Division of Imaging Sciences and Biomedical Engineering
School of Medicine
King's College London
University of London

For KR

Abstract

Myocardial fibrosis is associated with ventricular arrhythmia. Late gadolinium enhancement cardiac magnetic resonance (LGE-CMR) has been the standard approach to visualise regional myocardial fibrosis. T_1 mapping is a novel CMR technique that overcomes the inherent limitation of conventional LGE imaging to assess diffuse fibrosis.

The incidence of arrhythmia and sudden death continues to be high despite the benefits of cardiac resynchronisation therapy (CRT) in terms of symptomatic improvement and overall mortality. As myocardial scar can have a structural and functional impact on remodeling, there is a need to further elucidate the effect of CRT on electrophysiology and to better select patients for CRT.

Prospective clinical studies were conducted to assess the ability of CMR scar quantification to

1. predict the risk of ventricular arrhythmia in both ischaemic and non-ischaemic cardiomyopathy (ICM, NICM) patients;
2. predict reverse remodeling following CRT in dyssynchronous heart failure patients.

Investigative studies were also carried out to

1. explore CMR scar characterisation using high-resolution 3-dimensional scar image acquisition in heart failure patients;
2. explore clinical utilisation of T1 mapping for myocardial fibrosis quantification;

3. understand the relationship between scar heterogeneity and substrate for ventricular arrhythmia;
4. explore electrical remodeling effect of CRT in dyssynchronous heart failure patients

The present study is the first to demonstrate that non-contrast native T1 is an independent predictor of ventricular arrhythmia in patients with ICM or NICM. It provides confirmation that the extents of scar and grey zone derived from LGE-CMR are independently associated with ventricular arrhythmia. With regards to prediction of CRT remodeling, focal scar burden detected by LGE-CMR is associated with a poor response to CRT, whereas markers of diffuse interstitial fibrosis were not however predictive of CRT response.

These findings have important clinical implications, lending support for the use of quantitative myocardial scar quantification in selecting patients for complex device therapy.

Key words:

Ventricular arrhythmia; T1 mapping; grey zone; defibrillator; cardiac resynchronisation therapy; reverse remodeling.

Table of Contents

List of Figures

List of Tables

List of Abbreviations

AC = apparent conductivity

APD = action potential duration

ARI = activation recovery interval

CMR = cardiac magnetic resonance imaging

CE = contrast-enhanced

CRT = cardiac resynchronization therapy

ECV = extracellular volume index

EDV = end-diastolic volume

EF = ejection fraction

ESV = end-systolic volume

FWHM = full-width-half-maximum

ICD = implantable cardioverter-defibrillator

ICM = ischemic cardiomyopathy

LBBB = left bundle branch block

LGE = late gadolinium enhancement

LV = left ventricle

NICM = non-ischemic cardiomyopathy

NYHA = New York Heart Association

RBBB = right bundle branch block

RC = restitution curve

RV = right ventricle

SI = signal intensity

VF = ventricular fibrillation

VT = ventricular tachycardia

Acknowledgment

During this research period, it has been my privilege to meet and receive help from many talented individuals from a wide range of disciplines.

I would like to take this opportunity to thank my supervisor Prof C Aldo Rinaldi and Prof Reza Razavi for their guidance, encouragement, patience and wisdom. I owe them both a debt of gratitude for implanting that initial seed of research idea in me, then trusting me, supporting me, guiding me and allowing me to develop my own research acumen.

A special thank-you to Dr Tobias Voigt and Prof Tobias Shaeffter who provided the technical building blocks to this research project, this project could not have taken off the ground without their contributions.

I would also say a special thank-you to Prof Peter Taggart for his guidance. His wisdom and enthusiasm for exploring the science and physiology is an inspiration to all young researchers. It has been my privilege to work with him.

It was my pleasure to collaborate with Dr Jatin Relan, Dr Rocio Cabrera-lozoya under the supervision of Prof Maxime Sermesant who enlightened me with the power of computational modeling.

This work would not have been possible without the generous support from Medtronic Ltd and a Clinical Research Training Fellowship from the British Heart Foundation, and the assistance of my colleagues: Dr Manav Sohal, Dr Anoop Shetty, Dr Eva Sammut, Dr Nick Child, Dr Tom Jackson, Dr Julian Bostock, Dr Amedeo

Chiribiri, Dr Valentina Puntmann, Dr Ben Hanson, Dr Catalina Tabon-Gomez, Dr Rashed Karim and Dr Kawal Rhode.

The final words of gratitude go to my wife who is "my rock…" that wedges me against the hard place when the going gets tough.

Chapter 1 Thesis Outline

1.1 Thesis Aims

This thesis summarises the research work undertaken to test the hypothesis that quantitative left ventricular myocardial fibrosis assessment using cardiac magnetic resonance imaging can

1. predict the risk of ventricular arrhythmia and provide additional predictive value in identifying patients with increased risk of ventricular arrhythmia in both ICM and NICM patients;
2. predict reverse remodeling following CRT in dyssynchronous heart failure patients.

1.2 Chapter Overview

The following chapters describe the work undertaken to addressed the hypothesis listed above

Chapter 2 introduces the background information in support of the proposed study hypothesis with a focus on why there is a need for using CMR quantitative myocardial scar assessment and the relevance of addressing scar heterogeneity assessment (rather than the simple binary assessment of the presence of scar) using T1 mapping and grey zone assessment.

Chapter 3 describes the general methods if used in more than one study. Detailed methodology with respect to each individual study is further described in the respective study chapters.

Chapter 4 describes an exploratory study conducted to assess the clinical applications of T1 mapping for myocardial scar assessment.

Chapter 5 describes an exploratory study conducted to utilise a novel method of improving respiratory navigation during high-resolution scar imaging in patients with heart failure.

Important limitations and drawbacks learnt from the work described in Chapter 4 and 5 were used to refine the methods and develop data analysis tools for carrying out the large prospective clinical outcome study described in Chapter 7.

Chapter 6 describes a study to explore the association between scar heterogeneity detected by CMR imaging and ventricular tachycardia substrate.

Chapter 7 describes a large prospective clinical study that assesses the prognostic value of quantitative scar assessment using CMR in predicting ventricular arrhythmia in both patients with ICM and NICM. This included scar quantification using LGE images and T1 mappings with its associated derived index such as extracellular volume index (ECV).

Chapter 8 describes a study that assesses the impact of CRT on left ventricular (LV) electrical remodeling in terms of action potential duration (APD) changes between responders and non-responders. The findings may provide explanations to the persistent high incidence of arrhythmias in some patients with CRT and the additional mortality benefit observed in responders of CRT.

Chapter 9 describes a study that assesses the relationship between the mechanical remodeling (regional strain) and electrical remodeling (regional APD) induced by CRT, providing evidence that the two processes are linked.

Chapter 10 describes a prospective clinical study that assesses the prognostic value of quantitative scar assessment using CMR to predicting RR to CRT in both dyssynchronous patients with ICM and NICM.

Chapter 11 concludes the thesis by discussing the original contributions, clinical perspectives, implications, limitations and future directions of this work.

The following flow chart describes the development journey of the various hypotheses put forward in this thesis and thus the order of the chapters listed.

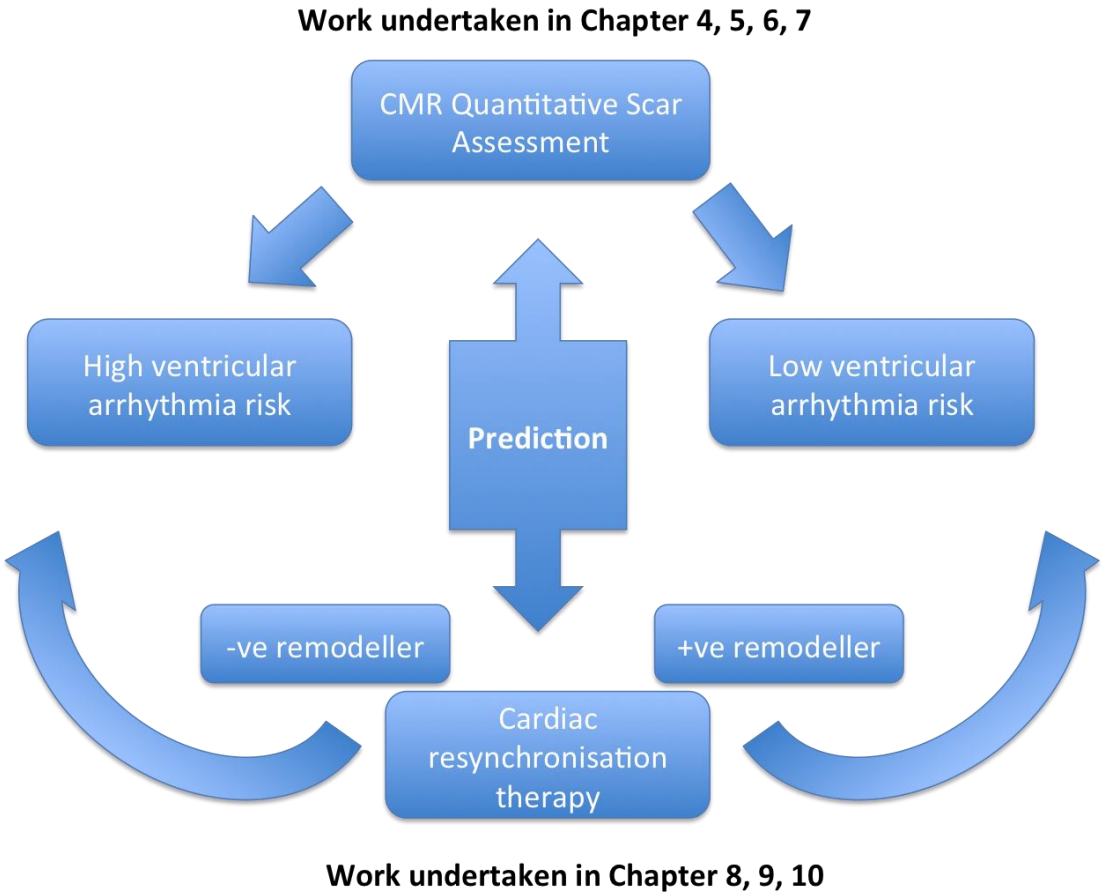

Chapter 2 Introduction

The aim of this thesis is to assess the prognostic value of quantitative myocardial scar assessment using cardiac magnetic resonance imaging (CMR) in predicting ventricular arrhythmia and myocardial remodeling.

In this chapter, I will briefly describe the principles of cardiac magnetic resonance imaging, focusing in particular on T1 mapping which has recently emerged as a useful tool that overcomes of the limitation of conventional late gadolinium enhanced (LGE) CMR technique and allows the quantitative assessment of interstitial diffuse fibrosis.

I will also describe the relevance of myocardial tissue scar heterogeneity in terms of providing substrate for ventricular arrhythmia and its potential impact on ventricular remodeling following cardiac resynchronisation therapy (CRT); and discuss the measure of CRT response.

In turn, I will introduce the background to the aim of study explaining the rationale for the hypothesis proposed.

2.1 Principles of cardiac magnetic resonance imaging

2.1.1 Basic physics of MRI

Cardiac magnetic resonance imaging (CMR) is the best noninvasive image modality to characterise human organ tissues. Visualisation of myocardial tissue is based on principles and technique using magnetic fields and radiofrequency (RF) pulses. Human organ tissues distinguish from one type to another by the amount of water and therefore hydrogen content. Each hydrogen atom consists of a central nucleus that contains one proton, surrounded by a single electron. Nuclei are in a constant state of

spin in their “rest” magnetic state or moment. When an external magnetic field is applied, the “rest” magnetic moment is therefore affected and the hydrogen nuclei align themselves with the directions of the magnetic field. The nuclei precess about the magnetic field direction like gyroscopes, a behavior called *Larmor precession*.

The frequency of the precession (ω0), measured in (M)Hz, is proportional to the applied magnetic field strength (B0).

$\omega 0 = \gamma B0$; where γ is the gyromagnetic ratio.

(Gyromagnetic ratio is a nuclei specific constant, for hydrogen, $\gamma = 42.6$ MHz/Tesla)

In order to obtain a magnetic resonance image, the subject is placed in a magnetic field, then a RF pulse is applied (with a frequency equal to the *Larmor* frequency of proton, so they are in “resonance”) to disturb the equilibrium state of the proton nuclei spin. This transfers the energy to, i.e. excite, the nuclei which then spin/precess to a greater degree. This leads to a measureable transverse magnetisation in 3-dimensional space. The z-axis usually refers to the direction of the external magnetic field, whilst x-axis or y-axis is perpendicular to the external magnetic field. The angle between the z-axis and the new net magnitisation vector is known as the flip angle and its magnitude depends on the amplitude and duration of the RF pulse.

When the RF signal is removed, the nuclei realign themselves with the external magnetic field and continue precessing at their precession frequency, until their net magnetic moment is again parallel to the external magnetic field. This return to equilibrium is referred to as “relaxation”. During realignment, the change in magnetic flux induces an electric voltage, which can be detected by an RF antenna resulting a receptive RF signal. This signal is referred to as the free-induction decay (FID)

response signal. The FID response signal is measured by a conductive field coil placed around the object being imaged. These signals are processed or reconstructed to obtain 3-dimensional (3D) grey-scale magnetic resonance (MR) image.

In order to produce a 3D image, the FID resonance signal must be encoded for each dimension. This is made possible by providing an additional gradient magnetic field. This gradient causes the *Larmor* frequency to change linearly in the axial direction. A 2D spatial reconstruction in each axial slice can be accomplished using frequency and phase encoding by giving two magnetic gradients that are perpendicular to each other consecutively. As a result, the resonant frequencies of the nuclei vary in one direction due to one gradient, and have a phase variation in the other direction due the previously applied gradient. Thus frequency and phase encode the signals in each of the directions. These signals are acquired in an array known as K-space. Usually K-space is filled linearly but it can also be filled with other pattern, for example radial. A Fourier transform can then be used to encode the image to the spatial domain and producing the MR images.

The contrast in MR images, distinguishing one tissue type to another depends on the intensity of the FID response signal each tissue type exhibits. This will depends on the proton density of the tissue, i.e. the higher the proton density, the stronger the FID response signal.

2.1.2 T1 and T2 relaxation

Two other important parameters also influence the image contrast, the longitudinal relaxation time, T1, and the transverse relaxation time, T2. Following removal of the RF signal, the longitudinal relaxation time measures the time by which the proton nuclei spin returns to the magnetisation vector along the direction of the external

magnetic field (i.e. the lattice), thus longitudinal relaxation is also referred to as spin-lattice relaxation. T1 time is defined as a time to reach 63% of the equilibrium longitudinal relaxation magnetisation. In contrast, T2 measures the time it takes for the transverse component of the magnetisation vector to exponentially decay towards its equilibrium value, i.e. spin-spin relaxation. T2 time is defined as the time it takes of the magnetic resonance signal to irreversibly decay to 37% of its initial value.

2.1.3 Cardiac and respiratory motion compensation

Another important aspect of CMR image processing is the correction for cardiac and respiratory motions. Electrocardiographic ECG gating is used to overcome cyclic cardiac motion. The timing of MR data collection is synchronised with each cardiac cycle. The pulse sequence is triggered according the amplitude of the ECG complex, R-wave. This can be achieved prospectively or retrospectively. Prospective gating detects the R-wave and starts RF excitation and data acquisition after a certain delay time (trigger delay). Figure 2.1 demonstrates the data acquisition window timed to the specific phase within the cardiac cycle.

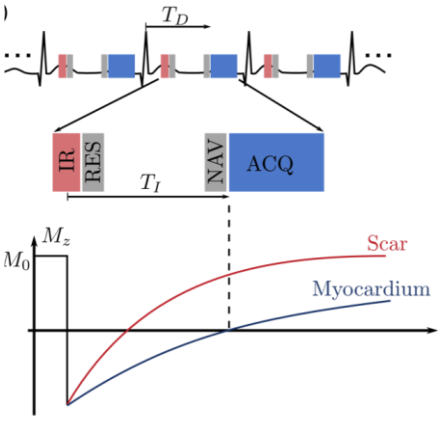

Figure 2- 1 Acquisition window (ACQ) timed to end-diastole when the cardiac motion is minimised.

In retrospective cardiac gating, data are continuously acquired throughout the scan whilst ECG data are monitored and recorded. During post acquisition image reconstruction, data within the windows of interest during the defined cardiac cycles are selected and processed. An interpolation process is then performed in order to reconstruct the desired number of cardiac phases.

Respiratory motion correction can be more challenging. Motion-compensation strategies such as breath-holding and the use of a respiratory belt and respiratory navigator echoes. Patients are asked to hold their breath at the end of expiratory phase because the position of the diaphragm is most reproducible due to the fixed end-expiratory volume. However, for high-resolution imaging, and especially for 3D imaging, acquiring all the data in a single breath-hold would be very difficult. Thus respiratory belt or respiratory navigator is used. The pneumatic belt fixed to the patient's upper abdomen has pressure sensors that detects the cyclic motion associated with respiration and is used to gate the image acquisition to a particular breathing phase. RF excitation pulse excites a rectangular slab or pencil beam of spins over a reference point within the thorax, usually over the diaphragm. The data is acquired along a single dimension (readout direction) in the direction of the movement of the diaphragm. MR image data is only acquired when the respiratory phases is within a predefined window of interest (again usually at the end-expiratory phase).

This is however problematic with patients who have significantly impaired LV function. They have irregular breathing patterns, resulting in poor respiratory navigator efficiency thus prolonging the MR data acquisition time. Figure 2.1 (below) illustrates the breathing patterns in a subject with normal LV function and some one with poor LV function.

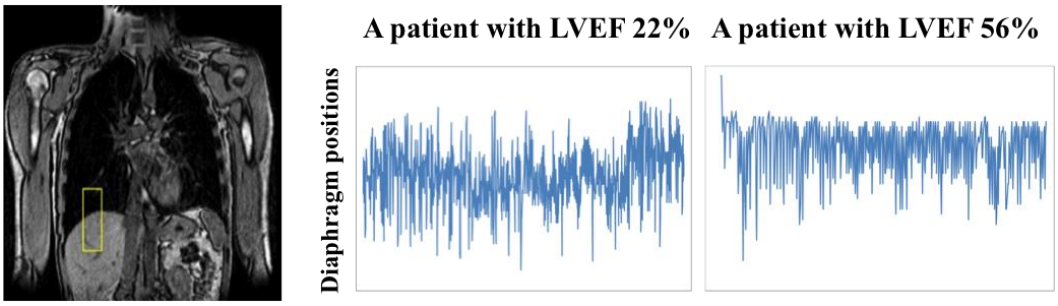

Figure 2- 2 Recording of diaphragm positions by the respiratory navigator over the right hemi-diaphragm showing an irregular breathing pattern often exhibited in patients with severely impaired LV dysfunction.

2.2 Inversion recovery sequences and late gadolinium enhancement for myocardial scar imaging

Inversion recovery (IR) sequences begin with a 180 degree pulse, which inverts the magnitisation. After a given time, known as the inversion time (TI), image data acquisition is carried out by a 90-degree RF pulse that brings the residual longitudinal magnetisation into the x-y or transverse plane where it can be detected by an RF coil.

Late gadolinium enhancement (LGE) imaging uses a T1 dependent IR technique to exploit the differential shortening of T1 by gadolinium contrast agents dependent on the different concentrations of gadolinium contrast accumulating in different tissue. Gadolinium is a small paramagnetic molecule that preferentially accumulates in the tissue extracellular space.

In normal myocardial tissue, the cells are closely packed with minimal interstitial space. This extracellular space is expanded in the presence where normal myocytes are replaced by fibrosis. This may be the result of inflammation, infarction or infiltrative pathologies. Furthermore, gadolinium is quickly washed out from the capillary circulation, but takes much longer to wash out of the extracellular space (10-

30 minutes) and therefore sufficient gadolinium will preferentially accumulate in these regions.

By imaging within this window, a TI is chosen to provide the greatest signal contrast between normal myocardium (where net vector magnetisation vector is "zero", i.e. magnetic resonance signal is "nulled" and appears black) and the region with expanded extracellular space (as a surrogate measure of myocardial fibrosis). See Figure 2.3 below.

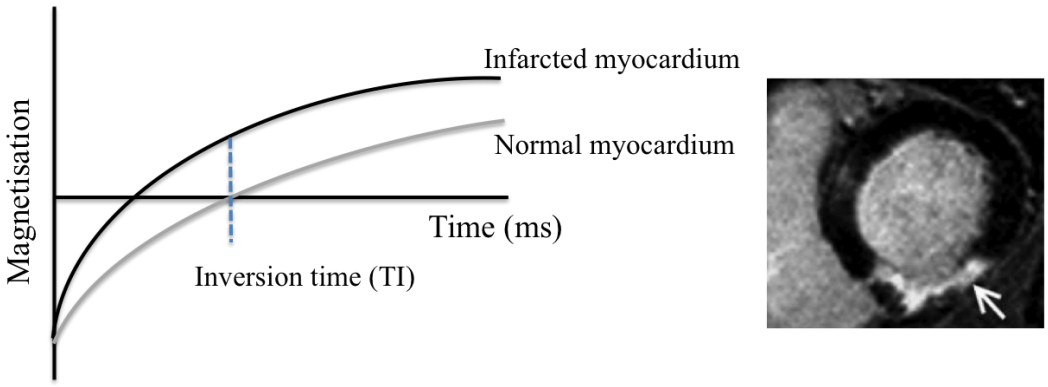

Figure 2- 3 Relative TI chosen to demonstrate the greatest image contrast difference between normal and scarred myocardium (shown in white in the LGE images on the right) from myocardial infarction.

2.3 Grey zone

Tissue death begins at the time of ischaemia with cellular necrosis. This is characterised by the rapid loss of cellular homeostasis and plasma membrane rupture. Collagen deposition then begins at the site of the MI several days after necrosis begins, forming scars.[1] Infarcted myocardial tissue has limited or no contractile activity and leads to impairment of the heart's functional capacity. Surrounding infarcted tissue is

an area that bridges the gap between non-viable and viable healthy myocardial tissue. This "peri-infarct" area consisting of an admixture of scar tissues and surviving myocytes is defined as the grey zone.

The standard image analysis technique for grey zone measurement is based on signal intensity quantification methods, classifying the grey zone with signal intensity somewhere between the scar core and normal myocardium with the classification varying between studies.[2-4]

Rather than providing a true quantitative assessment of tissue heterogeneity, these methods are susceptible to partial volume effects where both healthy and scarred tissues are found in a single voxel, especially when the 2D image slices are 8-10mm thick. This may lead to inaccurate quantification. This partial volume effect, a major criticism of grey zone characterisation, can potentially be reduced with higher spatial resolution 3D CMR acquisition.[5]

2.4 T1 mapping

The first medical application of magnetic resonance imaging measuring longitudinal proton relaxation time, T1, has been used to detect and characterise tumour.[6] Myocardial T1 map is a parametric reconstructed image where the signal intensity of each pixel represents the T1 longitudinal relaxation time of the corresponding myocardial voxel. The voxel-by-voxel T1 estimation is derived from multiple samplings along the recovery curve following a specific preparation sequence (Figure 2.4). It allows true quantitative signal quantification on a standardised scale of image voxel to characterise tissue heterogeneity. This eliminates the influence of imprecise

inversion time selection, which is needed to null the apparently normal remote myocardium with standard delayed enhanced CMR.

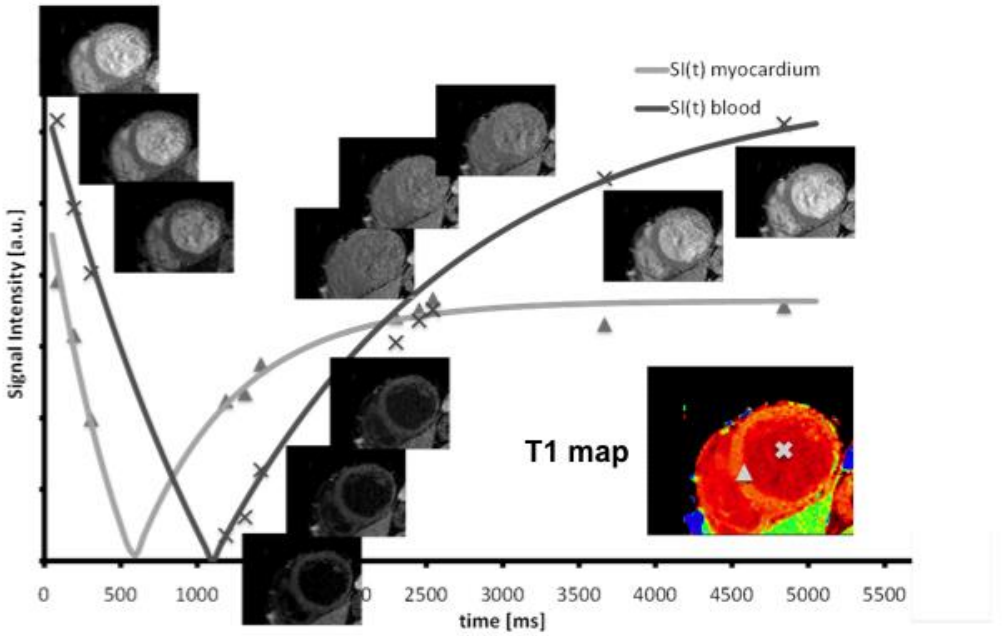

Figure 2- 4 Illustration of T1 mapping using Modified Look-Locker Inversion recovery imaging (MOLLI) sequence. The final T1 map merges images sampled from eleven different inversion times (TI). T1 value is determined by fitting a 3-parameter exponential model to the measured data on a voxel-by-voxel basis.

There are many ways of assessing T1. Two methods, based on the standard Look-Locker method, have largely been adopted and validated for T1 mapping in the literature.[7,8] The Modified Look-Locker Inversion recovery sequence (MOLLI), proposed by Messroghli *et al.*, merges images sampled from eleven different inversion times (TI) from three consecutive inversion-recovery (IR) experiments into one data set in a 17-heartbeat breath-hold; whereas Shortened Modified Look-Locker Inversion recovery (ShMOLLI), proposed by Piechnik *et al.*, samples from seven different TIs in a 9-heartbeat breath-hold. Both methods have been readily applied in

T1 mapping data acquisition in patients with a variety of cardiac pathologies. However, both methods are susceptible to underestimation of the true T1 values. Especially at high T1 values, MOLLI demonstrated a greater dependence on heart rate requiring adjustment whereas ShMOLLI required only an empirical adjustment.[7-9]

Myocardial fibrosis detection by delayed contrast enhancement CMR sequence is dependent on a greater distribution volume and slower wash-out of contrast agents within tissues of greater extracellular space. The delayed contrast-enhanced CMR pulse sequence has been the gold standard in detecting regional fibrosis. An important drawback of the method is the need for manual selection of IR time to generate an image with signal contrasts between the fibrotic region and apparently non-fibrotic region. Thus, delayed-enhancement imaging is good at differentiating between "normal" and diseased myocardium but less good at looking diffuse processes that affect the myocardium in a more homogeneous way. T1 mapping by assessing the voxel signal intensity on a standardised scale rather than an arbitrary scale does not depend on a "normal" reference and therefore has the advantage of detecting diffuse fibrosis.

In addition to the type of acquisition sequence, heart rate and scanner field strength, the post-contrast T1 value in T1 mapping measurements is also largely dependent on the properties of the gadolinium contrast agents, the dose of contrast, the time delay of the T1 mapping after contrast injection, the haematocrit level which affects the partition coefficient of the gadolinium contrast agent, the contrast kinetics between regions of fibrosis and normal myocardium and the contrast wash-out rate which is also influenced by the renal clearance rate. Myocardial contrast volume of distribution ($VD_{(m)}$) or extracellular volume (ECV) quantification has been therefore proposed as

a measure of myocardial fibrosis in order to circumvent some of these confounding factors related to standalone post-contrast T1 measurement.

ECV is estimated from the concentration of extracellular contrast agent such as gadolinium in the myocardium relative to the blood in a dynamic steady sate.

$$ECV = (1 - \text{haematocrit}) \times \left(\frac{(1/\text{Post-contrast T1myocardium} - 1/\text{Pre-contrast T1myocardium})}{(1/\text{Post-contrast T1blood} - 1/\text{Pre-contrast T1blood})} \right)$$

The formula holds true when the extracellular contrast concentration in the blood and the myocardium reaches equilibrium.

Kehr *et al.* demonstrated a correlation between ECV and collagen volume fraction (CVF) in human myocardium in vitro.[10] Using a bolus injection followed by a slow infusion of contrast protocol to ensure a steady contrast equilibrium when post-contrast T1 is measured, Flett *et al.* has demonstrated a close correlation between ECV and CVF measured on histological samples indicating diffuse fibrosis from a group of patients with either aortic stenosis or hypertrophic cardiomyopathy (HCM).[11]

There is an on going debate whether, instead of infusion, a bolus injection of contrast can achieve a steady state between the intravascular compartment and the myocardial interstitial compartment. A single bolus injection would make the CMR protocol simpler and easier to integrate into daily clinical practice. Schelbert *et al.* demonstrated that there is no significant difference between the measured ECV 12-50 minutes after a bolus injection of contrast compared with an infusion protocol in 10 volunteers with an age range between 20 and 81.[12] However, Kawel *et al.* demonstrated that serial measurements between 5 and 45 minutes after bolus injection of contrast revealed a small but significant increase in measured ECV in a group of

younger healthy volunteers, implying that post-contrast T1 values for the estimation of ECV should be made at the same intervals post bolus injection in order to improve the accuracy of ECV as a biomarker for diffuse fibrosis.[13] Messroghli *et al.* demonstrated a moderate correlation of ECV, estimated with post-contrast T1 measured 20 minutes after bolus injection of contrast, with CVF found on cardiac histology in a rat model of cardiac diffuse interstitial fibrosis.[14]

T1 mapping requires a fundamental post-imaging processing which is a voxel-by-voxel registration between the different T1 images taken at different IR times; in addition, in order to generate ECV maps and analysis, further registration is required to match the pre- and post-contrast T1 maps. In its clinical application, we are likely to encounter image motions due to body movement given the significant time lapse between the pre- and post-contrast T1 maps acquisition (typically 15-30 minutes apart), respiratory motion artefact due to inadequate breath-hold as well as cardiac motion due to arrhythmia and heart rate variability. Xue et al. has described and validated a method that is non-rigid, fully automated and integrated to the image acquisition and processing of T1 mapping.[15] Incorporating this method, Kellman *et al.* has devised a workflow that integrates the motion correction and co-registration of breath-holds to improve the accuracy of ECV mapping/calculation, which make its translation to clinical application feasible.[16] They correlated the ECV on a continuous scale with the severity of fibrosis in a variety of disease pathologies that included myocarditis, non-ischemic dilated cardiomyopathy (NIDCM), HCM, amyloidosis and chronic myocardial infarction.[16]

2.5 Relevance of myocardial scar to ventricular arrhythmia

The mixture of electrically conducting (viable) and non-conducting (scarred) tissue can lead to the formation of a re-entrant circuit and provide the substrate for VT.[5,17] Animal studies have shown that electrical remodelling occurs in the infarct border zone (the grey zone), leading to slow conduction within the myocardium and promoting re-entrant VT.[18,19] Pathological studies in humans have also shown that small patchy scars from infarcts might facilitate the development of complex 3-dimensional re-entry circuits.[20] Histological examination of myocardial specimens from patients with chronic MI and medically refractory VT has revealed isolated bundles of surviving myocytes interwoven with strands of fibrous tissue at the apparent arrhythmic focus. These data implicate a heterogeneous zone between the scar and the viable tissue i.e. the grey zone, in the pathogenesis of ventricular arrhythmias by providing a substrate for development of re-entrant VT.

The above evidence lends support to approaches for identifying the grey zone as a "potentially arrhythmic heterogeneous zone of viable and non-viable myocardium". CMR imaging allows assessment of the grey zone by quantifying the extent of infarct tissue heterogeneity.[21] Importantly, clinical studies have demonstrated a correlation between the grey zone size characterised by CMR and clinical outcome data including mortality, ventricular arrhythmia inducibility and appropriate ICD discharge.[2-4] These studies support the notion that MRI characterisation of the grey zone can provide unique and valuable information which can be used as a prognostic predictor for VT and sudden cardiac death incremental to that offered by current selection criteria for ICD therapy. Clinical electrophysiology studies have found that fractionated and isolated electrograms are more commonly seen in this heterogeneous grey zone which correlates to the propensity for VT.[22,23] Varying degree of the grey zone size may

explain why some patients with myocardial infarction are more prone to VT than the others despite similar sized infarcts.[24] Indeed, areas of grey zone appear to represent critical components of the re-entrant VT circuit and have been targeted during VT ablation with successful long-term outcomes.[25]

Currently left ventricular ejection fraction (LVEF) is used as the main clinical criteria in deciding ICD implantation for primary prevention of sudden cardiac death in post-MI patients. This is based on data from the Multicentre Automated Defibrillator Implantation Trial (MADIT II) and Sudden Cardiac Death in Heart Failure Trial (SCD-HeFT) which demonstrated that implantable cardioverter-defibrillator (ICD) reduced mortality rates in patients with evidence of ischaemic heart disease and reduced LVEF <30%, and NYHA class I and LVEF < 35% and NYHA class II or III, respectively.[26,27] Post hoc analysis of the MADIT II study population showed that only 35% of the patients who received an ICD developed ventricular arrhythmia requiring ICD therapy during a 3-year follow up.[28] In 2004, the number of ICDs (including ICDs combined with cardiac resynchronisation pacemakers) per million capita was approximately 100 in Western Europe compared with 550 in the USA.[29] MAVERIC registry study estimated that UK ICD implant rate would rise to at 18 per million of the population, costing the National Health Service £24.1 million per annum.[30] In addition to the financial cost to innovative health care service delivery, there is also a human cost. There is significant incidence of inappropriate shocks delivered which has an adverse effect on patient's quality of life.[31-33] Hence there is a need for more refined selection criteria for ICD implantation.

Previous studies of grey zone quantification and risks of arrhythmia have only been performed in the ischaemic patient population. Non-ischaemic dilated cardiomyopathy (NICM) patients have been shown to have prognostic benefit from

ICD therapy and account for a significant proportion (20% to 40%) of the ICD/CRT-D (ICD with cardiac resynchronisation therapy) patient population.[34-36] Although there is evidence supporting ICD implant in these NICM patients for primary and secondary prevention of sudden cardiac death, a clear risk stratification method in terms of ventricular arrhythmia risk prediction remains problematic. Though LV ejection fraction is used for risk stratification for ICD therapy, it is poor at predicting appropriate ICD therapy and therapy outcome. Histological studies have demonstrated varying degrees of fibrosis in NICM although the significance in terms of predicting ventricular arrhythmia is unclear.[37,38] Assomoll et al have demonstrated that mid-wall fibrosis detected with conventional MRI is associated with a poor clinical outcome in terms of heart failure hospitalisation and ventricular arrhythmia/sudden cardiac death.[39] Iles et al found that 50% of NICM patients had regional fibrosis detected by late gadolinium enhancement and that this was associated with a higher incidence of ventricular arrhythmia resulting in appropriate ICD therapy.[40] Nazarian et al demonstrated that fibrosis in NICM detected by DE-MR provided additional predictive value over the ejection fraction in VT inducibility.[41] These data demonstrate that regional fibrosis exist in a significant proportion of cardiomyopathy with non-ischaemic aetiology and support the notion that tissue heterogeneity characterisation may also be an important risk predictor for ventricular arrhythmia in patients with NICM.

2.6 Relevance of myocardial scar to cardiac resynchronisation therapy response

Since the first reported case of cardiac resynchronisation therapy (CRT) two decades ago, it has established its effectiveness, improving morbidity and mortality in

selective heart failure patients with evidence of dyssynchrony. [42,43] Prolonged QRS duration (QRS_d), usually manifests as left bundle branch block (LBBB) are the recommended criteria in patient selection for CRT.[44,45] However responder rates vary between half to two-thirds in reported cohorts, with left ventricular remodeling response (LV RR) rate being much lower than clinical response rate. [46,47] One explanation for this high non-response rate may be the presence of focal and diffuse interstitial myocardial fibrosis, which can disrupt the concordance between mechanical and electrical dyssynchrony mediated through lines of structural and functional block thus attenuating the effect of CRT. [48-52]

Heart failure patients with ischemic etiology tend to benefit less from CRT than patients with DCM.[53-55] Prior studies have demonstrated that total scar burden (without differentiating between scar core and grey zone) is lower in CRT responders defined by clinical functional status rather than LV volumetric response.[50,56] Long-term prognosis after CRT has been shown to correlate with LV RR rather than clinical symptomatic response.[57] Prior studies that assessed LV volumetric responses to CRT have focused on scar burden at the LV lead pacing site.[49,51,58]

The presence of diffuse fibrosis is overlooked in routine clinical CMR studies due to the inherent limitation of conventional LGE CMR technique. It requires the nulling of apparently "normal" myocardium in order to provide a contrast in image signal intensities to highlight the region of focal scar represented by gadolinium enhancement. The degree of transmurality in LGE has been shown to correlate with contractile improvement after revascularisation suggesting that the greater proportion of surviving myocardium the greater the capacity for the myocardium to recover.[59] Measures of diffuse interstitial myocardial fibrosis may likewise represent a measure of viable/recoverable myocardium.[60,61]

There is no clear consensus on the definition of a positive response to CRT. Prior studies have used different definitions that derived from clinical symptoms parameters, echocardiographic parameters and composite of the two.[62] Furthermore, the follow-up duration following CRT at which the response is measured also varied greatly. It is generally considered that the response rate measured by clinical criteria is higher than that measured by echocardiographic parameters. It is not surprising that there is little correlation between the two. [62] Echocardiographic parameters are susceptible to operator dependence. Whilst MLHFQ scores provide additional validity to the subjective NHYA class scores, a poor correlation has been found between NYHA class and some objective measures of cardiac function, such as peak oxygen consumption and 6-minute walk.[63]

The lack of universal definition of response to CRT is also a reflection of uncertainty regarding the effects of CRT.

QRS duration being a primary selection parameter for CRT yet is not used as a measure of response to CRT. It is mainly because it has been shown to be a relatively specific but not sensitive predictor of CRT response and there is a lack of standardisation in measuring QRS duration in CRT patients. [64]. A consistent feature of electrophysiological remodelling in heart failure is ventricular action potential duration (APD) prolongation.[65] However, the effect of reverse remodelling on APD during cardiac resynchronisation therapy (CRT) has not been determined in these patients.

Recently, the MultiCenter Automatic Defibrillator Implantation Trial with Cardiac Resynchronisation Therapy (MADIT-CRT) trial, the Resynchronisation Reverse Remodelling in Systolic Left Ventricular Dysfunction (REVERSE) trial and the

Resychronisation-Defribrillation for Ambulatory Heart Failure Trial (RAFT) trial have demonstrated that CRT provided an incremental overall survival benefit to ICD therapy alone in heart failure patients.[66-68] However, earlier studies showed that the incidence of arrhythmia and sudden death continues to be high despite CRT inferring the possible need for additional protection from implantable cardioverter defibrillator (ICD).[36,43]

These observations highlighted a need to further elucidate the effect of CRT on electrophysiology. Given the potential impact of regional or diffuse fibrosis that may impact on the electrical conduction through lines of structure or functional block during CRT pacing, quantitative scar assessment using CMR may add predictive value in CRT response. [48]

Chapter 3 General Methods

Where methods are applicable to more than one of the following chapters, the details are given below to avoid repetition. However, the individual study protocols are described within the respective chapters.

3.1 Ethics

Local institute ethics committee (Guy's and St Thomas' Hospital) approved the studies involving human subjects. All study participants gave written informed consent prior to participation.

3.2 Patient selection

ICD patients

All patients undergoing ICD implantation for primary and secondary preventions as per guidelines (ESC guideline 2012) at local institution between May 2011 to January 2013 to participate.[69] Ischemic etiology was defined as the presence of any epicardial coronary artery stenosis with more than 75% or any history of myocardial infarction or coronary revascularisation with a scar pattern consistent with myocardial infarction on CMR. Non-ischemic etiology was defined as the absence of the above criteria. Patients undergoing implantation of ICD for catecholaminergic VT, Brugada syndrome or long QT syndromes with normal CMR findings were not included in the final analysis.

CRT patients

Patients undergoing CRT pre-assessment clinic in local institution and fulfilling Class I and II recommendation for CRT were prospectively invited to participate in the study following local research ethics committee approval.[70]

Inclusion criteria

Heart failure with New York Heart Association (NYHA) Class III-IV symptoms

- Patients should be on optimal medical therapy
- Have significantly impaired LV function (ejection fraction <35%)
- QRS duration >150ms on ECG or QRS duration between120 and 149ms with evidence of dyssynchrony on echocardiography.
- Age > 18 years

Exclusion criteria

- Contra-indication to CMR scan
- Significant renal impairment (eGFR<30ml/min/1.73m^2)

3.3 Cardiac magnetic resonance imaging

3.3.1 CMR protocol

CMR imaging was performed using a 1.5T scanner with a 32–channel coil (Philips Healthcare, Best, Netherlands). After standardised patient-specific planning, a stack of breath-hold short axis balanced steady-state free precession cine slices covering the LV was acquired for quantification of volume, mass and EF. Following a Look-Locker scan to find the optimum inversion time, a stack of short axis slices of an

inversion-recovery gradient-echo sequence (repetition time/echo time = 3.4/2.0ms, flip angle = 25 degrees, voxel size = 1.8x1.8x8mm, ECG triggered to end-diastole with a patient-adapted pre-pulse delay) were acquired 10-15 minutes post contrast injection (gadobutrol, 0.2mmol/kg body weight) for CE-CMR scar assessment. A single mid-ventricular short axis slice (in the same geometry as the mid CE-CMR slice) using modified Look-Locker inversion recovery sequence (MOLLI) with 11 phases (3+3+5) was acquired for T1 mapping (repetition time/echo time = 3.3/1.5ms, a flip angle = 50 degrees, voxel size = 1.8x1.8x8mm, with heart rate adapted trigger delay, and adiabatic pre-pulse to achieve a complete inversion) both before and after the administration of contrast.

3.3.2 Image analysis

Ventricular volumes, function and mass were analyzed using dedicated software (ViewForum, Philips Healthcare, Best, Netherland) and were indexed to body surface area. LGE-CMR images were visually assessed by two independent CMR experts blinded to the study outcome. In case of discrepancy, the data were jointly reviewed by these experts to reach a consensus. Quantitative analysis of LGE was performed using CMR42 (Circle Cardiovascular Imaging Inc., Calgary, Canada). The extent of LGE was quantified using both the 2-standard deviation method ($Scar_{-2sd}$, defined as the region with SI 2sd above the remote reference myocardium) and the full-width-half-maximum method ($Scar_{-FWHM}$, defined as the region with SI above the 50% of the maximal SI of the enhanced area). The extent of grey zone was quantified using the $Greyzone_{-2sd\text{-}FWHM}$ method (defined as the region with SI between $Scar_{-FWHM}$ and $Scar_{-2sd}$), and the $Greyzone_{-2sd\text{-}3sd}$ method (defined as the region with SI between 2 and 3 SD above the remote reference myocardium). Each of these indices was expressed as a percentage of the LV mass (%LV).

T1 relaxation maps were processed using a customised software plugin, incorporating motion correction with open source software (Osirix environment, Pixmeo, Geneva, Switzerland). Motion correction was performed by applying a multi-resolution BSpline deformable registration, as implemented in the Insight Toolkit.[71] Due to the potential susceptibility of high T1 values to the effects of heart rate during image acquisition, we performed linear regression analysis of the measured native non-contrast T1 ($T1^{-native}$) values on heart rate and applied heart rate correction using a function of the mean heart rate of our study population to the non-contrast T1 values as previously described.[9] The T1 associated derivative, extracellular volume index (ECV), was also calculated as previously described using the following formula:[11]

$$(1-\text{hematocrit}) \times \left(\frac{\frac{1}{\text{Post-contrast T1myocardium}} - \frac{1}{\text{Pre-contrast T1myocardium}}}{\frac{1}{\text{Post-contrast T1blood}} - \frac{1}{\text{Pre-contrast T1blood}}} \right)$$

A region of interest (ROI) in the septum was chosen for estimation of non-contrast T1 ($T1^{-native}$), post-contrast T1 ($T1^{-contrast}$) and ECV, as previously described.[72] Care was taken to avoid the endocardium/blood pool interface. If regional enhancement was seen in the septum on the LGE image a septal ROI was chosen adjacent to the enhanced region for T1 mapping analysis. The geometry of the mid-ventricular T1 map slice was the same as that of the mid-ventricular LGE images to allow for this comparison.

3.4 Echocardiography

Transthoracic echocardiography was performed using a GE Vivid 7 scanner (General Electric-Vingmed, Milwaukee, WI, USA) to acquire standard 2D images of left

ventricular (LV) dimensions and ejection fractions (EF) during breath-hold in standard apical 2-chamber and 4-chamber views. LVEF and dimensions were measured using the 2-dimentional modified biplane Simpson's method. Analysis was done on EchoPac 6.0.1 (General Electric-Vingmed).

Echocardiographic evidence of inter- and/or intra-ventricular dyssynchrony was deemed present if any of the following criteria were fulfilled:[73]

- LV pre-ejection period > 140ms
- Interventricular mechanical delay (LV minus RV pre-ejection period) > 40ms

(Pulsed wave Doppler was used with the measurement made from the LV outflow tract (LVOT) in an apical 5-chamber view. The RV outflow tract (RVOT) was viewed in a parasternal short axis view. The pre-ejection period was defined as the time from the QRS onset on the ECG to the onset of flow.

- Septal to lateral wall motion delay (by tissue Doppler imaging, TDI) > 60ms

(The difference between septal to lateral peak velocity within the aortic valve opening and closing times)

3.5 Activation recovery interval measurement

LV unipolar electrogram (UEG) signal was made via the device programmer (Merlin Patient Care System, Model 3650, St Jude Medical). In order to eliminate the influence of variable heart rate on ARI. UEG recordings were made after at least 2 minutes of pacing at a constant rate of 10 beats above the patient's intrinsic heart rate. The 30 second LV UEG recordings were analysed off-line using a software script

developed by our group within the MATLAB environment (MathWorks, Massachusetts, USA) to derive the activation recovery interval (ARI). [74] ARIs were measured using conventional validated criteria from dv/dt min of the QRS of the UEG to dv/dt max of the local T wave.[75-79]An example showing the measurement and the stability of recordings is illustrated in Figure 3.1.

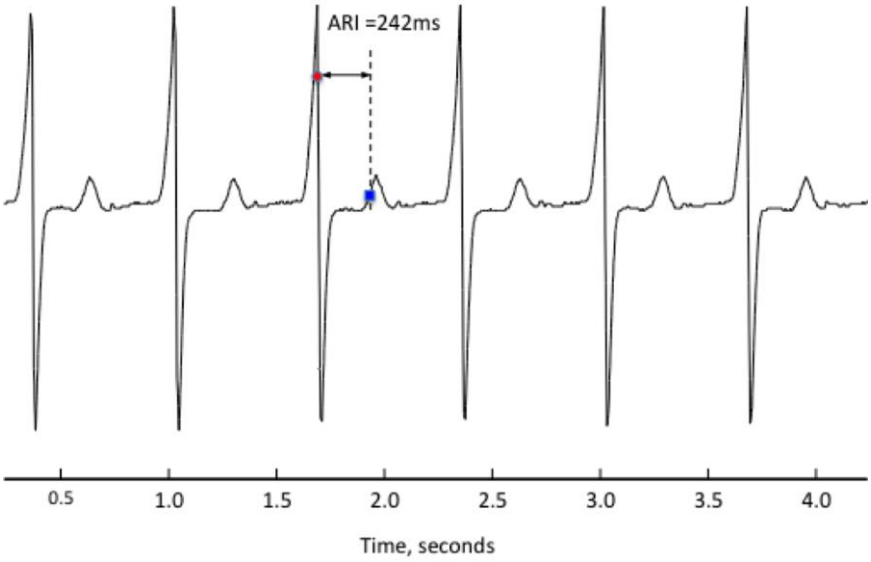

Figure 3- 1 An example of LV unipolar electrogram raw data recording demonstrating activation recovery interval (ARI).

3.6 Statistics

The baseline characteristics of the participants were studied in detail; continuous variables are reported as mean ± sd and categorical variables as number (and percentage) of participants. Between-group comparisons were made using the t-test for normally distributed continuous variables, otherwise the Mann-Whitney U or Wilcoxon tests were used, or the Chi-squared test (for categorical variables), with a two-tailed p-value < 0.05 indicating statistically significant differences between groups.

(Where applicable) The first episode of appropriate ICD therapy or sustained VT was considered as the event of interest for quantifying various associations.

Kaplan-Meier survival curves were plotted to study the cumulative event rates between groups of participant, with the log-rank test providing further evidence regarding any significant differences between them.

The univariate association between pre-specified variables of interest and the primary endpoint was examined using Cox proportional hazards regression models. For multivariable-adjusted analyses, a forward selection process using variables significantly associated with the outcome of interest in univariate analyses (at $p < 0.05$) was employed to further determine any independent predictors of the primary endpoint.

Chapter 4 Exploring T1 mapping for scar assessment

The clinical application of T1 mapping in myocardial tissue characterisation was in its infancy when this exploratory study was conducted. The aim of the study is to explore its application as a useful clinical tool for myocardial scar characterisation. Given the established experience with the use of LGE CMR for detection of regional myocardial scar, the study focused on comparing the quantitative assessment of regional scar, in particular the grey zone by T1 mapping with that by LGE CMR in the ischemic cohort population.

4.1 Abstract

Background: In ischaemic cardiomyopathy, grey zone is a strong predictor of ventricular arrhythmia. T1 relaxation-time mapping allows quantitative myocardium characterisation. We explored whether T1 measurements using images generated by a modified Look-Locker inversion-recovery (MOLLI) sequence can differentiate grey zone from healthy myocardium and scar core.

Methods: Twenty-one patients with a history of myocardial infarction underwent scar assessment with standard inversion-recovery gradient-echo sequence post-contrast (gadobutrol, 0.2mmol/kg) on a 1.5T scanner (Philips, Netherlands). Signal-intensity-based tissue heterogeneity assessment identified regions of remote healthy myocardium, scar core, and grey zone. These corresponding regions-of-interest were identified on the pre- and 20-minutes post-contrast MOLLI images. T1, R1 (1/T1) and relative ΔR1 (r ΔR1) values (Pre-contrast R1 – Post-contrast R1/ Pre-contrast R1) values for each region were analyzed.

Results: The mean T1 relaxation-times or R1 values for remote healthy myocardium, grey zone and scar core (n=63, respectively) were different on the pre- ($p<0.001$) and the post-contrast T1 maps ($p<0.001$). ROC analysis showed that r ΔR1 provided the best distinction between remote healthy myocardium, grey zone and scar core in comparison to either pre- or post-contrast R1 alone. Pre-contrast R1 is just as good at distinguishing the remote healthy myocardium from scar core and grey zone, but not as good at distinguishing the grey zone from scar core.

Conclusion: Using measurements derived from T1 mapping, pre-contrast R1 value can reliably distinguish healthy myocardium from scar and grey zone. However, rΔR1 provides a better distinction for grey zone from scar core and healthy myocardium than either pre- or post-contrast R1 alone.

Key words: grey zone, T1 mapping, late gadolinium enhancement

4.2 Introduction

Late gadolinium enhanced (LGE) inversion-recovery imaging in cardiac magnetic resonance (CMR) imaging is the standard approach to visualise regional myocardial fibrosis.[80,81] Studies have shown that the presence of regional fibrosis by LGE is an important prognostic indicator in both patients with ischaemic cardiomyopathy and patients with non-ischaemic cardiomyopathy.[39,59,82,83] With improvements in spatial resolution and contrast-to-noise ratio, it is now possible to perform a more detailed characterisation of the degree of scarring in the infarct border zone, where there is an admixture of fibrosis and surviving myocytes.[21] This area is referred to as the grey zone, because of the intermediate signal intensity (SI) between the hyper-enhanced

scar core and the nulled non-infarct myocardium seen on the LGE images. Studies based on semi-quantitative SI-based scar segmentation methods have demonstrated that the grey zone is an independent prognostic indicator of mortality and ventricular arrhythmia in post-infarct patients.[2-4]

Despite the wide adoption of the standard LGE-CMR imaging for regional myocardial fibrosis assessment, it is not without limitations such as inaccurate inversion-time selection and therefore suppression of diffuse fibrosis. An alternative method of characterizing the myocardium by assessing the tissue longitudinal relaxation time, T_1 mapping, would eliminate the influence of imprecise inversion time selection during image acquisition and allow true quantitative signal quantification on a standardised scale of each image voxel to characterise tissue heterogeneity. One of the best described methods of generating T_1 map of the myocardium is the modified Look-Locker inversion-recovery (MOLLI) sequence, which has been optimised and validated in patients with ischaemic cardiomyopathy.[7,9,84] MOLLI provides high resolution T_1 maps within a single breath-hold.

We hypothesised that the change in longitudinal relaxation times derived from pre- and post-contrast T_1 measurements acquired using MOLLI sequence would be best at characterizing the myocardium and differentiating between regions of healthy myocardium, grey zone and scar core in patients with ischaemic cardiomyopathy.

4.3 Methods

Patients

(See Chapter 3.2 for General patient selection criteria)

Patients with a known history of ischaemic cardiomyopathy and under assessment for implantable cardioverter defibrillator (ICD) for primary or secondary preventions were invited to participate in the study prior to their routine clinical CMR. Additional inclusion criteria included a history of myocardial infarction(s) at least > 3 months prior to CMR

Cardiovascular magnetic resonance imaging

(See Chapter 3.3.1 for General CMR methods protocol)

For left ventricular (LV) scar assessment, LGE-CMR was performed by full short axis coverage of LV 10-15 minutes post contrast injection[85] (gadobutrol, 0.2mmol/kg body weight).

Breath-hold MOLLI sequence was used for T_1 mapping.[84] Three separate gapless short-axis slices of MOLLI T_1 mapping images were acquired pre- and 20 minutes post-contrast in the same corresponding three mid-ventricular short-axis slices as the LGE images.

In order to maintain reasonable scanning duration, functional images were routinely acquired post contrast injection and we were limited to three MOLLI image slices per patient. Rather than having different MOLLI slices geometries for different patients, we decided to standardise the scanning protocol to three mid-ventricular slices. This allowed direct comparison with LGE scar images in the same slice geometry and maximised the likelihood of image acquisition of scar and grey zone, as in our experience nearly all patients with ischaemic cardiomyopathy have scars that extends to the mid-ventricular levels as demonstrated by our cohort.

Data analysis

Tissue sub-types selection

For the study, three mid-ventricular LGE short axis images with regional scar coverage were cross-referenced with the corresponding T_1 mapping images of the same geometry and analyzed using open source software OsiriX (Pixmeo, Geneva, Switzerland). Signal intensity (SI) based tissue heterogeneity assessment on the LGE images were analyzed with additional dedicated software plug-in for OsiriX as previously described.[86] On each LGE short-axis slice, we manually delineated the LV endocardial, epicardial borders and the border of a region of non-enhanced myocardium which was defined as the region of remote healthy myocardium. The maximum SI within the whole myocardium was automatically determined.

Using the full-width-half maximum method all pixels with SI values up to half of the maximum SI were automatically characterised as scar core.[87] Pixels with SI higher than 2 standard-deviation of the SI of the manually selected remote healthy myocardium but below the SI of the scar core were automatically assigned as being grey zone. The manually identified endocardial and epicardial borders and the three areas of region-of-interest (ROI), i.e. manually selected remote healthy myocardium, automatically segmented grey zone and scar core, were transferred to the corresponding pre- and post-contrast T_1 mapping images, as illustrated in Figure 1.

Motion correction

Though selective acquisitions at fixed points of the cardiac cycle in end-diastole and single breath holding would have largely suppressed the influence of cardiac and respiratory motion. The MOLLI sequence required eleven images to obtain the final

T_1 map which led to a relatively long breath-hold and therefore sometimes undesired residual respiratory motion. This would have resulted inaccurate T_1 value estimation for the ROI. We therefore applied manual motion correction using the endocardial and epicardial borders to adjust for in-plane respiratory motion between the eleven images used to construct the final T_1 map.

T_1 relaxation time analysis

The T_1 values for each of the three ROIs were calculated from the eleven pre- and post-contrast images by fitting a three parameter exponential model to the average voxel value of the measured data from each ROI, i.e. "ROI-by-ROI" method, and applying Look-Locker correction as previously described.[88] Due to the potential susceptibility of high T_1 values to the influence of heart rate during image acquisition, we also performed linear regression analysis on the measured pre-contrast T_1 values against heart rate and applied heart rate correction using a function of the mean heart rate of our study population to the pre-contrast T_1 values as previously described.[9]

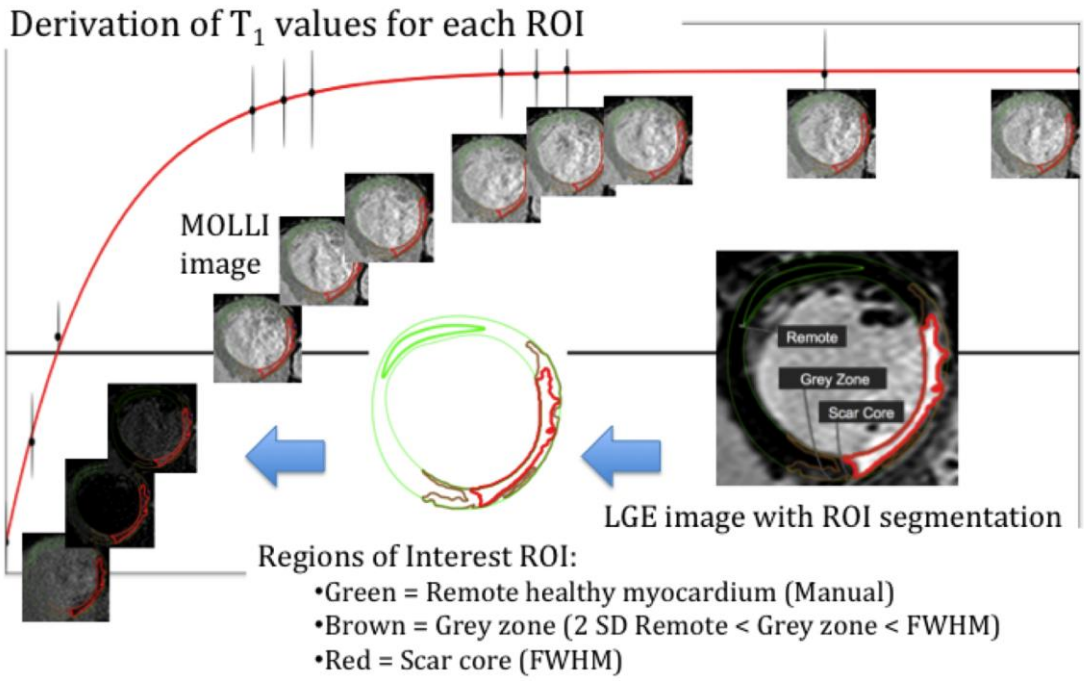

Figure 4- 1 Transposition of region of interest (ROI) from late-gadolinium-enhanced (LGE) image to modified Look-Locker inversion-recovery image for T_1 longitudinal relaxation time analysis.

ROI = region of interest; MOLLI = modified Look-Locker inversion-recovery; LGE = late gadolinium enhancement; SD = standard deviation; FWHM = full-width-half-maximum.

The final T1 value for each region of interest (ROI) is generated from curve fitting from the mean voxel data points gathered from eleven images, each acquired at different inversion-recovery time, with the MOLLI sequence. The error bars demonstrate the variance of voxel data points within selected ROI.

R_1 and *relative* ΔR_1 ($r\Delta R_1$)

In addition, R_1 values ($^1/_{T1}$) and $r\Delta R_1$ ($^{(\text{Pre-contrast R1} - \text{post-contrast R1})}/_{\text{pre-contrast R1}}$) for the respective ROI were also calculated.

T_1 longitudinal relaxation times were expressed as R_1 values, to allow a direct comparison of the post-contrast R_1 values ($R_{1,post}$) with native pre-contrast R_1 values ($R_{1,pre}$). The relationship between $R_{1,pre}$, $R_{1,post}$ and the contrast agent concentration C and its relaxivity r_1 is expressed by the function:[18]

$$R_{1,post} = R_{1,pre} + C \cdot r_1$$

The proposed quantity $r\Delta R_1$ takes into account the difference between R_{1post} and R_{1pre} which is then normalised against R_{1pre}:

$$r\Delta R_1 = \Delta R_1 / R_{1pre} = (R_{1,post} - R_{1,pre}) / R_{1pre} = (C \cdot r_1) / R_{1,pre}$$

Expressing the relative change in tissue T_1 longitudinal relaxation time pre- and post-contrast as $r\Delta R_1$ takes advantage of $r\Delta R_1$ being linearly proportional to the contrast agent concentration and its relaxivity constant. $r\Delta R_1$ is inversely proportional to pre-contrast R_1 as shown in the above equation, thus any difference in pre-contrast T_1 or R_1 between different ROI would be taken into account; and any changes in T_1 or R_1 values post contrast would potentially be magnified allowing greater separation of $r\Delta R_1$ between different ROI on a quantitative scale.

4.3.1 Statistics

(See Chapter 3.6 for General statistical methods)

Receiver-operating characteristics (ROC) analysis was used to identify the cut-off values with the best comparable sensitivity and specificity to discriminate different ROI. The predictive ability of pre-contrast R_1, post-contrast R_1 and $r\Delta R_1$ to identify each ROI was summarised using the area under curve (AUC). The best cut-off values derived from the ROC curve analysis for the distinction of remote healthy myocardium from scar and grey zone and that for the distinction of scar core from grey zone and healthy myocardium were then used as threshold values for the grey

zone. These different threshold values were retrospectively tested on the observed data to assess their predictability of the grey zone. The AUCs for pre-contrast R_1, post-contrast R_1 and $r\Delta R_1$ for each ROI (remote healthy myocardium, grey zone and scar core) were compared. Where a significant difference in the AUCs was detected between the three measures, pairwise comparisons were conducted using a Bonferroni correction (i.e. $p<0.05/3=0.016$ were considered statistically significant; the correction adjusts for multiple comparisons).

Analysis of the variables was conducted on a per-short axis slice basis. To assess the impact of including three short axis slices from each patient as independent data points on the final results estimation, a linear mixed effects model was used to adjust for within patient correlation and data analysis repeated using randomly selected single slice from each patients and compared with the final results. All statistics were performed using computer software SPSS Statistics, version 19, SPSS Inc., IBM, USA.

4.4 Results

Patients

Twenty-one patients were included in the study (nineteen males). The mean age was 61 ± 16 years. The baseline patient characteristics are outlined in Table 1. All patients had hematocrit levels within the normal reference range.

Characteristics	**Patient, n = 21 (100%)**
Male	19 (90%)
Hypertension	3 (14%)
Diabetes	2 (10%)
Renal impairment (estimated glomerular filtration rate, eGFR, 45-65ml/min/1.73m^2	5 (24%)
Indication for Implantable defibrillator therapy	Primary prevention: 16 (76%) Secondary prevention: 5 (24%)
Duration of last infarct to CMR, months	40 ±29
Left ventricular ejection fraction, %	35 ±10
Left ventricular end-diastolic volume, ml	232 ±49
Number of segments with evidence of late gadolinium enhancement / patient	7 ±3
Number of patient with evidence of late gadolinium enhancement at mid-ventricular level	21 (100%)
Culprit coronary artery territory of infarct	LAD: 11 (52%) Cx: 5 (24%) RCA: 13 (61%)
Scar transmurality at mid-ventricular levels: (per total scarred segment analyzed, n=180)	<25%: 0 (0%) 25-50%: 15 (8%) 50-75%: 51(28%) >75%: 114 (64%)

Table 4- 1 Baseline patient clinical characteristics

Data are expressed as n ± standard deviation, (%); LAD: left anterior descending artery, Cx: circumflex artery, RCA: right coronary artery. Left ventricular segments are classified according to the American Heart Association AHA 16-segment model.

Image analysis

All of the three mid-ventricular LGE scar images and the corresponding pre-contrast, 20 minutes post-contrast T_1 mapping images contained scar were suitable for ROI segmentation. The mean number of LV segments (American Heart Association 16-segment model) with enhancement on the LGE images were 7 ± 3 per patient, with 64% of the enhanced segments having >75% transmural scar at the mid- ventricular level. T_1 values, R_1 values and respective $r\Delta R_1$ from a total of 189 ROIs identified from the LGE images; remote healthy myocardium (n=63), grey zone (n=63) and scar core (n=63); were analyzed.

To account for the impact of including three short axis slices from each patient as independent data points on the final results estimation, a linear mixed effects model was used to compare the values between remote health myocardium, grey zone and scar core to adjust for within patient correlation. The mean T_1 relaxation times and R_1 values for each region, healthy myocardium, grey zone and scar core, were significantly different on both the pre- and the post-contrast T_1 maps (see Table 4-2).

N=63	Remote healthy myocardium	Grey zone	Scar core	P values
Pre-contrast T_1	971 ± 44 ms	1067 ± 57 ms	1186 ± 96 ms	< 0.001
$R1_{pre}$ x 10^3	1.03 ± 0.05	0.94 ± 0.05	0.85 ± 0.07	< 0.001
Post-contrast T_1	419 ± 51 ms	348 ± 36 ms	258 ± 36 ms	< 0.001
$R1_{post}$ x 10^3	2.42 ± 0.28	2.90 ± 0.30	3.94 ± 0.53	< 0.001
$r\Delta R_1$	1.35 ± 0.30	2.10 ± 0.38	3.68 ± 0.79	< 0.001

Table 4- 2 Pre-contrast T_1 relaxation time, post-contrast T_1 relaxation time, R_1 values ($1/T_1$) and the relative changes expressed by $r\Delta R_1$ ($^{R1,pre - R1,post}/_{R1,pre}$) for regions of remote healthy myocardium, grey zone and scar core; n=63, respectively.

Data are expressed as mean ± standard deviation.

At 20 minutes post-contrast, the T_1 values were significantly reduced in all regions with the greatest reduction seen in scar core. The distribution of R_1 and $r\Delta R_1$ for each region are plotted in Figure 4-2.

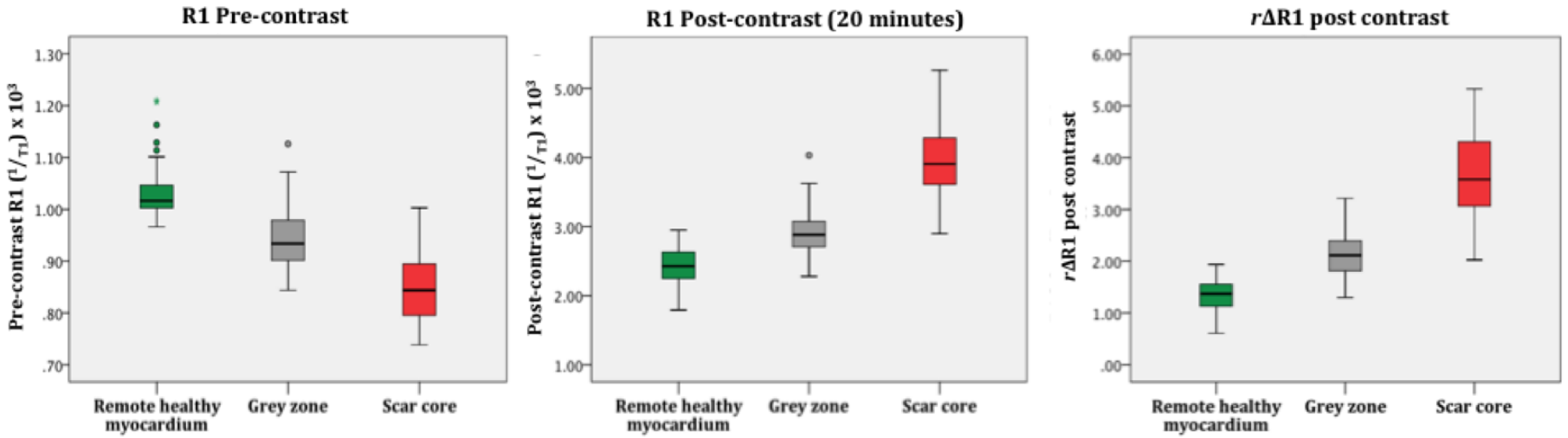

Figure 4- 2 Box plot demonstration of the distribution of pre-contrast R1 (1/T1 relaxation time), post-contrast R1 and rΔR1 (R1,pre - R1,post/R1,pre) for each region of interest: remote healthy (green), grey zone (grey) and scar core (red).

Box: median, interquartile ranges. Wiskers: minimum, maximum ranges. Different R1 scales are used on the pre- and post-contrasts graphs because of the effect of gadolinium on R1

ROC curve analysis, Figure 3, showed that the native pre-contrast R_1 (AUC: 0.96; 95% Confidence interval (CI): 0.93-0.97) and $r\Delta R_1$ (AUC: 0.97; 95% CI: 0.95-0.99) both provided a better distinction for healthy myocardium from scar core and grey zone than post-contrast R_1 value (AUC:0.94; 95% CI:0.91-9.97); $r\Delta R_1$ (AUC: 0.99; 95% CI: 0.98-1.00) and post-contrast R_1 value (AUC: 0.98; 95% CI: 0.96-0.99) provided a better distinction for scar core from grey zone and healthy myocardium than pre-contrast R_1 value (AUC: 0.92; 95% CI: 0.88-0.96). $r\Delta R_1$ (AUC: 0.98; 95% CI: 0.95-1.00) provided the best distinction for grey zone from scar core, with post-contrast R_1 also providing good differentiation (AUC: 0.95; 95% CI: 0.92-0.99), and pre-contrast R_1 being less good (AUC:0.85; 95% CI: 0.78-0.92).

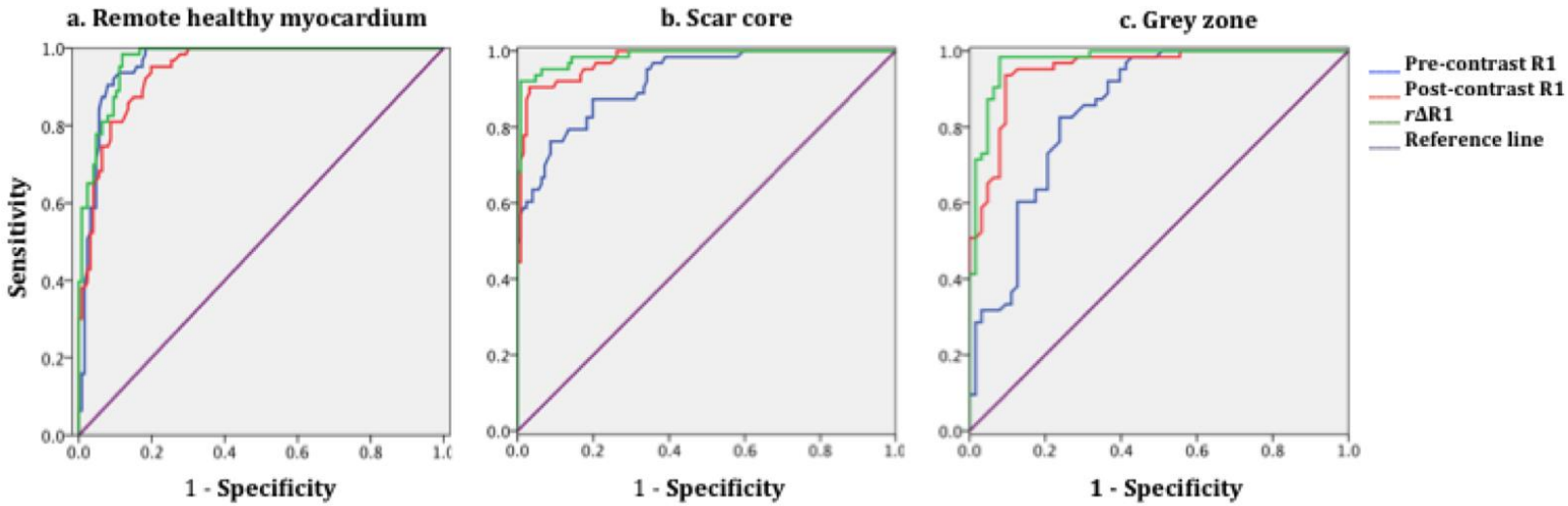

Figure 4- 3 ROC curve analysis of remote healthy myocardium, scar core and grey zone assessment by pre-contrast R1 (blue), post-contrast R1 (red) and rΔR1 (green); n = 63, respectively.

a: differentiation for remote healthy myocardium from scar core and grey zone; b: differentiation for scar core from grey zone and healthy myocardium; c: differentiation for grey zone from scar core.

A cut-off of pre-contrast R_1 $x10^3$ value of $\geq$0.986 provided a good distinction for healthy myocardium from scar core and grey zone with a sensitivity of 0.92 and specificity of 0.90 as did a cut-off $r\Delta R_1$ value of $\leq$1.78 with a sensitivity of 0.95 and specificity of 0.89; a $r\Delta R_1$ value of $\geq$2.68 provided the best distinction for the scar core from grey zone and healthy myocardium with a sensitivity of 0.92 and specificity 0.99. Using cut-off values for scar core and remote healthy myocardium derived from the ROC analysis as threshold values for grey zone, a $r\Delta R_1$ value between 1.78 and 2.68 provided the best prediction for the grey zone with a sensitivity of 0.75 and specificity of 0.94, see Table 4-3.

	Pre-contrast R1x10^3 cut-offs	**Post-contrast R1x10^3 cut-offs**	**rΔR_1cut-offs**
Remote healthy myocardium	≥986 (sens 0.92; spec 0.90) (ppv 0.83; npv0.96) (diag. accuracy 91%)	≤2677 (sens 0.81; spec 0.91) (ppv 0.82; npv 0.91) (diag. accuracy 88%)	≤1.78 (sens 0.95; spec 0.89) (ppv 0.80; npv 0.97) (diag. accuracy 90%)
Scar core	≤923 (sens 0.87; spec 0.80) (ppv 0.69; npv 0.93) (diag. accuracy 83%)	≥3226 (sens 0.91; spec 0.94) (ppv 0.93; npv 0.95) (diag. accuracy 95%)	≥2.68 (sens 0.92; spec 0.99) (ppv 0.98; npv 0.96) (diag. accuracy 97%)
Grey zone	923 < 986 (sens 0.46; spec 0.90) (ppv 0.71; npv0.77) (diag. accuracy 76%)	2677 < 3226 (sens 0.78; spec 0.86) (ppv 0.73; npv 0.89) (diag. accuracy 83%)	1.78 < 2.68 (sens 0.75; spec 0.94) (ppv 0.85; npv 0.88) (diag. accuracy 87%)

Table 4- 3 Prediction of Grey zone using pre-contrast R_1, post-contrast R_1 and rΔR_1

sens. = sensitivity; spec. = specificity; ppv = positive predictive value; npv = negative predictive value; diag. = diagnostic

For prediction of remote healthy myocardium from scar core and grey zone, the AUC of pre-contrast R_1 was not significantly different from the AUCs of post-contrast R_1 (p=0.377) and $r\Delta R_1$ (p=0.459). For prediction of grey zone from scar core, the AUC of $r\Delta R_1$ was significantly larger than the AUC of pre-contrast R_1 (p<0.001), but not

significantly different from the AUC of post-contrast R_1 (p=0.076); the AUC of post-contrast R_1 was also significantly larger than the AUC of pre-contrast R_1 (p=0.007).

Linear regression model analysis suggested within subject correlation may be a potential source of bias. To assess the impact of this correlation, data analysis was repeated using only one randomly selected image slice from each patient. The pre- and post-contrast T_1 for each ROI using a randomly selected single slice from each patient (see Table 4-4) were in good agreement with the final results shown above (see Table 4-2) encompassing all three short axis images from each patient.

N=21 (random slices)	**Remote healthy myocardium**	**Grey zone**	**Scar core**	**P values**
Pre-contrast T_1	969 ± 48 ms	1066 ± 59 ms	1191 ± 107 ms	< 0.001
Post-contrast T_1	416 ± 53 ms	350 ± 35 ms	262 ± 36 ms	< 0.001

Table 4- 4 T_1 values for each ROI derived from a randomly selected single short axis slice of MOLLI images from each patient.

Using data derived from randomly selected single slice of short axis images from each patient, repeated ROC analysis showed the same numbers for AUCs for remote healthy myocardium from scar core and grey zone using pre-contrast R_1 (AUC: 0.96, 95% CI 0.91-1.00); and in prediction for scar core from grey zone and remote healthy myocardium using $r\Delta R_1$ (AUC: 0.99, 95% CI 0.97-1,00). See supplement data provided.

4.5 Discussion

Our findings revealed that the pre-contrast and post-contrast T_1 maps derived from MOLLI and more specifically the R_1 ($^1/_{T1}$) and $r\Delta R_1$ ($^{R1,pre\ -\ R1,post}/_{R1,pre}$) values can be used for characterisation of different myocardial tissue sub-types in patients with ischaemic cardiomyopathy. We realise that the "healthy" non-enhancing areas in our conventional LGE images are not necessarily normal myocardium. There is some suggestions that patients with ischaemic cardiomyopathy may develop interstitial fibrosis in the remaining non-infarct region as the LV remodels, although histological study has not conclusively demonstrated this.[89,90] Conventional LGE images would have not been able to detect this as this region is nulled. Thus the T_1 longitudinal relaxation times for the remote "healthy" myocardium should be taken as delineating an area which is not scar core or grey zone but not necessarily normal myocardium. Further studies in healthy volunteers would be needed to characterise the true T_1 values for healthy myocardium.

For T_1 quantification, motion correction between the multiple images used to build the T_1 map is crucial to ensure accuracy. We applied manual in-plane motion correction to the 11 images for each slice by aligning the endocardial and epicardial borders. In addition, we adopted a more robust technique to calculate the ROI T_1 value of by using the mean signal intensity within the ROI using the "ROI-by-ROI" method as apposed to the "pixel-by-pixel" method that is less influenced by small amount of residual motion between the 11 images needed for T_1 mapping.

We used the term T_1 in the introduction, discussion and R_1 ($^1/_{T1}$) in the methods and results, as R_1 better represents the relationship between the pre- and post-contrast values, with post-contrast R_1 being a linear function of contrast concentration.

4.5.1 Pre-contrast T_1 values

We observed that the remote non-infarcted myocardium had a mean T_1 value that was significantly different from the grey zone and scar core. ROC analysis demonstrated pre-contrast R_1 value was just as good as post-contrast R_1 and $r\Delta R_1$ at distinguishing remote nulled myocardium from grey zone and scar seen on LGE images. This lends support to the suggestion that "healthy" myocardium could be reliably distinguished from abnormal myocardium (either grey zone or scar) without the need for contrast enhancement.

Messsroghli et al. also observed differences between pre-contrast T_1 values of "healthy" myocardium and areas of late enhancement in both patients with acute and chronic myocardial infarction.[7] They however did not assess the predictive values of T_1 mapping in identifying the different regions. The T_1 values for "healthy" myocardium in patients with chronic infarcts from both studies are comparable, however the T_1 values for scar were lower in the Messroghli's study than our values for scar core. This may be explained by our study's additional differentiation between grey zone and scar core.

The prevailing hypothesis for the difference in the native T_1 values between healthy myocardium and scar is that there is an increase in the extracellular matrix volume and loss of vasculature within the scar region, whilst healthy myocardium is packed with closely adherent parenchymal cells.[91] In addition, fibrillar type III and type I collagens are laid down substituting the loss of parenchymal cells in the scarred region.[92] These long-term histological changes in the infarcted myocardium are the likely explanation for the increase in native pre-contrast tissue longitudinal relaxation that we see in this study.

4.5.2 Post-contrast T_1 values

There was a significant drop in T_1 values in all regions in the 20 minutes post-contrast scans. Similar to the pre-contrast T_1 values, the post-contrast T_1 values for the different tissue regions were also significantly different. Our post-contrast T_1 values were lower than those observed by Messroghli et al.[7] This could be explained by the difference in our study protocol where post-contrast T_1 values were taken at 20 minutes post contrast administration rather than 10-15 minutes; and the higher concentration of gadolinium (0.2mmol/kg) used in our study.

Gadobutrol, used in our study, is an extracellular contrast agent. As a result of the disappearance of normal parenchymal cellular architecture and decreased capillary density within scarred myocardial regions, it preferentially distributes and accumulates for longer in the larger extracellular space, resulting in a reduction in the T_1 relaxation time in these regions.[91,92] The reduction in T_1 values in the scar borders zones with a mixture of scar and "healthy" myocardium will be less. Iles et al. have demonstrated that T_1 values, using images taken with a sequence similar to MOLLI fifteen minutes post-contrast, correlated with collagen volume fraction seen from biopsy samples in patients with heart failure with mixed aetiology.[93] Flett et al. have also demonstrated that regional myocardial T_1 values, taken after a slow infusion of contrast agent, correlated strongly with collagen volume fraction from biopsy results in patients with severe aortic stenosis.[11] Both these studies support the potential of using post contrast T_1 values to quantitatively assess the degree of collagen density within different myocardial regions.

We used LGE as a gold standard in our study as it has been validated in studies against histology for differentiating between "healthy" myocardium, scar core and infarct border zone i.e. grey zone.[21,87] We have demonstrated that each of the three

regions of "healthy" myocardium, grey zone and scar core with varying degrees of signal intensity seen in LGE have distinct post contrast T_1 and therefore R_1 values, presumably due to different levels of collagen volume fraction. We have also showed that post-contrast R_1 is much better than pre-contrast R_1 in distinguishing between grey zone and scar core with a greater degree of separation in post-contrast R_1 values ($x\ 10^3$) than pre-contrast R_1 values ($x\ 10^3$); 1.03 ± 0.51 vs. 0.09 ± 0.07. The observed non-linear differences in post-contrast R_1 between scar core, grey zone and remote "healthy myocardium" may be due to the non-linear differences in the regional contrast kinetics, which may vary depending on the regional tissue and microvascular constituents within each of the three ROIs.

4.5.3 Combining Pre-and Post-contrast T_1 values

We have shown the superiority of the simple index $r\Delta R_1$ ($^{R1,pre\ -\ R1,post}/_{R1,pre}$) to differentiating the three ROIs in patients with ischaemic cardiomyopathy. Though the difference between the AUCs of $r\Delta R_1$ and post-contrast R_1 were not statistically significant, there was a trend to suggest $r\Delta R_1$ being superior at distinguishing grey zone from scar core with higher specificity and diagnostic accuracy.

Expressing the relative T_1 values changes as $r\Delta R_1$, allows a measure that is linearly proportional to contrast agent concentration in the tissue and takes into account the differences in the pre-contrast R_1 values. This is important because when ΔR_1 is normalised against the pre-contrast R_1 values, represented by $r\Delta R_1$, there is a greater separation between the tissue subtypes on a quantitative scale ("healthy" remote myocardium has higher R_1 than scar core pre-contrast), thus allowing better distinction between regions of healthy myocardium, grey zone and scar core. This is due to the opposite orders in which scar-core and remote myocardium sits on the pre- and post-contrast R_1 quantitative scale. Indeed, retrospective analysis using different

cut-off thresholds for the grey zone derived from the ROC curve analysis showed $r\Delta R_1$ provided the best prediction for grey zone from the remote healthy myocardium and scar core with improved specificity and diagnostic value.

With conventional inversion-recovery LGE, tissue heterogeneity assessment is based on semi-quantitative signal intensity quantification on an arbitrary scale that can only differentiate between different tissue sub-types in contrast to a region of nulled myocardium. In comparison, T_1 mapping enables direct myocardial signal quantification on a standardised scale. It overcomes the inherent limitation of conventional inversion-recovery LGE imaging where the optimal imaging of different tissue sub-types requires the precise identification of the inversion time so that the "healthy" myocardium can be nulled. Therefore, T_1 mapping could also be a useful tool for assessing diffuse micro-fibrosis seen in other types of cardiomyopathy where myocardium fibrosis or scars are more homogeneous.

Several studies showed that myocardial extracellular volume fraction (Ve) provides a surrogate quantitative measure of myocardial collagen volume fraction.[11,94-96] Ve estimation is based on a calculation combining pre-and post-contrast T_1 value measurements and relies on prerequisite of an achieved steady state between the myocardial and blood pool contrast concentration. In addition, an assumption is made that there is a constant myocardial plasma volume fraction (reflecting capillary density) in regions of myocardium. After achieving an equilibrium following slow intravenous contrast infusion, Flett et al showed a close correlation between measured Ve and collagen volume fraction from histology. Schelbert et al. recently has demonstrated that a single bolus injection of gadolinium contrast at 0.2mmol/kg can also achieve this steady state 12-50 minutes post injection.[96] However their study involved a population of >50% subjects healthy volunteers, and only analyzed regions

of homogenous myocardium where there was no late gadolinium enhancement. This difference in study populations compared with ours meant that we could not extrapolate their observation to our study. In addition, in ischaemic cardiomyopathy there is a loss of vasculature in the infarct scar region,[91] therefore an assumption of normal myocardial capillary density or myocardial plasma volume fraction cannot be made. The heterogeneity between the different ROIs within the myocardium would influence the local contrast kinetics and timing of achieving contrast equilibrium between the scar core, grey zone, remote "healthy" myocardium and blood pool. Further studies comparing bolus injection and slow infusion to achieve contrast equilibrium state in the ischaemic cardiomyopathy patients are needed before we can apply Ve estimation in such selective patient population with myocardial tissue heterogeneity. In addition, the purpose of this study is to assess the ability of utilizing pre- and post-contrast T_1 values to separate scar core, grey zone and remote "healthy" myocardium. Variables such as blood pool pre and post-contrast R_1 values and hematocrit levels would be the same for the three ROIs within individual patient, thus removing the impact of these variables in distinguishing one ROI from the other. Our index, $r\Delta R_1$ ($^{R1,pre - R1,post}/_{R1,pre}$), takes into account of the pre-contrast R_1 value, which is different for the different ROI in heterogeneous myocardial tissue. It would therefore add additional predictive value in characterizing different myocardial subtypes. Although we used LGE as the gold standard in this study of patients with ischaemic cardiomyopathy, future studies that compare the two techniques against a histological gold standard will be of great interest. $r\Delta R_1$ can potentially be incorporated into an automated clustering tool that can quantitatively segment the tissue subtypes in a heterogeneous myocardium.[97]

4.5.4 Study Limitations

One limitation is the relatively small number of patients in our study. However, we were still able to demonstrate the ability of pre-contrast R_1, post-contrast R_1 and $r\Delta R_1$ at differentiating the different tissue sub-types. As with many previous studies,[84,98] multiple images, three separate short axis slices in our study, from each patient were used as independent data points which potentially introduces bias because of the intra-class correlation between the slices from the same individual. However, we found little difference in the T_1 values when we used a randomly selected single slice from each patient. In addition, the AUC for prediction of ROI from ROC analysis were also almost identical. Inaccurate manual endocardial border delineation may have introduced contamination of blood pool in the sub-endocardial scar regions due to similarity in signal intensity seen on the LGE images. All of our patients had close to or more than 50% transmural infarcts, thus minimizing the effect of blood pool contamination. Post-contrast T_1 or R_1 values also depend on individual pharmacokinetics and vary across a population as seen in the standard deviation of our values. A slow infusion technique that allows steady state between tissue and blood contrast concentrations proposed by Flett et al. that may overcome this issue, but is more time consuming.[11] There is however, some evidence to suggest that at 20 minutes following a bolus injection, relative steady state in tissue contrast concentration is reached within scarred myocardium,[98] we therefore acquired our post-contrast T_1 values 20 minutes post injection.

4.6 Conclusion

Using pre- and post-contrast T_1 measurements acquired with single-breath hold MOLLI sequence, $r\Delta R_1$ was best at distinguishing different tissue sub-types in

ischaemic cardiomyopathy. Pre-contrast R_1 was able to reliably distinguish “healthy myocardium” but was not as good in differentiating between grey zone and scar core.

Chapter 5 Improving respiratory navigator efficiency during high-resolution 3D delayed-enhancement CMR and its impact on myocardial scar assessment

One criticism of grey zone quantification by LGE CMR is the impact of imaging resolution on the quantification of LGE image signals. The quantification is semi-quantitative and is based on the signal intensities from the LGE images, therefore susceptible to partial volume effect of signal strength within each imaging voxel. With higher resolution LGE CMR, it is perceived that grey zone can be more accurately quantified with smaller voxel size. However this high-resolution data acquisition is at the cost of longer scanning time requiring patients to perform multiple long breath-holds. This is time consuming and laborious for the patients, especially to those with severely impaired LV function. One way of overcoming this is to acquire high-resolution 3-dimesional data with CMR sequence during free-breathing. This requires respiratory navigation with a selected window of interest for data acquisition during the respiratory phase (usually end-expiratory). However, patients with severely impaired LV function often have irregular breathing patterns, resulting in poor navigator efficiency and prolonging the scan time again. This chapter describes the work that explores a new technique to improve the navigator efficiency and the impact of high-resolution on LGE scar images and its quantification.

5.1 Abstract

Background: Myocardial scar characterisation and quantification by delayed-enhancement cardiac magnetic resonance imaging (DE-CMR) improves arrhythmia

risk stratification in patients with severely impaired left ventricular ejection function (LVEF). However, often the long breathhold required for routine multi-slice 2-dimensional (M2D) scar imaging are challenging for many of these patients, and irregular breathing resulting in prolonged free-breathing 3-dimensional (3D) scar imaging time. We proposed to combine high-resolution 3D DE-CMR with a more efficient respiratory-gating approach (HybridPAWS) to improve scan efficiency and asses its clinical efficacy in patients with significantly impaired LVEF who are being considered for defibrillator device therapy.

Methods: Breath-holding M2D and free-breathing high-resolution 3D DE-CMR were performed in 44 consecutive patients. During 3D data acquisition, the navigator efficiency (NE) for HybridPAWS and a standard respiratory-gated acquisition scheme were compared. Scar quality and quantification analyses were compared between the M2D and 3D images in short- and long-axis orientations, using a multi-planar reformatting tool.

Results: The mean LVEF of the study cohort was 30±12%. The mean respiratory NE was 47±15% with HybridPAWS *vs.* 39±18% with the standard respiratory-gated Cartesian scheme (p <0.01). HybridPAWS made the greatest impact in patients with NE <40%, achieving a mean improvement of 55±68% in NE. 3D scar image quality was comparable to M2D images and without any compromise when reformed to any clinically important image orientations to study region of interest. Quantitative delayed-contrast enhancement analyses showed that given similar in-plane resolutions, M2D and 3D images produced similar scar core and grey zone sizes. Increasing through-plane slice thickness did impact on the scar quantification beyond a thickness of 8mm.

Conclusion: HybridPAWS can improve respiratory NE and shorten scan time during high-resolution isotropic 3D DE-CMR. Isotropic 3D scar image has a potential for improving the accuracy of scar border zone quantification and allowing retrospective multi-plane reformatting for optimal myocardial scar assessment. Increasing through-plane slice thickness during 3D scar imaging may potentially shorten acquisition time without a significant impact on scar quantification.

Key words: high-resolution CMR, respiratory navigation, HybridPAWS

5.2 Introduction

Delayed-enhancement cardiac magnetic resonance imaging (DE-CMR) is the standard approach for visualising myocardial fibrosis.[80,81] The presence of myocardial fibrosis is an important prognostic indicator in patients with both ischemic and non-ischemic cardiomyopathies.[39,59,82,83] Signal intensity (SI) based analysis on regions of enhancement allows further characterisation of the scar region, separating the scar core and the scar border zone (often referred to as grey zone due to its intermediate signal intensity with a mixture of fibrosis and myocytes). This has been shown to improve patient arrhythmic risk stratification and assist cardiac arrhythmia ablation procedure.[4,24,99,100] Small areas of myocardial scar need to be characterised in high spatial resolution in order to detect complex arrhythmogenic substrates beyond the simple binary detection of scar. Conventional DE-CMR yields myocardial scar images by acquiring multiple two-dimensional (M2D) image slices over several breath-holds in order to give sufficient coverage of the whole ventricle. This image

acquisition process can be strenuous for some patients, particularly those with significantly impaired left ventricular (LV) function who often cannot hold their breath long enough for each image acquisition. Furthermore breathholds are often not reproducible resulting in misalignment of slices along the slice selection direction. Whilst the in-plane resolution of the image slice is sufficient for excellent visualisation of the ventricular myocardial scar, the slice thickness is much larger (resulting in an one order of magnitude lower through-plane resolution than the in-plane resolution). High-resolution three-dimensional (3D) free-breathing DE-CMR has been proposed to overcome these limitations and to allow for accurate depiction of scar tissue independent of the scan orientation.[5] However, the acquisition requires long scan time requiring compensation of cardiac and respiratory motions. Whilst cardiac motion is synchronised by electrocardiography (ECG) triggering, respiratory gating is commonly applied during the free breathing scan. For such scans, data are only accepted if a respiratory motion surrogate such as the position of the right diaphragm is within a pre-defined narrow gating window. This approach can be problematic especially in patients with impaired ventricular function who often have irregular breathing patterns leading to prolonged image acquisition times as a result of poor respiratory gating efficiency.[101-103]

In order to improve respiratory navigator efficiency (NE), a CMR data acquisition scheme called Phase ordering with Automatic Window Selection (PAWS) has been proposed to improve respiratory gating efficiency in non-contrast enhanced coronary magnetic resonance angiography.[104] Recently a Radial Phase Encoding (RPE)-PAWS approach for non-contrast enhanced 3D-MRI has been proposed, which is more efficient as it allows better under-sampling properties.[105] However, RPE usually

requires advanced image reconstruction techniques making its clinical translation cumbersome.

Here, a modified RPE-PAWS approach is proposed that acquires all phase encoding steps in a radial order but on a rectilinear grid. This allows immediate data reconstruction on the scanner platform allowing direct clinical assessment at the scanner. This method is referred to as HybridPAWS. The purpose of this study is to assess HybridPAWS in patients with impaired LVEF who are likely to have irregular breathing patterns resulting in poor navigation efficiency and evaluate the respiratory NE and image quality of high resolution isotropic 3D DE-CMR acquired. Furthermore, the study aims to assess the impact of the required through-plane slice thickness on the quantification of scar core and grey zone.

5.3 Methods

5.3.1 HybridPAWS combined with a 3D DE-CMR inversion-recovery (IR) sequence

In HybridPAWS all phase encoding steps are acquired in a radial order but located on a rectilinear grid allowing straightforward application of standard parallel imaging techniques and thus fast image reconstruction. Instead of defining the gating window at the beginning of the scan, PAWS is determining the most probable respiratory motion state during the acquisition ensuring a high NE over the complete scan. For this the data was obtained at multiple respiratory windows (referred to as bins) covering the entire amplitude of the respiratory signal. In each respiratory bin, data are radially distributed and thus cover both low and high spatial frequencies homogeneously. In addition, the proposed ordering scheme ensures that data acquisitions in two adjacent respiratory bins are complementary. Therefore the scan is

successfully finished if two neighboring bins can be combined for the reconstruction of a 3D image (Figure 5-1a). The acquisition scheme was combined with inversion recovery (IR) pre-pulse for late-enhancement MRI. The electrocardiograph (ECG) - triggered acquisition scheme and behavior of the longitudinal magnetisation for healthy and fibrotic myocardium post contrast enhancement is shown in Figure 5-1b.

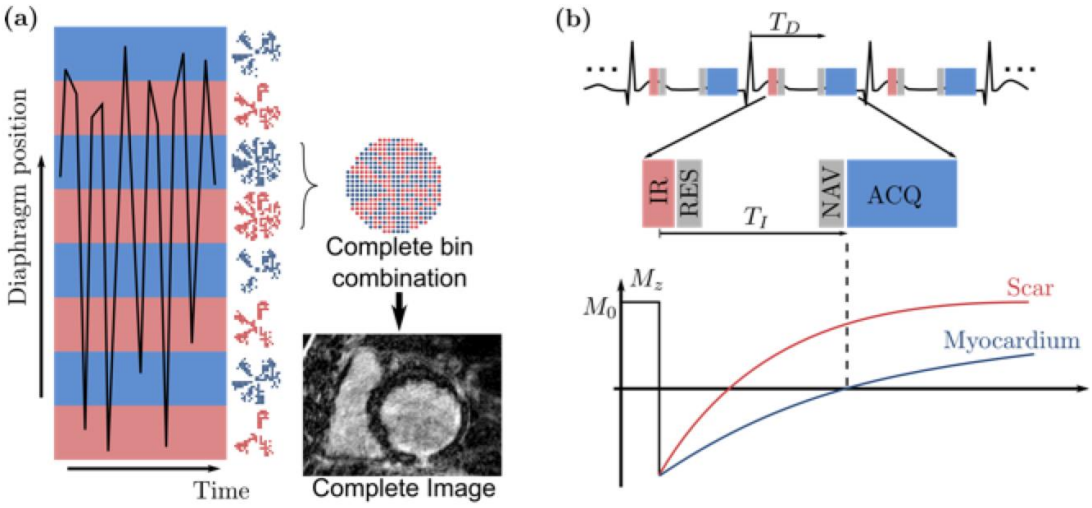

Figure 5- 13D DE-MR sequence combined with HybridPAWS.

(a) HybridPAWS acquires data in multiple respiratory bins (red/blue bars) covering the entire amplitude of diaphragm movement. An interleaved phase encoding scheme is used which allows for the combination of data from two adjacent bins. Data acquisition is successfully finished when one combination of two adjacent bins leads to a completely filled k-space allowing reconstruction of DE-3D images. (b) Data acquisition is cardiac triggered with the trigger delay (TD). An inversion recovery (IR) pre-pulse inverts the longitudinal magnetisation. Signal at the location of the respiratory navigator (NAV) is restored (RES). Data is obtained after an inversion time TI which is selected to optimally null healthy myocardium. IR inverts the longitudinal magnetisation Mz. The administered contrast agent leads to a shortening of the T1 time of scar tissue. Therefore, Mz of scar tissue (red) recovers faster than the longitudinal magnetisation of viable myocardium (blue). The inversion time TI is set to optimally null signal from healthy myocardium.

Patient selection

(See Chapter 3.2 for General patient selection criteria)

Cardiovascular magnetic resonance imaging

(See Chapter 3.3.1 for General CMR methods protocol)

For scar imaging, standard M2D DE-CMR was performed in the same views 10-15 minutes post contrast injection (gadobutrol, 0.2mmol/kg body weight), using a standard IR gradient echo sequence with repetition time/echo time of 3.4/2.0ms; flip angle 25 degrees; voxel size 1.8x1.8x8mm^3 and a field of view (FOV) of approximately 300x300x8mm^3; ECG triggered to end-diastole. Patient-specific inversion time (TI) for the IR sequences was selected individually based on a Look-Locker scan to ensure nulling of the myocardium just prior to the M2D DE-CMR imaging.[106] Immediately after M2D scar image acquisition, high-resolution 3D DE-CMR data was acquired using HybridPAWS with isotropic voxel size of 1.7x1.7x1.7mm^3, FOV approximately 300x300x100mm^3, repetition time/echo time of 5.4/2.6ms and flip angle 25 degrees. Parallel imaging was used in two directions with SENSE factors of 2 and 1.3 in phase and slice encoding direction, respectively. For respiratory gating of the 3D IR acquisition, a combination of a pencil beam navigator with a preceding restore pulse was applied.[107] Again, patient-specific TI was selected from a repeated Look-Locker scan.

Respiratory navigator efficiency (NE)

Respiratory navigator efficiency (NE) was defined as the number of accepted data points in the two bins divided by the overall obtained data points in all bins. During the acquisition of high-resolution 3D DE-CMR data, the NE was calculated for

HybridPAWS. All respiratory signals were stored to calculate the NE for a standard respiratory-gated Cartesian acquisition scheme (Std-gated Cartesian scheme), thus allowing a direct comparison of NE from the same respiratory motion information.

Image analysis

The scar images were compared between the conventionally acquired M2D and 3D DE-CMR images. In order to make comparison, the higher resolution 3D datasets were reformatted to the same slice thickness as that of the M2D datasets with a multi-planar reformatting tool (mean SI slabs with a thickness of 8mm), using OsiriX Imaging Software, version 3.9.2 (Geneva, Switzerland). The in-plane resolution between the two datasets was comparable, 1.7x1.7mm vs. 1.8x1.8mm, and was therefore not modified, as we expected the gain in image quality with 3D DE-CMR to be mainly in the slice direction. Two experienced observers blinded to the image acquisition methods visually scored each dataset to assess the quality of the scar images in short- and long-axis on a scale between 0 and 4: 0 = non-interpretable, 1 = poor quality, 2 = medium quality, 3 = good quality, and 4 = excellent quality. The scar signal noise ratio (SNR) was measured by the mean SI from the region of contrast enhanced region divided by the standard deviation (SD) of the SI in the lung field away from the myocardium. The scar_myocardium and scar_blood contrast noise ratios (CNR) were measured as the difference between the scar SNR and the respective remote normal myocardium SNR or blood pool SNR. 3D mages with the best visual quality score (i.e. score 4) were selected for further SI based scar quantification analysis. Scar core was defined by the full-width-half-maximum (FWHM) method; and the grey zone was defined by the region with SI above that defined by FWHM but below that defined by that of two standard deviation (2SD) from remote presumed normal myocardium (2SD – FWHM method). Scar

quantification analyses were also repeated with varying reformatted though-plane slice thickness (1mm, 2mm, 4mm, 8mm, 16mm) in order to assess its impact on the in-plane image scar quantification using 3D DE-CMR images.

5.3.2 Statistics

(See Chapter 3.6 for General statistical methods)

Between-group comparisons were made using the t-test or the Chi-squared test (for categorical variables), or the one-way ANOVA test (for more than two groups comparison), with a two-tailed p-value < 0.05 indicating statistically significant differences between groups. All statistics were performed using computer software Prism Version 6 (GraphPad Software, Inc. CA, USA)

5.4 Results

In total, 44 patients were enrolled in the study prior to CMR as part of their clinical assessment before ICD implantation. The mean LVEF was 30±12%. Of the cohort, 30 (68%) patients subsequently received combined cardiac resynchronisation therapy (CRT) with a defibrillator device. All patients completed standard M2D and high-resolution 3D DE-CMR with HybridPAWS implemented during data acquisition. The baseline patient characteristics and clinical CMR findings are outlined in Table 5.1.

Characteristics	**Patient, n = 44 (100%)**
Age (years)	65 ± 12
Female	11 (25)
Hypertension	8 (18)
Diabetes	6 (14)
Atrial fibrillation	5 (11)
COPD	9 (20)
Renal impairment (eGFR 45-65ml/min/1.73m^2)	15 (34)
NYHA class I/II/III/IV	5/12/23/4
ICM / NICM	30 (68)/14 (32)
Indications for ICD: primary/secondary	32/12
Combined cardiac resynchronisation therapy	30
CMR findings	
LV ejection fraction, %	30 ± 12
V end-diastolic volume index, ml/m^2	127 ± 40
LV mass index, g/m^2	72 ± 15
Culprit territories of infarct in ischemic cardiomyopathy (n=30), LAD/Cx/RCA	14 (47)/10 (33)/19 (63)
Presence of regional scar in non-ischemic cardiomyopathy (n=14)	10 (71)

Table 5- 1 Baseline patient and CMR characteristics

COPD indicates chronic obstructive pulmonary disease; eGFR, estimated glomerular filtration rate; NYHA, New York Heart Association; ICM, Ischemic cardiomyopathy; NICM, non-ischemic cardiomyopathy; ICD, implantable cardioverter defibrillator; LV, left ventricle/ventricular; LAD, left anterior descending artery; Cx, circumflex artery; RCA, right coronary artery.

5.4.1Respiratory navigator efficiency (NE) and scan time

Patients with significantly impaired LV function have irregular breathing patterns, resulting in poor respiratory navigator efficiency. **Figure 5-2** illustrates the breathing patterns with examples of high NE and low NE based on diaphragm positions.

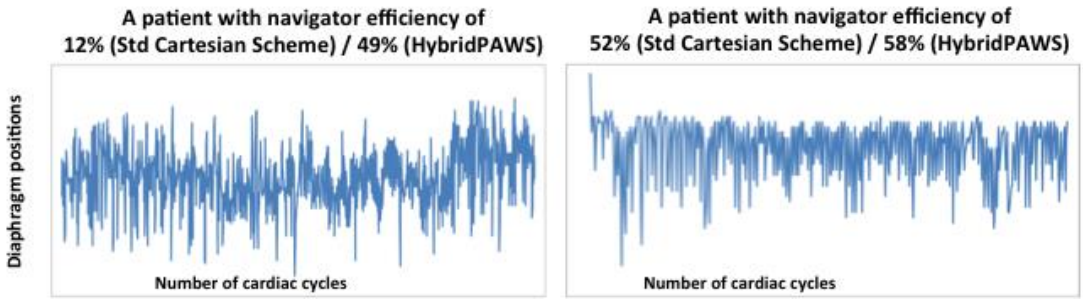

Figure 5- 2 Diaphragm positions recorded during 3D DE-CMR data acquisition

The mean respiratory NE was 47±15% (median: 47%; inter-quartile range IQR: 37-55%) with HybridPAWS compared to 39±18% (median 39%; IQR: 27-52%) with Std-gated Cartesian scheme, $p < 0.01$. Data acquisition with HybridPAWS led to a mean relative improvement of 36±59% in NE per individual patient.

The greatest improvement was achieved in patients with low NE, i.e. <40%, using Std-gated Cartesian scheme. In this group, HybridPAWS improved the overall NE from 27±8% to 38±9%, $p < 0.01$; achieving a mean relative improvement of 55±68% in NE per individual patient. In the group with NE ≥40%, HybridPAWS improved overall NE from 58±12% to 61±11%; achieving a mean relative improvement of 6±7% in NE per individual patient; as illustrated in Figure 5-3.

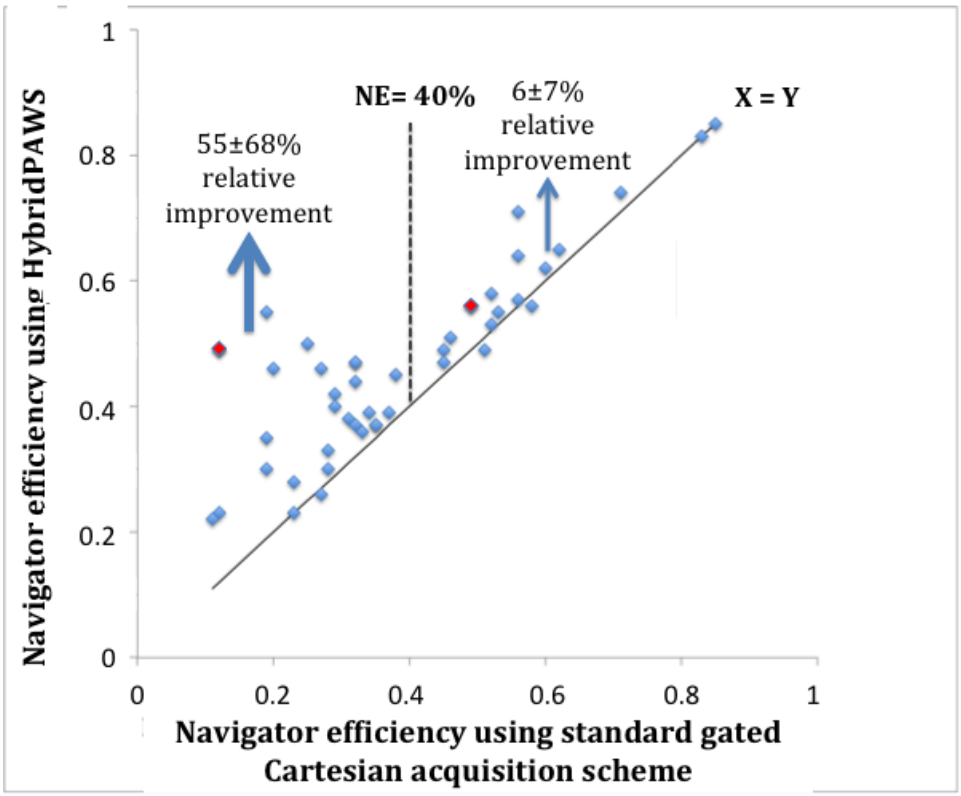

Figure 5- 3 Scatter plot of navigator efficiency (NE) achieved with HybridPAWS versus standard Cartesian respiratory gating sampling scheme.

HybridPaws significantly improves the NE for subjects with low NE using a standard gating scheme. (The respiratory patterns for subjects are illustrated in Figure 5-2)

The average nominal scan time for high-resolution 3D DE-CMR data acquisition was 4:09±1:30 minutes assuming an average heart rate of 70 beats per minute and a respiratory NE of 100%. HybridPAWS led to an average total scan time of 9:44±5:15 minutes with mean NE of 47±15%. M2D DE-CMR data acquisition took an average time of 9:59±2:02. (This included a SAX stack with 11-13 slices, a LAX slice in standard 4-, 3- and 2- chambers and any repeat slices needed to improve image quality). There was no significant difference in scan times between the total M2D data and the 3D data acquisition.

5.4.2 Image quality and scar quantification

One of the limitations of single slice 2D LAX images in standard orientations is that it does not always highlight areas of clinical interest. Two examples are illustrated in Figure 5-4. The top panel illustrates images from 2D single slices in standard orientations. The bottom panel illustrates retrospectively reformatted 3D images in orientations that best highlight areas of clinical interest such mural thrombus, complex scar structures with islands of surviving myocardium.

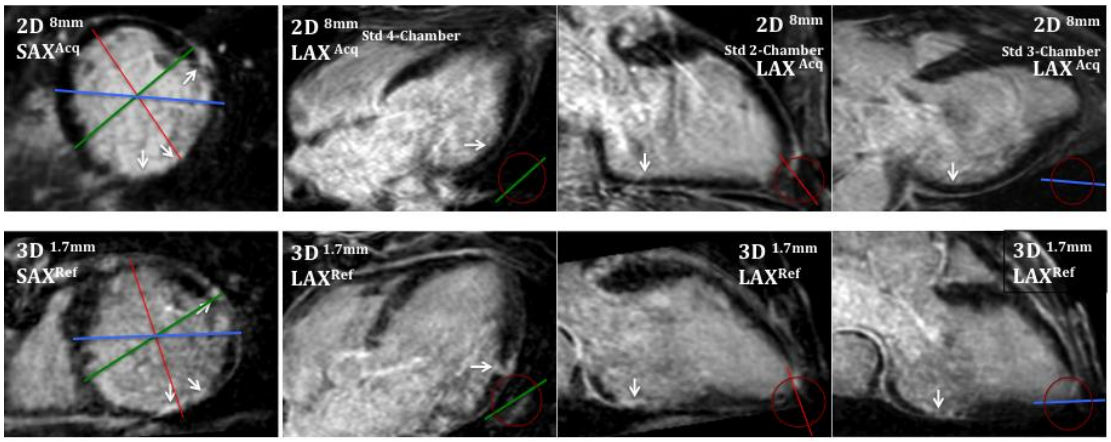

Subject 1 *is a patient with subendocardial scar from right coronary artery infarct (white arrow in inferior wall) with additional epicardial scar (white arrow in the lateral wall) from secondary post infarct pericarditis which are not demonstrated in standard LAX views.*

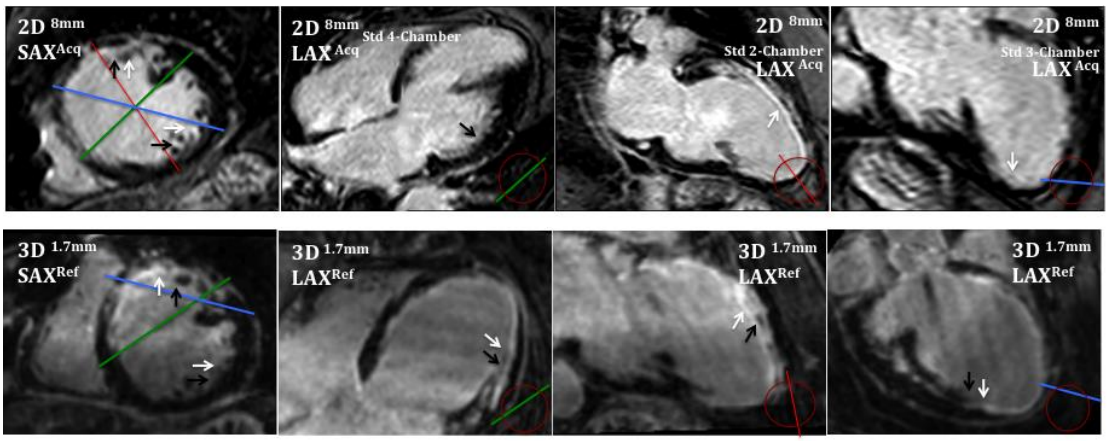

Subject 2 *is a patient with extensive left anterior descending artery and circumflex artery territory infarct, the 3D image allows the freedom of assessing the complex scar structures in any orientations without a reduction in image quality. Surviving myocardium is interwoven within the infarct zone (white and black arrows), providing potential substrate for re-entrant ventricular tachycardia.*

Figure 5- 4 Two examples of M2D scar images (top panel) in standard long axis (LAX) 2-, 3-, 4- chambers "missing" clinical regions of interest compared with 3D scar images (lower panels) allowing retrospective reformatting of different off-axis orientations.

In order to make a like-with-like comparison, we also reformatted the M2D SAX and 3D stacks to LAX in the same orientations that best illustrate regions of clinical interest such as complex scars and thrombus. The 3D images were reformatted to the same slice thickness as that of the M2D slices in the same orientation. 5 examples of M2D and 3D images in SAX and LAX orientations are shown in Figure 5-5, illustrating that the 3D data allowed the freedom of retrospective assessment in any orientations without a reduction in image quality of clinical regions of interest. Subjects 1-3 demonstrate the detections of fine structures such as thrombus, papillary muscle scar, the strands/islands of surviving myocardium within complex scar structure and at the infarct border zone in three ICM patients with previous histories of ventricular tachycardia. Subjects 4-5 demonstrate the different scar patterns that are more commonly associated with NICM. Subjective image quality from two independent experienced assessors were 3.4 ± 0.6 for M2D images versus 2.8 ± 1.0 for 3D images in SAX ($p<0.01$); 1.8 ± 0.7 for M2D images versus 2.9 ± 0.9 for 3D images in LAX ($p<0.01$).

Figure 5- 5 M2D and 3D DE-CMR images

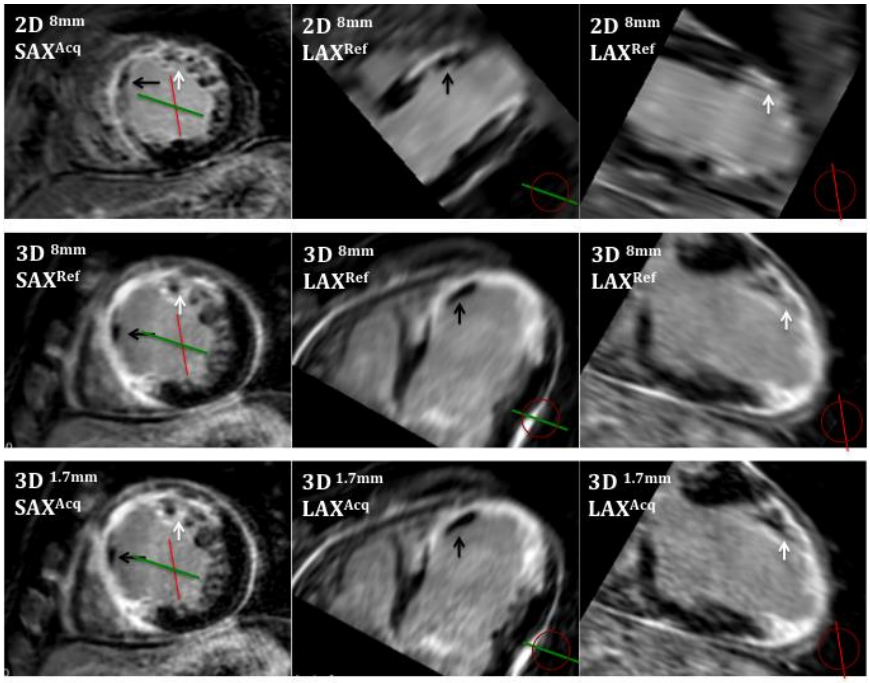

Subject 1: Left anterior descending artery infarct with complex scar structures surround islands/strands of surviving myocardium (white arrow) and thrombus in the antero-septal wall (black arrow).

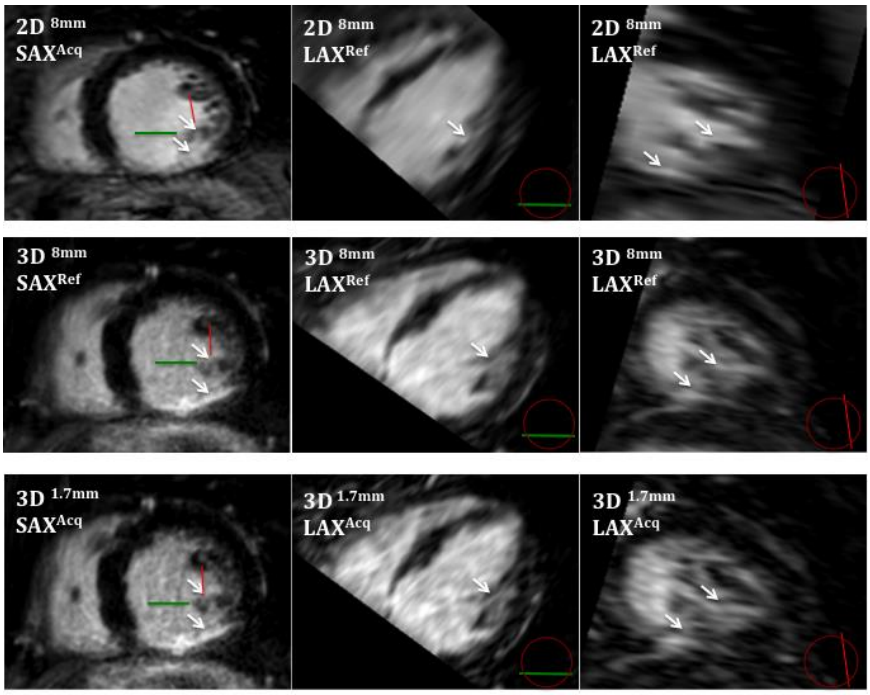

Subject 2: Right coronary artery territory infarct with a partial infarction of the inferior-posterior papillary muscle (white arrows).

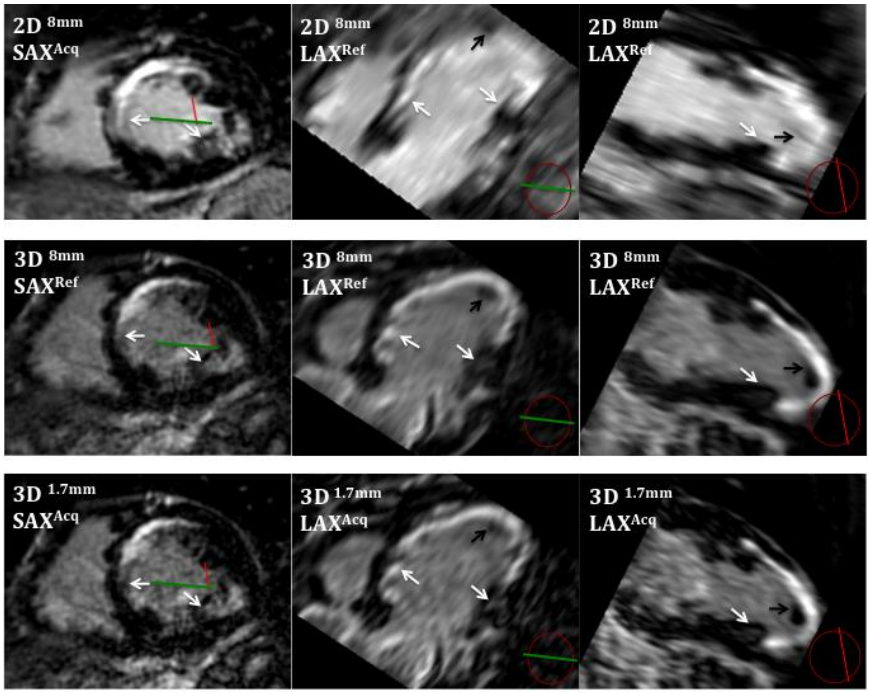

Subject 3: Left anterior descending artery and right coronary artery region infarct. The infarct border zone, the "grey zone", (white arrow) appears larger and the apical thrombus (black arrow) appears less sharp with larger voxel size due to the partial volume effect.

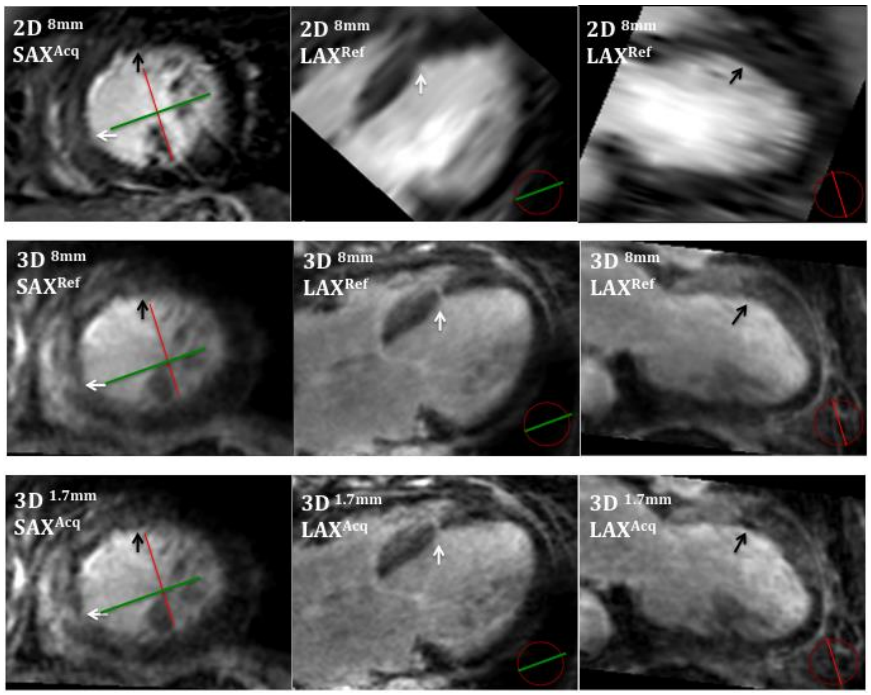

Subject 4: Non-ischemic dilated cardiomyopathy with island of focal fibrosis (white arrow) and strands of myocardium (black arrow) in regions of diffuse fibrosis.

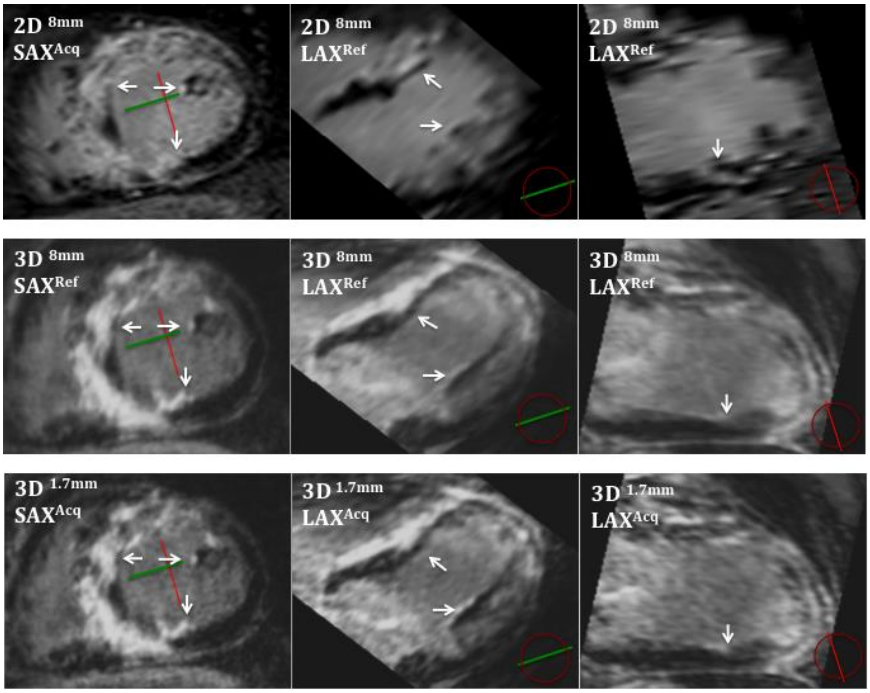

Subject 5: "Burnt-out" hypertrophic cardiomyopathy with complex diffuse patchy scars and regional scars involving the ventricular myocardium and the papillary muscles.

Scar quantification analysis on six reformatted 3D SAX images of 2mm, 4mm, 8mm and 16mm slice thickness showed that these changes did impact on scar quantification with a significant overestimation observed only when the slice thickness was increased than larger than 8mm, shown in Figure 5-6. This suggested an influence of partial volume effect with increasing slice thickness on scar core and grey zone definitions. The infarct border zone appeared to enlarge as the slice thickness is doubled with reducing SI.

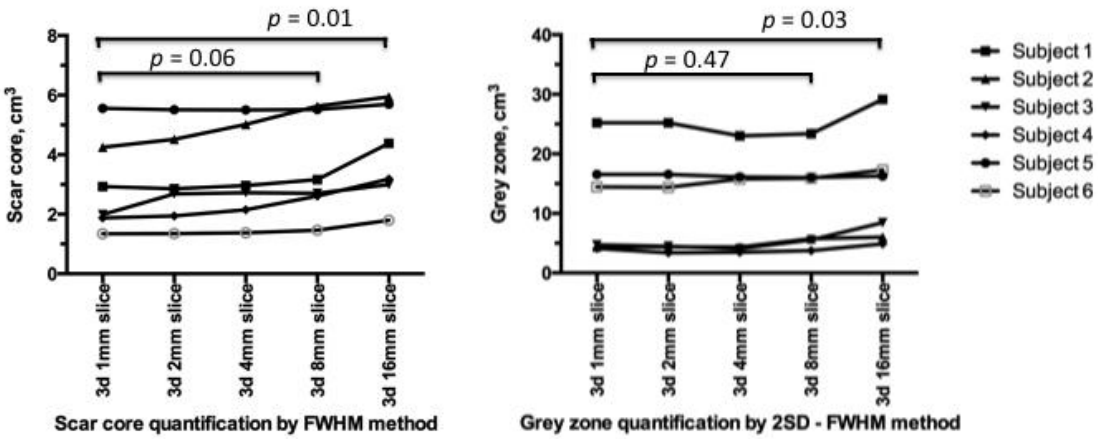

Figure 5- 6 Quantitative scar assessment with scar core (FWHM method) and grey zone (2SD – FWHM method) with varying slice thickness

3D image resolution: (acquired in-plane) 1.7mm x 1.7mm x (varying reformatted through-plane) 1mm/2mm/4mm/8mm/16mm; FWHM=full-width-half-maximum; SD=standard deviation.

The respective scar SNR, the scar_myocardium CNR and scar_blood CNR for patients with a previous history of myocardial infarction are illustrated in Table 5-2.

n = 30	2D	3D	*P values*
Scar SNR	21±5	43±11	*P<0.01*
Scar_Myocardium CNR	20±5	39±10	*P<0.01*
Scar_Blood CNR	4±2	16±7	*P<0.01*

Table 5- 2 Signal noise ratio (SNR) and contrast noise ratio (CNR)

5.5 Discussion

The current study, involving a cohort of patients with severely impaired LV systolic function, demonstrates that the implementation of HybridPAWS can reliably improve

NE and shortens scan time for the acquisition of high-resolution isotropic 3D DE-CMR with immediate image post process reconstruction. The technique is particularly effective in patients with poor respiratory breathing patterns, in whom the standard respiratory-gated Cartesian acquisition scheme would normally achieve less than 40% NE. Furthermore, qualitative and quantitative scar assessments show that isotropic 3D data allow post-scan multi-plane reformatting of optimal image planes without a compromise in image quality; and a higher resolution 3D image has the potential to improve the accuracy of scar quantification.

5.5.1 Navigator efficiency and scan time

Despite the implementation of HybridPAWS, which has the benefit of immediate reconstruction of the 3D data, the acquisition time is comparable with the time needed for M2D data acquisition. This however is coupled with the benefit of acquiring isotropic high-resolution image data. The relatively long acquisition time with both M2D and 3D image data is a reflection of clinical difficulties faced when scanning patients with severely impaired LV function, including difficulties in achieving long breath-holds and the need to rest between multiple breath-holds. The lengthy acquisition time of high-resolution 3D DE-CMR has hindered its routine clinical application. In addition, the long scan time makes the scar image quality more susceptible to the influence of contrast agent kinetics, thus the initially determined optimal inversion time (TI) for nulling of the myocardium to give the greatest signal contrast between scar and healthy myocardium will be incorrect by the end of the scan, causing image artifacts. By shortening the 3D DE-CMR scan time through improved NE, we can potentially limit the impact of inaccurate nulling due to changes in contrast kinetics during a prolonged scan. An additional advantage of the 3D HybridPAWS phase encoding scheme compared with standard PAWS is that, for an

IR pre-pulse, the TI is ensured for both phase encoding directions, i.e. for the central portion of the k-space (disc shape), therefore further minimise the influence of contrast kinetics on regional DE-CMR image quality during a prolonged scan.

5.5.2 Image quality

The 3D scar images were consistently acquired after 20 minutes of bolus injection whereas the M2D images were acquired between 10-20 minutes in this study. There is evidence to suggest that at 20 minutes following a bolus injection of gadolinium contrast, a relative steady state in tissue contrast concentration is reached within scarred myocardium in ICM.[98] The scar SNR was doubled for 3D scar images with an acquired voxel resolution of 1.7x1.7x1.7mm^3 when compared with the M2D images with a resolution of 1.8x1.8x8mm^3. The reason for the doubling of SNR for the 3D images is the additional phase encoding along the slice direction resulting in additional averaging and compensates for the thinner slice thickness. The scar_myocardium CNR was also 2-fold higher and the scar_blood CNR was 4-fold higher with the 3D compared with the M2D images. The additional increase in scar_blood CNR originates from a higher blood signal in the 2D images due to inflow effects.

Despite the higher SNR and CNR, the mean in-plane SAX subjective scar image quality score was lower for the reformatted 3D images than for the M2D images. The image quality achieved with HybridPAWS should be less dependent on the breathing pattern than with the original PAWS because it potentially suppresses residual motion artifacts by distributing them evenly along both phase directions rather than along one encoding direction. However, one reason for the reduction in image quality could be due to the residual motion artifacts introduced during the continuous 3D data acquisition scan which can affect all slices of 3D image without the benefit of

immediate correction. In contrast to that, a failing breath-hold would usually impact only those M2D slices when motion occurred. This suboptimal M2D image was immediately repeated during the clinical study and the improved image slices were used for the image qualitative score assessment. Furthermore, the 3D images were reformatted to the same slice thickness as that of the M2D SAX images for image quality score assessment, effectively reducing the acquired resolution.

SI-based assessment on regions of delayed contrast enhancement with further scar characterisation demonstrated a potential of influence of acquired voxel resolution on the accuracy of scar core and grey zone quantification. A major criticism of the quantification of the grey zone is the effect of partial volume given the relative large voxel size of the standard M2D scar images. Schelbert *et al* have demonstrated this using reformatting the ultra-high resolution at cellular level in ex-vivo rat heart scar images.[12] Peters *et al* have demonstrated that a reduction in voxel size (a reduction in in-plane as well as through-plane resolutions) that is more relevant to standard clinical in vivo human scans can produce a larger peri-infarct zone in heterogeneous scar and conversely a smaller peri-infarct zone in homogenous scar. [5]The current study has however found that when the in-plane (SAX) resolutions are comparable, the slice thickness in the slice encoding direction only has a significant impact on the analyses when it is multiple orders of magnitude of the in-plane resolution.

5.5.3 Clinical relevance

The 3D DE-CMR enables a greater degree of freedom to visualise scar structure by allowing multi-plane reformatting of the images without compromising image quality. Post-acquisition multi-plane analysis of 3D images with isotropic voxel is therefore helpful in characterising complex heterogeneous scar structure in different orientations. This is important because there is a growing need to achieve better scar

characterisation at a higher resolution other than simply binary detection of the presence of scar. Fused displays of myocardial scar images with other imaging modalities such as fluoroscopy and electro-anatomical mapping have been shown to aid therapeutic decisions during cardiac resynchronisation therapy and ventricular tachycardia ablative therapy.[99,108-110] The high spatial resolution 3D DE-CMR is capable of providing structural information in regions of tissue heterogeneity, potentially exceeding the resolution that can be achieved with contact electrode mapping.[111] Scar quantifications have demonstrated additional clinical prognostic benefit in terms of assessing arrhythmia risk in both ischemic and non-ischemic cardiomyopathy.[2-4,112,113] In order to reduce free-breathing 3D data acquisition time in patients who are unable to hold sufficiently long breathhold, the through-plane acquisition resolution can be further reduced without significantly impacting on the scar quantification assessment provided the in-plane resolution of scar imaging remains sufficient high.

5.5.4 Study limitation

The study is limited by a relative small number of patients. Although it is the largest study to-date that focused on a patient population with severely impaired LV function and irregular breathing patterns. Though we reformatted the high-resolution 3D data to the lower resolution of the M2D images for "like-with-like" comparison, it could have introduced a systemic bias favoring the image quality assessment of the 3D images. The 3D dataset was acquired 5-10 minutes after the first M2D scar images due to constraints of the clinical protocol. This would have resulted in a systemic bias on the image quality by potentially giving additional time for the contrast kinetics to reach an equilibrium state during 3D data acquisition. Randomising both scan types would avoid this.

5.6 Conclusions

This study has shown for the first time that HybridPAWS can reliably improve respiratory navigator efficiency and shorten scan time during high-resolution isotropic 3D DE-CMR. The technique is particularly effective at improving the poor navigator efficiencies in patients with irregular respiratory patterns. Isotropic 3D DE-CMR acquired with the assistance of HybridPAWS has the additional advantage of allowing multi-plane characterisation of myocardial scar without compromising image quality and the potential to improve the accuracy of scar quantification assessment. However suboptimal motion compensation may still affect the image quality without the freedom of real-time correction. Non-isotropic 3D imaging with sufficient high in plane resolution can help to speed up the scan time without compromising scar quantifications.

Chapter 6. Exploring the association between scar heterogeneity using cardiac magnetic resonance imaging with ventricular tachycardia substrate – a clinical and computer modeling approach

Computational modelling of cardiac arrhythmogenesis and arrhythmia maintenance has made a significant contribution to the understanding of the underlying mechanisms of arrhythmia. In collaboration with biomedical engineers from Inria, Asclepios Team, Sophia Antipolis, France, we sought to explore the relationship between the myocardial scar heterogeneity detected by CMR with VT arrhythmia substrate through a combined clinical and computer modelling approach. The following chapter describes the work involved in a clinical pilot validation study of a biophysical model to predict VT inducibility and circuit morphology.

6.1 Abstract

Background: Computational modelling of cardiac arrhythmogenesis and arrhythmia maintenance has made a significant contribution to the understanding of the underlying mechanisms of arrhythmia. We hypothesised that cardiac model using personalised electro-anatomical parameters can represent the underlying VT substrate and predict re-entrant VT circuits. We used a combined modelling and clinical approach in order to validate the concept.

Methods: Non-contact electroanatomic mapping studies were performed in seven patients (5 ICM, 2 NICM). Three ICM patients underwent a clinical VT stimulation study. Anatomical information was obtained from cardiac magnetic resonance imaging (CMR) including high-resolution scar imaging. A simplified biophysical

mono-domain action potential model personalised with the patients' anatomical and electrical information was used to perform *in silico* VT stimulation studies for comparison.

Results: The personalised *in silico* VT stimulations were able to predict VT inducibility as well as the macroscopic characteristics of the VT circuits in patients who had clinical VT stimulation studies. Patients 1 and 2 with positive clinical VT stimulation studies had wider distribution of APD-RC slopes and APDs than Patient 3 with a negative VT stimulation study. The exit points of re-entrant VT circuits encompassed a higher percentage of the maximum APD-RC slope compared to the scar and non-scar areas, 32%, 4% and 0.2% respectively.

Conclusions: VT stimulation studies can be simulated *in silico* using a personalised biophysical cardiac model. Myocardial spatial heterogeneity of APD restitution properties and conductivity may help predict the location of crucial entry/exit points of re-entrant VT circuits.

Keywords: Ventricular tachycardia; computer modelling; APD restitution; conductivity; cardiac magnetic resonance imaging.

6.2 Introduction

Implantable cardioverter defibrillator (ICD) shocks are a cause of substantial morbidity in patients with ventricular arrhythmias.[114] Radiofrequency ablation is increasingly used to treat ventricular tachycardia (VT) to reduce ICD discharges and improve patient quality of life and mortality. The current arrhythmia risk stratification strategy is imperfect and is determined largely on left ventricular (LV) function with

not all high-risk patients receiving an ICD, and those who received ICDs never experiencing appropriate therapies. Similarly ablation of VT is technically challenging with a recurrence rate of up to 40% with a lack of clinical consensus on the optimal ablation strategy.[1152] Better risk stratification and higher ablation success rates would potentially improve patient outcomes. There is therefore a need to identify individuals at high risk of developing ventricular arrhythmia and the arrhythmia substrate in order to guide the optimal ablation strategy.

Computational modelling of cardiac arrhythmogenesis and arrhythmia maintenance can be used to contribute to the understanding of the underlying mechanisms of arrhythmia. Image-based computational models have incorporated cardiac structural information such as heterogeneity of scars into such simulations.[1163] However, the heterogeneity in action potential duration (APD) restitution, the adaptation of APD as a function of the cardiac cycle length, has a crucial role in arrhythmogenesis.[117,118] The integration of both personalised structural and functional data has not previously been performed.

We hypothesised that, using personalised electrophysiological mapping data and structural anatomical data acquired respectively from electrophysiology studies and high-resolution cardiac magnetic resonance imaging (CMR) we could develop a patient-specific biophysical model to perform *in silico* VT stimulation studies to assess inducibility of VT and circuit morphology.

6.3 Methods

Patients

(See Chapter 3.2 for General patient selection criteria)

Patients under consideration for primary prevention ICD on the basis of their LV function were prospectively invited to participate in the study following local research ethics committee approval. Seven patients, 5 with ischaemic cardiomyopathy (ICM) and 2 with non-ischaemic dilated cardiomyopathy (NICM) gave written consent prior to study inclusion.

CMR Acquisition and Image Processing

(See Chapter 3.3.1 for General CMR methods protocol)

CMR was performed on a Philips Achieva 1.5T scanner using a 32 channel cardiac coil. All 7 patients completed CMR morphological and volumetric assessment as well as high-resolution scar characterisation by late-gadolinium-enhanced (LGE) imaging with acquired voxel size 1.3x1.3x2.6mm^3. A personalised 3D model of the ventricles was derived from the CMR images: a tetrahedral mesh was generated from the binary mask of the ventricles. The LV myocardial scar distribution was segmented using signal intensity (SI) based analysis from the high-resolution LGE images to distinguish between scar core and grey zone. Each element of the mesh was labelled (healthy/scar core/grey zone).

6.3.1 Invasive Electrophysiological Study with Electroanatomic Mapping and Signal Processing

LV electroanatomic mapping (EAM) was performed using a multi-electrode array catheter (EnSite Velocity System, St Jude Medical, MN, USA) in all 7 patients. The chamber geometry was reconstructed using locator signals from a steerable electrophysiological catheter. Three patients (patients 1-3) with ICM underwent a simultaneous VT stimulation study according to the Wellens protocol during the mapping study.[119] Unipolar electrograms (UEG) derived were filtered with a band-pass filter (10Hz/300Hz and 0.5Hz/30Hz) to optimise QRS complex and T wave detections. The depolarisation times were detected within the QRS window and derived from the zero crossings of the laplacian of the measured UEGs, the repolarisation times were detected within the ST window for the signals.[117] The difference between the depolarisation and repolarisation times was used to estimate the activation recovery time (ARI) which is used as a surrogate marker for APD. The APD restitution curve (APD-RC) was estimated from steady-state RV pacing (500ms) with sensed pacing extras at progressively shorter coupling interval at a decrement of 20ms till 200ms or refractory period. The APD-RC was represented by a non-linear equation using a least-squares fit to the mono-exponential function as previously detailed on experimental and clinical data: a single APD-RC was fitted for each measured point from the EAM and the maximum APD was estimated as the asymptotic APD of the APD-RC when the diastolic interval tends to infinity.[120,121]

6.3.2 Construction of Personalised 3D Cardiac Model

Building on the framework that we have previously described and validated, the anatomical mesh was registered with the electrical information offline and used to generate a personalised 3D cardiac model, which combines the benefits of an Eikonal (EK) model (fast and robust for conduction velocity (CV) personalisation) and those

of a simplified biophysical mono-domain action potential Mitchell-Schaeffer (MS) model (well suited for personalising APD restitution properties).[120-122] The MS model was personalised with the apparent conductivity (AC) values derived from the patient's CV computed from the EAM data. AC is the diffusion coefficient that represents an intrinsic parameter of the cardiac tissue electrical conductivity in the electrophysiological cardiac model. AC (m^2s^{-2}) is proportional to the product of the square of CV and a time constant parameter in the model.[121] AC is used as an independent estimation of the intrinsic biophysical electrical conductivity property of the tissue rather than CV which could be dependent on the activation sequence and the shape of the propagation wave front. The process of building the models from the CMR and EAM data is illustrated in Figure 6-1.

(The estimation of the electrical parameters and computer modelling is described in detail in the Supplemental material: Computer modelling)

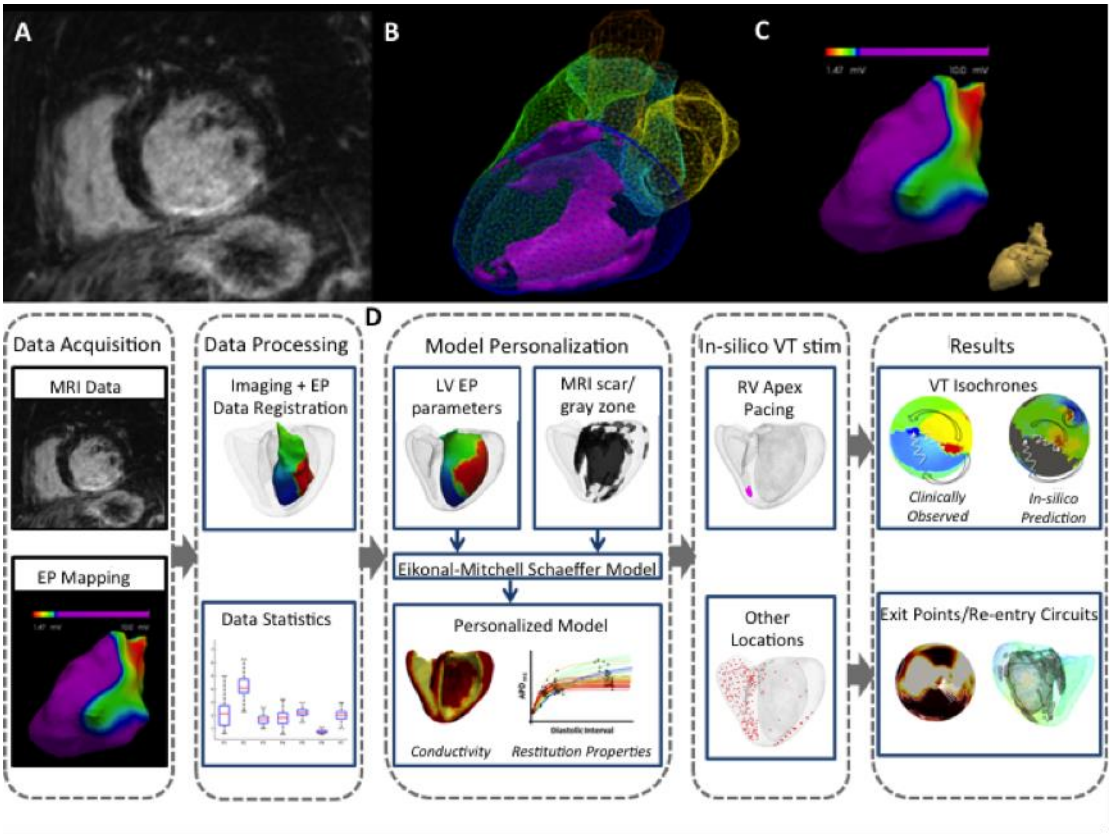

Figure 6- 1(A) high-resolution contrast-enhanced CMR scar images; (B) whole heart model segmented from 3D steady-state free precession (SSFP) CMR with scar (core and grey zone) in violet; (C) low voltage areas from electroanatomical mapping. Lower panel: (D) model personalisation and *in silico* VT stimulation study procedure workflow.

6.3.3 In silico VT Stimulation Study

In three patients (patients 1-3) with ICM, the personalised cardiac model was used to simulate a clinical VT stimulation study *in silico* in order to predict the initiation and maintenance of ventricular arrhythmia induced during clinical study. The simulated study was performed in accordance with the clinical study protocols that were carried out: the pacing stimuli were applied from the RV apex following the Wellens protocol. We also simulated the study from alternate pacing sites in the RV and LV that encompassed the basal and apical freewall/lateral/septum/anterior and inferior walls. The exit points identified from the clinical VT stimulation studies and the *in silico*

simulations were characterised in terms of the spatial heterogeneities of the AC, APD restitution properties.

6.3.4 Statistical analysis

The electrical parameters consisted of multiple data points, each corresponding to a different location within the LV of an individual patient. The data were expressed by median and inter-quartile range (IQR) or mean and standard deviation. Continuous variables were compared using Median test. A p value < 0.05 was considered to be statistically significant. All statistics were performed using computer software SPSS Statistics, version 21, SPSS Inc., IBM, USA.

6.4 Results

Baseline patient characteristics and CMR findings are summarised in Table 1. During the clinical VT stimulation studies, patients 1 and 2 developed sustained monomorphic VT; patient 3 was non-inducible. All 7 patients were implanted with ICDs for primary prevention following clinical assessment. During a median follow-up period of 22months, IQR 9 months, patient 2 received appropriate ICD therapy for sustained VT.

Patient	**1**	**2**	**3**	**4**	**5**	**6**	**7**
Condition	ICM	ICM	ICM	ICM	ICM	NICM	NICM
Gender	M	M	M	M	F	M	M
Age	73	69	64	60	65	75	81
Co-morbidities	HTN	None	HTN, AF	DM	None	AF	PAF
B-blocker	Yes	Yes	Yes	Yes	Yes	Yes	Yes
ACE-I/ARB	Yes	Yes	Yes	Yes	Yes	Yes	Yes
Statins	Yes	Yes	Yes	Yes	Yes	No	Yes
LVEF, %	27	35	35	25	31	36	17
LVEDV, ml	199	292	245	304	185	196	285
LV mass, g	129	172	147	182	118	89	206
Scar on CMR	Yes	Yes	Yes	Yes	Yes	Yes	Yes
Scar core, g	8	22	20	12	16	7	12
Grey zone, g	12	26	4	19	7	8	5

Table 6- 1 Baseline patient characteristics and CMR findings.

ACE-I= angiotensin converting enzyme inhibitor; AF= atrial fibrillation; ARB= angiotensin receptor blocker; CMR= cardiac magnetic resonance imaging; EDV= end-diastolic volume; EF= ejection fraction; ICM= ischaemic cardiomyopathy; LV= left ventricle/ventricular; NICM= non-ischaemic dilated cardiomyopathy; PAF= paroxysmal atrial fibrillation.

6.4.1 Heterogeneities in Apparent Conductivity (AC) and APD Restitution Properties

The IQRs of AC and APD restitution data representing the heterogeneities of these electrical parameters were calculated for each patient, shown in Figure 2. The range of AC across the LV was comparable across the 7 patients. “Apparent Conductivity” (AC) rather than “Conduction velocity” (CV) for the computer modeling was used.

AC (m^2s^{-2}) is proportional to the product of the square of CV and a time constant parameter in the model. In brief, the observed conduction velocity (CV) is responsible for the estimation of the intrinsic electrical parameters of the cardiac tissue. A simple Eikonal (EK) model is used to measure the electrical apparent conductivity (AC) parameters, which are then used to set the parameters of a biophysical model, the Mitchell-Schaeffer (MS) model. Contrary to CV, AC is independent of the propagation direction and curvature. As only endocardial data is measured, the acquired parameters are extrapolated through the myocardium using a diffusion-like process and global measurements such as the QRS durations are used to control this extrapolation. The MS model intrinsically incorporated CV restitution parameters adjusted according to AC. In the present study, a greater emphasis is placed on the impact of APD restitution, as in our experience CV restitution has a greater impact on propagation at much higher pacing frequencies. The AC range across the tissues subtypes (healthy, grey zone and scar) between patients with inducible VT and patients with non-inducible VT were $3.5 \pm 1.3 m^2s^{-2}$ vs. $2.7 \pm 1.0 m^2s^{-2}$ (healthy); $2.3 \pm 0.7 m^2s^{-2}$ vs. $0.4 \pm 0.2 m^2s^{-2}$ (grey zone); $0.4 \pm 0.2 m^2s^{-2}$ vs. $0.1 \pm 0.1 m^2s^{-2}$ (scar core). The median APD-RC slopes and maximum asymptotic APD for NICM patients was lower than that for ICM patients ($p<0.01$). Amongst the 3 patients who underwent a clinical VT stimulation study, patients 1 and 2 with positive clinical VT stimulation studies had APD-RC slopes IQRs of 1.50 and 1.02; and maximum asymptotic APD IQRs of 123ms and 66ms. These IQRs were greater than that of patient 3 with a negative clinical VT stimulation study; in whom the APD-RC slope IQR and APD IQR were 0.48 and 36ms, respectively.

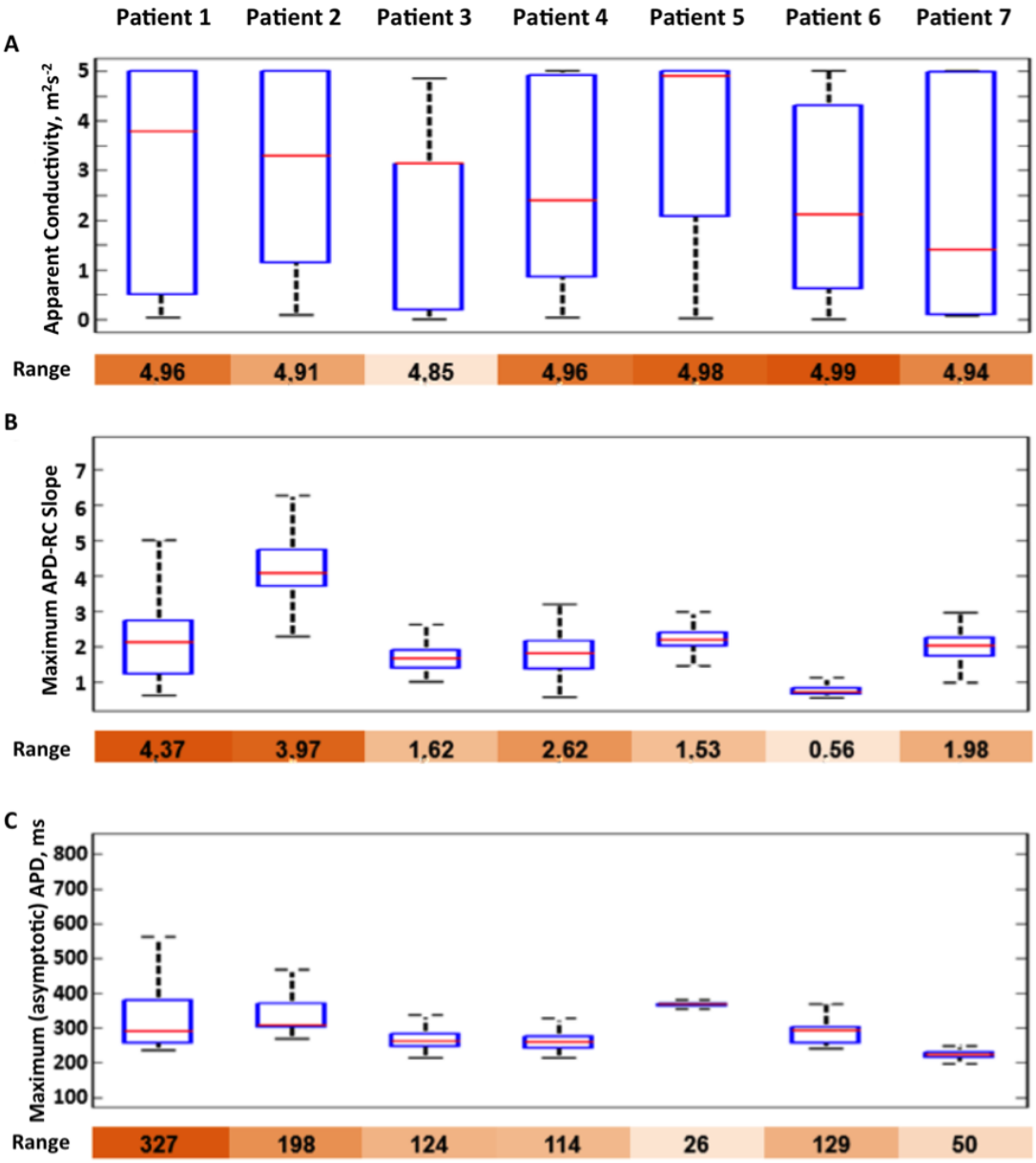

Figure 6- 2 Box-whiskers plots of (A) spatial heterogeneity of apparent conductivity; (B) maximum APD-RC slope; and (C) maximum (asymptotic) APD for each of the patients.

Box = median and quartile ranges; whiskers = total range. Data range values for each of the boxplots are shown at the bottom of each box-plot. Colour coding shows the range varies from the largest (darker brown) and the smallest (lighter brown) for each parameter.

The APD-RC properties and ACs are also illustrated with LV polar plots to provide a qualitative assessment of the spatial heterogeneity of these parameters across the LV in Figure 6-3.

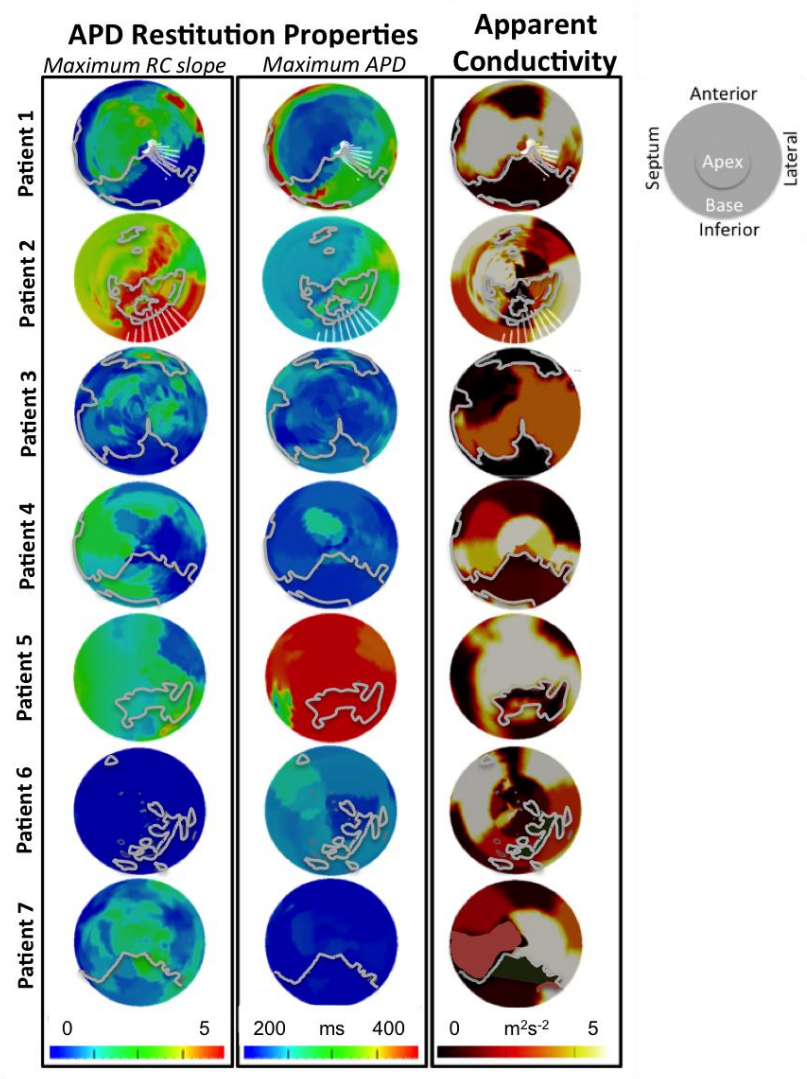

Figure 6- 3 LV polar plot representation of the spatial distribution of the maximum slope for APD-RCs, maximum asymptotic APD and AC.

Scars identified by LGE CMR with its border zone (highlighted by grey contours) and clinically observed exit points (highlighted in Patient 1 and 2 by fang-shaped* white contours during re-entrant VT are overlaid to the polar plots.

*Fang-shaped due to unfolding of 3D volume surface to 2D polar plot)

There appeared to be the same broad spatial heterogeneity in AC in all the study patients including the 2 patients with NICM who also had regions of low AC in areas without scars seen on CMR. However, there was a wide variation in the spatial heterogeneity of APD-RC properties across the cohort, with patients 1 and 2 showing the most heterogeneity.

Visually, the VT exit points that were observed during the clinical VT stimulation studies in patients 1 and 2 appear to be at the neighbouring regions with varying degree of APD-RC properties and AC. These VT exit points were in the scar border zone/grey zone as determined by the LGE CMR scans. In order to explore the role of local spatial heterogeneity of electrical properties play in arrhythmogenesis we assessed the differences in AC, APD and APD-RC between neighbouring regions in LV (each region $\approx 3mm^3$) by evaluating the gradient of the parameters in polar coordinates in Figure 3. The gradient amplitude reflects how smooth or abrupt the transition is between values in the spatial domain. Using a definition of "high gradient" being greater than the 90th percentile of the gradient range, the proportion of LV regions with high gradients was analysed for each patient. For each of the electrical parameters, AC, APD and APD-RC, there was no statistically significant difference in the number of elements with high gradients ($\geq$ 90 percentile) between patients. However, patient (1 and 2) with inducible VT had a combined greater heterogeneity of both AC and APD-RC, shown in Figure 4.

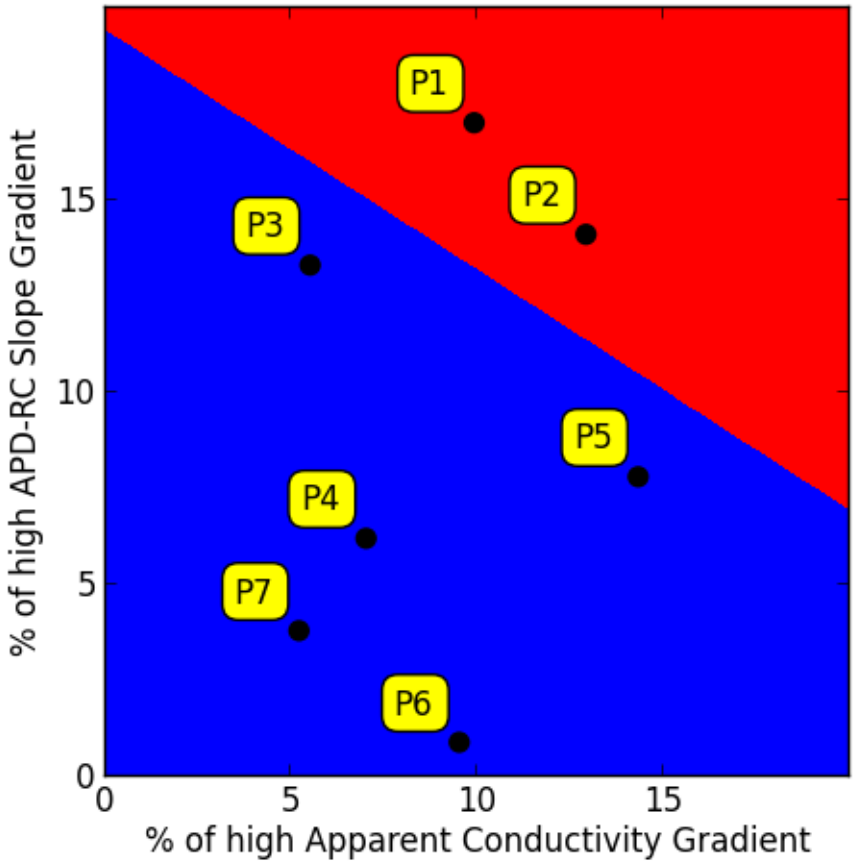

Figure 6- 4 Percentages of LV spatial domains with high gradient (> 90th percentile of the gradient range) as a representation of spatial differences between neighbouring regions in terms of AC and APD-RC slope for each patient (P1-P7).

The separating line with a maximal margin was computed here using the Support Vector Machine algorithm.

6.4.2 Induction of VT and Clinically Observed Monomorphic VT Exit Points

Patient 1 had induced sustained monomorphic VT (SMVT) with a cycle length (CL) of 275ms at Wellens' stage 11. Patient 2 had induced SMVT with a cycle length of 245ms at Wellens' stage 4. The patterns of activation for both re-entrant VT circuits are illustrated in Figure 5. Analysis of the UEG recording from the EAM showed a higher percentage of maximum APD-RC slope that is 2 standard deviation (*SD)* above

the mean LV APD-RC slope at the observed exit points (32%) compared to the scar (4%) and non-scar regions (0.2%). The absolute values in APD and tissue conductivity between the three areas were not as distinct although the exit point values (APD: median 319ms, IQR 45ms; AC: median 3.4m^2s^{-2}, IQR 2.5m^2s^{-2}) appeared to lie between those of the scar (APD: median 385ms, IQR 136ms; AC: median 0.4m^2s^{-2}, IQR 2.1m^2s^{-2}) and non-scar regions (APD: median 305 IQR 49ms; AC: median 4.7m^2s^{-2}, IQR 2.4 m^2s^{-2}). It is possible that it is the heterogeneity in regional tissue electrical properties distributions rather than the absolute value (mean or median) that may allow us to identify the exit points from other regions of the myocardium.

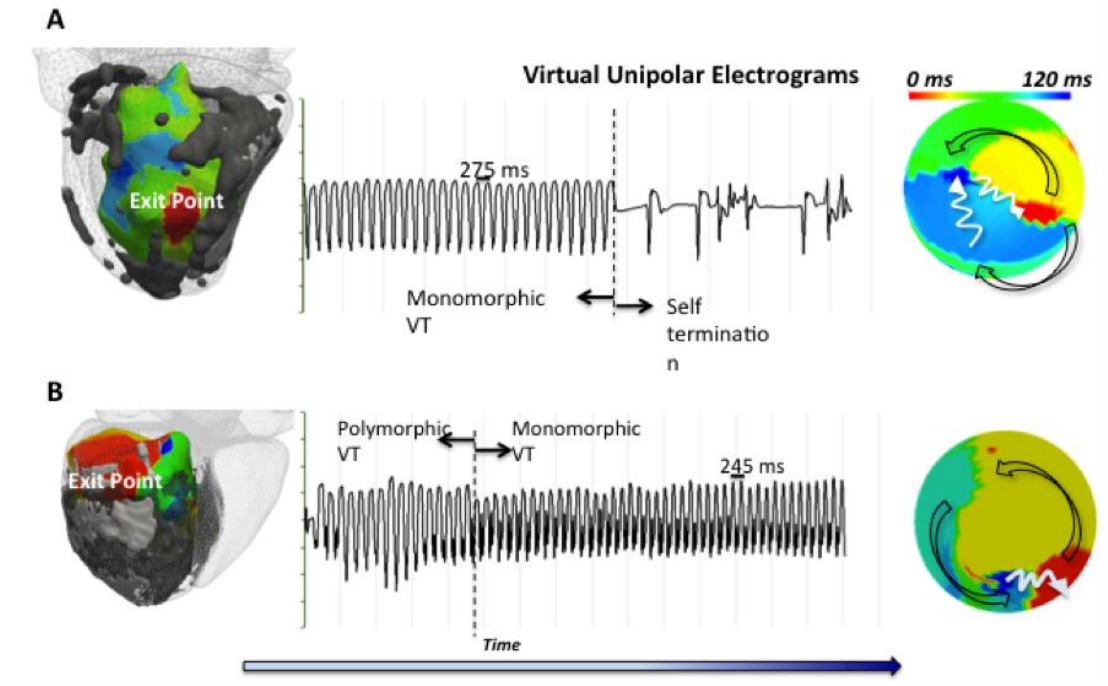

Figure 6- 5 Isochrones mapping during re-entrant VT.

(A) Patient 1 with VT cycle length 275ms; (B) Patient 2 with VT cycle length 245ms.

In Patient 1, the sustained VT self-terminated 42 seconds after failed attempts of

overdrive pacing given due to patient's stable hemodynamic response. In Patient 2, the sustained VT required DC-cardioversion due to patient's unfavorable hemodynamic response. The 3D VT isochrones with exit points (red) in relation with scar core (white) and grey zone (grey) are shown in the left panels. Unipolar electrograms recording during VT are shown in the middle panels. LV polar plots of VT isochrones illustrating the direction of activation pattern are shown in the right panels. In Patient 1, the endocardial activation recorded from EAM showed the re-entrant VT circuit initiating from the LV lateral wall, spreading anteriorly and then posteriorly before returning to the lateral wall. In Patient 2, the re-entrant VT circuit exited from the LV infero-lateral wall, spreading antero-laterally and then towards the septum, before returning to the infero-lateral wall.

6.4.3 Comparison of Model-Predicted and Clinically-Observed Induced VT

Sustained monomorphic VT was induced *in silico* at stage 7 of the virtual Wellens protocol for Patient 1 and stage 5 for patient 2. Sustained VT was not inducible in *silico* for patient 3. LV polar plots of the clinical and virtual VT isochrones are illustrated in Figure 6 for comparison. Both macroscopic re-entrant VT circuit and exit points were matched between the clinical and simulated studies, shown in Figure 6-6

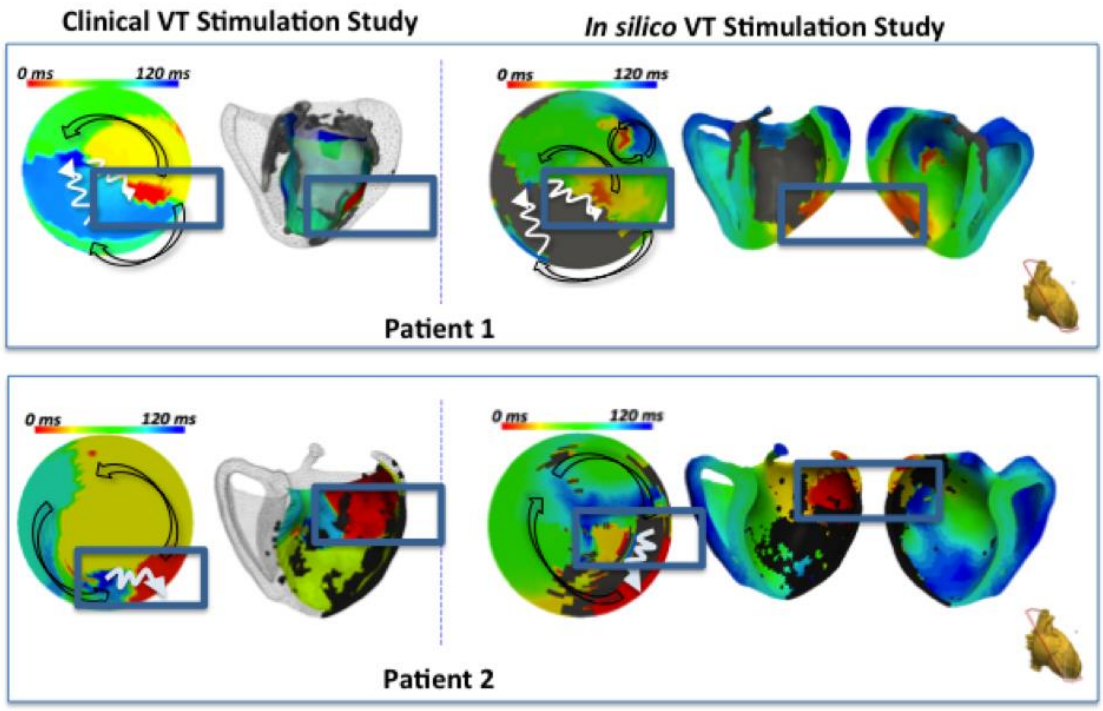

Figure 6- 6 VT isochrones of induced re-entrant VT during clinical VT stimulation study (left panel) and during *in silico* VT stimulation study (right panel).

The arrows point towards the directions of propagation. Scars (core and grey zone) are superimposed to the LV shell shown in darkened regions. The personalised model of patient 1 predicted a sustained re-entrant VT circuit with a cycle length of 260ms compared with the clinically observed cycle length of 275ms with a macroscopically similar activation pattern and a predicted exit point that matched with the observed clinical one. The personalised model of patient 2 also predicted a positive VT stimulation study with a cycle length of 250ms compared with 245ms for the clinical VT. The induced VT was sustained and the re-entrant pathway stable. Notably the direction of the activation pattern during the predicted re-entrant VT was reversed from that observed clinically; however, the predicted exit point correlated with the clinically observed one.

6.4.4 Three-Dimensional VT Circuit Visualisation

By taking into account the 3D geometric information including transmural scar core and grey zone across the LV wall, the computer model enabled the prediction of a 3D VT circuit as opposed to the 2D VT activation pattern observed by endocardial EAM. Computational simulation allowed this additional insight to the wave propagation within the myocardium. For patient 2, the activation wave front of the re-entrant VT is shown propagating in the region of the grey zone. The estimated wave front path surrounds the scar core and lies within the scar border zone, entering from the endocardial surface, meandering within the ventricular wall, and exiting via the epicardial surface, shown in Figure 6-7.

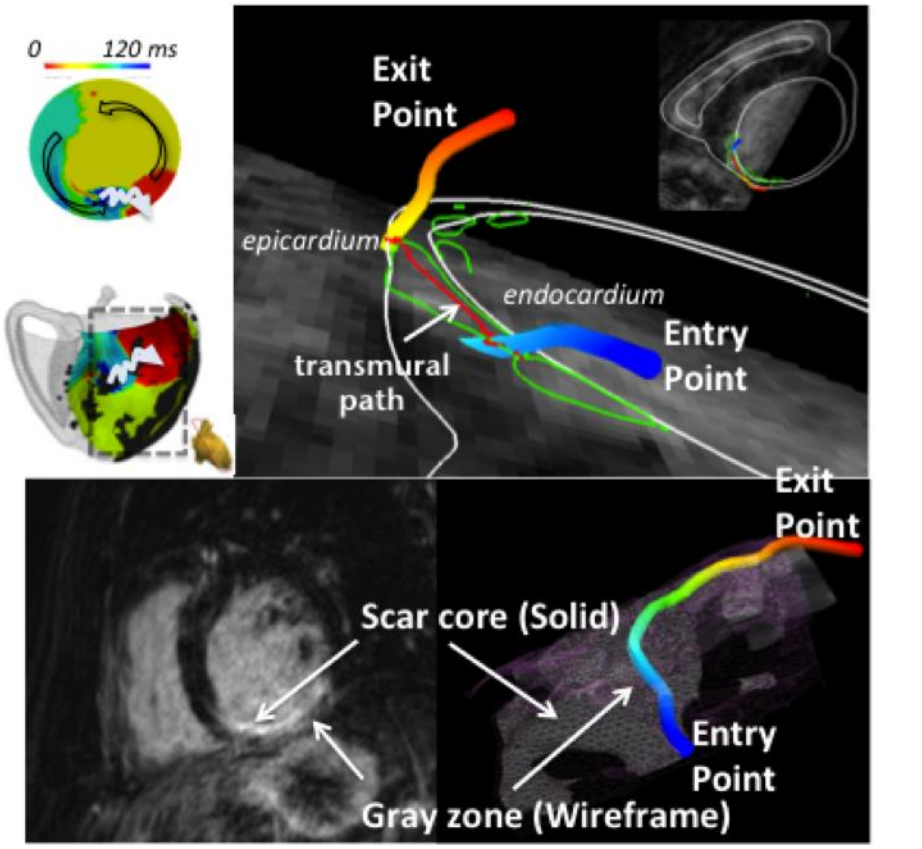

Figure 6- 7 Estimation of the intra-myocardial path between the entry and exit points during re-entrant VT.

Estimated endocardial 2D geodesic path between the entry and exit points from electroanatomical study during clinical VT stimulation study is demonstrated by the isochrones map. Estimated intra-myocardial 3D geodesic path (red line) takes into account of the scar heterogeneity from the high-resolution CMR images. The entry and exit points are illustrated by the graded colours on the 3D path with blue denoting late activation and red denoting early activation. The activation wave front of the re-entrant VT propagates in the region of the grey zone. The estimated wave front path surrounds the scar core and lies within the scar border zone, entering from the endocardial surface, meandering within the ventricular wall, and exiting via the epicardial surface.

A comparison of clinically observed and predicted exits points in terms of anatomic location were made. We defined the exit region compassing anatomical points with an activation time within 10ms of the earliest activation. The distance between the clinically observed and simulated exit points was defined as the 3D Euclidean distance between the centres of both exit regions. A difference of 7mm and 8mm were found, respectively, for patients 1 and 2.

6.4.5 Simulated VT Stimulation from Additional Sites

VT stimulation study was also performed *in silico* by pacing from other sites than the RV apex used during the clinical study for patients 1 and 2. Different VT circuits with three additional exit points were observed in both patients. The exit points were located on the boundary of scar in the region of the grey zones from the CMR LGE images. Similar to the clinically observed exit points, they were mostly in the region

of maximum APD-RC slope. The composite of different exit points are plotted in Figure 6-8 in terms of their APD restitution properties and AC.

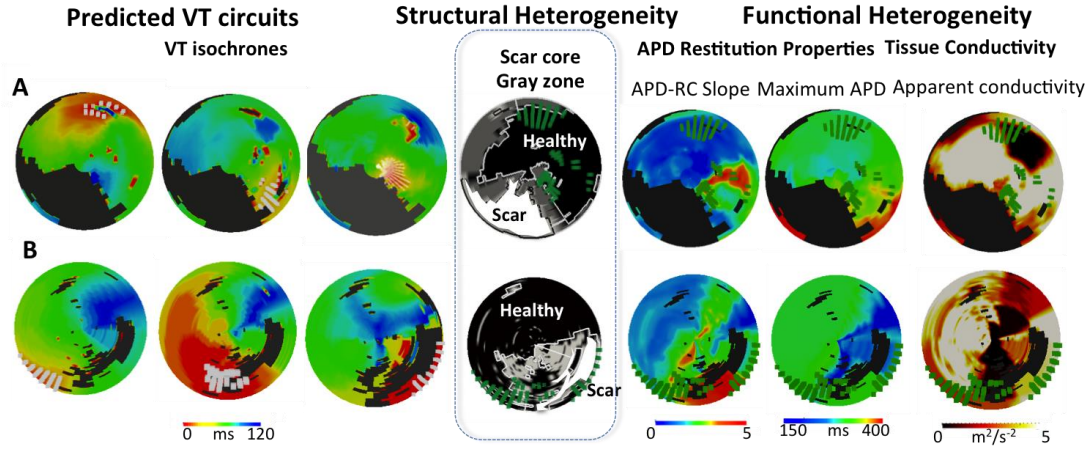

Figure 6- 8 Correlation of predicted exits points with structural heterogeneity and functional heterogeneity.

A = Patient 1. B = Patient 2. The left panel shows the isochrones for the three predicted VT circuits with fangs of white lines denoting the exit points. The middle panel demonstrates the LV scar distribution with black region denoting healthy myocardium, white region denoting the scar core and the grey region denoting the grey zone/scar boarder zone with overlying composite exit points (fanged green lines). The right panel demonstrates the electrical properties with overlying composite exit points (fanged green lines).

6.5 Discussion

The present study provides new insights into the prediction of VT circuits using a biophysical model. The principal findings of our study are as follows: 1) the location of scar border zone (grey zone) on high-resolution CMR correlates with areas of abnormal measured and model derived electrical properties; 2) the VT exit points have a substantially higher percentage of tissue with steep APD-RC slopes compared to surrounding tissues; and combined tissues heterogeneity in APD-RC and CV may underlie the substrate for the inducibility of VT; 3) *in silico* VT stimulation studies

were able to predict inducibility of VT in patients at risk of ventricular arrhythmia; 4) the characteristics of the modeled VT circuits correlated well with the clinically observed circuits in terms of cycle length, macroscopic activation patterns and VT exit sites.

6.5.1 Tissue Heterogeneity (admixture of scar and myocardium) co-location with Heterogeneity in APD Restitution Properties and Tissue Conductivity

A correlation between the spatial heterogeneity in APD, APD-RC slopes and AC and the location of grey zone detected on high-resolution CMR supports the notion that myocardial scars can alter the regional restitution properties and provide potential substrate for arrhythmia.[61] Data from the two patients who developed sustained VT suggest that VT exit points are co-located with heterogeneous APD-RC slopes. Ciaccio *et al.* has demonstrated potential mechanisms using a geometric model that could account for this co-location between exit zones and conducting channels in terms of tissue conductivity.[123] The presence of clumps of fibroblasts, although electrically non-excitable, results in a slowing of the electrical wave front propagation in the myocardial tissue in which they are embedded. Fibroblasts can modulate cellular ion channel remodelling and therefore tissue electrical properties through a variety of mechanisms including mechano-electric feedback via stretch-activated ion channels, close coupling of nearby cardiac myocytes via connexin, and by altering surrounding myocardial fibres anisotrope.[61,124] Some of these mechanisms have been shown in vitro, but remains speculative in vivo. The suggested relationship between the degree of heterogeneity demonstrated by the electrical gradients between neighbouring tissue domains and the propensity for sustained ventricular arrhythmia is therefore likely be non-linear as observed in the present study. The present study

supports the notion that potential successful ablation sites for VT lie in areas of heterogeneous tissue zones that can be identified with CMR.[99,125]

Heterogeneity in electrical properties have been observed in LV.[117,118] Computation modellings have demonstrated that theoretically APD-RC slope >1 is needed to result in electrical instability and initiate ventricular arrhythmia.[126] In keeping with the observed tissue functional heterogeneity at the VT exit points in the present study, others have also demonstrated that the heterogeneity in APD-RC slopes is needed for the initiation and stability of re-entry VT.[118,126,127] These prior studies did not have the benefit of high-resolution CMR scar information, and so could not explain the anatomical cause of this. Nash *et al.* speculated that regional stretch strain pattern resulting from ischemia might have led to electrical remodelling through mechano-electric feedback.[118] It may well have been that these regions had areas of grey zone as they correlated to the territories of the diseased coronary arteries.

Restitution hypothesis has suggested that electrical alternans was a dynamic consequence of the slope of the APD restitution curve and if the slope of was ≥ 1, then APD alternans was possible.[128,129] However, in-vivo studies (Nash et al 2006 and Orini et al 2016) have found a large region of normal left ventricle tissue express APD restitution properties > 1, in accordance with our finding.[118,130] There are also significant regional heterogeneities observed within the LV (basal vs. apical; epicardial vs. endocardial). This suggests the importance of restitution parameters other than slope per se in the mechanisms underlying arrhythmogenesis. It is reflected in our result that it is the spatial heterogeneity and heterogeneity in the neighbouring

tissue that provide substrate for ventricular arrhythmia. APD restitution property is a function of both activation and repolarization. Orini et al has recently demonstrated the relationship in a systematic assessment of these parameters in a human whole heart in vivo study.[130] At shorter cycle length, conduction delay significantly increases the APD slope by interacting with the diastolic interval; and ARI restitution slope does not depend on baseline APD, but more dependent on the activation time than the repolarization time. In the present study, the exact correlation was not made. However significant heterogeneity in terms of APD slopes and conductivity were observed at the re-entrant arrhythmia exit zone. Further correlation of the these parameters would be of great interest in exploring the mechanism by which these parameters interact in order to set up the critical substrate "arrhythmia window" for reentry arrhythmia.

6.5.2 In silico VT stimulation studies in patients

Encouragingly the personalised cardiac models encompassing both anatomical and electrical properties were able to predict not only the inducibility of VT, but also the re-entrant VT circuit properties and anatomical locations of the substrate. The present study is unique in that, as well as anatomical and scar information it incorporated personalised functional data including APD-RC properties and tissue conductivities into the patient-specific cardiac models. Previously, Arevalo H et al. suggested that VT dynamics were primarily governed by the geometric parameters of the scar-core and border zone using image-based computational VT modelling work.[131] The present study highlighted the advantage of incorporating detailed geometric information gained from CMR, demonstrating the possibility of using high-resolution 3D scar data

to help predict potential critical isthmus on the epicardial surface. This is important, as conventional mapping techniques used during ablative therapy are limited to two-dimensional geometry when the substrate of the VT circuit could be on the opposite side of the mapping surface.

Whilst we realise that CMR can provide important scar geometry that governs the substrate of re-entrant VT, we also recognise that the resolution of the current standard clinical CMR technique is limited (common voxel size $2x2x8mm^3$) in providing the level of spatial geometry details that we would like to see at the border zone. We believe that additional knowledge and understanding of patient-specific heterogeneities in local electrical parameters would assist in predicting the likely culprit conduction channels/isthmus, and not the bystanders, that is critical to the clinical VT. We have performed additional sensitivity analysis using empirical electrical parameters instead of personalised patient-specific electrical data in the two patients with positive clinical VT stimulation studies and found that using combined personalised electrical and image data can potentially improve the accuracy of VT inducibility and predictions regarding the location of exit zones predictions. (See Supplemental Material: Personalised vs. non-personalised empirical electrical parameter)

Given the interaction between activation and repolarization wave front, Taggart et al has proposed a re-entry vulnerability index (RVI) which may predict the susceptibility of re-entry in tissue.[132] Coronel et al demonstrated that the critical parameter for differentiating between the occurrence of reentry and the mere occurrence of a line of activation block between the two myocardial regions was not the magnitude of the

repolarization gradient but the timing of arrival of the premature activation wave at the distal side of the line of activation block relative to the repolarization time of the premature beat proximal to the line of block.[78] Thus during electrophysiology study, by evoking an extra simulation and then measuring the local unipolar electrograms at different points within the ventricle, one can calculate the activation time and repolarization at those points. With the additional anatomical information in terms of distance between neighboring points, an algorithm is created to allow identification of sites of block and subsequent reentry. Such analysis can potentially be retrospectively applied to the dataset in the present study. However the inherent limitation of NCM with T wave morphologies may potentially impact on the analysis.

6.5.3 Clinical application: Potential for Circuit Prediction using Personalised Computer Models to Guide Ablation

Whilst cardiac modelling has been an active research area for decades, personalised cardiac modelling using patient-specific clinical data is in its infancy. *In silico* personalised models may offer significant clinical benefit in predicting the risk of ventricular arrhythmia in patients and guiding treatments including ICD implantation and VT ablation. Successful VT termination through ablation may be achieved when the critical isthmus is successfully interrupted with ablation lesions. If VT exit points can be predicted with biophysical models then this information may be used to guide ablation. Such models also offer additional flexibility as the model can simulate any combination of paced stimuli from different locations with varying pacing cycle lengths, which may not be feasible in clinical practice. Predicted VT exit points could be Recently, Ashikaga *et al.* presented a retrospective study that found a good

correlation between the predicted ablation sites and the actual target VT ablation sites at the scar border zone.[133] We have indeed demonstrated that additional exit points can be induced from *in silico* VT stimulation studies which could be potential targets for ablation. Our results suggest that patient-specific cardiac models may offer incremental clinical benefit in terms of ventricular arrhythmia risk stratification and in the planning and delivery of ablation strategies for re-entrant ventricular arrhythmias. Non-invasive body surface mapping could be incorporated to routine simple electrophysiology study to gain such personalised whole heart electroanatomic data in order to facilitate the translation of the biophysical cardiac model processing pipeline to clinical practice.[134]

Arevalo H et al. suggested that VT dynamics were primarily governed by the geometric parameters of the scar-core and border zone using image-based computational VT modeling work with scar data acquired from high-resolution CMR of ex-vivo canine heart (reconstructed voxel size 200um3) and empirical ionic cell parameters.[131] Recently, Ashikaga et al. elegantly demonstrated that such image-based simulation can estimate ablation target site in a retrospective study in patients who underwent catheter ablation of VT.[133] Others previously have shown that conducting channels of viable myocardium between the scars detected with CMR, in regions of scar border zone, have correlated with potential ablation sites for reentrant VT.[99,125]

Whilst we realize that contrast-enhanced CMR provides important scar geometry that governs the substrate of reentrant VT, we also recognize that the resolution of current standard clinical CMR imaging technique is limited (common voxel size 2x2x10mm3) in providing the level of spatial geometry details that we would like to

see at the border zone. Thus the term “gray zone” reflecting the spectrum of intermediate signal intensity seen on CMR scar images at the scar border zone was originated.

We therefore adopted a slightly different computational approach to the simulated VT model by incorporating not only a higher resolution than standard CMR scar images to obtain the geometry information in our study but also patient-specific endocardial electrical parameters from endocardial non-contact electrical mapping. We believe that at the current standard resolution achieved with clinical CMR scar images, additional personalized electrical parameters would assist in predicting the likely culprit conduction channels/isthmus that is critical to the clinical VT and not the bystanders.

6.5.4 Study limitations

Given the invasive nature of the study precludes analysis of a large number of patients, the study is limited by the small number of patients included with only a subset of patients undergoing a VT stimulation procedure. The electro-anatomical data are derived from non-contact mapping with the inherent limitations of this type of mapping. It was chosen for its ability to provide ‘beat-to-beat’ mapping in the setting of rapid and unstable VT circuits. The cardiac model also made several simplifications in particular for the Purkinje network and pathological changes of cardiac fibre orientations. With any personalisation of computational physiology model, there is a degree of uncertainty due to the limitations in acquired temporal and spatial resolution clinical data. Extending computational methods used in the study to incorporate an efficient Bayesian inference method could account the uncertainties in the application of the model.[13520] The action potential duration (APD) restitution

represents the APD as a function of the preceding diastolic interval or local cycle length. The curve produced when APD is plotted against cycle length is not linear and is usually flatter for longer cycle length and steeper for shorter cycle length. The estimation accuracy of restitution curve using a mono-exponential function will be dependent on the range of the cycle length tested. Its inaccuracy increases over the shorter cycle length range and with fewer sampling intervals, giving an over/underestimation of the restitution curve where the restitution curve is usually steeper. In the present study, the MS model was used. It is a simplified ionic model for fast simulation and personalization using clinical data, thus limited parameter was used. A bi- (or higher) exponential function may allow more degree of freedom in estimating the shape of the restitution curve as others have found a secondary peak and plateau in the shape of APD restitution curve.

6.6 Conclusion

Patient-specific spatial heterogeneity of restitution properties were the distinguishing features of ventricular arrhythmogenicity, with re-entrant VT exit points present in regions of higher maximum APD-RC slopes compared with the surrounding tissue. These regions were within the grey zone identified by LGE CMR. Personalised biophysical model was able to predict macroscopic VT circuits and exit point locations in agreement with clinically observed datasets.

6.7 Supplementary material

Rocio Cabrera-lozoya PhD and Jatin Relan PhD (Inria, Asclepios Team, Sophia Antipolis, France) under the guidance of Maxime Sermesant PhD. carried out the following computational work.

6.7.1 Computer Modeling

The present study used a coupled personalisation framework that was previously evaluated in details.[120,121] It combines the benefits of two different kinds of mathematical models while keeping the computational complexity tractable. The Eikonal (EK) model was used to estimate the conductivity parameters over the ventricle derived from non-contac *diffusion-like process* t mapping of the ventricular endocardial surface potential, which were then used to set the parameters for the Mitchell-Schaeffer (MS) model. Additionally, the MS model is able to hold the memory of one preceding cycle and has restitution properties, thus is able to simulate arrhythmias macroscopically. Both models are computed on the whole 3D myocardium. This personalisation framework has already been detailed in a previous publication and the predictive power of such personalised model was evaluated on experimental data. [120,121] A summary on the personalisation of each of the models is included in the following sections.

Cardiac Electrophysiology Models

Eikonal (EK) Model

The EK model simulates the propagation of the depolarisation wave in cardiac tissue by computing the local activation time. It is governed by the eikonal-diffusion equation and solved using the fast marching method. It can be written as:

$$c_o\sqrt{d_{EK}}\left(\sqrt{\nabla T(x)^t M \nabla T(x)}\right) - \nabla \cdot \left(d_{EK} M \nabla T(x)\right) = \tau(x)$$

Where:

c_o – is a dimensionless constant (=2.5)

$\tau(x)$ – is the cell membrane time constant (=0.003s)

d_{EK} – is the square of the tissue space constant along the fiber and is related to the specific conductivity of the tissue in the fiber direction, it has units of m^2

$M = diag(1, \rho, \rho)$ – is a diffusion tensor that incorporates the tissue anisotropy into the model

$\rho = 1/2.5^2$ – is the anisotropy ratio between longitudinal and transverse diffusion. This value is given to have a conduction velocity (CV) 2.5 times faster in the fiber direction

Details for solving the previous non-linear equation are explained in a prior publication.[1363]

Mitchell Schaeffer (MS) Model

The MS model is a simplified biophysical model derived from the Fenton Karma ionic model.[122,137] It models the trans-membrane potential as the sum of a passive diffusive current and several active reactive currents including combination of all inward and outward phenomenological ionic currents. This is described in the MS model by a system of partial differential equations:

$$\begin{cases} \partial_t u = div\,(d_{MS} M \nabla u) + \dfrac{z u^2 (1-u)}{\tau_{in}} + \dfrac{u}{\tau_{out}} + J_{stim}(t) \\ \partial_t z = \begin{cases} \dfrac{(1-z)}{\tau_{open}} & if\ u < u_{gate} \\ \dfrac{-z}{\tau_{close}} & if\ u > u_{gate} \end{cases} \end{cases}$$

Where:

u – is a normalised transmembrane potential variable

z – is a gating variable which depicts the depolarisation and repolarisation phases by opening and closing the currents gate

$J_{in} = \frac{z u^2 (1-u)}{\tau_{in}}$ – represents the inward currents (primarily Na^+ and Ca^{2+}) which raise the action potential voltage

$J_{out} = \frac{u}{\tau_{out}}$ – represents the outward currents that decrease the action potential voltage (mainly K^+), describing repolarisation

J_{stim} – is the stimulation current at the pacing location

$\tau_{in}, \tau_{out}, \tau_{open}, \tau_{close}$ – have units of seconds

M – is a diffusion tensor that controls the diffusion term in the model

This model incorporates both APD and CV restitution effects, and the restitution curves can be written in an analytical formulation, which can be used to estimate restitution parameters.

Depolarisation and Repolarisation time extraction

The electrical data was collected with high pass filter settings for prominent QRS detection and with low pass filter for T-Wave detection. The depolarisation times were detected within the QRS window and were derived from the zero crossings of the laplacian of the measured unipolar electrograms. The repolarisation times were detected within the ST window and derived using the alternative method.[117] The

alternative method has repolarisation times derived from dV/dt_{max} for the negative T-wave, at the dV/dt_{min} for the positive T-wave, and the mean time between dV/dt_{max} and dV/dt_{min} for the biphasic T-waves.

Model Personalisation

Apparent Conductivity Parameter Estimation

The apparent conductivity (AC) of tissue can be measured by the parameter d_{EK} in the EK model. It is initially estimated on the endocardial surface as a global value using a bisection method that matches the average conduction velocity of the measured depolarisation time (DT) isochrones to the simulated ones. It is used as an initial estimate in an adaptive multi-level domain decomposition algorithm, which minimises the mean-squared difference of the simulated and measured DT isochrones.[1387] One particular aim of this step is to estimate areas with high conduction velocity, which can represent parts of the Purkinje network.

Extrapolation of myocardial volumetric parameters from endocardial data, imaging and body surface ECG

In order to propagate the estimated parameters to the whole myocardium, the present approach uses a diffusion-like process that smoothly extrapolates the estimated endocardial parameters. This estimation is based on the model using the anatomical 3D information from the CMR scar images and the global electrical information (ECG). The transmural AC value is estimated in order to fit the measured QRS duration, by a one-dimensional minimisation of the following cost function: (mean-squared difference of simulated and measured isochrones at endocardium + squared

difference of simulated and measured QRS duration). The simulated QRS duration is calculated as the difference between the maximum and the minimum depolarisation times in the biventricular mesh and the measured QRS duration is estimated from the surface ECG. The AC values for RV endocardium and RV myocardial mass are set at $5mm^2$ and $0.64mm^2$ as previously described.[139] Such estimation method has been validated by experimental data.[121]

Due to the absence of transmural electrical propagation information, no variation is assumed across the healthy left ventricular myocardium, excluding the LV endocardium which was personalised as described in the previous paragraphs and the scar personalised from imaging, see below.

Coupling of EK and MS Model Parameters

The AC parameter for EK model d_{EK} is a scale for the diffusion speed of the depolarisation wave front in the tissue. In 3D, the model Conduction Velocity (CV) is related to d_{EK} as

$$c_{EK} = \alpha_{EK}\sqrt{d_{EK}} + \beta_{EK}$$

where the constants α_{EK} and β_{EK} are introduced to take into account the discretisation errors (in particular of the curvature) in 3D.
The corresponding conductivity parameter for MS model, d_{MS} is also a scale for the wave diffusion speed in the tissue. The model CV here is related to d_{MS} as:

$$c_{MS} = \alpha_{MS}\sqrt{d_{MS}} + \beta_{MS}$$

where the constants α_{MS} and β_{MS} are introduced for the same reasons as of EK model, while τ_{in} is kept as a constant. The estimated AC parameter d_{EK} can then be used to estimate the parameter d_{MS} as previously described.[120]

To represent the volumetric heterogeneity of the border zone, the intensity values derived from the 3D LGE CMR images were used to modulate the spatial variation in the AC values of scar border zone (the higher the signal intensity seen on LGE-CMR images, the lower the tissue conductivity). AC values were assigned to zero in the scar core, to reflect the paucity of viable cardiac myocytes.

APD Restitution Curves

APD restitution is an electrophysiological property of the cardiac tissue and defines the adaptation of APD as a function of the heart rate. Its slope has a heterogeneous spatial distribution. The APD restitution curve (APD-RC) defines the relationship between the diastolic interval (DI) of one cardiac cycle and the APD of the subsequent cardiac cycle. The slope of these RCs is controlled by a model parameter τ_{open} of the MS model and depicts the APD heterogeneity present at multiple heart rates. APD-RC for MS model is explicitly derived as:

$$APD_{n+1} = f(DI_n) = \tau_{close} \ln\left(\frac{1-(1-h_{min})e^{\frac{-DI_n}{\tau_{open}}}}{h_{min}}\right)$$

where $h_{min} = 4(\tau_{in}/\tau_{out})$ and n is the cycle number. The maximum value of APD is also explicitly derived as $APD_{max} = \tau_{close} \ln\left(\frac{1}{h_{min}}\right)$.

CV Restitution Curves

In the current study, a greater emphasis is placed on the impact of APD restitution, as in our experience CV restitution has a greater impact on propagation at a much higher pacing frequencies than our sampling pacing range. If deemed relevant, CV restitution can also be personalised, as the parameters to adjust CV restitution are also present in the Mitchell-Schaeffer model. Its mathematical formulation is described in the following equation: with $g(DI)$ = CV as the next cycle CV.

$$g(DI) = \left(\frac{1}{4}\left(1 + \sqrt{1 - {h_{min}}/{h(DI)}}\right) - \frac{1}{2}\left(1 - \sqrt{1 - {h_{min}}/{h(DI)}}\right)\right)\sqrt{\frac{2dh(DI)}{\tau_{in}}}$$

However, these parameters also impact the APD restitution formula, so a slightly more complex model like the Fenton-Karma model may be better suited in such application.[137]

6.7.2 Personalised vs. Non-Personalised Empirical Electrical parameters

VT simulation with patient-specific personalised parameters

The personalised model was finally used to predict VT circuits, using an *in silico* programmed ventricular stimulation study from RV apex with Wellens protocol. Each stage for the VT stimulation *in silico* was simulated in parallel on a cluster of computers, and tested for induced VT. Simulated induced VT cycle isochrones were computed to locate the earliest activation time site, which corresponded to the exit point of the re-entrant VT circuit.

VT simulation with non-personalised parameters

A sensitivity analysis where the performance of a model constructed using non-personalised empirical electrical parameters was compared to that using personalised patient-specific electrical data. For all cases, patient anatomy and scar geometry was preserved. The VT simulation procedure was performed as described in the previous sections.

The personalised mesh was divided into three different types of tissue, guided by the LGE CMR imaging information: healthy myocardium, grey zone and scar core. Nodes within the scar core tissue were set to have zero apparent conductivity values. Conduction and restitution parameters in the healthy myocardium tissue were set to the average value computed from the personalised models across patients. This yielded values of $4m^2s^2$ for the apparent conductivity and Tau close = 180ms, tau in = 0.3ms, tau out = 6ms, tau open = 160 ms for the restitution model parameters. According to the described values of conduction velocity and restitution parameters in the literature, model parameters were modified in the grey zone areas.[19,140] Conduction velocity parameters were reduced by 90% with respect to those in the healthy myocardium. Restitution parameter values in the grey zone regions were set to have 25% longer action potential duration (increase in tau close parameter) and 31% slower upstroke velocity (increase in the tau in parameter) than those in the healthy myocardium.

Using non-personalised empirical electrical parameters, VT was not inducible in Patient 1. It also induced a different macroscopic VT circuit morphology from the one seen during the clinical study in Patient 2. The Euclidean distance between the centre

of the clinical exit region and that predicted using non-personalised electrical parameters was 37mm, and with using personalised electrical parameters it was 8mm.

Chapter 7 Myocardial tissue characterisation by cardiac magnetic resonance imaging using T1 mapping predicts ventricular arrhythmia in ischemic and non-ischemic cardiomyopathy patients with implantable cardioverter defibrillators

This chapter describes the work of a prospective clinical study that assessed the prognostic value of quantitative scar assessment using CMR in predicting ventricular arrhythmia in both patients with ischaemic and non-ischaemic cardiomyopathies. This included scar quantification using conventional late gadolinium enhancement images and T1 mappings with its associated derived index such as extracellular volume index (ECV). The analyses also demonstrated how results of the present study would have impacted on the current risk stratification strategy used in selecting patients for ICD therapy.

7.1 Abstract

Background: Diffuse myocardial fibrosis may provide substrate for the initiation and maintenance of ventricular arrhythmia. T1 mapping overcomes the limitations of the conventional delayed contrast-enhanced cardiac magnetic resonance imaging (CE-CMR) technique by allowing quantification of diffuse fibrosis. We assessed whether myocardial tissue characterisation using T1 mapping would predict ventricular arrhythmia in ischemic and non-ischemic cardiomyopathy.

Methods: A prospective longitudinal study of consecutive patients receiving implantable cardioverter defibrillators (ICD) in a tertiary cardiac center. Participants underwent CMR myocardial tissue characterisation using T1 mapping and

conventional CE-CMR scar assessment prior to device implantation. The primary endpoint was appropriate ICD therapy or documented sustained ventricular arrhythmia.

Results: One hundred and thirty patients (71 ischemic; 59 non-ischemic) were included with a mean follow-up period of 430 ±185 days (median: 425 days; IQR: 293 days). At follow-up, 23 (18%) patients experienced the primary endpoint. In multivariable-adjusted analyses, the following factors showed a significant association with the primary endpoint: secondary prevention (hazard ratio [HR] 1.70, confidence interval [CI] 1.01-1.91), non-contrast $T1_{-Native}$ for every 10ms increment in value (HR 1.10, CI 1.04-1.16; *90ms difference between the endpoint positive and negative groups*), and $greyzone_{-2sd-3sd}$ for every 1% LV increment in value (HR 1.36, CI 1.15-1.61; *4% difference between the endpoint positive and negative groups*). Other CE-CMR indices including $scar_{-2sd}$, $scar_{-FWHM}$ and $greyzone_{-2sd-FWHM}$ were also significantly, albeit less strongly, associated with the primary endpoint as compared to $greyzone_{-2sd-3sd}$.

Conclusions: Quantitative myocardial tissue assessment using T1 mapping is an independent predictor of ventricular arrhythmia in both ischemic and non-ischemic cardiomyopathies.

Key words: ventricular arrhythmia; T1 mapping; grey zone; defibrillator

7.2 Introduction

Ventricular arrhythmia is a major cause of sudden cardiac death in patients with impaired left ventricular (LV) function. Implantable cardioverter defibrillators (ICDs)

are effective in reducing mortality but are associated with both peri-operative complications and post-implant morbidity including inappropriate therapies.[26,27] Risk stratification is therefore critical to select patients most likely to benefit from ICD therapy. Although LV ejection fraction (LVEF) plays a central role in patient selection, there is considerable risk heterogeneity amongst patients with impaired LVEF.[141] Myocardial fibrosis provides potential substrate for the initiation and maintenance of re-entrant ventricular arrhythmia circuits, which propagate around localised regions of scars and along zones of slow conduction containing a mixture of scar and "healthy" myocardial tissue (grey zone). Cardiac magnetic resonance imaging techniques using late contrast enhancement (CE-CMR) are considered the gold standard for the non-invasive assessment of myocardial regional fibrosis, with a growing body of evidence showing the presence and the magnitude of the region of delayed contrast enhancement predict arrhythmia in ischemic and non-ischemic cardiomyopathies (ICM, NICM).[112,113,142,143] Diffuse LV fibrosis has also been shown to be arrhythmogenic by affecting electrical propagation between individual myocytes, which might provide evidence of increased risk for ventricular arrhythmia.[144,145] Assessment of diffuse fibrosis as seen in patients with NICM is not possible with conventional CE-CMR techniques since they rely on an arbitrary scale of relative signal intensity (SI) difference detected between regions of dense scar and regions of user-defined "normal" tissue. Even in patients with ICM, the non-infarct regions of the LV seen as "normal" myocardium on CE-CMR may contain diffuse interstitial fibrosis as a result of adverse remodeling.[60,146] Myocardial tissue characterisation using T1 mapping has emerged as a new CMR application, which has the potential to overcome the limitations of conventional CE-CMR techniques and allows characterisation of diffuse fibrosis, providing a reliable quantitative assessment of

myocardial tissue on a standardised scale. Several studies have shown a good correlation between measured T1 values and its associated derivative, extracellular volume index (ECV), with quantitative histological measures of fibrosis.[11,93,147]

We therefore hypothesised that T1 mapping techniques, which enable better assessment of diffuse myocardial fibrosis, would help predict the occurrence of ventricular arrhythmia in patients with ischemic or non-ischemic cardiomyopathy undergoing ICD implantation.

7.3 Methods

Patients

(See Chapter 3.2 for General patient selection criteria)

We prospectively invited all patients undergoing ICD implantation for primary and secondary preventions as per guidelines at our institution between May 2011 to January 2013 to participate.[148] Over 90% of patients gave written informed consent and were recruited to the study. All study participants underwent CMR assessment and coronary angiography prior to device implant. Patients undergoing implantation of ICD for catecholaminergic VT, Brugada syndrome or long QT syndromes with normal CMR findings were not included in the final analysis.

Cardiac magnetic resonance imaging protocol

(See Chapter 3.3.1 for General CMR methods protocol)

Image analysis

Ventricular volumes, function and mass were analyzed using dedicated software (ViewForum, Philips Healthcare, Best, Netherland) and were indexed to body surface area. CE-CMR images were visually assessed by two independent CMR experts blinded to the study outcome (RR and AC). In case of discrepancy, the data were jointly reviewed by these experts to reach a consensus. Quantitative analysis of late gadolinium enhancement (LGE) was performed using CMR42 (Circle Cardiovascular Imaging Inc., Calgary, Canada). The extent of LGE was quantified using both the 2-standard deviation method ($Scar_{-2sd}$, defined as the region with SI 2sd above the remote reference myocardium) and the full-width-half-maximum method ($Scar_{-FWHM}$, defined as the region with SI above the 50% of the maximal SI of the enhanced area). The extent of grey zone was quantified using the $Greyzone_{-2sd\text{-}FWHM}$ method (defined as the region with SI between $Scar_{-FWHM}$ and $Scar_{-2sd}$), and the $Greyzone_{-2sd\text{-}3sd}$ method (defined as the region with SI between 2 and 3 SD above the remote reference myocardium). Each of these indices was expressed as a percentage of the LV mass (%LV).

T1 relaxation maps were processed using a customised software plugin, incorporating motion correction with open source software (Osirix environment, Pixmeo, Geneva, Switzerland). We performed motion correction by applying a multi-resolution BSpline deformable registration, as implemented in the Insight Toolkit.[71] Due to the potential susceptibility of high T1 values to the effects of heart rate during image acquisition, we performed linear regression analysis of the measured native non-contrast T1 ($T1_{-native}$) values on heart rate and applied heart rate correction using a function of the mean heart rate of our study population to the non-contrast T1 values as previously described.[9] The T1 associated derivative, extracellular volume index (ECV), was also calculated as previously described using the following formula:[13]

$$(1\text{- hematocrit}) \times \left(\frac{\frac{1}{\text{Post-contrast T1myocardium}} - \frac{1}{\text{Pre-contrast T1myocardium}}}{\frac{1}{\text{Post-contrast T1blood}} - \frac{1}{\text{Pre-contrast T1blood}}} \right)$$

We chose a region of interest (ROI) in the septum for estimation of non-contrast T1 ($T1^{-native}$), post-contrast T1 ($T1^{-contrast}$) and ECV, as previously described.[72] Care was taken to avoid the endocardium/blood pool interface. If regional enhancement was seen in the septum on the LGE image a septal ROI was chosen adjacent to the enhanced region for T1 mapping analysis. The geometry of the mid-ventricular T1 map slice was the same as that of the mid-ventricular LGE images to allow for this comparison.

7.3.1 Follow-up and endpoint

All patients were implanted with an ICD or an ICD combined with cardiac resynchronisation therapy device (CRTD) capable of storing electrograms that met the criteria for detection. A standardised programme for ventricular arrhythmia detection and therapy was employed: ventricular arrhythmias > 170 bpm were detected (detection count: 16 intervals) and treated with anti-tachyarrhythmia pacing (ATP) and then shock therapy if ATP failed. Ventricular arrhythmias > 210bpm were detected (detection count: 24/30 intervals) and were treated with shock therapy as the first line. Standard supraventricular tachycardia detection discriminators were enabled according to device manufactures' recommendations. (St Jude Medical, St. Paul, Minnesota; Medtronic, Minneapolis, Minnesota. Onset: 81% for Medtronic devices, 18% for St Jude devices; stability: 40ms for both types of devices; morphology: passive.) These settings were altered only if clinically indicated. Patients were followed up at three-monthly intervals. At each follow-up visit, the device was interrogated for system integrity and any recorded events were reviewed by an experienced device physiologist and trained electrophysiologist who were blinded to

the CMR data. The primary endpoint for our study was the delivery of appropriate ICD therapy for VT or VF, or documented sustained VT greater than 30-second duration as documented by the device. Multiple therapies may occur in a single triggered event and we defined any additional appropriate therapy five minutes apart from the preceding therapy to be a separate episode of therapy.

7.3.2. Statistical analysis

(See Chapter 3.6 for General statistical methods)

The first episode of appropriate ICD therapy or sustained VT was considered as the event of interest for quantifying various associations. Kaplan-Meier survival curves were plotted to study the cumulative event rates between groups of participant, with the log-rank test providing further evidence regarding any significant differences between them. The univariate association between pre-specified variables of interest and the primary endpoint was examined using Cox proportional hazards regression models. For multivariable-adjusted analyses, a forward selection process using variables significantly associated with the outcome of interest in univariate analyses (at $p < 0.05$) was employed to further determine any independent predictors of the primary endpoint. All reported associations in this study are hazard ratios (HR) and their corresponding 95% confidence intervals (CI). To overcome limitations of missing data, only patients who had complete information on CE-CMR derived indices and T1 mapping derived indices were included in our multivariate analysis. Moreover, to avoid spurious associations due to the inclusion of correlated variables in a single Cox model, the multivariate analysis studied each of the CE-CMR indices separately. Receiver-operating characteristic (ROC) curves were plotted to identify variable cut-off points with 90% sensitivity to discriminate the primary endpoint. The estimated cut-off values for the chosen scar index and T1 index to predict the primary

endpoint was retrospectively used to re-classify and dichotomise the study subjects into high and low risk categories. All data analyses were performed using SPSS statistical software (version 21, IBM, New York, USA).

7.4 Results

7.4.1 Study population

A total of 138 patients agreed to participate in the study, of whom, 3 did not complete the CMR protocol due to claustrophobia and 2 additional participants were lost to follow-up. Three patients with Brugada or long QT syndromes were excluded from the analysis, leaving a total of 130 patients for further analysis. Of these, 71 patients had ICM and 59 had NICM (1 sarcoidosis, 5 hypertrophic cardiomyopathy, 53 dilated cardiomyopathy). One hundred study participants underwent T1 myocardial tissue characterisations and of this subset, 95 paired native and post-contrast T1 mapping images were suitable for analysis, 5 T1 mapping images were not suitable for analysis due to image corruption due to excessive motion artifacts. Table 7-1 shows the baseline characteristics of all 130 participants according to the underlying etiology.

	ICM	NICM	P
N (%)	71(100)	59(100)	
Age	66±10	58±18	n/s
Female	14 (20)	12 (20)	n/s
ICD	34 (48)	25 (42)	n/s
CRTD	37 (52)	34 (57)	n/s
1 °prevention	48 (68)	44 (75)	n/s
2 °prevention	23 (32)	15 (25)	n/s
COPD	10 (14)	10 (17)	n/s
Diabetes	14 (20)	7 (12)	n/s
Hypertension	25 (35)	20 (34)	n/s
CVA	6 (8)	2 (3)	n/s
AF	14 (20)	19 (32)	n/s
eGFR<60mls$_{/min/1.73m2}$	25 (35)	15 (25)	n/s
LVEF, %	26±11	35±18	n/s
QRS, ms	123±25	124±30	n/s
Pre-implant NSVT (1 °prevention)	13 (27)	17(38)	n/s
Aspirin/Clopidgrel*	65 (92)	28 (47)	<0.001
B-blocker	70 (99)	53 (90)	n/s
Ca-antagonist	2 (3)	3 (5)	n/s
ACEi/ARB	69 (97)	57 (97)	n/s
Statins*	65 (92)	37 (63)	<0.001
Amiodarone*	12 (17)	3 (5)	0.036
Digoxin	7 (10)	6 (10)	n/s
Loop diuretic	27 (38)	30 (51)	n/s
K-sparing diuretic	33(45)	25 (42)	n/s

Table 7- 1 Baseline patient characteristics

ICD = implantable cardioverter defibrillator; CRTD = cardiac resynchronisation therapy with defibrillator; COPD = chronic obstructive pulmonary disease; AF = atrial fibrillation; CVA = cerebral vascular accident; LVEF = left ventricular ejection fraction; NSVT = non-sustained ventricular tachycardia.

* = Variable with a statistical significant difference between groups.

7.4.2 Primary endpoint

During a mean follow-up of 430±185 days (median: 425 days; IQR: 293 days), 23 (18%) patients experienced appropriate ICD therapy. Three patients experienced

more than one episode of appropriate ICD therapy. The median time to first ICD therapy was 178 days, IQR 420 days. Of the 4 cardiovascular deaths (3 in ICM and 1 in NICM; 1 died of primary heart failure, 3 died of heart failure following sepsis), only 1 patient had experienced appropriate ICD therapy following implant and before death. There was a greater proportion of appropriate ICD therapy in the secondary [11/38 (29%)] versus primary prevention [12/92 (13%)] group (p = 0.031), as was the cumulative event rate for the primary endpoint (p=0.033, Figure 7-1A). The cumulative event rate was similar, however, between the ICM and NICM cohorts (p=0.479, Figure 7-1B).

Figure 7-1A

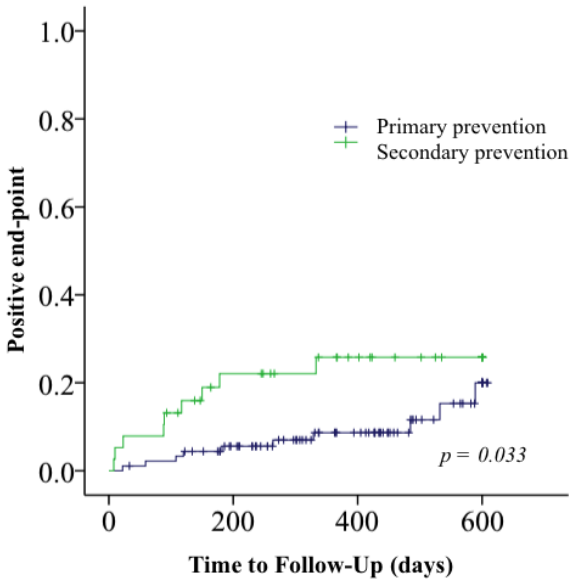

Figure 7-1B

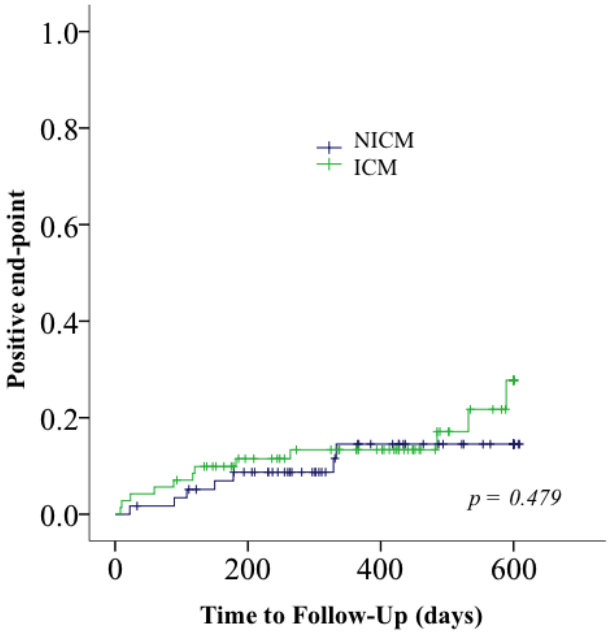

Figure 7- 1 Kaplan-Meier survival curves of appropriate ICD therapy for primary *vs.* secondary prevention (A); and for ICM vs. NICM (B).

ICD = implantable cardioverter defibrillator; ICM = ischemic cardiomyopathy; NICM = non-ischemic cardiomyopathy.

7.4.3 CE-CMR and T1 myocardial tissue characteristics

When patients were dichotomised into endpoint +ve and endpoint –ve groups, there were significant differences in the CE-CMR derived indices with both scar and grey zone being significantly higher in the endpoint +ve group. In addition, non-contrast native T1 value was significantly higher in the endpoint +ve group (Table 7-2).

	Endpoint -ve		Endpoint +ve		P
	ICM	NICM	ICM	NICM	
LV EF, %;	32 ±15		30 ±12		0.893
	28 ±10	36 ±19	31 ±13	30 ±12	
LV mass, g	151 ±42		155 ±34		0.588
	146 ±35	155 ±49	162 ±33	144 ±36	
Scar$_{-2sd}$*, %LV	18 ±11		30 ±11		<0.001
	23 ±8	13 ±12	33 ±9	26 ±13	
Scar$_{-FWHM}$*, %LV	11 ±7		18 ±8		<0.001
	14 ±6	7 ±8	19 ±7	15 ±9	
Greyzone$_{-2sd\text{-}FWHM}$*, %LV	8 ±5		12 ±7		0.006
	9 ±4	6 ±6	14 ±7	11 ±7	
Greyzone$_{-2sd\text{-}3sd}$*, %LV	5 ±3		9 ±3		<0.001
	5 ±2	5 ±4	8 ±2	9 ±5	
T1$_{-native}$*†, ms	1033 ±65		1123 ±80		0.029
	1031 ±70	1035 ±59	1088 ±63	1158 ±93	
T1$_{-contrast}$†, ms	421 ±72		415 ±43		0.592
	418 ±56	425 ±87	421 ±34	408 ±56	
ECV†	0.29 ±0.06		0.31 ±0.05		0.262
	0.29 ±0.06	0.29 ±0.06	0.31 ±0.04	0.32 ±0.07	

Table 7- 2 CMR derived indices

EF = ejection fraction; FWHM = full-width half-maximum; ECV = extracellular volume index; LV = left ventricular; +ve = positive; -ve = negative

(*$T1_{-native}$ <1000ms were considered to be the normal reference in our institution. 1.5T scanner with a 32–channel coil, Philips Healthcare, Best, Netherlands. There were no significant differences, p > 0.05, in age, gender distribution, comorbidities such as hypertension/diabetes/renal impairment and patient heart rate during image acquisition between the Endpoint-ve and Endpoint+ve groups.*)

* Variable with a statistical significant difference between groups

† T1 derived indices, n = 95

7.4.4 Predictors of ICD therapy

Univariate analysis showed that secondary prevention, CE-CMR derived indices of scar and grey zone (n = 130), and non-contrast native T1 values (n=95) were significantly associated with appropriate ICD therapy (Table 7-3). In multivariable-adjusted analysis, secondary prevention, CE-CMR derived indices of scar and grey zone and non-contrast native T1 values were all significantly associated with ICD therapy (Table 7-3). To overcome limitations of missing data, only patients who had complete information on CE-CMR derived indices and T1 mapping derived indices were included in our multivariate analysis. The HR of secondary prevention was 1.70, a mean difference of 4% in $Greyzone^{-2sd\text{-}3sd}$ between the endpoint +ve and endpoint –ve groups gave a 2.4-fold excess risk of the primary outcome. Similarly, for non-contrast native T1, a mean difference of 90ms between the end-point +ve and –ve groups was associated with a 1.4-fold excess risk of the primary outcome. The respective HR with associated confidence interval for each index is described in Table 7-3.

Univariate analyses

Variables	Hazard ratio	Confidence intervals	P
Age, + 1year	0.99	0.96-1.03	n/s
Female	1.53	0.45-5.16	n/s
COPD	2.16	0.84-5.55	n/s
Diabetes	2.23	0.87-5.68	n/s
Hypertension	1.89	0.83-4.29	n/s
CVA	2.84	0.83-9.69	n/s
AF	1.48	0.61-3.59	n/s
eGFR<60mls$_{/min/1.73m2}$	1.37	0.75-2.24	n/s
QRS ≥120ms	1.18	0.51-2.73	n/s
2 °prevention	1.59	1.04-1.82	0.039
LVEF, +1%	0.99	0.96-1.02	n/s
LV mass, +1g	1.01	0.99-1.01	n/s
Scar$_{-2sd}$, +1%LV	1.09	1.05-1.14	<0.001
Scar$_{-FWHM}$, +1%LV	1.09	1.04-1.15	0.001
Greyzone$_{-2sd-FWHM}$, +1%LV	1.14	1.08-1.22	<0.001
Greyzone$_{-2sd-3sd}$, +1%LV	1.31	1.17-1.47	<0.001
T1$_{-native}$, +10ms	1.06	1.01-1.11	0.021
T1$_{-contrast}$, -10ms	1.03	0.98-1.09	n/s
ECV, +1%	1.01	0.94-1.11	n/s

Multivariate analyses*†

Variables	Hazard ratio	Confidence intervals	P
QRS ≥120ms			n/s
2 °prevention	1.70	1.01-1.91	0.048
LVEF≤35%			n/s
Scar$_{-2sd}$, +1%LV	1.10	1.04-1.15	<0.001
Scar$_{-FWHM}$, +1%LV	1.11	1.05-1.19	0.001
Greyzone$_{-2sd-FWHM}$, +1%LV	1.13	1.05-1.22	0.001
Greyzone$_{-2sd-3sd}$, +1%LV	1.36	1.15-1.61	<0.001
T1$_{-native}$, +10ms	1.10	1.04-1.16	0.001

Table 7- 3 Findings from univariate and multivariate Cox regression analyses

EF = ejection fraction; FWHM = full-width half-maximum; ECV = extracellular volume index; LV = left ventricular; n/s = non-significant; +ve = positive; -ve = negative. For multivariable-adjusted analyses, each of the factors listed in the table has been mutually adjusted for all the other factors mentioned for the corresponding regression analysis.

* To overcome limitations of missing data, only patients who had complete information on CE-CMR derived indices and T1 mapping derived indices were included in our multivariate analysis, n = 95.

† To avoid spurious associations due to the inclusion of correlated variables in a single Cox model, the multivariate analysis studied each of the scar or grey zone indices separately, i.e. for the analysis of Scar$_{-2sd}$ +1%LV, the adjustment included QRS ≥120ms, 2° prevention, LVEF≤35% and T1$_{-native}$ +10ms; for analysis of Scar$_{-FWHM}$ +1%LV, the adjustment included QRS ≥120ms, 2° prevention, LVEF≤35% and T1$_{-native}$ +10ms; for the analysis of Greyzone$_{-2sd-FWHM}$ +1%LV, the adjustment included QRS ≥120ms, 2° prevention, LVEF≤35% and T1$_{-native}$ +10ms; for the analysis of Greyzone$_{-2sd-3sd}$ +1%LV, the adjustment included QRS ≥120ms, 2° prevention, LVEF≤35% and T1$_{-native}$ +10ms.

7.4.5 Risk re-classification

Risk re-classification was assessed for Greyzone$_{-2sd-3sd}$ and T1$_{-native}$ values that allowed 90% sensitivity for detecting the primary endpoint. Based on ROC analyses, a cut-off value of ≥1015ms was used for T1$_{-native}$ and a value of ≥5.5% of the LV mass was used for Greyzone$_{-2sd-3sd}$ to dichotomise the study participants into high-risk (i.e. those requiring an ICD) and low-risk (i.e. those not requiring an ICD) groups. In the primary prevention group, 50 of the 80 participants (62.5%) who had an ICD implanted but who never experienced the endpoint were correctly reclassified into the low risk category based on Greyzone$_{-2sd-3sd}$ data, whilst none of the participants experiencing a positive endpoint were mistakenly reclassified into the low risk group. By comparison, 25 of the 57 participants (43.9%) with a primary prevention ICD and a negative endpoint were correctly reclassified to low risk group based on T1$_{-native}$ measures, whilst none of the patients with a positive endpoint were mistakenly reclassified into the low risk group. The net reclassification improvement (NRI) was 62.5% and 26.3%, respectively, compared with original clinical risk classification. However, in the secondary prevention group, the use of neither Greyzone$_{-2sd-3sd}$ nor T1$_{-native}$ was effective in risk re-classification (NRI 26.3% and -7.9%, respectively, Figure 7-2A). The value of using risk reclassification is illustrated in Figure 7-2B using Kaplan-Meier survival curves. Risk re-stratification using either the

Greyzone$^{-2sd\text{-}3sd}$ or T1$^{-native}$ value to high or low risk categories resulted in significantly different cumulative event rates in the primary prevention cohort but not in the secondary prevention cohort.

Figure 7-2A. Risk reclassification with Greyzone$^{-2sd-3sd}$ (high risk ≥5.5% LVmass) or T1$^{-native}$ (high risk ≥1015ms) in the primary prevention and secondary prevention cohort

Primary prevention	**Original clinical risk prediction** / **Prediction with Greyzone$^{2sd-3sd}$**		
ICD event	Low risk	High risk	Total
Endpoint -ve	0 / 50*	80 / 30	80 / 80
Endpoint +ve	0 / 0	12 / 12	12 / 12
Total	0 / 50	92 / 42	92 / 92
Net reclassification improvement = 62.5%			
Secondary prevention			
ICD event	Low risk	High risk	Total
Endpoint -ve	0 / 12*	27 / 15	27 / 27
Endpoint +ve	0 / 2*	11 / 9	11 / 11
Total	0 / 14	38 / 24	38 / 38
Net reclassification improvement = 26.3%			
Primary prevention	**Original clinical risk prediction** / **Prediction with T1$^{-native}$**		
ICD event	Low risk	High risk	Total
Endpoint -ve	0 / 25*	57 / 32	57 / 57
Endpoint +ve	0 / 0	8 / 8	8 / 8
Total	0 / 25	65 / 40	65 / 65
Net reclassification improvement = 43.9%			
Secondary prevention			
ICD event	Low risk	High risk	Total
Endpoint -ve	0 / 3*	21 / 18	21 / 21
Endpoint +ve	0 / 2*	9 / 7	9 / 9
Total	0 / 5	30 / 25	30 / 30
Net reclassification improvement =-7.9%			

* denotes changes affected by risk reclassification.

Figure 7-2B Kaplan-Meier curves for the reclassified high and low risk categories

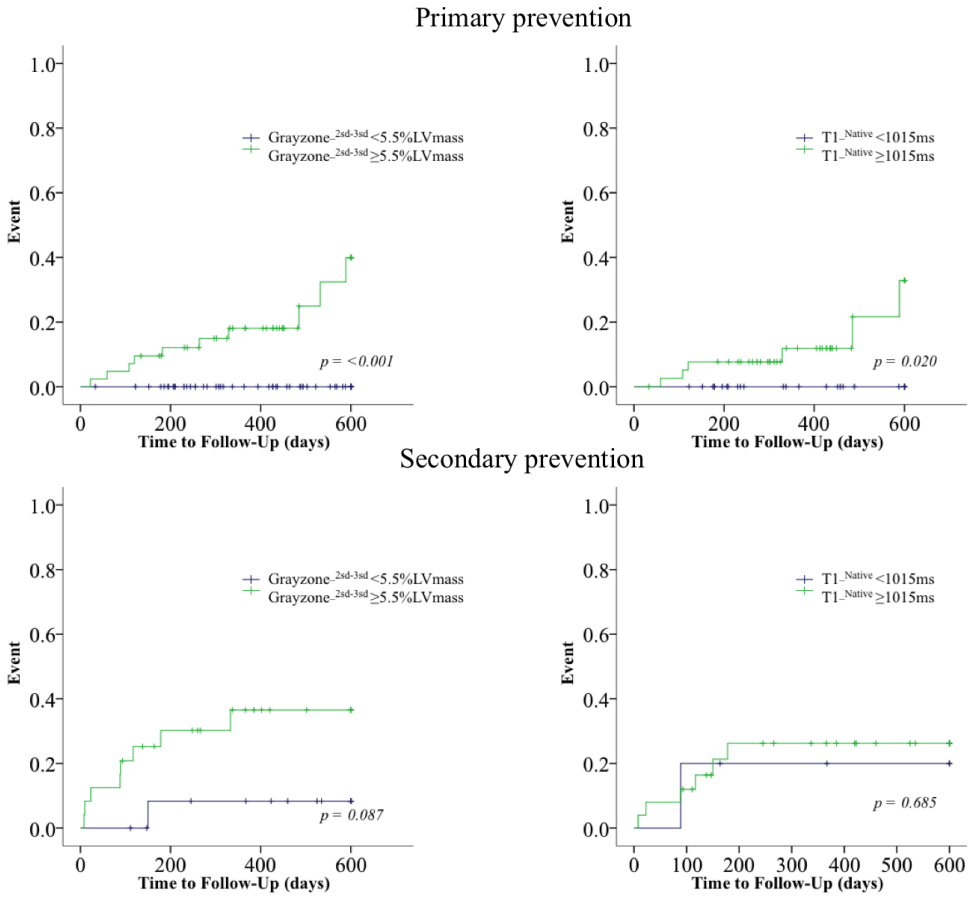

Figure 7- 2 Risk reclassification with Greyzone$^{-2sd\text{-}3sd}$ (high risk ≥5.5% LVmass) or T1$^{-native}$ (high risk ≥1015ms) in the primary prevention and secondary prevention cohort (A), with corresponding Kaplan-Meier curves for the reclassified high and low risk categories (B).

7.4.6 Reproducibility of T1 measurement

T1 measurements were repeated in a subgroup of randomly selected patients from the study cohort (10 ICM and 10 NICM). For T1$^{-native}$ measurement, the intra-observer average difference in values was 5±3ms, coefficient of variation (COV) was 0.3±0.2%; the inter-observer average differences in values were 6±5ms and COV was 0.4±0.3%. For T1$^{-contrast}$ measurement, the intra-observer average difference in values was 5±4ms and COV was 0.8±0.6%; the inter-observer average differences in values

were 5±4ms and COV was 0.9±0.7%. There were good agreements in inter and intra-measurements of native T1 and contrast T1 (Pearson's r = 0.99; p≤0.01).

7.5 Discussion

The current study is the first to demonstrate that non-contrast native T1 estimated with T1 mapping is an independent predictor of ventricular arrhythmia in patients with ICM and NICM. It also provides further confirmation that the extents of scar and grey zone derived from CE-CMR are independently associated with ventricular arrhythmia, and highlights the importance of grey zone in patients with NICM.

7.5.1 Diffuse fibrosis and ventricular arrhythmia

It has long been recognised that diffuse interstitial fibrosis occurs at various stages in the pathological progression of cardiomyopathies of different etiologies. [60,89,93,146,149] Fibroblasts are not electrically "inert" and can modulate cellular ion channel remodelling, thereby affecting tissue electrical properties through a variety of mechanisms including mechano-electrical feedback mediated via stretch activated ion channels; gap junctions via connexin with close coupling of nearby cardiac myocytes; and altering the orientation of cardiac fibres. Collectively, these effects can provide a substrate for ventricular arrhythmia.[61,124] Electroanatomical mapping study suggests that diffuse interstitial fibrosis plays a critical role in the maintenance of re-entrant VT and propensity to degenerate to VF.[150] Studies using myocardial biopsy specimens to look for diffuse fibrosis in patients with deemed normal hearts and those with hypertrophic cardiomyopathy have also shown a strong association between interstitial fibrosis and ventricular arrhythmia.[151,152]

T1 mapping of the myocardium provides a true quantitative assessment of the voxel SI and is used to detect regions of diffuse interstitial fibrosis with higher native T1 values than normal myocardium. In comparison, conventional CE-CMR techniques require an arbitrary reference "normal" myocardium to generate an image with a signal contrast between fibrotic and apparently non-fibrotic regions. It is therefore less discriminative in "highlighting" the diffuse fibrosis that affects the myocardium in a more homogeneous way. Native T1 values reflecting the presence of diffuse interstitial fibrosis, not detectable by conventional CE-CMR, have been found to be higher in myocardial regions free of delayed contrast enhancement in a number of different cardiomyopathies.[153,154] The current study is the first to show that native myocardial T1 is independently associated with ventricular arrhythmia in patients with advanced cardiomyopathies of both ischemic and non-ischemic etiologies.

T1 values have also been measured following the administration of gadolinium contrast agents and in addition to the patients' hematocrit levels can be used to calculate ECV. Several studies have demonstrated a close correlation between ECV and histological measures of fibrosis in cardiomyopathies of various etiologies.[155-157] Others have demonstrated a correlation between ECV and mortality.[16,158,159] Accurate ECV assessment depends on the time delay of T1 mapping after contrast injection, the haematocrit level which affects the partition coefficient of the gadolinium contrast agent, the contrast kinetics between regions of fibrosis and normal myocardium and the contrast wash-out rate which is influenced by the renal clearance rate. In the current study, ECV was not a significant independent predictor of ventricular arrhythmia which may be explained by several factors including the fact that the time delay after contrast injection for post-contrast T1 mapping varied between 10 and 25 minutes and that the hematocrit levels were measured using blood samples taken from

a time range within 24hrs before and after the time of image acquisition due to clinical constraints. It is known that hematocrit levels may vary significantly depending on the time of the day, posture, physical activity and post-prandial state.[160] Similarly the formula from which ECV is derived holds true when the extracellular contrast concentration in the blood and myocardium reaches equilibrium and there are uncertainties whether this equilibrium is achievable with the bolus technique we used rather than the slow contrast infusion technique.[16134] Finally, in our cohort of advanced cardiomyopathies, variations in diuretic therapy and varying degrees of renal function are likely to have an impact on renal clearance of gadolinium and therefore contrast kinetics.

7.5.2 Regional fibrosis and ventricular arrhythmia

Regional fibrosis provides an important substrate for ventricular arrhythmias and is an independent predictor of ventricular arrhythmia in both ICM and NICM with several electroanatomical mapping studies demonstrating that scar border zone (grey zone) is important in the initiation and maintenance of ventricular arrhythmia.[99,125] Further characterisation of the enhanced region with intermediate SI to further differentiate the grey zone from the scar core has provided incremental prediction of ventricular arrhythmia in ICM but has not been studied so far in NICM.[3,4]

A criticism of grey zone assessment is the effect of partial volume and image acquisition voxel size which may influence its quantification. Furthermore the multitude of SI-based quantitative methods used in various studies makes direct comparison of the predictive value of each index difficult. To overcome these limitations, an automated computer analysis was used to improve the reproducibility of the quantification by standardizing the SI-based assessment; and comparison was made between two grey zone indices on the same cohort of patients (Greyzone$_{-2sd-3sd}$

and Greyzone$_{-2sd\text{-}FWHM}$). This study systematically tested the predictive values of each index expressed as a percentage of LV mass and found both to be independent predictors of ventricular arrhythmia in a multivariate model that included adjustments for established variables used for arrhythmia risk stratification. Greyzone$_{-2sd\text{-}3sd}$ gave the highest HR for every 1% LV mass increment compared to other indices, although ROC analysis showed the areas under the curve were not significantly different between the grey zone and other scar indices. This study is the largest cohort to date to demonstrate the incremental value of grey zone quantification for arrhythmia prediction and to highlight the potential of arrhythmia prediction by grey zone in patients with NICM.

7.5.3 Clinical relevance

Native T1 removes the dependence on contrast kinetics and makes its potential translation to routine clinical application attractive. In addition, it allows myocardial tissue characterisation free of the potential risk associated gadolinium contrast in patients with severe renal impairment. In the sub-analysis assessing the impact of utilizing greyzone$_{-2sd\text{-}3sd}$ and T1$_{-native}$ values for risk re-stratification, additional risk assessment based on the cut-off values derived from this study could correctly re-classify primary prevention patients from high risk to the low risk category. In the secondary prevention group, some patients were wrongly risk stratified to the low risk group when tested using either Greyzone$_{-2sd\text{-}3sd}$ or T1$_{-native}$ alone, however the specificity may be improved if both indices were considered simultaneously. These results are in line with others that showed scar quantification with CE-CMR as the only independent predictor of adverse ventricular arrhythmia outcome in the patients with a previous history of non-sustained VT.[162]

7.5.4 Study limitations

This study is limited by a relatively short follow-up and use of a surrogate end point (i.e. appropriate ICD therapy) which does not necessarily equate to sudden arrhythmic death. The absolute T1 values of interest can be influenced by a number of technical parameters including magnetic field strength and acquisition sequence as well as post-acquisition image processing including motion correction and image registration. T1-mapping was limited to just a single slice of myocardium and an assumption made that diffuse fibrosis imaged is truly diffuse/uniform in the remote myocardium. Conducting a single center study allowed standardisation of the imaging protocol across the entire cohort, however it may have introduced systematic bias including the timing of post-contrast T1 measurement. Only one type of sequence was used for T1 image acquisition. A shorter T1 mapping acquisition sequence with shorter breathholds during image acquisition may potentially reduce motion artifact and impact on the post-contrast T1 value analysis. In light of the results from MADI-RIT study, optimzd ICD programming aimed at reducing ICD therapy could have potentially reduced the event rate of the study.[163] However by standardizing the ICD programming within our cohort, it is unlikely that our programming asset up would have introduced any systemic bias in the associations studied. This study included a heterogeneous patient population, though diffuse fibrosis may be present in advanced cardiomyopathies of various etiologies, a more homogenous population group would have improved the power of detection of suggested association. A multicenter study with a larger sample would be of great value to further assess our findings.

7.6 Conclusion

The study has shown for first time that quantitative myocardial tissue assessment using T1 mapping is an independent predictor of ventricular arrhythmia with a hazard ratio comparable to scar or grey zone quantification detected by conventional CE-CMR in both ischemic and non-ischemic cardiomyopathies. Our results suggest a potential for the use of myocardial tissue characterisation using CMR to refine the current risk stratification decisions regarding ICD implantation especially in the context of primary prevention for sudden arrhythmic death.

Chapter 8. Exploring electrical remodeling in response to cardiac resynchronisation therapy

This chapter describes the work that assessed the impact of CRT on LV electrical remodeling in terms of action potential duration (APD) changes between responders and non-responders. The findings may provide explanation to the persistent high incidence of arrhythmias in some patients with CRT and the additional mortality benefit observed in responders of CRT.

8.1 Abstract

Background: A consistent feature of electrophysiological remodelling in heart failure is ventricular action potential duration (APD) prolongation. However, the effect of reverse remodelling on APD during cardiac resynchronisation therapy (CRT) has not been determined in these patients. We hypothesised (1) CRT may alter APD and (2) that the effect of CRT on APD may be different in patients who exhibit a good haemodynamic response to CRT compared to those with a poor response.

Methods: LV activation recovery intervals (ARI), as a surrogate for action potential duration, were measured from the LV epicardium in thirteen patients at day 0, 6 weeks and 6 months following CRT implant. Responders to CRT were defined as those demonstrating a ≥15% reduction in LV end-systolic volume at 6 months.

Results: The responder group had a significant reduction in LVARI (mean: -13ms ±12ms; median: -16ms, IQR -2ms to -19ms) during RV pacing at 6 months ($p<0.05$). Conversely the non-responders showed a significant increase in ARI (mean:

+22ms ±16; median: 17ms, IQR 8ms to 35ms) ($p<0.05$). (One patient in each group was on Amiodarone.)

Conclusions: In patients with heart failure left ventricular epicardial APD (ARI) altered during CRT. The effect on APD was opposite in patients showing a good haemodynamic response compared to non-responders. The findings may provide explanation for the persistent high incidence of arrhythmias in some patients with CRT and the additional mortality benefit observed in responders of CRT.

Key words:

action potential duration; activation recovery interval; cardiac resynchronisation therapy; mechano-electrical feedback.

8.2 Introduction

A consistent feature of electrophysiological remodelling in heart failure is ventricular action potential duration (APD) prolongation.[65] The effect of cardiac resynchronisation therapy (CRT) and reverse remodelling on APD duration has not been determined in these patients.

Cardiac resynchronisation therapy (CRT) in patients with heart failure has been shown to be beneficial in terms of symptomatic improvement and overall mortality. Recently, the MultiCenter Automatic Defibrillator Implantation Trial with Cardiac Resynchronisation Therapy (MADIT-CRT) trial, the Resynchronisation Reverse Remodelling in Systolic Left Ventricular Dysfunction (REVERSE) trial and the

Resychronisation-Defribrillation for Ambulatory Heart Failure Trial (RAFT) trial have demonstrated that CRT provided an incremental overall survival benefit to ICD therapy alone in heart failure patients.[66-68] However, earlier studies showed that the incidence of arrhythmia and sudden death continues to be high despite CRT inferring the possible need for additional protection from implantable cardoverter defibrillator (ICD).[36,43] These observations highlighted a need to further elucidate the effect of CRT on electrophysiology.

CRT is associated with anatomical and electrical remodelling and evidence suggests these two processes are linked.[164-166] The effect of CRT on APD has been studied in a canine heart failure model which showed APD shortening in cells from the lateral LV wall.[16710] However, evidence suggests that the electrophysiological effects of CRT may vary according to the anatomic and haemodynamic profiles,[168-171] underlining the need to obtain information directly from the hearts of patients with heart failure.

We hypothesised that APD may be modified during CRT, and the effect on APD may vary in patients who exhibit a beneficial response to CRT compared to those with a poor response. To assess this we set out to record activation recovery intervals (ARI) as a surrogate measure of APD from the left ventricular epicardial lead of a CRT device at intervals over the first 6 months following implantation. ARI has been theoretically and experimentally validated as a reliable surrogate marker of regional action potential duration.[75-79] It has advantages over other measures of repolarisation including enabling analysis of regional electrical properties, unlike the QT interval which is a more global measurement. It also avoids the need for long pacing protocols required for effective refractory period (ERP) and the pro-arrhythmic risk of premature stimulation required to measure ERP.

8.3 Methods

8.3.1 Study population and protocol

(See Chapter 3.2 for General patient selection criteria)

Thirteen patients who fulfilled the standard criteria for CRT were prospectively recruited to the study prior to their device implant. The selection criteria included drug refractory symptomatic heart failure with New York Heart Association (NYHA) class II-IV, impaired left ventricular ejection fraction (LVEF) ≤ 35% with a QRS duration ≥ 120ms.

Clinical status according to NYHA class and Minnesota heart failure questionnaires and echocardiographic measures of LV function were assessed at baseline (day 0) and 6 months post device implant.

Transthoracic echocardiography was performed at baseline and 6 months post implant to acquire standard 2D images of left ventricular (LV) dimensions and ejection fractions (EF) during breath-hold in standard apical 2-chamber and 4-chamber views. LVEF and dimensions were measured using the 2-dimentional modified biplane Simpson's method.

(See Chapter 3.4 for General echocardiography methods)

All thirteen patients were implanted with the Quartet Model 1458Q LV pacing lead (St. Jude Medical, Minnesota, USA) via the coronary sinus in conjunction with a Unify Quadra CD 3251-40Q generator (St. Jude Medical, Minnesota, USA). The atrial-ventricular (AV) and ventricular-ventricular (VV) delays were empirically set at

120ms and LV 30ms ahead of RV at implant. CRT device optimisation was performed at 6 weeks post-implant per our institute's standard clinical care protocol. At this time the AV and VV delays were adjusted under echocardiographic guidance using mitral valve inflow Doppler signals and aortic valve outflow velocity-time-intervals to achieve the best haemodynamic benefit. There were no changes in the LV pacing vectors and output stimulus strength in the patients over the 6 months period. The LV pacing output strength was 2.0V at 0.5ms pulse width for all patients.

At day 0 post-implant, a 30 second recording of the LV unipolar electrogram (UEG) signal was made via the device programmer (Merlin Patient Care System, Model 3650, St Jude Medical) during DDD-RV or VVI-RV pacing, depending on whether the patient was in sinus rhythm or in atrial fibrillation. This enabled comparisons between patients with sinus rhythm and those with atrial fibrillation at identical heart rate, in order to eliminate the influence of heart rate on ARI. This study protocol is also clinically relevant in that during CRT, in addition to LV pacing, the RV is also paced which would change the regional ARI when patient is in intrinsic ventricular rhythm.[172] In order to eliminate the influence of variable heart rate on ARI. UEG recordings were made after at least 2 minutes of pacing at a constant rate of 10 beats above the patient's intrinsic heart rate. The same recordings were repeated 6 weeks and 6 months post implant at the same heart rate. The 30 second LV UEG recordings were analysed off-line using a software script developed by our group within the MATLAB environment (MathWorks, Massachusetts, USA) to derive the activation recovery interval (ARI).[21] ARIs were measured using conventional validated criteria from dv/dt min of the QRS of the UEG to dv/dt max of the local T wave.[75] An

example showing the measurement and the stability of recordings is illustrated in Figure 8-1.

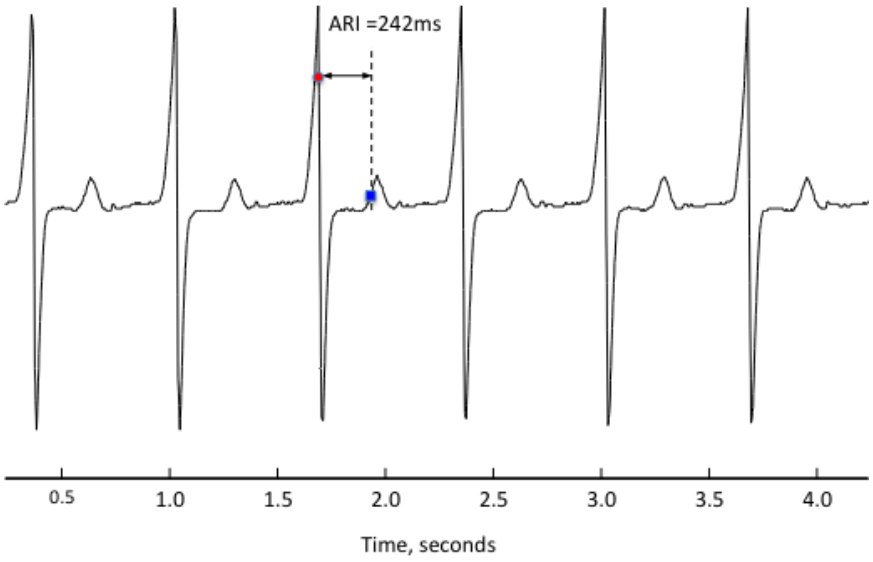

Figure 8- 1 An example of LV unipolar electrogram raw data recording demonstrating activation recovery interval (ARI)

Responders to CRT were defined as those demonstrating a ≥15% reduction in LV end-systolic volume (ESV) at 6 months. The echocardiography assessor was blinded to the ARI results.

8.3.2 Statistical analysis

(See Chapter 3.6 for General statistical methods)

Additional post hoc power analysis based on the collected data assuming non-parametric distribution was performed using G*Power, version 3.1.5, Kiel, Germany.

8.4 Results

The baseline patient characteristics are shown in Table 8-1.

	Responders	Non-responders
Patient, n (%)	7 (100)	6 (100)
Age	70 ±7	69 ±11
Male n (%)	4 (57)	6 (100)
NYHA Class (II/III/IV)	0/5/2	1/5/0
Minnesota heart failure score	50 ±32	42 ±23
LVEF (%)	22 ±6	29 ±5
LVEDV (ml)	199 ±57	188 ±32
LVESV (ml)	157 ±50	130 ±24
Ischaemics/Non-ischaemics n (%)	1 (14) /6 (86)	4 (67) / 3 (33)
Sinus rhythm/atrial fibrillation n (%)	4 (57) /3 (43)	3(50) /3 (50)
QRS duration pre-implant (ms)	150 ±28	166 ±28
QRS duration during CRT (ms)	134 ±19	161 ±16
QRS morphology (LBBB/RBBB/nonspecific IVCD) n	5/0/2	6/0/0
Bi-V pacing (%)	97 ±4	97 ±3
Bisoprolol* n (%)	6 (85)	6 (100)
Amdiodarone* n (%)	1 (14)	1 (17)
ACEi/ARB n (%)	7 (100)	6 (100)
Statins n (%)	3 (43)	4 (67)

Table 8- 1 Baseline patient characteristics

*During the follow-up, three of the six patients in the responder group had increased Bisoprolol dosages. None of the patients in the non-responder group had changed Bisoprolol dosages. The only patient who was on Amdiodarone in the responder group continued its usage during the follow up, whereas the only patient who was on Amdiodarone in the non-responder group discontinued its usage 2 months after CRT. These changes in

medication could not have accounted for the divergent changes in the ARI observed in our study.

EF=ejection fraction; EDV=end-diastolic volume; ESV=end-systolic volume; IVCD=intraventricular conduction delay; LBBB=left bundle branch block; RBBB=right bundle branch block; ACE=angiotensin converting enzyme inhibitor; ARB=angiotensin receptor blocker.

All thirteen patients underwent successful CRT implant. The epicardial LV leads were targeted in the lateral and posterior walls in all subjects. The positions of the LV lead tip where UEG recordings were made are illustrated in Figure 2. There were no significant difference between the positions of the RV lead between the responder and non-responders.

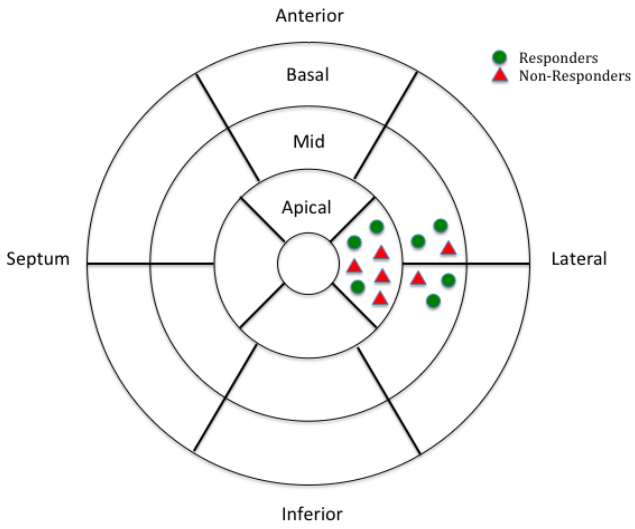

Figure 8- 2 Positions of the left ventricular lead tip where unipolar electrograms are made, according to American Heart Association 17-segments heart model

Although four of six patients in the non-responder group, compared with three of seven patients in the responder group, had LV lead tip positioned in the apical region,

the use of quadripolar leads allowed pacing sites away from the apex in some cases in order to maximise clinical benefit for the patient and avoid phrenic nerve stimulation. The mean absolute distance between the LV lead tip from which ARI was measured to the LV pacing cathode were 10mm±13mm in the in responder group and 11mm±19mm in the non-responder group. (Note that these measures are derived from the absolute distance between the vectors along the quadripolar leads and absolute accuracy is limited due to the oblique course of epicardial vein and the position and shape of lead sitting within the vein.) During the 6 months CRT, all the patients (responders and non-responders) were paced via bipolar vectors (LV and RV). The pacing vectors and pacing outputs were not changed during the 6 months study duration. The percentages of the bi-ventricular pacing were the same between the two groups. There were no major differences between the optimised A-V delays and V-V delays between the responder and non-responders in the study cohort. A-V delays were 127ms±10ms and 123±5ms in the patients with sinus rhythm in the responders and non-responder groups. Four of seven patients in the responder group had V-V delays of 0ms, the other three patients had LV ahead of RV by 30ms. Three of six patients in the non-responder group had V-V delays of 0ms, one of six patients had LV ahead by 20ms, and the other two had LV ahead by 30ms.

Based on the LVESV reduction ≥ 15% at 6 months post implant, 7 patients (54%) were considered to be echocardiographic responders. The mean change in LVESV at 6 months post CRT device implant was -36%±15% in the responder group and +3%±5% in the non-responder group compared with baseline, $p<0.001$. The mean LVEF at 6 months was 39%±7% in the responder group and 31%±5% in the non-responder group, $p=0.045$. The mean NYHA class improved by 1.5±0.9 class in the

responder group and remained unchanged in the non-responder group. Minnesota heart failure questionnaires score at 6 months were 31±23 in both groups. The clinical and echocardiographic indices at 6 months post CRT are shown in Table 8-2.

	Responders	**Non-responders**	***P values***
Patient, n	7	6	
NYHA Class	1.8±0.6	2.6±0.5	P<0.01
Minnesota heart failure score	31±23	31±23	NS
LVEF (%)	39±7	31±4.5	P=0.04
LVEDV (ml)	157±45	192±29	NS
LVESV (ml)	98±37	134±27	NS
Δ LVEDV (%)	-20±12	-3±5	P<0.01
Δ LVESV (%)	-36±15	-3±5	P<0.01

Table 8- 2 Table 8-2. Patient clinical and echocardiographic indices at 6 months

Δ=% change compared with baseline echocardiographic parameters; NS=not significant.

LV UEGs were recorded during DDD-RV or VVI-RV pacing at a fixed heart rate ranged from 80bpm to 120 bpm within the cohort (the same heart rates were maintained during recordings at day 0, 6 weeks and 6 months for individual patients). The LV ARI during RV pacing at day 0, 6 weeks and 6 months are summarised in Table 8-3.

LV ARI	(ms)	Responders		Non-responders	
Day 0	mean	259±53		253±25	
	median	238; IQR: 213, 303		262; IQR: 224, 270	
			Δ at 6weeks		Δ at 6weeks
Week 6	mean	255±50	-4±18	*265±25	13±12
	median	252; IQR: 224, 287	0; IQR -20-11	*278; IQR: 234, 284	12; IQR: 7, 21
			Δ at 6 months		Δ at 6 months
Month 6	mean	*246±47	-13±12	*272±22	19±16
	median	*235; IQR: 215, 287	-16; IQR: -19, -2	*277; IQR: 258, 284	17; IQR: 8, 35

Table 8- 3 Epicardial LV ARI during steady rate RV pacing at day 0, 6 weeks and 6 months of CRT

Δ=changes compared with day 0. Data are expressed as mean±standard deviation and median and interquartile range (IQR). * where $p<0.05$ compared with day 0.

The paired changes in LVARI at 6 weeks and 6 months compared with day 0 among the responders and non-responders are shown in Figure 8-3. At 6 months the responders showed a significant decrease in ARI ($p = 0.043$) whereas conversely the non-responders showed a significant increase in ARI ($p=0.046$). These divergent effects were evident by 6 weeks although not reaching significance for the responders. Mean, median values and confidence intervals for the data are shown in Table 8-3.

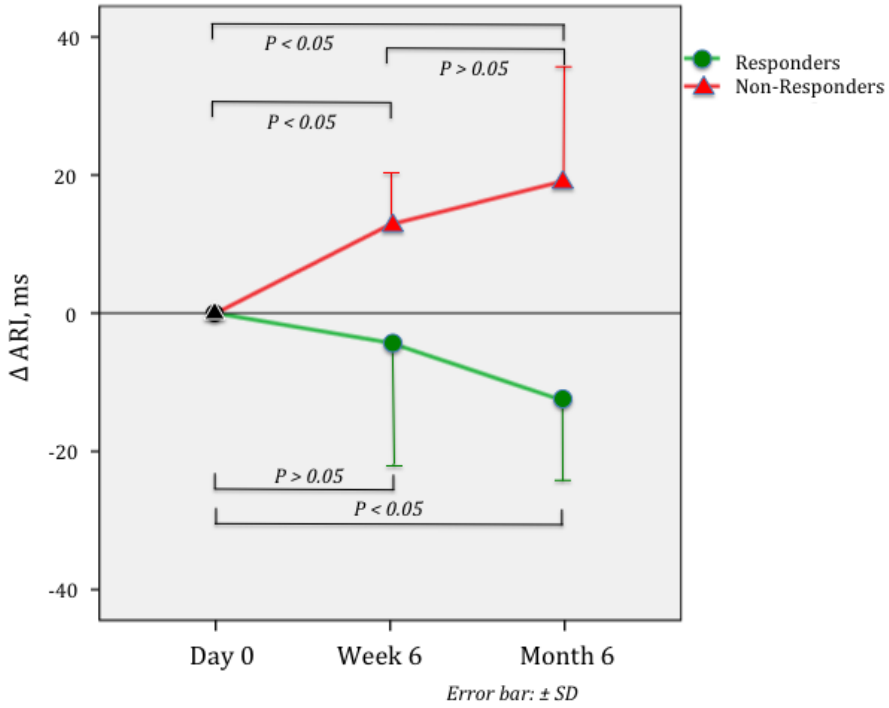

Figure 8- 3 Changes in regional left ventricular activation recovery intervals, ΔARIs, during right ventricular pacing at day 0, 6 weeks and 6 months post-cardiac resynchronisation therapies.

In Figure 8-4, changes in LVARI at 6 months compared with day 0 amongst the responders and non-responders are plotted against changes in LVEF response to CRT. The changes between the LV ARI and the changes in LV function were not linear. In the responders, the LV ARI during RV pacing decreased with an improvement in LV function however the LVARI increased in the non-responders despite insignificant changes in LV function.

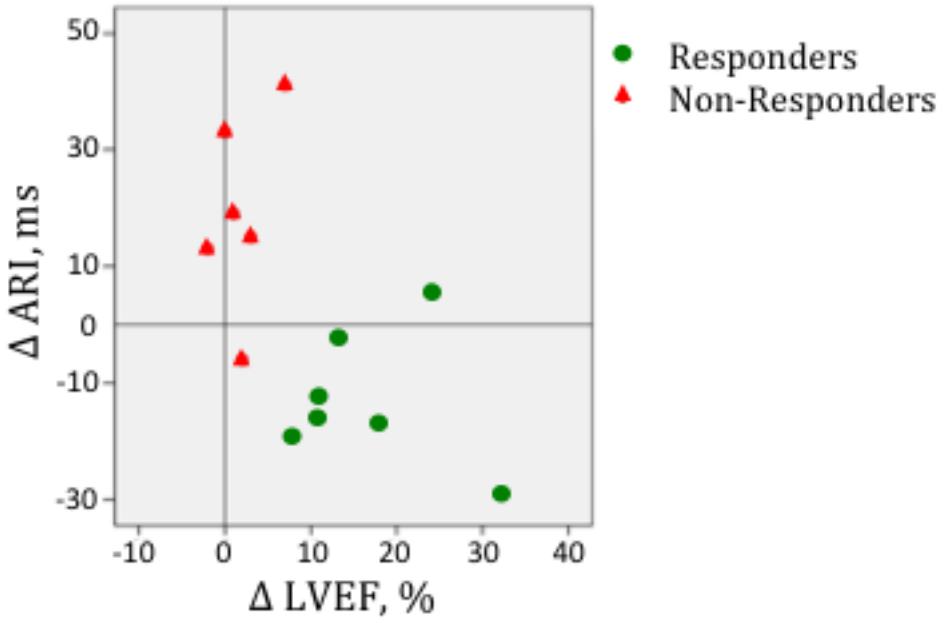

Figure 8- 4 Scatter plots of changes in LV ARI with changes in LVEF, from day 0 to 6 months post cardiac resynchronisation therapy

Post hoc power calculation showed that the study had a 95% power to detect a change in LVARI at 6 months post CRT between responders and non-responders at the 0.05 significance level.

8.5 Discussion

We have shown, for the first time, that LV APD (ARI) changes during CRT with APD shortening in responders and lengthening or remaining the same in non-responders to CRT. These changes appear to be coupled with positive reverse remodelling in the CRT responders. This supports the hypothesis that electrical remodelling accompanies the haemodynamic remodelling associated with CRT in heart failure patients with dyssynchrony.

8.5.1 Comparison with previous studies

Our results are in keeping with the observed APD shortening in the LV lateral wall after three weeks of resynchronisation therapy in a canine dyssynchrony heart failure model.[173] Recent human studies using ECG QT and T wave measurements have shown evidence suggestive of remodelling of APD associated with CRT in heart failure patients with dyssynchrony. Wecke et al. demonstrated an increase in repolarisation changes, measured by T-wave vectors and T-peak to T-end intervals, in the first two weeks of initiating CRT therapy treatment in heart failure patients with LBBB.[174] In a group of established responders of CRT, Braunschweig et al. demonstrated a transient initial increase followed by a sustained reduction of QT and JT interval following re-initiation of resynchronisation therapy.[175] Perhaps more comparable with the results of our study, Lellouche et al. observed a reduction in QT intervals in responders to CRT which was associated with a lower incidence of appropriate ICD therapies.[176] Our results also lend support to the *in silico* modelling of the adaptive effects of mechano-electrical coupling relationship in the dyssynchronous heart by Kuijpers et al.[177]

8.5.2 Mechanisms for APD changes

APDs are lengthened in the myocytes of the failing heart. The mechanisms underlying APD changes in heart failure and APD changes during CRT are at present unclear. A fairly consistent finding is a down-regulation of repolarising K^+ currents together with changes in depolarizing Na^+ and Ca^{2+} currents and calcium cycling.[65,173,178,179] Studies of animal models of heart failure have demonstrated that considerable heterogeneity exist in these changes.[180]

Dyssynchronous heart failure, as in the present patient cohort, is associated with regional variation in myocardial strain patterns; with low strain occurring in early activated antero-septal regions and high strain in late activated lateral posterior LV walls. In heart failure patients with LBBB, the lateral wall is usually the latest area of activation. This discordant contraction between the early and late activated segments increases the strain and workload of the late activated regions.[181,182] As a result there is an increase in the left ventricular preload, further stretching the myocardium leading to long term structural modelling. However mechanical dyssynchrony can also occur in the absence of intraventricular electrical delays. An animal study has demonstrated that simple changes in LV afterload by clamping the aorta can acutely induce dyssynchrony in the presence of normal ventricular electrical delays,[183] suggesting a close mechano-electrical coupling involved in the LV activation. Studies with canine dyssynchrony heart failure models have demonstrated APD shortening in the early activated low strain regions and APD prolongation in the late activated regions of high strain.[168,173] These observations suggest that the myocardium can respond to changes in stretch by altering its electrical properties through a process of mechano-electrical feedback.[168,173,184-186] This mechanism may be a trigger for the changes in APD seen with dyssynchronous heart failure and with its reversal through CRT. Jeyaraj et al.[16811] have suggested that this trigger may be mediated through intermediates including stretch activated non-selective ion channels,[187,188] cytoskeletal proteins,[189] and stretch activated signal transduction pathways.[190]

However, the observation that sarcolemmal ion channels and even individual potassium channels appear to be differentially regulated in models of heart failure suggests that multiple mechanisms may be involved.[173] CRT results in partial reversal of the electrophysiological consequences of heart failure including the down-

regulation of repolarising K^+ currents. This would be consistent with the shortening of APD at the lateral LV wall that we observed at 6 weeks and 6 months following the initiation of CRT in the responders. Our results are also in line with the APD shortening observed in an animal dyssynchrony heart failure model by Aiba and colleagues.[173]

The mechanisms of reverse electrical remodelling during CRT have yet to be fully elucidated. Several mechanisms have been proposed including reversal of the abnormal activation pattern, reversal of abnormal regional strain patterns, and a role for improved beta-adrenergic function. Considerable overlap is likely to exist between these multiple mechanisms that underlie remodelling and reverse remodelling. For example, mechano-electrical feedback and changes in electrotonic current load due to altered activation sequence are component of myocardial memory.[168] It is possible therefore that the memory function may play a role in our results. Varied coupling between these mechanisms in responders and non-responders may in part explain the non-linear relationship between the differential changes in action potential we observed in the responders and non-responders. It is worth noting there were a greater proportion of patients with ischaemic cardiomyopathy in the non-responder group. The regional scars may hinder both mechano- and electrical remodelling to CRT in patients with previous myocardial infarction. During device implant, LV leads were positioned outside scarred myocardium on the basis of electrical sensing parameters and prior knowledge of scar location identified from cardiac magnetic resonance imaging. Our study is underpowered to assess the influence of the ischemic aetiology on the changes in LVARI. However it would be of interest for future studies to combine with cardiac magnetic resonance imaging with scar geometry and examine the possible influence of scar on reverse remodelling.

Relation of electrophysiology to mechanical changes

Several mechanisms could underlie the parallel changes in APD and mechanical strain during CRT, and the differences between responders and non-responders.

(a) Mechano-electric feedback: In patients with heart failure and LBBB the lateral wall is usually the latest to be activated. The discordant contraction between early and late activate regions increases strain and work in late activated regions resulting in increased preload, further increased stretch and structural remodeling.[181,182] Canine models of myocardial dyssynchrony show APD changes with APD shortening in the early activated low strain regions and APD lengthening in the late activated high strain regions, suggesting the myocardium responds to stretch by altering the electrophysiology by MEC.[167,191] In humans, Kroon et al have recently demonstrated a good correlation between LV depolarization pattern and strain pattern in heart failure patients,[192] and our group has also found a similar correlation in heart failure patients with LBBB.[193]

The notion of MEC as a mechanism for functional remodeling and its reversal by CRT receives support from computer modeling studies highlighting a role of L-type Ca^{2+} current and calcium handling.[194] A number of studies have demonstrated changes in gene and protein expression resulting in abnormal calcium handling and distribution in dyssynchronous hearts.[169,173] In canines with dyssyncronous heart failure L-type Ca^{2+} current was 20% higher in early activated regions and 20% lower in late activated regions and CRT normalized the distribution of the calcium transient.[173] It has been suggested that feedback of external work on the L-type calcium current could represent a true feedback mechanism whereby regional

contractility of the myocardium is regulated in order to maintain or restore uniform mechanical load.[195] It has been proposed that changes in stress and strain may be sensed by the Z discs which modulate regulatory proteins of L type calcium channels.[196]

Our finding of divergent changes in responders and non-responders supports the hypothesis of a breakdown in the MEC amongst non-responders whereas the coupling relationship is maintained in the responder group. One plausible cause for this decoupling may be the presence or the extent of myocardial fibrosis as the presence of scar at the LV pacing sites adversely affects CRT response.[51],,

(b) Other mechanisms

A number of other mechanisms could be involved in reverse electrical remodeling during CRT. There is increasing evidence for a role of cardiac mitochondria in modulating calcium handling and the electrophysiology.[197] Changes in a variety of ionic currents have been observed in animal experiments following prolonged dyssynchony induced by ventricular pacing or LBBB, including L-type calcium current, several potassium currents (Ito, Ik1, Iks, Ikr), and calcium handling proteins.[173,179,198]

8.5.3 Significance of APD changes, impact on arrhythmogenesis

The effect of CRT on arrhythmogenesis remains controversial. It has been suggested on the basis of clinical and experimental evidence that CRT incorporating left ventricular epicardial pacing may promote rather than reverse electrical remodelling and be potentially proarrhythmic.[169,170,199-201] APD changes in heart failure are characteristically heterogeneous resulting in increased dispersion of repolarisation

which is potentially proarrhythmic. Biventricular pacing incorporating an LV epicardial lead reverses the normal activation sequence across the lateral LV wall. This has been shown in canine wedge preparations to result in increased dispersion of transmural repolarisation across the LV wall and be proarrhythmic.[169,170] Others have further demonstrated that in the canine dyssynchrony heart failure model, the trans-regional dispersion of APD occurs to a greater extent than the trans-mural dispersion of APD in response to dyssynchrony.[168,202] In a recent clinical study, increased dispersion of repolarisation measured by interlead difference in T-peak to T-end intervals were associated with a higher incidence of ICD therapies in patients with CRT.[203]

Reversal of APD lengthening by CRT has been shown experimentally to reduce dispersion and hence be potentially arrhythmia protective.[173] Interpreting our results in this context must remain speculative, as we have no evidence that APD at the lateral LV wall at the site of our recordings was actually prolonged as a result of heart failure. However, since it is well known that APD prolongation at the lateral LV wall is a consistent finding in heart failure we would suggest that APD shortening at this site in the responders would generate a more favourable anti-arrhythmia substrate profile. Conversely the APD lengthening that we observed in the non-responders would create a less favourable arrhythmia substrate. The observation that APD prolongs in non-responders despite insignificant changes in LV function and dimension suggests in the absence of positive reverse functional and structural remodelling, LV epicardial pacing may potentially be proarrhythmic.[169,170] This would be in keeping with clinical observations suggesting a reduced arrhythmia risk in responders to CRT[164,204] and an increased arrhythmic risk in non-responders.[199] It is possible the additional electrical remodelling that accompanies the structural and

functional remodelling observed in responders of CRT outweighs the initial pro-arrhythmic increase in repolarisation dispersion caused by LV epicardial and biventricular pacing.[175]

8.5.4 Limitations

Our study was limited, but was large enough to demonstrate significant result at 95% power. Due to a limitation of the device programmer we were only able to record unipolar electrograms from distal pole of the quadripolar lead; improved spatial mapping could be of interest for future studies. Though we did not have a measure of regional wall stress or strain in our study, previous studies have demonstrated CRT results in a more synchronous LV strain patterns in responders compared to non-responders.[45,46] Further study is needed to explore the regional strain pattern in the accompanying regions where we measured LV ARI in order to elucidate whether mechanical stretch or strain may be the trigger for our observed changes in APD. It has been shown that increased dispersion of repolarisation measured from body surface ECG leads varied between responders and non-responders. The ARI measured only reflected regional electrical activity at the site of the distal LV lead. It would be of interest to see how this regional change related to the global LV repolarisation time and dispersion. A much larger patient cohort with longer follow-up period is needed to achieve this and relate to the arrhythmic outcomes in these patients.

8.6 Conclusion

In patients with dyssynchronous heart failure left ventricular epicardial APD measured by ARI altered during CRT, the effect on APD was opposite in patients showing a positive echocardiographic remodelling response compared to non-responders. The findings may provide explanation to the persistent high incidence of

arrhythmias in some patients with CRT and the additional mortality benefit observed in responders of CRT.

Chapter 9. Coupling of ventricular action potential duration and local strain patterns during reverse remodeling in responders and non-responders to cardiac resynchronization therapy

This chapter describes the work built on the foundation outlined in chapter 8. Using the new technique (developed during the work described in the last chapter) of measuring regional activation recovery interval via LV pacing lead and coupling that with echocardiographic myocardial speckle tracking measurement of strain, the study assessed the relationship between the mechanical remodeling (regional strain) and electrical remodeling (regional APD) induced by CRT. This provides the evidence that suggests the two processes are linked.

9.1 Abstract

Background: Ventricular action potential duration (APD) changes in patients with dyssynchronous heart failure during cardiac resynchronisation therapy (CRT). Evidence suggests the electrophysiological effect may vary dependent on the myocardial contractile properties. We hypothesized that diverse APD changes occuring between responders and non-responders to CRT would correlate with similar diverse changes in regional myocardial strain.

Methods: ARI were recorded from the left ventricular epicardium in 20 CRT patients 6 weeks and 6 months post implant. Two-dimensional speckle tracking echocardiography was performed at the same time to assess myocardial strains. Patients with ≥15% reduction in end-systolic volume at 6-months were classified as responders.

Results: ARI reduced in responders, 263±46ms vs. 246±47ms, p<0.01; and increased in non-responders, 235±23ms vs. 261±20ms, p<0.01. Time-to-peak (TPS) radial, circumferential and longitudinal strains increased in responders (+41±27ms, +35±25ms, +56±37ms; p<0.01); and reduced in non-responders (-58±26ms, -47±26ms, -64±27ms; p<0.01). There was a non-linear correlation between changes in TPS and ARI (r≥0.70; p<0.01). Baseline QRS >145ms and QRS shortening with biventricular pacing was associated with ARI shortening during CRT.

Conclusions: Changes in ventricular wall mechanics predict local APD lengthening or shortening during CRT. Non-responders have a worsening of myocardial strain and local APD. Baseline QRS >145ms and QRS shortening on biventricular pacing identified patients who exhibited improvement in APD.

Key Words: Cardiac remodeling, cardiac resynchronisation therapy, mechano-electric feedback, activation recovery interval, action potential duration, myocardial strain

9.2 Introduction

Cardiac resynchronization therapy (CRT) has been demonstrated to provide symptomatic improvement, induce structural reverse remodeling and improve survival in heart failure patients with prolonged QRS durations.[66-68] However, approximately one third of patients do not derive benefit and the incidence of arrhythmias remains substantial.[36,43] The further understanding of the electromechanical changes during CRT therefore remains an important challenge.

The response to CRT in patients with broad QRS complex is generally considered to be multifactorial including QRS width, mechanical dyssynchrony, the presence of scar, lead position and the reversibility of advanced heart failure.[205] Several studies demonstrating the beneficial effects of CRT on LV remodeling have suggested that improvement of LV mechanical synchrony was the predominant mechanism,[206] while others have in addition focused on the molecular and cellular effects that it chronically induces.[173,207,208]

Numerous ion channels changes are associated with heart failure usually resulting in prolonged action potential duration (APD) and hence prolonged refractoriness together with slowed conduction.[173,207,208] Studies in a canine model of heart failure showed APD prolongation to be inhomogeneous occurring preferentially in the late activated lateral wall where circumferential strain was shown to be increased.[168] Aiba and colleagues have demonstrated APD prolongation in cells from late activated regions and detailed a range of cellular alterations involved in the remodeling process.[173] However, Spragg et al. found APD shortening in the late activated segment in dyssynchronous animal model in the absence of LV dysfunction.[186] Both APD and the abnormal strain pattern were partially normalized by CRT. As has been pointed out, these observations during CRT have been made in an animal model where chamber dilatation and dysfunction persist and therefore most likely represent the effect of dis-coordinated contraction that is resynchronized.[208]

Information in humans is limited. We have recently reported activation recovery interval (ARI), as a surrogate measure of APD, changes in heart failure patients during CRT, with LV free wall APD shortening in subjects classified as responders and lengthening in non-responders.[209] The clinical response to CRT is known to be closely linked to reversal of dyssynchrony.[210] Improved LV function by CRT has

been shown to be associated with a reduced arrhythmia burden,[211] whereas persistent or new radial dyssynchrony or abnormal longitudinal strain is associated with an increased rate of ventricular arrhythmias or death.[212,213] The effect of LV resynchronization on the electrophysiologic substrate is a suggested mechanism. However, at present it has not been determined whether changes in APD during CRT relate to changes in regional mechanical function in humans.

We aimed to explore the relationship between LV APD and strain following LV reverse remodeling in response to CRT. To assess this we recorded ARI from the epicardial CRT LV lead as a conventional measure of local APD together with speckle tracking analysis of regional ventricular strain at 6 weeks and 6 months following the initiation of CRT.

9.3 Methods

9.3.1 Study population and protocol

(See Chapter 3.2 for General patient selection criteria)

We prospectively studied 20 consecutive patients receiving CRT in our institution. All patients were invited to participate in the study in the pre-CRT assessment clinic. The selection criteria included drug refractory symptomatic heart failure with New York Heart Association (NYHA) class II-IV, impaired left ventricular ejection fraction (LVEF) $\leq$ 35% with a QRS duration $\geq$ 120ms.

Clinical status according to NYHA class and Minnesota heart failure questionnaires (MLHFQ) and echocardiographic measures of LV function were assessed pre and 6 months post CRT implant.

Simultaneous echocardiography and LV unipolar electrogram recordings were performed 6 weeks and 6 months post CRT implant to assess LV functional and electrical remodeling in response to CRT.

A positive LV functional response was defined by ≥ 15% reduction in LV ESV on TTE assessment coupled with improvement in clinical heart failure symptoms at 6 months post implant.

9.3.2 Functional remodeling assessed by transthoracic echocardiography

Transthoracic echocardiography were performed by independent operators who were blinded to the outcome of the electrical remodeling data, at baseline, 6 weeks and 6 months post implant.

(See Chapter 3.4 for General echocardiography methods)

Short axis and longitudinal images focusing on the AHA segment of LV lead position were acquired at 6 weeks and 6 months post CRT implant in preparation for off-line speckle tracking analysis in order calculate the time (gated from the onset of QRS body surface electrocardiography complex) to peak radial, circumferential and longitudinal strain of the respective myocardial segment (see Figure 9-1). Speckle-tracking analysis was performed using independent 2D Cardiac Performance Analysis software (TomTec, Unterschleissheim, Germany).

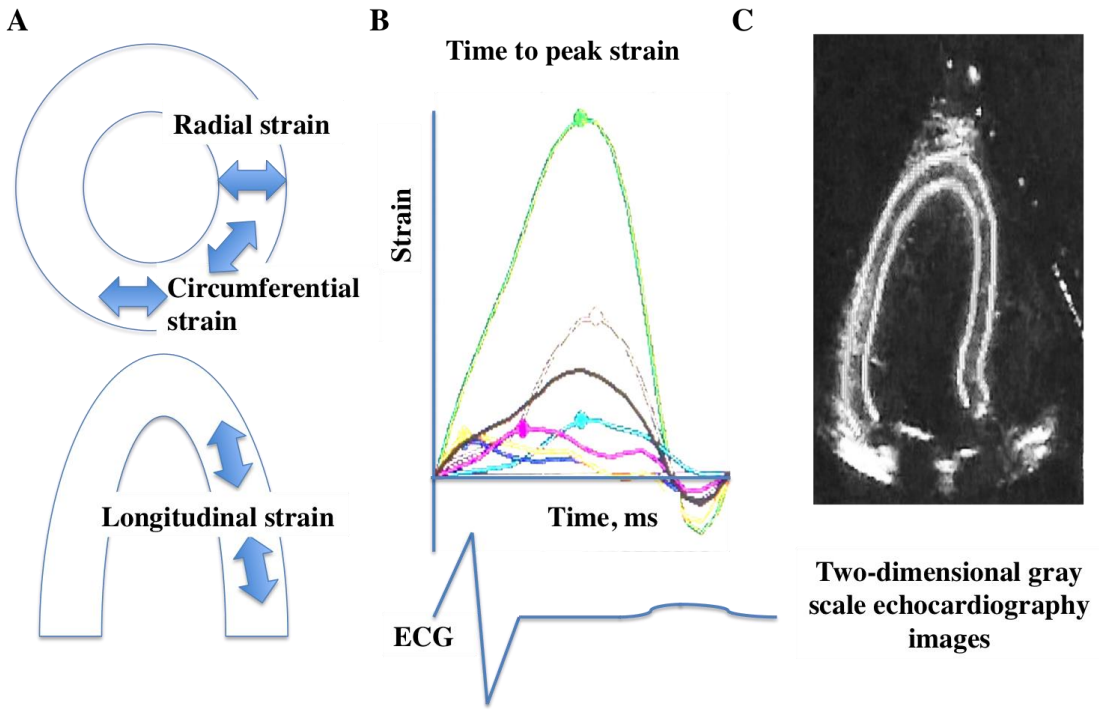

Figure 9- 1 Speckle tracking analysis

A: Different types of left ventricular myocardial strains during contraction

B: Strain curve with time to peak strain gated to ECG, different color represent different left ventricular segment (AHA classification)

C: Transthoracic echocardiographic grey scale images for automated speckle tracking analysis

CRT device optimisation was performed at 6 weeks post-implant as per our standard clinical protocol. At this time the AV and VV delays were adjusted under echocardiographic guidance using mitral valve inflow Doppler signals and aortic valve outflow velocity-time-intervals to achieve the best hemodynamic benefit.

Fluoroscopic image acquisitions in right and left anterior oblique views during CRT implant were used to estimate the LV segment where the LV lead was positioned for

each individual. Each segment was classified according to the American Heart Association 16 segment classification.

9.3.3 Electrical remodeling assessed by activation recovery interval, ARI, measurement

All 20 patients were implanted with a LV pacing lead via the coronary sinus (St. Jude Medical, Minnesota, USA). At 6 weeks and 6 months post CRT implant, a 30 second recording of the LV unipolar electrogram (UEG) signal was made via the device programmer (Merlin Patient Care System, Model 3650, St Jude Medical) during DDD-RV or VVI-RV pacing, depending on whether the patient was in sinus rhythm or in atrial fibrillation. In order to eliminate the influence of variable heart rate on ARI, UEG recordings were made after at least 2 minutes of pacing at a constant rate of 10 beats above the patient's intrinsic heart rate. This enabled comparisons between patients with sinus rhythm and those with atrial fibrillation at identical heart rate and eliminated the influence of heart rate on ARI. The 30 second LV UEG recordings were analyzed off-line using a custom software script within MATLAB (MathWorks, Massachusetts, USA) to derive the activation recovery interval (ARI). ARIs were measured using conventional validated criteria from minimum dv/dt of the QRS of the UEG to maximum dv/dt of the local T wave as previously described.[209] There were no changes in the LV pacing vectors and output stimulus strength in the patients between 6 weeks and 6 months post CRT implant. The LV pacing output strength was unchanged at 0.5ms pulse width for all patients during this period.

9.3.4 Statistical analysis

(See Chapter 3.6 for General statistical methods)

Correlation between time to peak strain and ARI were expressed using Spearman's correlation coefficient. A p value < 0.05 was considered to be statistically significant.

All statistics were performed using Prism version 6, (GraphPad software, California, USA)

9.4 Results

9.4.1 Study population

Twenty patients fulfilling standard indications for CRT[45] participated and completed the study. 25% of the cohort was female and mean age was 61±12yrs. All of the patients were in NYHA class III or IV. The mean QRS duration was 143±21ms, 45% of the patient had an ischemic etiology and 55% dilated cardiomyopathy on the basis of World Health Organisation criteria. The baseline characteristics of the patients including the positions of the LV leads are shown in Table 9-1.

	Responders	Non-responders	*P*
Patient, n	11	9	
Age, years	60±11	61±13	n/s
Female	3	2	n/s
COPD,	2	2	n/s
DM,	4	2	n/s
HTN,	3	2	n/s
CVA,	2	1	n/s
AF (persistent),	1	1	n/s
eGFR<60	2	5	n/s
Etiology: ICM/DCM	4/7	5/4	n/s
Beta blocker	11	8	n/s
Amiodarone	1	1	n/s
ACEI/ARB	11	9	n/s
Loop diuretics	6	7	n/s
MR antagonist	7	5	n/s
Statins	8	6	n/s
NYHA class II/III/IV	0/10/1	0/9/0	n/s
MLHFQ score	51±22	51±21	n/s
LVEF, %	23±9	22±4	n/s
LVESV, ml	177±87	173±50	n/s
QRS duration, ms	148±25	133±7	n/s
QRS morphology LBBB	11	9	n/s
LV lead positions			
basal/mid/apex	6/5/0	2/7/0	n/s
anterior/antero-lateral	2/1	1/2	n/s
infero-lateral/inferior	6/2	5/1	n/s
RV lead positions			
septum/apex	4/7	5/4	n/s
A-V delays, 120/130/140ms	4/5/2	4/4/1	n/s
LV>RV offset, 30/20/10/0	7/3/0/1	6/2/0/1	n/s
>25% transmural scar near LV pacing site	2	5	n/s
>50% transmural scar near LV pacing site	0	3	0.038

Table 9- 1 Baseline patient characteristics

ICM = ischemic cardiomyopathy; DCM = dilated cardiomyopathy; COPD = chronic obstructive pulmonary disease; AF = atrial fibrillation; CVA = cerebral vascular accident; ACEI = angiotensin converting enzyme inhibitor; ARB = angiotensin receptor blocker; LV= left ventricular; EF = ejection fraction; ESV = end-systolic volume; MR = mineralcorticoid receptor.

9.4.2 Left ventricular functional remodeling

At 6 months post CRT, LVESV reduction ≥15% occurred in 11 patients (55%), all of whom reported an improvement in heart failure symptoms (NHYA class reduction ≥ 1 class and quality of life questionnaires reduction of ≥20% in MLHFQ scores). These patients were considered to be positive responders with functional reverse remodeling. The mean LV ESV in the responders group improved from 177±87ml at the baseline pre CRT implant to 107±51ml ($p<0.01$) at 6 months post CRT. The mean LV EF improved from 23±9% to 36±11%. In contrast, the mean LV EF in the non-responders group was 22±4ml at the baseline and was 23±4ml at 6 months post CRT. The changes in clinical LV functional status between responders and non-responders at 6 months are shown in Table 9-2.

	Responders	Non-responders	P
Patient, n	11	9	
NYHA Class	2±1	3±0	P=0.01
Minnesota heart failure score	27±15	45±23	P<0.01
Δ LVEF, %	+13±7	+1±6	P<0.01
Δ LVESV, %	-37±15	+8±23	P<0.01

Table 9- 2 Clinical and LV functional response at 6 months

Δ = change; LVEF = left ventricular ejection fraction, LVESV = left ventricular end-systolic-volume, NYHA = New York Heart Association

9.4.3 Changes in LV electrical remodeling and time to peak strains

During the 6 months receiving CRT, all the patients (responders and non-responders) were paced via bipolar vectors (LV and RV). The pacing vectors and pacing outputs were not changed during the 6 weeks to 6 months post CRT implant study period. The percentages of the bi-ventricular pacing were the same between the two groups. There were no major differences between the optimized AV delays and VV delays between the responder and non-responders in the study cohort. Median AV delays were 130ms ±10ms and 130 ±10ms in the patients with sinus rhythm in the responders and non-responder groups. Variations in VV delays between responders and non-responders group were not significantly different.

LV UEGs were recorded during DDD-RV or VVI-RV pacing at a fixed heart rate ranged from 70bpm to 100 bpm within the cohort (the same heart rates were maintained during recordings at 6 weeks and 6 months for individual patients; paced heart rate of the two patients with atrial fibrillation were 75bpm and 80bpm, which were similar to the other patients in sinus rhythm, mean 80bpm). There was a clear divergent change in ARI seen between CRT responders and non-responders from 6 weeks to 6 months post CRT implant. In the responders ARI decreased from 263 +/- 46 to 246 +/-47 ($p<0.01$) whereas in the non-responders ARI increased from 235+/-23 to 261+/-20 ($p<0.01$). This trend is shown in Figure 9-2.

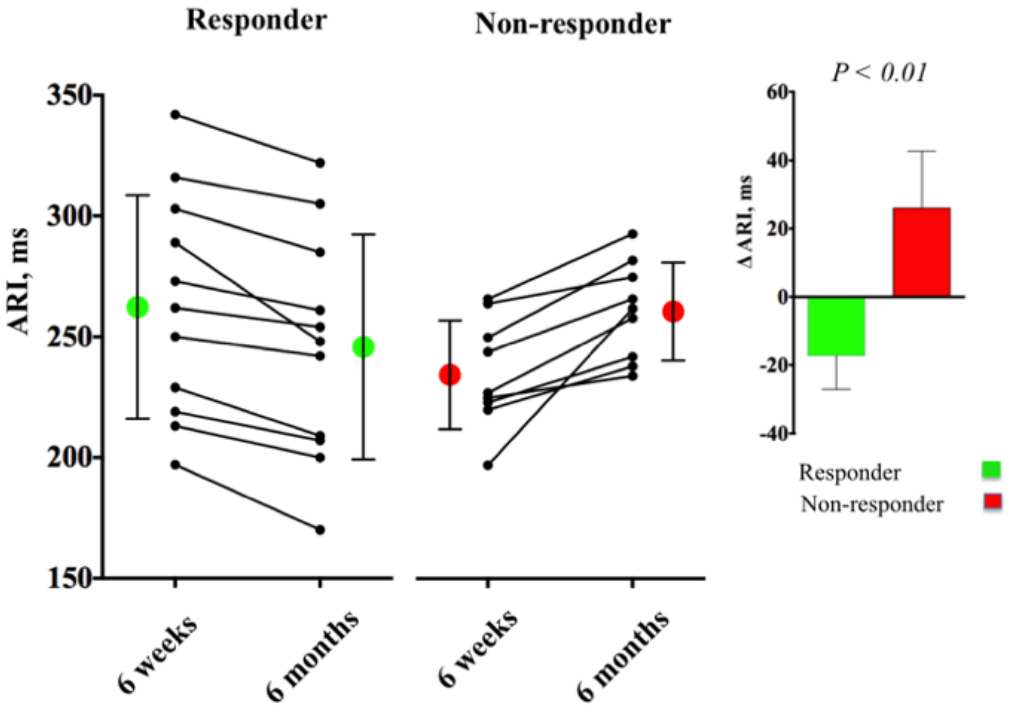

Figure 9- 2 Divergent changes in activation recovery interval ARI between 6-weeks and 6-months post CRT between responders and non-responders.

Δ = changes between 6weeks and 6months post CRT

The corrected QT (QTc, Bazett's correction) intervals averaged across all 12 surface ECG leads estimated by an electronic caliper were manually checked at 6-weeks and 6-months post CRT during RV pacing to allow comparison with ARI data. The trend of changes in QTc intervals reflected regional ARI measured in the responders and the non-responders. At 6 weeks, the QTc was 554±52ms (responders), 543±50ms (non-responders); and at 6 months 536±54ms, 558±49ms, respectively. The changes were Δ -17±14 for responders; and Δ +16±11 for non-responders, $p<0.01$. A weak correlation was observed between Δ ARI and Δ QTc, $r= 0.59$, $p <0.01$.

A similar divergent change was observed in TPS between the two groups with responders showing a decrease in TPS in radial, circumferential and longitudinal

strains between 6 weeks and 6 months of CRT and non-responders showing an increase. (See Figure 9-3 and Table 9-3). The mean values of LVARI at 6 weeks differed (263±46ms vs. 235±23ms), although not significantly different, p=0.12. The difference in ARI between the responders and the non-responders at the 6 weeks post CRT is reflected in the time to peak strain between the responders and the non-responders. A possible explanation for this perceived difference is the differences (although not statistically significant) in baseline QRS duration between the responders and the non-responders.

The LV ARI and times to peak strains during RV pacing at 6 weeks and 6 months post CRT are summarised in Table 9-3 and Figure 9-3.

Time, ms	Responders n = 11	Non-responders n = 9	p
6-week ARI,	263±46	235±23	
	Δ -17±10	Δ +26±17	<0.01
6-month ARI,	246±47	261±20	
6-week TPS radial,	375±59	311±34	
	Δ -58±26	Δ +41±27	<0.01
6-month TPS radial,	317±58	352±50	
6-week TPS circumferential	370±58	322±39	
	Δ -47±26	Δ +35±25	<0.01
6-month TPS circumferential	322±59	357±43	
6-week TPS longitudinal	397±61	333±31	
	Δ -64±27	Δ +56±37	<0.01
6-month TPS longitudinal	332±63	389±46	

ARI = activation recovery interval; TPS = time to peak strain.

Table 9- 3 ARI and time to peak strains (TPS) in responder and non-responder groups

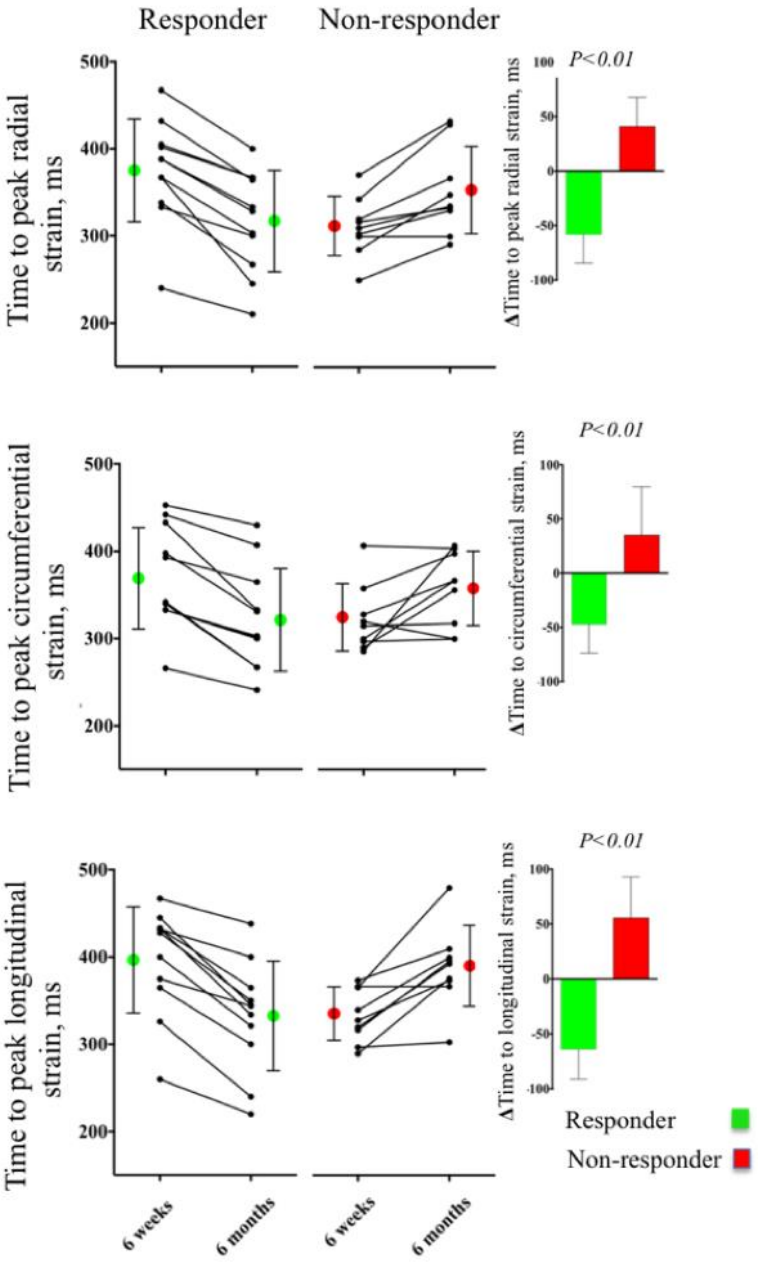

Δ = changes between 6weeks and 6months post CRT; Rad. = radial strain; Circ. = circular strain; Long. = longitudinal strain; ARI = activation recovery time, ms, Strain = % myocardial displacement

Figure 9- 3 The LV activation recovery times and times to peak strains during RV pacing at 6 weeks and 6 months post CRT

9.4.4 The relationship between changes in ARI and changes in TPS

Although for each of the strain measures (radial, circumferential and longitudinal strain), shortening during CRT was associated with APD shortening and vice-versa, the relationship between ARI local strain and TPS was likely to be non-linear (Spearman correlation coefficient 0.72 radial; 0.70 circumferential; 0.71 longitudinal strain). Nevertheless whether local strain increased or decreased indicated whether APD shortened or lengthened with a high degree of sensitivity and specificity. See Figure 9-4.

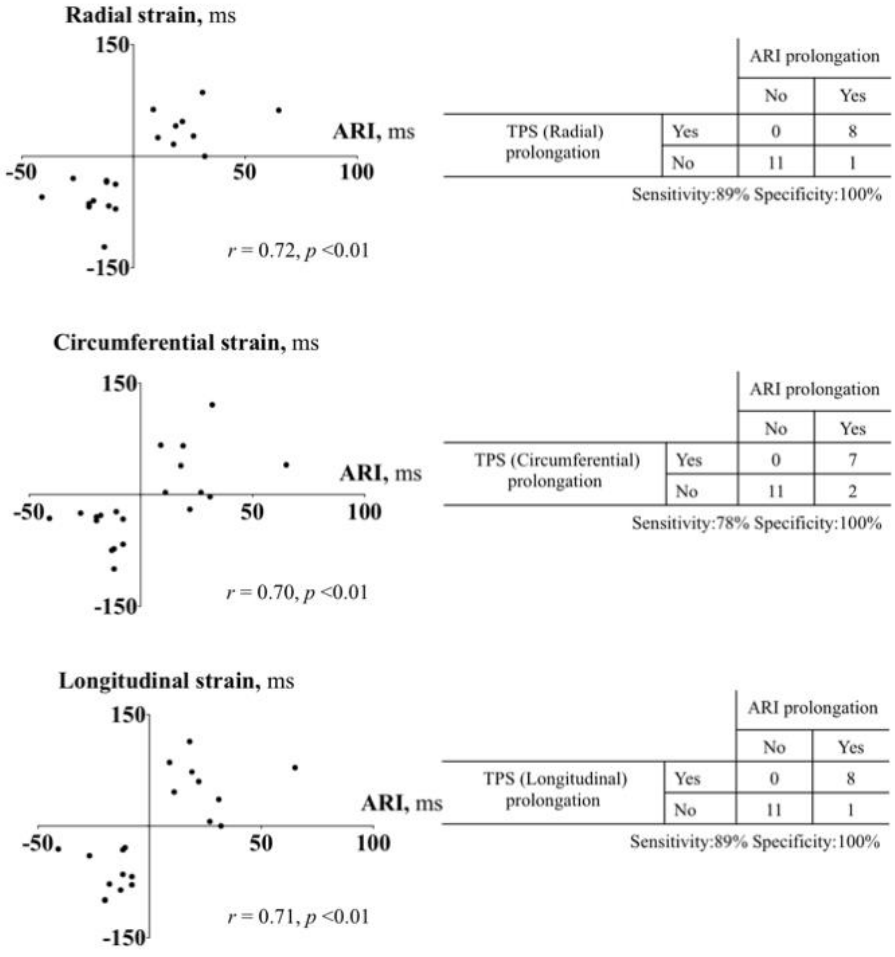

		ARI prolongation	
		No	Yes
TPS (Radial) prolongation	Yes	0	8
	No	11	1

Sensitivity:89% Specificity:100%

		ARI prolongation	
		No	Yes
TPS (Circumferential) prolongation	Yes	0	7
	No	11	2

Sensitivity:78% Specificity:100%

		ARI prolongation	
		No	Yes
TPS (Longitudinal) prolongation	Yes	0	8
	No	11	1

Sensitivity:89% Specificity:100%

r = Spearman's correlation coefficient

Figure 9- 4 Correlation between changes in activation recovery time (ARI) and changes in time to peak strain (TPS)

9.4.5 *Changes in ARI and QRS duration*

The relation between changes in ARI during CRT and baseline QRS duration is shown in Figure 9-5 (upper panel). Above a QRS duration of 145ms ARI shortened during CRT in all patients whereas patients with a baseline QRS below 145ms showed either ARI shortening or lengthening. Changes in ARI in relation to the effect of biventricular pacing on the QRS duration (i.e. difference in QRS duration during biventricular pacing vs. baseline QRS), are shown in Figure 9-5 (lower panel). A QRS decrease during biventricular pacing was associated with ARI shortening whereas a QRS increase was associated with either ARI shortening or lengthening.

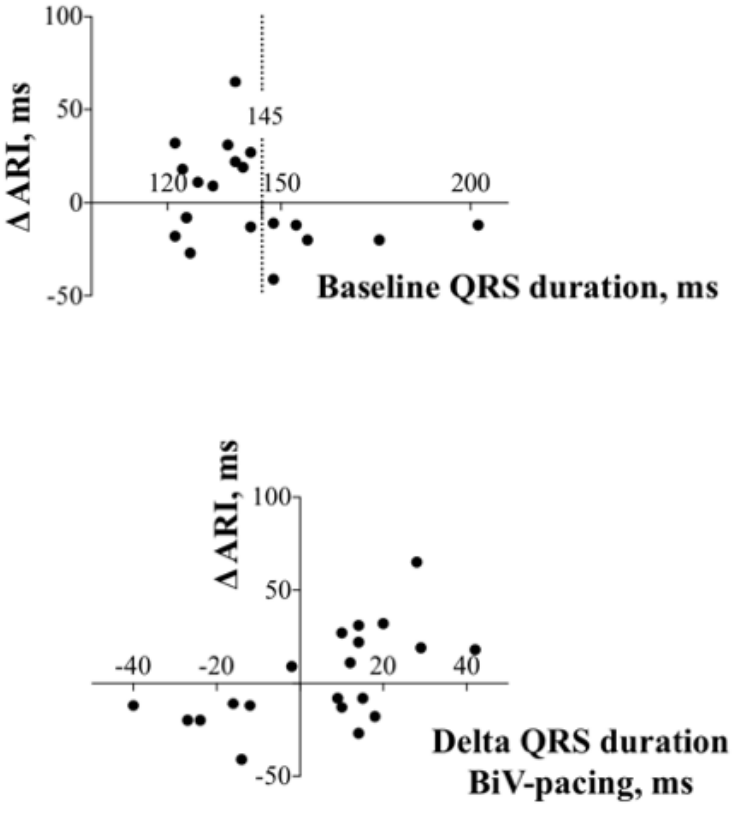

Figure 9- 5 Relationship between changes in activation recovery interval ARI and baseline QRS duration and CRT paced QRS duration

9.5 Discussion

The main findings of our study are: (1) patients with heart failure receiving CRT classified as responders exhibit LV ARI shortening in the late activated region, whereas non-responders show ARI lengthening confirming our previous observations; (2) ARI shortening was associated with local decrease in time to peak radial, circumferential and longitudinal strain, whereas ARI lengthening was associated with an increase in all three strain patterns; (3) non-responders have a worsening of local myocardial strain and prolongation of local ARI; (4) the relationship between changes in ARI and changes in local strain patterns was non-linear; (5) a baseline QRS of 145ms separated patients in whom ARI and local strain decreased (>145ms) from patients in whom ARI and local strain either decreased or increased (<145ms) in response to CRT; (6) a decrease in QRS duration during biventricular pacing compared to baseline was associated with ARI shortening in response to CRT, whereas an increase in QRS duration was associated with either ARI shortening or lengthening.

Comparison with previous work

9.5.1 Electrophysiology

A consistent finding in experimental models of heart failure is ventricular action potential duration prolongation.[65] In a canine model with LBBB ablation, cells isolated from the LV lateral wall after 6 weeks showed APD prolongation which was attenuated by CRT.[173] In humans several studies using body surface ECG measurements have reported repolarization changes during CRT. Braunschweig and colleagues found an initial increase in QT and JT interval followed by a sustained reduction in a group of responders.[175] Lellouche and colleague compared the peak to end of T wave and corrected QT measurements at the time of CRT implantation and

after 1 year, and observed a decrease in responders and an increase in QT dispersion and T wave peak-to-end dispersion in non-responders.[176] We recently reported APD shortening in responders and APD lengthening in non responders during CRT in patients with heart failure using ARI recordings from the LV epicardial free wall.[209]

9.5.2 Mechanical strain pattern

While the mechanism underlying reverse electrical remodeling during CRT in heart failure is considered to be multifactorial a general consensus is that LV mechanics play an important role.[173,205-208] Canine models of myocardial dyssynchrony show APD changes with APD shortening in the early activated low strain regions and APD lengthening in the late activated high strain regions.[167,191] In humans, Kroon et al have recently demonstrated a good correlation between LV depolarization pattern and strain pattern in heart failure patients,[192] and our group has also found a similar correlation in heart failure patients with LBBB.[193] Several studies have investigated the effect of CRT on LV mechanics. Strain patterns have been shown to improve in CRT in responders with lesser changes or worsening in non-responders.[214]

At the present time we are unaware of any previous report on the relationship between APD and regional wall mechanics in humans. In the present study we showed concordance between the change in APD and the change in strain pattern during CRT. However, the relation between delta APD and delta strain was not linear. Such a relationship would be consistent with the interaction of dyssynchronous contraction with the electrophysiology being multifactorial resulting in ion channel remodeling involving stretch activated receptors, gap junctions via connexins, calcium handling, beta adrenergic responsiveness, mitochondrial function, fibrosis and other changes.[173,205-208]

9.5.3 Relation of electrophysiology to mechanical changes

APD prolongation, particularly in the late activated lateral wall, is a consistent manifestation of heart failure and may contribute to the substrate for ventricular arrhythmias. Changes in all three strain patterns identified whether APD would lengthen or shorten during CRT with a high degree of sensitivity and specificity (Figure 9-4). Therefore an increase in regional strain would indicate a likely worsening of APD. If this effect were inhomogeneous it would favor re-entry arrhythmia. The prolongation in ARI observed in the non-responders may provide an explanation for the potential harmful effects of CRT in patients with narrow baseline QRS duration.[215] Conversely, improvement in strain pattern has been shown to be an independent predictor of CRT response in terms of long-term outcome including death and hospitalization.[216]

The trend of changes in QTc intervals appears to reflect that of regional ARI measured in the responders and the non-responders. Our results are in keeping with prior findings that QTc interval shortened amongst the responders to CRT.[176] However the weak association between the ARI and QTc reflects that ARI is a local measure of repolarization unlike the QT interval which is a global measure. Other mechanisms in addition to changes in local strain may contribute to the global electrical remodeling following CRT.

Above a baseline QRS duration of 145ms all patients showed APD shortening during CRT whereas below QRS of 145ms patients showed either shortening or lengthening (Figure 5). These electrophysiological changes lend support to the current recommendation for heart failure patients with baseline QRS ≥150ms to receive CRT. In our data a shortening of QRS during biventricular pacing compared to baseline was associated with APD shortening and a lengthening of QRS was associated with either

APD shortening or lengthening. This is in keeping with findings of other studies.[217,218] Bonakdar and colleague also found baseline QRS >145ms to be an independent predictor of CRT response with the best sensitivity and specificity.[218]

In the studied cohort, I observed that above a baseline QRS duration of 145ms ARI shortened during CRT in all patients whereas patients with a baseline QRS below 145ms showed either ARI shortening or lengthening. A QRS decrease during biventricular pacing was associated with ARI shortening whereas a QRS increase was associated with either ARI shortening or lengthening. This implies that in patient with broad baseline LBBB QRS and its reversal with CRT, there is sufficient electrical resynchrony and as a result positive electrical remodeling as reflected the local ARI shortening. The narrower QRS duration with CRT is a reflection of inter- and intra-ventricular synchrony, which is largely determined by the RV-LV transeptal time. The lack of QRS shortening with CRT coupled with ARI prolongation in the non-responder group is a reflection of adverse electrical remodeling. LV epicardial may further exacerbate adverse electrical remodeling through a reversal of electronic gradient across myocardium, increasing dispersion of repolarization, especially in patient cohort with narrower baseline QRS.

9.5.4 Methodological considerations

ARI has been extensively theoretically and experimentally validated as a reliable surrogate for local APD.[79] Unlike other measures of repolarization ARI has the advantage of providing local information in contrast to the QT interval and avoids the proarrhythmic risk of premature stimulation during estimation of refractory periods. Two dimensional speckle tracking echocardiography has been shown to be effective and simple in providing useful insights to the mechanics of myocardial contraction. Based on standard grey scale images, strain defined by percentage change of the

myocardial fiber length from its relaxed state in end systole is used to quantify myocardial deformation.[219]. Speckle tracking echocardiography has certain advantages compared with tissue velocity imaging and is an accurate way of indexing the complex ventricular contraction motions with radial, circumferential and longitudinal strain measurements.[220]

I did not specifically study any beat-to-beat dynamic variations in AT and ARI. I ensured a steady rate of pacing for two minute before taking ARI measurement in order to eliminate the influence of variable heart rate on ARI. Our research group however did investigate the effects of respiratory oscillation (at a frequency approximately at 0.25Hz) and arterial pressure oscillation (at a frequency of approximately 0.1Hz, coupled with synchronous oscillations of sympathetic nerve activity) on ventricular APD in heart failure patients. We found that ARI oscillated with the respiratory frequency in all heart failure patients, but only oscillated with the arterial pressure frequency in a third of heart failure patients with mental arousal (through provocative visual stimuli). These finding may help to understand the role of sympathetic activity-related arrhythmogenesis.

9.5.5 Limitations

The study cohort is relatively limited in number, but has sufficient power (>95%) to detect a change in LV remodeling based on the data gathered previously.[209] The device programmer only enables recordings of unipolar electrograms to be made from the distal pole of the LV lead, consequently limiting to single site recordings. It has been shown that increased regional dispersion of repolarization varied between responders and non-responders.[168,203] It would be of interest to see how this regional change related to the global LV repolarization time and dispersion as depending on the extent of the region exhibiting the changes; there might be either pro- or

antiarrhythmic effects. We are unable to comment on the initial response because no LV strain measurements were acquired immediately after CRT implant due to clinical constraints of patient discomfort. Anatomical features such as regional scars may alter local stress / strain relations and influence the remodeling process. The present study however was not designed to assess the influence of pathogenesis on the ARI.

Regional scars at the site of the LV lead implant has been shown to impact on the response to CRT. This has been the focus on several prior studies.[49,50,58] I did not make a direct comparison between the locations of the scar and the proposed qualitative scar assessment indices and their association with CRT response for two reasons. Firstly, in the present study correlation analysis between scar location and LV lead position showed that none of the LV pacing segment had evidence of focal LGE≥ 50% of myocardial wall thickness. This is because given the prior clinical efforts and with the benefit of scar information on CMR prior to device implant, conscious efforts were made by the implanter to avoid regions of high scar burden. This however precluded us to make the same analysis on impact of scar location as previously studied. Secondly, our study cohort consisted both ischemic cardiomyopathy and non-ischemic cardiomyopathy patients. The pattern and distribution of scar are distinct between these two cohorts. ICM typically has segmental scar in the distribution of coronary artery territories that extend from an endocardium to epicardium direction. In comparison, the scar pattern seen with DCM can be patchy, diffuse, mid-myocardial and epicardial in distribution on LGE image. The co-correlation of two distinct scar patterns with aetiology is likely to create confounder in the regression analysis.

9.6 Conclusions

Cardiac resynchronization therapy in heart failure patients with dyssynchronous LV electromechanical activation sequence resulted in LV epicardial APD shortening in CRT responders and APD lengthening in non-responders. Changes in regional ventricular wall mechanics, i.e. radial, circumferential and longitudinal strain patterns predicted local APD shortening or lengthening during CRT. Baseline QRS duration and change in QRS between baseline and biventricular pacing could identify patients showing APD shortening during CRT.

Chapter 10. Focal but not diffuse myocardial fibrosis burden quantification using cardiac magnetic resonance

imaging predicts left ventricular reverse modeling following cardiac resynchronisation

The prior studies have demonstrated a close coupling between the electrical and mechanical remodeling processes secondary to CRT. As myocardial scar can have a structural and functional impact on the remodeling process, I aimed to prospectively assess the prognostic value of quantitative scar assessment using CMR in predicting reverse remodeling to CRT in dyssynchronous heart failure patients

10.1 Abstract

Background: Many heart failure patients with dyssynchrony do not reverse remodel (RR) in response to cardiac resynchronisation therapy (CRT). The presence of focal and diffuse interstitial myocardial fibrosis may explain this high non-response rate. T1 mapping is a new cardiac magnetic resonance imaging (CMR) technique that overcomes the limitations of conventional contrast CMR and provides reliable quantitative assessment of diffuse myocardial fibrosis. The study tested the hypothesis that focal and diffuse fibrosis quantification would correlate with a lack of left ventricular (LV) RR to CRT.

Methods: In a prospective study of 48 consecutive patients (27 ischemic cardiomyopathy, 21 dilated cardiomyopathy) LV scar burdens were quantified (scar core and grey zone using late gadolinium enhancement LGE CMR; interstitial fibrosis using T1 mapping) before CRT implant. LV RR was defined by a ≥ 15% reduction in LV end-systolic volume 6 months post implant.

Results. Twenty-seven (56%) patients were responders with RR. Association between scar quantification and LV RR were assessed using Poisson regression model. Univariate analysis showed that QRS duration/morphology, scar core and grey zone volumes expressed as % of LV mass and extracellular volume index (ECV) (a measure of interstitial fibrosis from T1 mapping) to be significant predictors of LV RR. Multivariable-adjusted analyses demonstrated scar core quantification (≥13.7% LVmass) to be the only independent predictor of LV RR (Prevalence ratio 0.40, p=0.038).

Conclusions: Focal scar burden detected by LGE CMR is associated with a poor response to CRT. Diffuse interstitial fibrosis assessment by T1 mapping however is not independently predictive of CRT response.

Key words: fibrosis; T1 mapping; cardiac resynchronisation therapy; reverse remodeling

10.2 Introduction

Since the first reported case of cardiac resynchronisation therapy (CRT) two decades ago, it has established its effectiveness, improving morbidity and mortality in selective heart failure patients with evidence of dyssynchrony.[43] Prolonged QRS duration (QRS_d), usually manifests as left bundle branch block (LBBB) are the recommended criteria in patient selection for CRT.[44] However responder rates vary between half to two-thirds in reported cohorts, with left ventricular remodeling response (LV RR) rate being much lower than clinical response rate.[46] One

explanation for this high non-response rate may be the presence of focal and diffuse interstitial myocardial fibrosis, which can disrupt the concordance between mechanical and electrical dyssynchrony mediated through lines of structural and functional block thus attenuating the effect of CRT.

Cardiac magnetic resonance imaging (CMR) using late gadolinium enhancement (LGE) is the gold standard for the non-invasive assessment of myocardial regional fibrosis. Regional scar imaging with LGE is well known to be associated with a poor response to CRT especially if there is postero-lateral scar at the usual site of LV lead placement.[49] Patients with heart failure may however have more diffuse myocardial fibrosis which is not imaged using LGE-CMR that may be associated with a diminished response to CRT. Myocardial tissue characterisation using T1 mapping is a new CMR technique with the potential to overcome the limitations of conventional LGE-CMR and provide reliable quantitative assessment of diffuse myocardial fibrosis on a standardised scale.[159]

We hypothesised that diffuse myocardial fibrosis assessment on a quantitative scale may contribute to the selection of patients prior to CRT implant and identify those less likely to demonstrate volumetric response. We therefore tested the hypothesis that diffuse fibrosis detected by CMR would correlate with a lack of LV RR in patients with ischemic and non-ischemic dilated cardiomyopathies (ICM, DCM) receiving CRT. The ability of diffuse fibrosis to predict non-response was also tested against the burden of scar core and scar border zone i.e. grey zone (an area of admixture of viable myocardium and scar) detected by conventional LGE CMR in this cohort.

10.3 Methods

10.3.1 Study population and protocol

(See Chapter 3.2 for General patient selection criteria)

We undertook a prospective study of 48 consecutive patients undergoing CRT pre-assessment clinic in our institution.

Clinical status according to NYHA class and Minnesota living with heart failure questionnaires (MLHFQ) were assessed at pre- and 6 months post-CRT implant.

Trans-thoracic echocardiographic (TTE) assessment of cardiac structure and function were assessed at the same consultation as the clinical assessment, using a GE Vivid 7 scanner (General Electric-Vingmed, Milwaukee, Wisconsin). Standard 2-dimensional images of LV dimensions and ejection fraction (EF) were acquired during breath-hold in standard apical 2- and 4-chamber views. LV end-diastole and end-systole volumes (EDV, ESV) were used to estimate LVEF using the 2-dimensional modified biplane Simpson's method (EchoPac 0.0.1, General Electric Vingmed).

Cardiac magnetic resonance imaging protocol

(See Chapter 3.3.1 for General CMR methods protocol)

All patients underwent CMR assessment on the same day as their TTE, prior to their CRT implant.

10.3.2 Quantitative scar measurement

Focal fibrosis quantification using LGE CMR

Two independent CMR experts blinded to the study outcome visually assessed LGE CMR images. In case of discrepancy, these experts jointly reviewed the data to reach a consensus.

Patient specific LV mass was quantified using dedicated software CMR42 (Circle Cardiovascular Imaging Inc., Calgary, Canada) and used to index the LGE quantification, representing myocardial focal scar burden. The extent of LGE was quantified using the 2-standard deviation (2SD) method, defined as the region with signal intensity (SI) 2SD above the remote reference myocardium, i.e. $Scar_{-2SD}$. The full-width-half-maximum (FWHM) method, defined as the region with SI above the 50% of the maximal SI of the enhanced area was used to quantify the scar core, i.e. $Scarcore_{-FWHM}$. The extent of grey zone was quantified by the difference in SI between $Scarcore_{-FWHM}$ and $Scar_{-2SD}$, i.e. $Greyzone_{-2SD\text{-}FWHM}$. Each of these indices was expressed as a percentage of the LV mass (%LV).

Diffuse interstitial fibrosis quantification

We chose a region of interest (ROI) in the septum for estimation of $T1_{-Native}$, post-contrast T1 ($T1_{-Contrast}$) and ECV, as previously described.[72] Care was taken to avoid the endocardium/blood pool interface. If regional enhancement was seen in the septum on the LGE image a ROI was chosen away from the enhanced region for analysis. The geometry of the T1 map slice was the same as that of the LGE images to allow for this comparison. $T1_{-Native}$ <1000ms were considered to be the normal reference in our institution (1.5T scanner with a 32–channel coil, Philips Healthcare, Best, Netherlands). Blood tests were taken 1-2 hours immediately post CMR for estimation of patients' hematocrit levels.

The T1 derivative, extracellular volume index (ECV), was calculated as using the following formula:

$$ECV = (1 - \text{hematocrit}) \times \left(\frac{\frac{1}{\text{Post-contrast T1myocardium}} - \frac{1}{\text{Pre-contrast T1myocardium}}}{\frac{1}{\text{Post-contrast T1blood}} - \frac{1}{\text{Pre-contrast T1blood}}} \right)$$

Device implant

All patients underwent CRT implant successfully. The LV lead was preferentially targeted in a postero-lateral, lateral or anterolateral branch at the discretion of the operator and the confines of patient-specific anatomy; with a pacing site preferentially chosen in a position more basal than apical and away from regions of scar seen on CMR and to ensure optimal pacing parameters.

10.3.3 Outcome measure – LV RR

At 6 months post implant, a positive LV RR was defined as ≥ 15% reduction in LV ESV on TTE assessment and improvement in patient clinical heart failure symptoms by ≥1 NYHA class and ≥20% reduction in MLHFQ scores.

10.3.4 Statistical analysis

(See Chapter 3.6 for General statistical methods)

The univariate and multivariate associations between pre-specified variables of interest and outcome (LV RR) were examined using Poisson regression model with robust standard errors estimation.

This was used to avoid overestimation of the risk ratio by odds ratio in view of the high prevalence of positive outcome.[221]

All reported associations in this study were prevalence ratios (PR) and their corresponding 95% confidence intervals (CI). Moreover, to avoid spurious associations due to the inclusion of correlated variables in a single model, the multivariate analysis studied each of the LGE CMR and T1 mapping derived indices separately, thus limiting the maximum number of variables to four in a single multivariate model.

Intra- and inter-observer assessments of T1 values were assessed for reproducibility. The differences in repeated continuous variables measurements were expressed as mean ± SD and coefficient of variation (COV), and the correlation assessed using Pearson correlation coefficient (*r*). All data analyses were performed using SPSS statistical software (version 21, IBM, New York, USA)

10.4 Results

10.4.1 Study population

Forty-eight patients fulfilling class I and II indication guidelines for CRT[45] participated and completed the study, 17% were female, the mean age was 65±11 years, 92% of the patients were in NYHA class III and the mean QRS_d was 139±26ms. Significant mechanical inter- and/or intra-ventricular mechanical dyssynchrony were demonstrated in all patients with tissue Doppler imaging. Twenty-two patients had "strict" LBBB, defined by QRS≥140ms for men / ≥130ms for women and mid QRS notching/slurring in ≥ 2 contiguous leads. On the basis of World Health Organisation criteria 56% of subjects had an ischemic etiology. The baseline characteristics including focal and diffuse scar quantification are shown in Table 10-1 with patients categorised as ICM or DCM. There were no significant differences in terms of pre-implant baseline characteristics in terms of QRS duration/morphology and heart failure symptoms. Baseline LVEF was lower in the DCM group. Notably at baseline the ICM had higher levels of regional fibrosis although this was not statistically significant; 27/27(100%) of ICM patients had LGE vs. 19/21(90%) of DCM patients; scar core burden as a percentage of the LV was non-significantly higher in ICM (14±6 vs. 10±9, p=0.094). In terms of diffuse fibrosis quantification, there was no significant

difference between the ICM and DCM cohorts in the measured T1 indices ($T1^{-Native}$, $T1^{-Contrast}$ and ECV).

	Whole cohort	ICM	DCM	P
N (%)	48	27 (56)	21 (44)	
Age, years	66 ±12	68 ±9	64 ±14	0.486
Female,	8 (17)	6	2	0.437
COPD,	8 (17)	4	4	0.715
DM,	14 (29)	8	6	1.000
HTN,	17 (35)	9	8	0.769
CVA,	4 (8)	2	2	1.000
AF (persistent),	10 (21)	3	7	0.081
eGFR<60	24 (50)	14	10	1.000
Beta blocker	47 (98)	26	21	1.000
ACEI/ARB	47 (98)	26	21	1.000
Loop diuretics	37 (77)	21	16	1.000
MR antagonist	27 (56)	15	12	0.776
NYHA class				0.160
II	3 (6)	3	0	
III	44 (92)	24	20	
IV	1 (2)	0	1	
MLHFQ score	51 ±22	50 ±23	51 ±20	1.000
LVEF, %	24 ±8	27 ±6	22 ±8	0.011
LVESV, ml	173 ±84	156 ±61	189 ±108	0.388
QRS_d, ms	139 ±26	136 ±25	142 ±26	0.512
QRS_m "strict" LBBB	22	12	10	1.000
Presence of LGE	46 (96)	27	19	0.077
$Scarcore^{-FWHM}$, %LV	12 ±8	14 ±6	10 ±9	0.094
Greyzone $^{-2SD-FWHM}$, %LV	8 ±5	9 ±4	7 ±7	0.112
$T1^{-Native}$, ms	1060 ±78	1048 ±72	1075 ±83	0.262
$T1^{-Contrast}$, ms	419 ±72	428 ±54	407 ±91	0.117
ECV	0.32 ±0.06	0.32 ±0.06	0.32 ±0.06	0.925

Table 10- 1 Baseline patient characteristics

ICM = ischemic cardiomyopathy; DCM = dilated cardiomyopathy; COPD = chronic obstructive pulmonary disease; AF = atrial fibrillation; CVA = cerebral vascular accident; ACEI = angiotensin converting enzyme inhibitor; ARB = angiotensin receptor blocker; LVEF = left ventricular ejection fraction; LVES = left ventricular end-systolic volume; QRS_d =

QRS duration; QRS_m = QRS morphology; FWHM = full width half maximum; SD = standard deviation; ECV = extracellular volume index; MR = mineralcorticoid receptor

10.4.2 Outcome measure

At 6 months post CRT, LVESV reduction ≥15% occurred in 27 patients (56%), all of whom reported an improvement in heart failure symptoms, assessed by NHYA class (reduction ≥ 1 class) and quality of life questionnaires (a reduction of ≥20% in MLHFQ scores). These patients were considered to be positive responders with reverse remodeling. The mean LV ESV in the responder group was 180±69mls at baseline which improved to 146±47 ml ($p<0.01$) 6 months post CRT. Amongst the 21 patients who failed to demonstrate LV RR, 9 patients reported an improvement in clinical symptoms with an improvement in at least 1 NYHA class and ≥20% improvement in quality of life score giving a symptomatic response rate of 75%. The patient characteristic separated by responder demonstrating LV RR and non-responders are shown in Table 10-2. There were no significant differences in terms of LV lead position using a modified clock-face method in left anterior oblique and right anterior oblique projection taken with fluoroscopy at the time of lead implant as previously described.[222] Despite efforts of avoiding scarred segments by the operators during LV lead implants, 5 patients (3 non-responders, 2 responders, $p = 0.641$) had ≥ 50% transmural focal LGE in close proximity of the LV pacing site. Biventricular pacing percentage was comparable between responders and non-responders (96±4% and 97±2% respectively) at the time of 6 months follow-up.

	Non-responder	Responder	P
N	21	27	
Etiology: ICM/DCM	14/7	13/14	0.248
Age, years	63±14	68±9	0.323
Female	3	5	1.000
COPD,	3	5	1.000
DM,	7	7	0.750
HTN,	7	10	1.000
CVA,	2	2	1.000
AF (persistent),	2	8	0.152
eGFR<60	15	9	0.019
Beta blocker	21	26	1.000
ACEI/ARB	20	27	0.438
Loop diuretics	15	22	0.498
MR antagonist	8	19	0.040
NYHA class*			0.092
II	3	0	
III	18	26	
IV	0	1	
MLHFQ score *	50±21	51±22	0.780
LVEF, % *	25±7	23±8	0.486
LVESV, ml *	154±103	183±68	0.478
QRS_d, ms	129±22	146±26	0.031
QRS_m, "strict" LBBB	5	17	0.009
Scarcore $^{-FWHM}$, %LV	16±8	9±7	0.002
Greyzone $^{-2SD-FWHM}$, %LV	11±4	7±6	0.002
T1$^{-Native}$, ms	1071±77	1051±79	0.271
T1$^{-Contrast}$, ms	406±71	430±73	0.304
ECV	0.34±0.06	0.30±0.06	0.043

Table 10- 2 Characteristics of responder vs. non-responders

ICM = ischemic cardiomyopathy; DCM = dilated cardiomyopathy; QRS_d = QRS duration; QRS_m = QRS morphology; FWHM = full width half maximum; SD = standard deviation; ECV = extracellular volume index; MR = mineralcorticoid receptor

* Baseline measurement.

10.4.3 Characteristics of responders

QRS duration was significantly greater in the responder group versus the non-responder group (146±26ms vs.129±22ms, P=0.031). The prevalence of "strict" LBBB was markedly higher in responders (63% vs. 24%, P=0.009).

Focal fibrosis and diffuse fibrosis quantification with CMR:

The responder group had a significantly reduced regional scar burden with a smaller scar core and grey zone– expressed as a percentage of LV mass compared to non-responders (Scar$_{-FWHM}$: 9±7% vs. 16±8, p=0.002; and Greyzone$_{-2sd\text{-}FWHM}$: 7±6 vs. 11±4%, p=0.002). None of the LV pacing segment had evidence of focal LGE ≥ 50% of myocardial wall thickness.

In terms of diffuse fibrosis assessment, T1$_{-native}$ and T1$_{-contrast}$ were not statistically different in responders and non-responders (1051±79 vs. 1071±77ms, p=0.271; and 430±73 vs. 406±71, p=0.304). ECV was lower in the responders group (0.30±0.06 vs. 0.34±0.06, p=0.043) suggesting a lesser degree of diffuse interstitial fibrosis in the responders.

10.4.4 Predictors of response

The association between the variables of QRS, focal and diffuse fibrosis quantifications and the LV RR were assessed using Poisson regression model. Univariate analysis demonstrated a significant association between 1ms increment in QRS duration and presence of "strict" LBBB in relation to positive LV RR. Percentage increment in Scarcore^{-FWHM} and ECV were negatively associated with LV RR. The results of the univariate analyses are shown in Table 10-3.

Variables	Prevalence ratio	Confidence intervals	P
QRS_d, +1ms	1.01	1.00-1.02	0.009
QRS_m "strict" LBBB	2.01	1.18-3.35	0.011
$Scar^{-FWHM}$, +1%LV	0.94	0.89-1.00	0.010
$Greyzone^{-2sd\text{-}FWHM}$, +1%LV	0.94	0.89-1.00	0.074
$T1^{-Native}$, +10ms	0.98	0.95-1.02	0.427
$T1^{-Contrast}$, +10ms	1.02	0.99-1.05	0.206
ECV, +1%	0.96	0.92-1.00	0.028

QRS_d = QRS duration; QRS_m = QRS morphology; FWHM = full width half maximum; SD = standard deviation; ECV = extracellular volume index

Table 10- 3 Univariate analyses

Receiver operator curve analysis identified optimal cut-off values for focal and diffuse fibrosis indices in order to predict LV RR in the study cohort. These cut-off values were then used to dichotomise the focal and diffuse fibrosis indices and tested in multivariate analyses including QRS variables in the total patient cohort. $Scarcore^{-FWHM}$ using a thresholding value of ≥13.7% of the LV was shown to be the only significant independent variable associated with LV RR with a PR 0.39 (p=0.029), suggesting a strong negative predictor of LV reverse remodeling. The results from the multivariate analyses and Forest plot of the PR for each variable and are shown in Figure 10-1.

Variables	Prevalence ratio	Confidence intervals	P
QRS_m "strict" LBBB	1.35	0.79-2.29	0.272
$Scar^{-FWHM}$ ≥13.7%LV	0.40	0.17-0.95	0.038
$Grayzone^{-2SD-FWHM}$ ≥9.1%LV	0.48	0.23-1.01	0.053
$T1^{-Native}$ ≥1060ms	0.66	0.43-1.00	0.055
$T1^{-Contrast}$ ≥400ms	1.17	0.76-1.78	0.480
ECV ≥32%	0.77	0.46-1.31	0.486

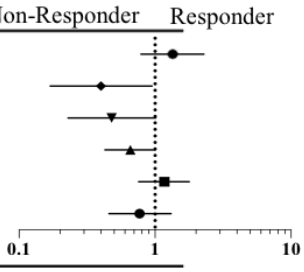

* In order to avoid spurious associations due to the inclusion of correlated variables in a single model, the multivariable adjusted analysis studied each of the T1derived indices separately. QRS_m "strict" LBBB but not QRS_d was included in the multivariate analyses because the definition of "strict" LBBB has already included QRS duration into consideration (≥140ms for men / ≥130ms for women). This is to avoid potential confound effect in the analyses due to correlation between these variables.

Figure 10- 1 Multivariate analyses*

10.4.5 Reproducibility of T1 measurements

T1 measurements were repeated in a subgroup of randomly selected patients from the study cohort (10 ICM and 10 DCM). For $T1^{-native}$ measurement, the intra-observer average difference in values was 5±3ms, coefficient of variation (COV) was 0.3±0.2%; the inter-observer average differences in values were 6±5ms and COV was 0.4±0.3%. For $T1^{-Contrast}$ measurement, the intra-observer average difference in values was 5±4ms and COV was 0.8±0.6%; the inter-observer average differences in values were 5±4ms and COV was 0.9±0.7%. There were good agreements in inter and intra-measurements of native T1 and contrast T1 (Pearson's r = 0.99; p≤0.01).

10.5 Discussion

We assessed whether regional myocardial scar characterisation and diffuse fibrosis quantification was able to predict LV volumetric response to CRT.

The main findings of the current study in a prospective cohort of patients with both ICM and DCM undergoing CRT are as follows:

1) CRT responders had a significantly reduced focal scar burden with a smaller scar core and grey zone (expressed as % of LV mass) compared to non-responders. Scar core burden of ≥13.7% of the LV was a strong independent negative predictor of LV RR to CRT in a combined cohort of ICM and DCM patients.

2) Diffuse fibrosis assessment with $T1^{-native}$ and $T1^{-contrast}$ was not statistically different in responders and non-responders (1051±79 vs. 1071±77ms, p=0.271; and 430±73 vs. 406±71,p=0.304). ECV, was lower in the responder group (0.30±0.06 vs. 0.34±0.06, p=0.043) but was predictive of response only in univariate analysis

10.5.1 Comparison with previous studies

Heart failure patients with ischemic etiology tend to benefit less from CRT than patients with DCM. Prior studies have demonstrated that total scar burden (without differentiating between scar core and grey zone) is lower in CRT responders defined by clinical functional status rather than LV volumetric response.[50] Long-term prognosis after CRT has been shown to correlate with LV RR rather than clinical symptomatic response.[57] Prior studies that assessed LV volumetric responses to CRT have focused on scar burden at the LV lead pacing site.[49,51,58] Our results confirm these previous findings and further show that regional scar differentiation with focal scar core burden quantification from LGE images assessed before CRT implant is a

strong independent negative predictor of LV RR even when compared with "strict" LBBB morphology.

To our knowledge the current study is the first to assess the prognostic value of T1 mapping and its derived indices (ECV) in predicting volumetric response to CRT. The presence of diffuse fibrosis is overlooked in routine clinical CMR studies due to the inherent limitation of conventional LGE CMR technique. It requires the nulling of apparently "normal" myocardium in order to provide contrasting image signal intensities to highlight the region of focal scar represented by gadolinium enhancement. The degree of transmurality in LGE has been shown to correlate with contractile improvement after revascularisation suggesting that the greater proportion of surviving myocardium the greater the capacity for the myocardium to recover.[59] Measures of diffuse interstitial myocardial fibrosis may likewise represent a measure of viable/recoverable myocardium.

10.5.2 Diffuse fibrosis assessment

In order to address the clinical need for better myocardial tissue characterisation, native T1 and ECV are the two indices that have been the main focus of clinical research interest. The derivation of ECV from native, post contrast myocardial/blood T1 values and haematocrit level is based on an important assumption that the contrast concentration reaches equilibrium between blood and tissue. It has been well validated against histological measures of interstitial fibrosis and has been shown to be a sensitive and robust measurement of collagen volume fraction, whereas post contrast T1 is more susceptible to contrast kinetics.[223] Native T1 removes the dependence of contrast kinetics and has been shown to be a valid biomarker of changes in extracelluar volume and matrix composition.[224] It is a relative simpler measurement making its translation to clinical practice attractive. However we must

exercise caution in interpreting the native T1 value because though we speculate it reflects similar changes based on its accordance with the trend observed with post-contrast T1 and ECV, others has failed to find a significant difference in non-contrast T1 value between the regions with and without LGE in the septum in patients with HCM or DCM.[154] Furthermore, a stronger correlation of native T1 with impaired myocardial energetics measured by magnetic resonance spectroscope than with LGE suggests that native T1 may additionally reflect intracellular metabolic state associated with myocardial disease.[153]

10.5.3 Clinical implications

Given that the burden of scar core, i.e. homogeneously non-viable myocardium, is ubiquitously high amongst advanced heart failure patients, the assessment of the remaining viable tissue may play an important role in predicting the capacity of the LV to positively remodel with CRT. ICM typically has segmental scar in the distribution of coronary artery territories that extend from an endocardium to epicardium direction. In comparison, the scar pattern seen with DCM can be patchy, diffuse, mid-myocardial and epicardial in distribution on LGE image. The presence of focal fibrosis detected by LGE in our DCM cohort appeared to be higher than previous studies which focused on the presence of mid-wall fibrosis.[112,225] The presence of mid-wall fibrosis has been shown to have a strong correlation with long-term mortality and morbidity in DCM patients and lack of RR post CRT.[225] Past studies that assessed the association between scars detection by LGE CMR and CRT response have largely focused on the locations of LGE scars i.e. its presence at the site of LV lead implant.[49,50,58] In practice, LV lead placement is mostly dictated by coronary venous anatomy and electrical parameters. So dictating the precise site of LV lead implant according to LGE sites from CMR in order to influence CRT

response is sound in theory but often not always practical. The results of the current study suggest that global LV diffuse scar quantification does not predict volumetric response to CRT in a cohort combined of ICM and DCM.

10.5.4 Limitations

Although this was the largest clinical study to date to address the importance of extracellular volume mapping with CMR for the response to CRT, we acknowledge the fact that the study may be underpowered given the sample size. Nevertheless this is a real world prospective study of consecutive patients undergoing CRT at our institution. The optimal thresholding values for the scar and T1 mapping indices should be taken in the context of the study and a larger population study is needed to validate these optimal thresholding values. T1-mapping was limited to a single slice of myocardium and the assumption is made that diffuse fibrosis imaged is truly diffuse/uniform in the remote myocardium. Notably T1-mapping was performed not at the site of myocardium where the LV lead is sited. This "selective" sampling may be biased against ECV measurement when "whole heart ECV" have been showed to best correlated with collagen volume fraction.[226] Knowledge of the degree of diffuse fibrosis at the site of LV lead placement may be of importance and should be addressed in further studies. The absolute T1 values of interest can be influenced by a number of technical parameters including magnetic field strength and acquisition sequence as well as post-acquisition image processing including motion correction and image registration. Conducting a single center study allowed standardisation of the imaging protocol across the entire cohort, however it may have introduced systematic bias including the timing of post-contrast T1 measurement. A multicenter study with a larger sample would be of great value to further assess our findings.

10.6 Conclusion

We have systematically characterised and quantified the burden of scar core and grey zone from conventional LGE CMR images and the degree of interstitial fibrosis using T1 mapping technique in predicting LV volumetric response to CRT. Our results confirm that focal scar burden detected by LGE CMR is associated with a poor response to CRT. CMR markers of diffuse interstitial fibrosis were not however predictive of CRT response. This finding may have an important bearing on patient selection for CRT and requires further investigation in large scale studies.

Chapter 11 Conclusion

The over all aim of this thesis is to assess whether quantitative left ventricular myocardial fibrosis assessment using cardiac magnetic resonance imaging can

1) predict the risk of ventricular arrhythmia and provide additional predictive value in identifying patients with increased risk of VT in both ischaemic and non-ischaemic cardiomyopathy (ICM, NICM) patients;
2) predict reverse remodeling following CRT in dyssynchronous heart failure patients.

11.1 Original contributions

The proceeding chapters in this thesis have demonstrated that these primary aims have been achieved.

1. Chapter 5 has shown for first time that quantitative myocardial tissue assessment using T1 mapping is an independent predictor of ventricular arrhythmia with a hazard ratio comparable to scar or grey zone quantification detected by conventional LGE-CMR in both ischemic and non-ischemic cardiomyopathies.

2. Chapter 10 has systematically characterised and quantified the burden of scar core and grey zone from conventional LGE CMR images and the degree of interstitial fibrosis using T1 mapping technique in predicting LV volumetric response to CRT. The results confirm that focal scar burden detected by LGE CMR is associated with a poor response to CRT. CMR markers of diffuse interstitial fibrosis were not however predictive of CRT response.

In the course of setting up the prospective clinical outcome study, other exploratory studies have also made original contributions.

3. Chapter 4 revealed some of the important limitations T1 mapping in terms of imaging acquisition and data analysis. It demonstrated that pre-contrast and post-contrast T_1 maps derived from MOLLI and more specifically the R_1 ($^{1}/_{T1}$) and $r\Delta R_1$ ($^{R1,pre\ -\ R1,post}/_{R1,pre}$) values could be used for characterisation of different myocardial tissue sub-types in patients with ischaemic cardiomyopathy. There was a suggestion that $r\Delta R_1$ was best at distinguishing different tissue sub-types in ischaemic cardiomyopathy.

4. Chapter 5 has shown for the first time that HybridPAWS can reliably improve respiratory navigator efficiency and shorten scan time during high-resolution isotropic 3D LGE-CMR. However suboptimal motion compensation may still affect the image quality without the freedom of real-time correction.

5. Chapter 6 provided new insights into the prediction of VT circuits using a biophysical model. Patient-specific spatial heterogeneity of restitution properties were the distinguishing features of ventricular arrhythmogenicity, with re-entrant VT exit points present in regions of higher maximum APD-RC slopes compared with the surrounding tissue. These regions were within the grey zone identified by LGE CMR. Personalised biophysical model was able to predict macroscopic VT circuits and exit point locations in agreement with clinically observed datasets.

6. Chapter 8 and 9 have shown for the for the first time, that LV APD (ARI) changed during CRT with APD shortening in responders and lengthening or remaining the

same in non-responders to CRT. The opposite changes in APD in responders *vs.* non-responders were strongly correlated with similar changes in regional myocardial strain. These findings were consistent with a role of MEC in ventricular remodeling in patients with heart failure. This supported the hypothesis that electrical remodelling accompanies the haemodynamic remodelling associated with CRT in heart failure patients with dyssynchrony.

11.2 Clinical perspective, implications and limitations

At present, international guidelines for selecting patients for ICD or CRT do not include myocardial scar quantifications. Evidences from the studies described in the current thesis support the notion that scar quantification by CMR may add incremental prognostic value to the current selection criteria.

Regional myocardial fibrosis, conventionally detected by LGE-CMR provides potential substrate for the initiation and maintenance of ventricular arrhythmia. Myocardial tissue characterisation using T1 mapping has emerged as a new CMR application, which has the potential to overcome the limitations of conventional LGE-CMR techniques and characterise diffuse fibrosis. The current study demonstrated that an incremental increase in non-contrast native T1 measurement (a marker of diffuse fibrosis) is independently associated with the incidence of ventricular arrhythmia in patients with ICD. The study also provided further confirmation that the extent of scar and grey zone derived from LGE-CMR are independently associated with ventricular arrhythmia, and highlights the importance of grey zone in patients with NICM. Such CMR applications have the potential to improve risk

stratification in selecting patients for ICD therapy and may be particularly useful for the primary prevention group in whom there is considerable risk heterogeneity.

Given that the burden of scar core, i.e. homogeneously non-viable myocardium, is ubiquitously high amongst advanced heart failure patients, the assessment of the remaining viable tissue may play an important role in predicting the capacity of the LV to positively remodel with CRT. ICM typically has segmental scar in the distribution of coronary artery territories that extend from an endocardium to epicardium direction. In comparison, the scar pattern seen with DCM can be patchy, diffuse, mid-myocardial and epicardial in distribution on LGE image. The presence of mid-wall fibrosis has been shown to have a strong correlation with long-term mortality and morbidity in DCM patients and lack of remodelling post CRT.[225] Past studies that assessed the association between scars detection by LGE CMR and CRT response have largely focused on the locations of LGE scars i.e. its presence at the site of LV lead implant.[49,50,58] In practice, LV lead placement is mostly dictated by coronary venous anatomy and electrical parameters. So dictating the precise site of LV lead implant according to LGE sites from CMR in order to influence CRT response is sound in theory but often not always practical.

The association between myocardial scar and ventricular arrhythmia is long recognised, however the relationship between the two and the mechanism by which one contribute to another remains clear-cut. Though the number of clinical subjects studied in order to validate the computational VT modeling is small, the initial results nevertheless support the notion that personalised computational model incorporating both scar (from CMR scar imaging) and electrical parameters can help us to gain insights to this relationship. The study showed that patient-specific spatial heterogeneity of restitution properties were the distinguishing features of ventricular

arrhythmogeneicity, with re-entrant VT exit points present in regions of higher maximum APD-RC slopes compared with the surrounding tissue. These regions were within the grey zone identified by LGE CMR.

This implies that scar heterogeneity has a major influence to the functional and electrical remodeling of the ventricle. Heart failure is associated with mechanical and electrophysiological remodeling. A consistent feature of importance in arrhythmogenesis is ventricular APD prolongation. CRT is associated with anatomic and electric reverse remodeling. Using ARI as a surrogate measure of APD from the left ventricular epicardial lead of a CRT device at intervals during the first 6 months after implantation, we found that in patients with dyssynchronous heart failure, left ventricular APD changed during CRT. APD shortened in responders with clinical improvement and lengthened or remained the same in non-responders to CRT. This supports the hypothesis that electric remodeling accompanies the reverse remodeling associated with CRT in heart failure patients with dyssynchrony. The effect on APD was the opposite in patients showing a positive echocardiographic remodeling response compared with non-responders. These findings may provide an explanation for the persistent high incidence of arrhythmias in some patients with CRT and the additional mortality benefit observed in responders of CRT.

I acknowledge that there is currently a lack of standardisation of quantitative myocardial tissue assessment with CMR in clinical practice and we are limited by our continuing understanding of this emerging T1 mapping technique. The initial research into the clinical applications of T1 mapping has focused on post-contrast T1 values. Iles *et al.* first demonstrated a correlation between post-contrast T1 values with a quantitative histological measure of fibrosis, CVF, in patients with heart failure of various aetiologies.[93] Lower post-contrast T1 values were correlated with a higher

histological percentage of collagen and associated with worsening diastolic function markers detected by transthoracic echocardiograph. Recently, in a larger cohort of forty-five patients with cardiomyopathies of mixed aetiologies, most of whom had evidence of diffuse fibrosis on histology, Sibley *et al.* also found that post-contrast T1 values had a significant correlation with histological measure of fibrosis.[147] Ng *et al.* also found lower global post-contrast T1 correlated with diastolic dysfunction in diabetic patient free of coronary artery disease and regional fibrosis.[116] Sparrow *et al.* showed that segmental post-contrast T1 values were increased in regions with impaired wall motion in a small number of patients with chronic aortic regurgitation.[227]

T1 measurements can also be performed in regional fibrosis caused by scar post myocardial infarction. Messroghli *et al.* found lower post-contrast T1 values in the infarct region compared with non-infarct region in acute and chronic myocardial infarction.[7] Increases in the interstitial space can also be caused by processes such as the protein deposition in amyloidosis and Maceira *et al.* found an association of lower subendocardial post-contrast T1 in patients with amyloidosis compared with controls.[228] However the application of T1 measurements in these areas with regional changes is potentially problematic because the derived ECV measurement relies on the prerequisite of a two-compartment model with contrast equilibrium between the blood and the myocardium. An assumption is made that there is a constant myocardial plasma volume fraction, reflecting homogeneous capillary density in the myocardium, which is not necessarily the case in conditions such as amyloidosis and replacement fibrosis post myocardial infarction.

It was recognised early on that converse to post-contrast T1, non-contrast T1 is higher in infarct regions compared with non-infarct regions in ischemic cardiomyopathy.[8,9]

Though still susceptible to the influence of acquisition sequence and magnetic field strength, native non-contrast T1 can remove the dependence on contrast kinetics and avoid the potential of contrast associated nephrogenic systemic fibrosis. In two separate studies, Puntmann *et al.* and Dass *et al.* have both recently demonstrated a significant higher non-contrast T1 values in hypertrophic cardiomyopathy (HCM) and non-ischemic dilated cardiomyopathy (NIDCM) compared with normal controlled group with T1 mapping acquired on 3Tesla scanners.[153,154] Dass *et al.* not only noticed a difference between regions with LGE, but also regions without LGE, in the cardiomyopathy group and the normal control group. Both studies suggest the potential implication of non-contrast native T1 being a useful biomarker in detecting diffuse disease in cardiac pathologies. Puntmann *et al.* further demonstrated a higher non-contrast native T1 in systemic lupus erythematous patients with normal myocardial function, implying that native T1 mapping can be a sensitive detector of subclinical myocardial disease.[229][21] Indeed, Karamitsos *et al.* found a higher non-contrast T1 value in patients with amyloid light-chain (AL) amyloidosis in the absence of definitive cardiac manifestations.[156] The scale of T1 value correlated with markers of cardiac systolic and diastolic function. Others have found non-contrast native T1 value to be useful for assessing areas of myocardial oedema in Takotsubo cardiomyopathy and quantifying areas-at-risk in acute myocardial infarction, comparable with the conventional T2 weighted images.[230-232] In a systematic analysis and an attempt to establish a normal reference range of non-contrast T1 values acquired with ShMOLLI on 1.5T scanner (a cohort of 342 healthy volunteers, 50% females, age 11-69), Piechnik *et al.* found the non-contrast T1 to be a highly reproducible and stable biomarker for characterizing the myocardium.[233]

Given the reported correlation of non-contrast native T1 with disease pathology, we must however be cautious in interpreting the value of native T1. We know that T1 increases with increased water content. We therefore speculate that the increase in native non-contrast T1 is due to an expansion of extracellular volume and change in extracellular matrix composition. This assumption seems to be in accordance with the trend observed with post-contrast T1 and ECV, for example Scholz *et al.* demonstrated a correlation between T1 with the amount of free water content and collagen in canine hearts.[234] Bull et al also found a correlation between native T1 with CVF on histology samples from patients with moderate and severe aortic stenosis.[224] This however may not be the complete picture. Puntmann *et al.* did not find a significant difference in non-contrast T1 value between the regions with and without LGE in the septum in patients with HCM or NIDCM[154] and Dass *et al.* found a stronger correlation of non-contrast T1 with impaired myocardial energetics measured by magnetic resonance spectroscope than with LGE, suggesting that non-contrast T1 may additionally reflect intracellular metabolic state associated with myocardial disease.[153]

11.3 Future directions

Like with any emerging technique, we can only explore the potentials of T1 mapping through a better understanding of its limitations. Though, differences in T1 mapping acquisition sequences and protocols make the absolute T1 values difficult to compare across studies, the evidence presented so far shows great promise for T1 mapping in becoming another cornerstone in the clinical application of CMR, but it needs to be performed in rigorous conditions with accurate post-processing registration in order to

improve its efficacy. Larger cohort studies are needed to establish the "ideal" thresholding values of diffuse and regional fibrosis to enable the translation of non-invasive myocardial fibrosis quantification using LGE-CMR and T1 mapping to the clinical management of patients at risk of life threatening arrhythmias or predicting CRT positive response.

These threshold levels can then be tested prospectively to quantify an "area-at-risk". The thresholding mapping can be generated through an automated image process algorithm pipeline (Figure 11-1) to improve reproducibility and shorten processing time to aid clinical translation.

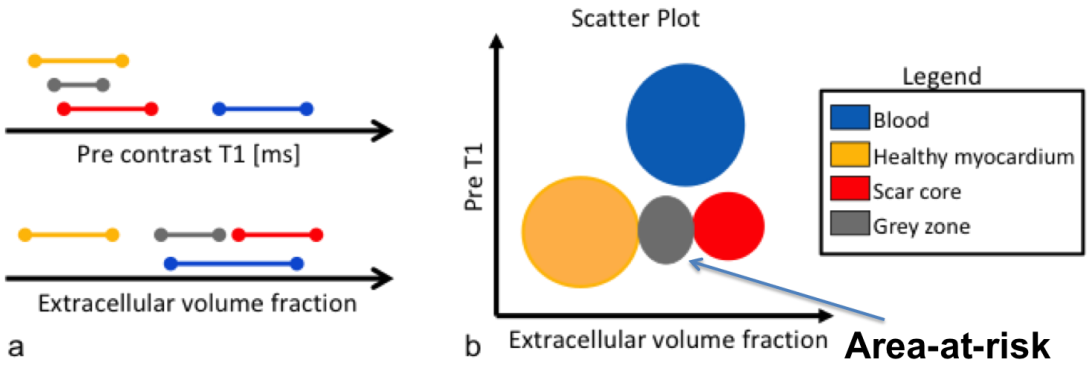

Figure 11- 1 Proposed automatic segmentation of area at risk for CMR scar quantification.

Typical ranges of T_1 and ECV values of myocardial tissue, scar core, grey zone and blood are shown in (a). Single T_1 or ECV maps cannot be used for area at risk segmentation using thresholds since the different tissue classes overlap in their value ranges. By combining the images, the different tissue types can be separated (b). In this work, native T_1 and ECV were used to segment and quantify scar core, grey zone and healthy myocardium.

Publications related to the work

Chen Z, Hanson B, Sohal M, Sammut E, Jackson T, Child N, Claridge S, Behar J, Niederer S, Gill J, Carr-White G, Razavi R, Rinald CA, Taggart P. Coupling of ventricular action potential duration and local strain patterns during reverse remodeling in responders and non-responders to cardiac resynchronization therapy. Heart Rhythm. 2016 Accepted, pending publication.

Chen Z, Cabrera-Lozoya R, Relan J, Sohal M, Shetty A, Karim R, Delingette H, Gill J , Rhode K, Ayache N, Taggart P, Rinaldi CA, Sermesant M, Razavi R. Biophysical Modelling Predicts Ventricular Tachycardia Inducibility and Circuit Morphology: A Combined Clinical Validation and Computer Modelling Approach. J Cardiovasc Electrophysiol. 2016 Apr 20. doi: 10.1111/jce.12991. [Epub ahead of print]

Chen Z, Sohal M, Sammut E, Child N, Jackson T, Claridge S, Cooklin M, O'Neill M, Wright M, Gill J, Chiribiri A, Schaeffter T, Carr-White G, Razavi R, Rinaldi CA. Focal but not diffuse myocardial fibrosis burden quantification using cardiac magnetic resonance imaging predicts left ventricular reverse modeling following cardiac resynchronization therapy.J Cardiovasc Electrophysiol. 2015 Oct 14. doi: 10.1111/jce.12855. [Epub ahead of print]

Chen Z, Reza R, Rinaldi CA. Reply to the Editor--Myocardial tissue characterization by cardiovascular magnetic resonance. Heart Rhythm. 2015 Sep;12(9):e118-9. doi: 10.1016/j.hrthm.2015.06.013. Epub 2015 Jun 27.

Chen Z, Sohal M, Voigt T, Sammut E, Tobon-Gomez C, Child N, Jackson T, Shetty A, Bostock J, Cooklin M, O'Neill M, Wright M, Murgatroyd F, Gill J, Carr-White G, Chiribiri A, Schaeffter T, Razavi R, Rinaldi CA. Myocardial tissue characterization by cardiac magnetic resonance imaging using T1 mapping predicts ventricular arrhythmia in ischemic and non-ischemic cardiomyopathy patients with implantable cardioverter-defibrillators. Heart Rhythm. 2015 Apr;12(4):792-801.

Chen Z, Hanson B, Sohal M, Sammut E, Child N, Shetty A, Boucher R, Bostock J, Gill J, Carr-White G, Rinald CA, Taggart P. Left ventricular epicardial electrograms show divergent changes in action potential duration in responders and non-responders to cardiac resynchronization therapy. Circ Arrhythm Electrophysiol. 2013;6(2):265-71.

Chen Z, Kotecha T, Crichton S, Shetty A, Sohal M, Arujuna A, Kirubakaran S, Bostock J, Cooklin M, O'Neill M, Wright M, Gill J, Rinaldi CA. Lower incidence of inappropriate shock therapy in patients with combined cardiac resynchronization therapy defibrillators (CRT-D) compared to patients with non-CRT defibrillators (ICDs). Int J Clin Pract. 2013;67(8):733-9.

Chen Z, Kapetanakis S, Carr-White G, Rinaldi CA, Chiribiri A. Extensive myocardial 'fatty-metaplasia' 20-years post-myocardial infarction. Eur Heart J Cardiovasc Imaging. 2012 Oct 10

Claridge S, **Chen Z,** Jackson T, Sammut E, Sohal M, Behar J, Razavi R, Niederer S, Rinaldi CA. Current concepts relating coronary flow, myocardial perfusion and

metabolism in left bundle branch block and cardiac resynchronisation therapy. Int J Cardiol. 2015 Feb 15;181:65-72.

Sammut E, Zarinabad N, Wesolowski R, Morton G, **Chen Z**, Sohal M, Carr-White G, Razavi R, Chiribiri A.Feasibility of high-resolution quantitative perfusion analysis in patients with heart failure. J Cardiovasc Magn Reson. 2015 Feb 12;17:13.

Hanson B, Child N, Van Duijvenboden S, Orini M, **Chen Z**, Coronel R, Rinaldi CA, Gill JS, Gill JS, Taggart P. Oscillatory behavior of ventricular action potential duration in heart failure patients at respiratory rate and low frequency. Front Physiol. 2014 Oct 28;5:414.

Sebag FA, Lellouche N, **Chen Z**, Tritar A, O'Neill MD, Gill J, Wright M, Leclercq C, Rinaldi CA. Positive response to cardiac resynchronization therapy reduces arrhythmic events after elective generator change in patients with primary prevention CRT-D. J Cardiovasc Electrophysiol. 2014 Dec;25(12):1368-75.

Jackson T, Sohal M, **Chen Z,** Child N, Sammut E, Behar J, Claridge S, Carr-White G, Razavi R, Rinaldi CA. A U-shaped type II contraction pattern in patients with strict left bundle branch block predicts super-response to cardiac resynchronization therapy. Heart Rhythm. 2014 Oct;11(10):1790-7.

Karim R, Ma Y, Jang M, Housden RJ, Williams SE, **Chen Z,** Ataollahi A, Althoefer K, Rinaldi CA, Razavi R, O'Neill MD, Schaeftter T, Rhode KS. Surface flattening of the human left atrium and proof-of-concept clinical applications. Comput Med Imaging Graph. 2014 Jun;38(4):251-66.

Sohal M, **Chen Z,** Sammut E, Jackson T, Behar J, Carr-White G, Razavi R, Rinaldi CA. New developments in the delivery of cardiac resynchronization therapy: targeted lead placement, multi-site and endocardial pacing. Expert Rev Med Devices. 2014 May;11(3):295-304.

Sohal M, Shetty A, Niederer S, **Chen Z,** Jackson T, Sammut E, Bostock J, Razavi R, Prinzen F, Rinaldi CA.Delayed trans-septal activation results in comparable hemodynamic effect of left ventricular and biventricular endocardial pacing: insights from electroanatomical mapping. Circ Arrhythm Electrophysiol. 2014 Apr;7(2):251-8.

Sohal M, Amraoui S, **Chen Z,** Sammut E, Jackson T, Wright M, O'Neill M, Gill J, Carr-White G, Rinaldi CA, Razavi R. Combined identification of septal flash and absence of myocardial scar by cardiac magnetic resonance imaging improves prediction of response to cardiac resynchronization therapy. J Interv Card Electrophysiol. 2014 Aug;40(2):179-90

Shetty AK, Sohal M, **Chen Z**, Ginks MR, Bostock J, Amraoui S, Ryu K, Rosenberg SP, Niederer SA, Gill J, Carr-White G, Razavi R, Rinaldi CA.A comparison of left ventricular endocardial, multisite, and multipolar epicardial cardiac resynchronization: an acute haemodynamic and electroanatomical study. Europace. 2014 Feb 12.

Karim R, Housden RJ, Balasubramaniam M, **Chen Z**, Perry D, Uddin A, Al-Beyatti Y, Palkhi E, Acheampong P, Obom S, Hennemuth A, Lu Y, Bai W, Shi W, Gao Y, Peitgen HO, Radau P, Razavi R, Tannenbaum A, Rueckert D, Cates J, Schaeffter T, Peters D, MacLeod R, Rhode K. Evaluation of current algorithms for segmentation of

scar tissue from late Gadolinium enhancement cardiovascular magnetic resonance of the left atrium: an open-access grand challenge. J Cardiovasc Magn Reson. 2013. 20;15:105

Sohal M, Shetty A, Duckett S, **Chen Z,** Sammut E, Amraoui S, Carr-White G, Razavi R, Rinaldi CA. Non-invasive assessment of left ventricular contraction patterns using cardiac magnetic resonance imaging to identify responders to cardiac resynchronization therapy. JACC Cardiovasc Imaging 2013;6(8):864-73.

Puntmann VO, Voigt T, **Chen Z**, Mayr M, Karim R, Rhode K, Pastor A, Carr-White G, Razavi R, Schaeffter T, Nagel E. T1 mapping in differentiation of normal myocardium from diffuse disease in hypertrophic and dilative cardiomyopathy. JACC Cardiovasc Imaging. 2013;6(4):475-84.

Karim R, **Chen Z**, Obom S, Ma YL, Acheampong P, Gill H, Gill J, Rinaldi A, O'Neill M, Razavi, R, Schaeffter T, Rode KS. "Infarct Segmentation of the Left Ventricle using Graph cuts" in Medical Image Computing and Computer Assisted Intervention (MICCAI) 2013. Lecture Notes in Computer Science. 2012, Vol. 7746, pp.71

Karim R, Claus P, **Chen Z,** House RJ, obom S, Ma YL, Acheampong P, Gill H, O'Neill M, Razavi R, Schaeffter T, Rhode RS. "Infarct Segmentation Challenge on Delayed Enhancement MRI of the Left Ventricle" in Medical Image Computing and Computer Assisted Intervention (MICCAI) 2013, Lecture Notes in Computer Science. 2012, Vol. 7746, pp. 97

Presentations related to the work

Chen Z, Sohal M, Voigt T, Sammut E, Child N, Jackson T, Bostock J, Cooklin M, O'Neill M, Wright M, Gill J, Chiribiri A, Carr-White G, Chiribiri A, Razavi R, Rinaldi CA. Focal and diffuse myocardial fibrosis burden quantification using cardiac magnetic resonance imaging to predict left ventricular reverse modeling following cardiac resynchronization therapy. Heart Rhythm 2015, 36th Annual Scientific Sessions. AB16-04

Chen Z, Manav Sohal, Eva Sammut, Nick Child, Tom Jackson, Anoop Shetty, Julian Bostock, Francis Murgatroyd, Jaswinder Gill, Gerry Carr-White, Valentina O Puntmann, Reza Razavi, C Aldo Rinaldi Myocardial tissue characterization using T1 mapping predicts ventricular arrhythmia in ischemic and non-ischemic cardiomyopathies. Heart Rhythm 2014, 35th Annual Scientific Sessions. PO01-186

Chen Z, Hanson B, Sohal M, Sammut E, Child N, Shetty A, Boucher R, Bostock J, Gill J, Carr-White G, Rinaldi CA, Taggart P. Divergent Changes In Left Ventricular Epicardial Action Potential Duration In Responders And Non-responders To Cardiac Resynchronisation Therapy. Heart Rhythm 2013, 34th Annual Scientific Sessions. PO03-41

Chen Z, Relan J, Schulze WH, Karim Rashed, Sohal M, Shetty A, Ma YL, Ayache N, Sermesant M, Delingette H, Bostock J, Razavi R, Rhode K, Rinaldi1 CA. Simultaneous non-contact mapping fused with CMR derived grey zone to explore the relationship with ventricular tachycardia substrate in ischaemic cardiomyopathy. Journal of Cardiovascular Magnetic Resonance 2013, 15(Suppl 1):P64

Rault ME Karim R, **Chen Z,** Schaeffter T, Voigt T, Manav S, Sammut E, Buerger C, Child N, Nagel E, Rinaldi CA, Razavi R, Rhode K, Puntmann VO. Motion correction using hierarchical local affine registration improves image quality and myocardial scar characterisation from T1 maps acquired with MOLLI. Journal of Cardiovascular Magnetic Resonance 2013, 15(Suppl 1):P73

Sammut E, Zarinabad N, **Chen Z,** Razavi R, Nagel E, Chiribiri A. Feasibility of quantitative perfusion CMR in patients with poor left ventricular function. Journal of Cardiovascular Magnetic Resonance 2013, 15(Suppl 1):E60

Z Chen, T Kotecha, S Crichton, S Kirubakaran, M Sohal, A Arujuna, A Shetty, B Julian, M Cooklin, M O'Neill, M Wright, JS Gill, CA Rinaldi. Reduction Of Inappropriate Shock Therapy In Patients With Combined Cardiac Resynchronization Therapy And Implantable Cardioverter-defibrillators Is Related To A Reduction In Atrial Arrhythmia Burden. Heart Rhythm 2012, 33rd Annual Scientific sessions. PO3-45

Z Chen, T Kotecha, S Crichton, A Shetty, A Arujuna, S Kirubakaran, M Sohal, J Bostock, JS Gill, CA Rinaldi. Does cardiac resynchronisation therapy reduce inappropriate shock therapy in Patients with implantable cardioverter-defibrillators? World Congress of Cardiology, 2012. Circulation 2012; 125:e741-e925.

Z Chen, T Voigt, A Wiethoff, S Crichton, D Murday, A Shetty, CA Rinaldi, E Nagel, VO Puntmann, T Schaeffter, R Razavi. Infarct myocardium tissue heterogeneity

assessment using pre-contrast and post-contrast T1 maps acquired with Modified Look-Locker Inversion Recovery (MOLLI) imaging. Journal of Cardiovascular Magnetic Resonance 2012, 14(Suppl 1):P263

Z Chen, C Kolbitsch, J Smink, J Harrison, V O Puntmann, E Nage, R Razavi, CA Rinaldi, T Schaeffter. Hybrid Phase ordering with Automatic Window Selection (HybridPAWS) improves respiratory-navigator efficiency during 3D late-gadolinium enhancement CMR in patients with chronic heart failure and irregular respiratory pattern. Journal of Cardiovascular Magnetic Resonance 2012, 14(Suppl 1):P256

Pastor A, Chen Z, Voigt T, Razavi R, Schaeffter T, Nagel E, Puntmann VO. Application of high resolution T1 mapping with MOLLI (hrMOLLI) to differentiate patients with diffuse and regional myocardial disease from healthy subjects. Journal of Cardiovascular Magnetic Resonance 2012, 14(Suppl 1):P225.

Pastor A, Chen Z, Voigt T, Schaeffter T, Razavi R, Nagel E, Puntmann VO. Application of a high resolution T1 mapping with MOLLI (hrMOLLI) in patients in clinical setting: a reproducibility study. Journal of Cardiovascular Magnetic Resonance 2012, 14(Suppl 1):O82.

Voigt T, Chen Z, Buerger C, Puntmann VO, Razavi R, Schaeffter T, Wiethoff AJ. Automated area at risk detection using myocardial t1 maps acquired pre- and post contrast agent administration. Proceedings of the 20th Annual Meeting of ISMRM. 2012, p0159.

Z Chen, C Kolbitsch, J Smink, J Harrison, V Puntman, E Nagel, R Razavi, A Rinaldi, T Schaeffter. Hybrid Phase ordering with Automatic Window Selection (HybridPAWS) improves respiratory-navigator efficiency during 3D late-gadolinium enhancement CMR in patients with chronic heart failure and irregular respiratory pattern. 15th Annual SCMR Scientific Sessions: 2012. http://www.jcmr-online.com/supplements/14/S1

References

1. Krijnen PAJ, Nijmeijer R, Meijer CJLM, Visser CA, Hack CE, Niessen HWM. Apoptosis in myocardial ischaemia and infarction. *J Clin Pathol*. 2002;55:801–811.

2. Yan AT, Shayne AJ, Brown KA, Gupta SN, Chan CW, Luu TM, Di Carli MF, Reynolds HG, Stevenson WG, Kwong RY. Characterization of the peri-infarct zone by contrast-enhanced cardiac magnetic resonance imaging is a powerful predictor of post-myocardial infarction mortality. *Circulation*. 2006;114:32–39.

3. Schmidt A, Azevedo CF, Cheng A, Gupta SN, Bluemke DA, Foo TK, Gerstenblith G, Weiss RG, Marban E, Tomaselli GF, Lima JA, Wu KC. Infarct tissue heterogeneity by magnetic resonance imaging identifies enhanced cardiac arrhythmia susceptibility in patients with left ventricular dysfunction. *Circulation*. 2007;115:2006–2014.

4. Roes SD, Borleffs CJ, van der Geest RJ, Westenberg JJ, Marsan NA, Kaandorp TA, Reiber JH, Zeppenfeld K, Lamb HJ, de Roos A, Schalij MJ, Bax JJ. Infarct tissue heterogeneity assessed with contrast-enhanced MRI predicts spontaneous ventricular arrhythmia in patients with ischemic cardiomyopathy and implantable cardioverter-defibrillator. *Circulation: Cardiovascular Imaging*. 2009;2:183–190.

5. Peters DC, Appelbaum EA, Nezafat R, Dokhan B, Han Y, Kissinger KV, Goddu B, Manning WJ. Left ventricular infarct size, peri-infarct zone, and papillary scar measurements: A comparison of high-resolution 3D and conventional 2D late gadolinium enhancement cardiac MR. *J Magn Reson Imaging*. 2009;30:794–800.

6. Damadian R, Zaner K, Hor D, DiMaio T. Human Tumors Detected by Nuclear Magnetic Resonance. *Proceedings of the National Academy of Sciences of the United States of America*. 1974;71:1471–1473.

7. Messroghli DR, Walters K, Plein S, Sparrow P, Friedrich MG, Ridgway JP, Sivananthan MU. Myocardial T1 mapping: application to patients with acute and chronic myocardial infarction. *Magn Reson Med*. 2007;58:34–40.

8. Piechnik SK, Ferreira VM, Dall'Armellina E, Cochlin LE, Greiser A, Neubauer S, Robson MD. Shortened Modified Look-Locker Inversion recovery (ShMOLLI) for clinical myocardial T1-mapping at 1.5 and 3 T within a 9 heartbeat breathhold. *J Cardiovasc Magn Reson*. 2010;12:69.

9. Messroghli DR, Plein S, Higgins DM, Walters K, Jones TR, Ridgway JP, Sivananthan MU. Human myocardium: single-breath-hold MR T1 mapping with high spatial resolution--reproducibility study. *Radiology*. 2006;238:1004–1012.

10. Kehr E, Sono M, Chugh SS, Jerosch-Herold M. Gadolinium-enhanced

magnetic resonance imaging for detection and quantification of fibrosis in human myocardium in vitro. *Int J Cardiovasc Imaging*. 2008;24:61–68.

11. Flett AS, Hayward MP, Ashworth MT, Hansen MS, Taylor AM, Elliott PM, McGregor C, Moon JC. Equilibrium contrast cardiovascular magnetic resonance for the measurement of diffuse myocardial fibrosis: preliminary validation in humans. *Circulation*. 2010;122:138–144.

12. Schelbert EB, Hsu LY, Anderson SA, Mohanty BD, Karim SM, Kellman P, Aletras AH, Arai AE. Late gadolinium-enhancement cardiac magnetic resonance identifies postinfarction myocardial fibrosis and the border zone at the near cellular level in ex vivo rat heart. *Circulation: Cardiovascular Imaging*. 2010;3:743–752.

13. Kawel N, Nacif M, Zavodni A, Jones J, Liu S, Sibley CT, Bluemke DA. T1 mapping of the myocardium: intra-individual assessment of post-contrast T1 time evolution and extracellular volume fraction at 3T for Gd-DTPA and Gd-BOPTA. *J Cardiovasc Magn Reson*. 2012;14:26.

14. Jellis C, Martin J, Narula J, Marwick TH. Assessment of nonischemic myocardial fibrosis. *J Am Coll Cardiol*. 2010;56:89–97.

15. Xue H, Shah S, Greiser A, Guetter C, Littmann A, Jolly M-P, Arai AE, Zuehlsdorff S, Guehring J, Kellman P. Motion correction for myocardial T1 mapping using image registration with synthetic image estimation. *Magn Reson Med*. 2012;67:1644–1655.

16. Kellman P, Wilson JR, Xue H, Bandettini WP, Shanbhag SM, Druey KM, Ugander M, Arai AE. Extracellular volume fraction mapping in the myocardium, part 2: initial clinical experience. *J Cardiovasc Magn Reson*. 2012;14:64.

17. de Bakker JM, van Rijen HM. Continuous and discontinuous propagation in heart muscle. *J Cardiovasc Electrophysiol*. 2006;17:567–573.

18. Ursell PC, Gardner PI, Albala A, Fenoglio JJ, Wit AL. Structural and electrophysiological changes in the epicardial border zone of canine myocardial infarcts during infarct healing. *Circ Res*. 1985;56:436–451.

19. Yao J-A, Hussain W, Patel P, Peters NS, Boyden PA, Wit AL. Remodeling of gap junctional channel function in epicardial border zone of healing canine infarcts. *Circ Res*. 2003;92:437–443.

20. Bolick DR, Hackel DB, Reimer KA, Ideker RE. Quantitative analysis of myocardial infarct structure in patients with ventricular tachycardia. *Circulation*. 1986;74:1266–1279.

21. Fieno DS, Kim RJ, Chen EL, Lomasney JW, Klocke FJ, Judd RM. Contrast-enhanced magnetic resonance imaging of myocardium at risk: distinction between reversible and irreversible injury throughout infarct healing. *J Am Coll Cardiol*. 2000;36:1985–1991.

22. Wiener I, Mindich B, Pitchon R. Determinants of ventricular tachycardia in patients with ventricular aneurysms: results of intraoperative epicardial and endocardial mapping. *Circulation*. 1982;65:856–861.

23. Cassidy DM, Vassallo JA, Miller JM, Poll DS, Buxton AE, Marchlinski FE, Josephson ME. Endocardial catheter mapping in patients in sinus rhythm: relationship to underlying heart disease and ventricular arrhythmias. *Circulation*. 1986;73:645–652.

24. Haqqani HM, Kalman JM, Roberts-Thomson KC, Balasubramaniam RN, Rosso R, Snowdon RL, Sparks PB, Vohra JK, Morton JB. Fundamental differences in electrophysiologic and electroanatomic substrate between ischemic cardiomyopathy patients with and without clinical ventricular tachycardia. *J Am Coll Cardiol*. 2009;54:166–173.

25. Marchlinski FE, Callans DJ, Gottlieb CD, Zado E. Linear ablation lesions for control of unmappable ventricular tachycardia in patients with ischemic and nonischemic cardiomyopathy. *Circulation*. 2000;101:1288–1296.

26. Moss AJ, Zareba W, Hall WJ, Klein H, Wilber DJ, Cannom DS, Daubert JP, Higgins SL, Brown MW, Andrews ML, Multicenter Automatic Defibrillator Implantation Trial II Investigators. Prophylactic implantation of a defibrillator in patients with myocardial infarction and reduced ejection fraction. *N Engl J Med*. 2002;346:877–883.

27. Bardy GH, Lee KL, Mark DB, Poole JE, Packer DL, Boineau R, Domanski M, Troutman C, Anderson J, Johnson G, McNulty SE, Clapp-Channing N, Davidson-Ray LD, Fraulo ES, Fishbein DP, Luceri RM, Ip JH. Amiodarone or an implantable cardioverter-defibrillator for congestive heart failure. *N Engl J Med*. 2005;352:225–237.

28. Moss AJ, Greenberg H, Case RB, Zareba W, Hall WJ, Brown MW, Daubert JP, McNitt S, Andrews ML, Elkin AD, Multicenter Automatic Defibrillator Implantation Trial-II (MADIT-II) Research Group. Long-term clinical course of patients after termination of ventricular tachyarrhythmia by an implanted defibrillator. *Circulation*. 2004;110:3760–3765.

29. Camm J, Klein H, Nisam S. The cost of implantable defibrillators: perceptions and reality. *Eur Heart J*. 2007;28:392–397.

30. Pathmanathan RK, Lau EW, Cooper J, Newton L, Skehan JD, Garratt CJ, Griffith MJ. Potential impact of antiarrhythmic drugs versus implantable defibrillators on the management of ventricular arrhythmias: the Midlands trial of empirical amiodarone versus electrophysiologically guided intervention and cardioverter implant registry data. *Heart*. 1998;80:68–70.

31. Germano JJ, Reynolds M, Essebag V, Josephson ME. Frequency and causes of implantable cardioverter-defibrillator therapies: is device therapy proarrhythmic? *Am J Cardiol*. 2006;97:1255–1261.

32. Glikson M, Lipchenca I, Viskin S, Ballman KV, Trusty JM, Gurevitz OT,

Luria DM, Eldar M, Hammill SC, Friedman PA. Long-term outcome of patients who received implantable cardioverter defibrillators for stable ventricular tachycardia. *J Cardiovasc Electrophysiol*. 2004;15:658–664.

33. Tung R, Zimetbaum P, Josephson ME. A critical appraisal of implantable cardioverter-defibrillator therapy for the prevention of sudden cardiac death. *J Am Coll Cardiol*. 2008;52:1111–1121.

34. Desai AS, Fang JC, Maisel WH, Baughman KL. Implantable defibrillators for the prevention of mortality in patients with nonischemic cardiomyopathy: a meta-analysis of randomized controlled trials. *JAMA*. 2004;292:2874–2879.

35. Duray GZ, Schmitt J, Richter S, Israel CW, Hohnloser SH. Arrhythmic death in implantable cardioverter defibrillator patients: a long-term study over a 10 year implantation period. *Europace*. 2009;11:1462–1468.

36. Bristow MR, Saxon LA, Boehmer J, Krueger S, Kass DA, De Marco T, Carson P, DiCarlo L, DeMets D, White BG, DeVries DW, Feldman AM. Cardiac-resynchronization therapy with or without an implantable defibrillator in advanced chronic heart failure. *N Engl J Med*. 2004;350:2140–2150.

37. de Leeuw N, Ruiter DJ, Balk AH, de Jonge N, Melchers WJ, Galama JM. Histopathologic findings in explanted heart tissue from patients with end-stage idiopathic dilated cardiomyopathy. *Transpl Int*. 2001;14:299–306.

38. Hughes SE, McKenna WJ. New insights into the pathology of inherited cardiomyopathy. *Heart*. 2005;91:257–264.

39. Assomull RG, Prasad SK, Lyne J, Smith G, Burman ED, Khan M, Sheppard MN, Poole-Wilson PA, Pennell DJ. Cardiovascular magnetic resonance, fibrosis, and prognosis in dilated cardiomyopathy. *J Am Coll Cardiol*. 2006;48:1977–1985.

40. Iles L, Pfluger H, Lefkovits L, Butler MJ, Kistler PM, Kaye DM, Taylor AJ. Myocardial fibrosis predicts appropriate device therapy in patients with implantable cardioverter-defibrillators for primary prevention of sudden cardiac death. *J Am Coll Cardiol*. 2011;57:821–828.

41. Nazarian S, Bluemke DA, Lardo AC, Zviman MM, Watkins SP, Dickfeld TL, Meininger GR, Roguin A, Calkins H, Tomaselli GF, Weiss RG, Berger RD, Lima JA, Halperin HR. Magnetic resonance assessment of the substrate for inducible ventricular tachycardia in nonischemic cardiomyopathy. *Circulation*. 2005;112:2821–2825.

42. CAZEAU S, RITTER P, BAKDACH S, LAZARUS A, LIMOUSIN M, HENAO L, MUNDLER O, Daubert JC, MUGICA J. Four Chamber Pacing in Dilated Cardiomyopathy. *Pacing Clin Electro*. 1994;17:1974–1979.

43. Cleland JGF, Daubert J-C, Erdmann E, Freemantle N, Gras D, Kappenberger L, Tavazzi L, Cardiac Resynchronization-Heart Failure (CARE-HF) Study Investigators. The effect of cardiac resynchronization on morbidity and

mortality in heart failure. *N Engl J Med*. 2005;352:1539–1549.

44. Epstein AE, DiMarco JP, Ellenbogen KA, Estes NAM, Freedman RA, Gettes LS, Gillinov AM, Gregoratos G, Hammill SC, Hayes DL, Hlatky MA, Newby LK, Page RL, Schoenfeld MH, Silka MJ, Stevenson LW, Sweeney MO, Tracy CM, Epstein AE, Darbar D, DiMarco JP, Dunbar SB, Estes NAM, Ferguson TB, Hammill SC, Karasik PE, Link MS, Marine JE, Schoenfeld MH, Shanker AJ, Silka MJ, Stevenson LW, Stevenson WG, Varosy PD, American College of Cardiology Foundation, American Heart Association Task Force on Practice Guidelines, Heart Rhythm Society. 2012 ACCF/AHA/HRS focused update incorporated into the ACCF/AHA/HRS 2008 guidelines for device-based therapy of cardiac rhythm abnormalities: a report of the American College of Cardiology Foundation/American Heart Association Task Force on Practice Guidelines and the Heart Rhythm Society. J. Am. Coll. Cardiol. 2013;61:e6–75.

45. Camm AJ, Lip G, De Caterina R. 2012 focused update of the ESC Guidelines for the management of atrial fibrillation An update of the 2010 ESC Guidelines for the management of atrial …. *European heart …*. 2012;

46. Chung ES, Leon AR, Tavazzi L, Sun J-P, Nihoyannopoulos P, Merlino J, Abraham WT, Ghio S, Leclercq C, Bax JJ, Yu C-M, Gorcsan J, St John Sutton M, De Sutter J, Murillo J. Results of the Predictors of Response to CRT (PROSPECT) trial. *Circulation*. 2008;117:2608–2616.

47. Ypenburg C, van Bommel RJ. Long-term prognosis after cardiac resynchronization therapy is related to the extent of left ventricular reverse remodeling at midterm follow-up. *Journal of the …*. 2009;

48. Ginks MR, Lambiase PD, Duckett SG, Bostock J, Chinchapatnam P, Rhode K, McPhail MJ, Simon M, Bucknall C, Carr-White G, Razavi R, Rinaldi CA. A Simultaneous X-MRI and Non Contact Mapping Study of the Acute Hemodynamic Effect of Left Ventricular Endocardial and Epicardial Cardiac Resynchronization Therapy in Humans. *Circ Heart Fail*. 2011;

49. Bleeker GB, Kaandorp TAM, Lamb HJ, Boersma E, Steendijk P, de Roos A, van der Wall EE, Schalij MJ, Bax JJ. Effect of Posterolateral Scar Tissue on Clinical and Echocardiographic Improvement After Cardiac Resynchronization Therapy. *Circulation*. 2006;

50. Bilchick KC, Dimaano V, Wu KC, Helm RH, Weiss RG, Lima JA, Berger RD, Tomaselli GF, Bluemke DA, Halperin HR, Abraham T, Kass DA, Lardo AC. Cardiac magnetic resonance assessment of dyssynchrony and myocardial scar predicts function class improvement following cardiac resynchronization therapy. *JACC Cardiovasc Imaging*. 2008;1:561–568.

51. Bilchick KC, Kuruvilla S, Hamirani YS, Ramachandran R, Clarke SA, Parker KM, Stukenborg GJ, Mason P, Ferguson JD, Moorman JR, Malhotra R, Mangrum JM, Darby AE, Dimarco J, Holmes JW, Salerno M, Kramer CM, Epstein FH. Impact of mechanical activation, scar, and electrical timing on cardiac resynchronization therapy response and clinical outcomes. *J Am Coll*

Cardiol. 2014;63:1657–1666.

52. Leong DP, Chakrabarty A, Shipp N, Molaee P, Madsen PL, Joerg L, Sullivan T, Worthley SG, De Pasquale CG, Sanders P, Selvanayagam JB. Effects of myocardial fibrosis and ventricular dyssynchrony on response to therapy in new-presentation idiopathic dilated cardiomyopathy: insights from cardiovascular magnetic resonance and echocardiography. *Eur Heart J*. 2012;33:640–648.

53. Wikstrom G, Blomström-Lundqvist C, Andren B, Lönnerholm S, Blomström P, Freemantle N, Remp T, Cleland JGF, CARE-HF study investigators. The effects of aetiology on outcome in patients treated with cardiac resynchronization therapy in the CARE-HF trial. *Eur Heart J*. 2009;30:782–788.

54. Barsheshet A, Goldenberg I, Moss AJ, Eldar M, Huang DT, McNitt S, Klein HU, Hall WJ, Brown MW, Goldberger JJ, Goldstein RE, Schuger C, Zareba W, Daubert JP. Response to preventive cardiac resynchronization therapy in patients with ischaemic and nonischaemic cardiomyopathy in MADIT-CRT. *Eur Heart J*. 2011;32:1622–1630.

55. McLeod CJ, Shen W-K, Rea RF, Friedman PA, Hayes DL, Wokhlu A, Webster TL, Wiste HJ, Hodge DO, Bradley DJ, Hammill SC, Packer DL, Cha Y-M. Differential outcome of cardiac resynchronization therapy in ischemic cardiomyopathy and idiopathic dilated cardiomyopathy. *Heart Rhythm*. 2011;8:377–382.

56. White JA, Yee R, Yuan X, Krahn A, Skanes A, Parker M, Klein G, Drangova M. Delayed enhancement magnetic resonance imaging predicts response to cardiac resynchronization therapy in patients with intraventricular dyssynchrony. *J Am Coll Cardiol*. 2006;48:1953–1960.

57. Yu CM. Left Ventricular Reverse Remodeling but Not Clinical Improvement Predicts Long-Term Survival After Cardiac Resynchronization Therapy. *Circulation*. 2005;112:1580–1586.

58. Wong JA, Yee R, Stirrat J, Scholl D, Krahn AD, Gula LJ, Skanes AC, Leong-Sit P, Klein GJ, McCarty D, Fine N, Goela A, Islam A, Thompson T, Drangova M, White JA. Influence of pacing site characteristics on response to cardiac resynchronization therapy. *Circulation: Cardiovascular Imaging*. 2013;6:542–550.

59. Kim RJ, Wu E, Rafael A, Chen E-L, Parker MA, Simonetti O, Klocke FJ, Bonow RO, Judd RM. The Use of Contrast-Enhanced Magnetic Resonance Imaging to Identify Reversible Myocardial Dysfunction. *N Engl J Med*. 2000;343:1445–1453.

60. Jugdutt BI. Ventricular Remodeling After Infarction and the Extracellular Collagen Matrix. *Circulation*. 2003;

61. Souders CA, Bowers SLK, Baudino TA. Cardiac fibroblast: the renaissance

cell. *Circ Res*. 2009;105:1164–1176.

62. Fornwalt BK, Sprague WW, BeDell P, Suever JD, Gerritse B, Merlino JD, Fyfe DA, Leon AR, Oshinski JN. Agreement is poor among current criteria used to define response to cardiac resynchronization therapy. *Circulation*. 2010;121:1985–1991.

63. Smith RF, Johnson G, Ziesche S, Bhat G, Blankenship K, Cohn JN. Functional capacity in heart failure. Comparison of methods for assessment and their relation to other indexes of heart failure. The V-HeFT VA Cooperative Studies Group. *Circulation*. 1993;87:VI88–93.

64. Molhoek SG, van Erven L, Bootsma M, Steendijk P, van der Wall EE, Schalij MJ. QRS duration and shortening to predict clinical response to cardiac resynchronization therapy in patients with end-stage heart failure. *Pacing Clin Electrophysiol*. 2004;27:308–313.

65. Aiba T, Tomaselli GF. Electrical remodeling in the failing heart. *Curr Opin Cardiol*. 2010;25:29–36.

66. Moss AJ, Hall WJ, Cannom DS, Klein H, Brown MW, Daubert JP, Estes NAM, Foster E, Greenberg H, Higgins SL, Pfeffer MA, Solomon SD, Wilber D, Zareba W, MADIT-CRT Trial Investigators. Cardiac-resynchronization therapy for the prevention of heart-failure events. *N Engl J Med*. 2009;361:1329–1338.

67. Linde C, Abraham WT, Gold MR, St John Sutton M, Ghio S, Daubert C, REVERSE (REsynchronization reVErses Remodeling in Systolic left vEntricular dysfunction) Study Group. Randomized trial of cardiac resynchronization in mildly symptomatic heart failure patients and in asymptomatic patients with left ventricular dysfunction and previous heart failure symptoms. *J Am Coll Cardiol*. 2008;52:1834–1843.

68. Tang ASL, Wells GA, Talajic M, Arnold MO, Sheldon R, Connolly S, Hohnloser SH, Nichol G, Birnie DH, Sapp JL, Yee R, Healey JS, Rouleau JL, Resynchronization-Defibrillation for Ambulatory Heart Failure Trial Investigators. Cardiac-resynchronization therapy for mild-to-moderate heart failure. *N Engl J Med*. 2010;363:2385–2395.

69. McMurray JJV, Adamopoulos S, Anker SD, Auricchio A, Böhm M, Dickstein K, Falk V, Filippatos G, Fonseca C, Gomez-Sanchez MA, Jaarsma T, Køber L, Lip GYH, Maggioni AP, Parkhomenko A, Pieske BM, Popescu BA, Rønnevik PK, Rutten FH, Schwitter J, Seferovic P, Stepinska J, Trindade PT, Voors AA, Zannad F, Zeiher A, ESC Committee for Practice Guidelines. ESC Guidelines for the diagnosis and treatment of acute and chronic heart failure 2012: The Task Force for the Diagnosis and Treatment of Acute and Chronic Heart Failure 2012 of the European Society of Cardiology. Developed in collaboration with the Heart Failure Association (HFA) of the ESC. Eur. Heart J. 2012;33:1787–1847.

70. Epstein AE, DiMarco JP, Ellenbogen KA, Estes NAM, Freedman RA, Gettes

LS, Gillinov AM, Gregoratos G, Hammill SC, Hayes DL, Hlatky MA, Newby LK, Page RL, Schoenfeld MH, Silka MJ, Stevenson LW, Sweeney MO, Smith SC, Jacobs AK, Adams CD, Anderson JL, Buller CE, Creager MA, Ettinger SM, Faxon DP, Halperin JL, Hiratzka LF, Hunt SA, Krumholz HM, Kushner FG, Lytle BW, Nishimura RA, Ornato JP, Page RL, Riegel B, Tarkington LG, Yancy CW, American College of Cardiology/American Heart Association Task Force on Practice Guidelines (Writing Committee to Revise the ACC/AHA/NASPE 2002 Guideline Update for Implantation of Cardiac Pacemakers and Antiarrhythmia Devices), American Association for Thoracic Surgery, Society of Thoracic Surgeons. ACC/AHA/HRS 2008 Guidelines for Device-Based Therapy of Cardiac Rhythm Abnormalities: a report of the American College of Cardiology/American Heart Association Task Force on Practice Guidelines (Writing Committee to Revise the ACC/AHA/NASPE 2002 Guideline Update for Implantation of Cardiac Pacemakers and Antiarrhythmia Devices) developed in collaboration with the American Association for Thoracic Surgery and Society of Thoracic Surgeons. *J Am Coll Cardiol*. 2008;51:e1–62.

71. Ibáñez L, Schroeder W, Ng L, Cates J. Ibáñez: Consortium TIS, Hamming R - Google Scholar. *The ITK software guide ebook*. 2003;

72. Rogers T, Dabir D, Mahmoud I, Voigt T, Schaeffter T, Nagel E, Puntmann VO. Standardization of T1 measurements with MOLLI in differentiation between health and disease -- the ConSept study. *J Cardiovasc Magn Reson*. 2013;15:78.

73. Ghio S, Constantin C, Klersy C, Serio A, Fontana A, Campana C, Tavazzi L. Interventricular and intraventricular dyssynchrony are common in heart failure patients, regardless of QRS duration. *Eur Heart J*. 2004;25:571–578.

74. Western D, Taggart P, Hanson B. Real-time feedback of dynamic cardiac repolarization properties. *Conf Proc IEEE Eng Med Biol Soc*. 2010;2010:114–117.

75. Wyatt RF, Burgess MJ, Evans AK, Lux RL, Abildskov JA, Tsutsumi T. Estimation of ventricular transmembrane action potential durations and repolarization times from unipolar electrograms. *The American Journal of Cardiology*. 1981;47:488.

76. Millar CK, Kralios FA, Lux RL. Correlation between refractory periods and activation-recovery intervals from electrograms: effects of rate and adrenergic interventions. *Circulation*. 1985;72:1372–1379.

77. Haws CW, Lux RL. Correlation between in vivo transmembrane action potential durations and activation-recovery intervals from electrograms. Effects of interventions that alter repolarization time. *Circulation*. 1990;

78. Coronel R, de Bakker JMT, Wilms-Schopman FJG, Opthof T, Linnenbank AC, Belterman CN, Janse MJ. Monophasic action potentials and activation recovery intervals as measures of ventricular action potential duration: experimental evidence to resolve some controversies. *Heart Rhythm*.

2006;3:1043–1050.

79. Potse M, Vinet A, Opthof T, Coronel R. Validation of a simple model for the morphology of the T wave in unipolar electrograms. *Am J Physiol Heart Circ Physiol*. 2009;297:H792–801.

80. Lima JA, Judd RM, Bazille A, Schulman SP, Atalar E, Zerhouni EA. Regional heterogeneity of human myocardial infarcts demonstrated by contrast-enhanced MRI. Potential mechanisms. *Circulation*. 1995;92:1117–1125.

81. Kim RJ, Fieno DS, Parrish TB, Harris K, Chen EL, Simonetti O, Bundy J, Finn JP, Klocke FJ, Judd RM. Relationship of MRI delayed contrast enhancement to irreversible injury, infarct age, and contractile function. *Circulation*. 1999;100:1992–2002.

82. Austin BA, Tang WHW, Rodriguez ER, Tan C, Flamm SD, Taylor DO, Starling RC, Desai MY. Delayed hyper-enhancement magnetic resonance imaging provides incremental diagnostic and prognostic utility in suspected cardiac amyloidosis. *JACC Cardiovasc Imaging*. 2009;2:1369–1377.

83. Rubinshtein R, Glockner JF, Ommen SR, Araoz PA, Ackerman MJ, Sorajja P, Bos JM, Tajik AJ, Valeti US, Nishimura RA, Gersh BJ. Characteristics and clinical significance of late gadolinium enhancement by contrast-enhanced magnetic resonance imaging in patients with hypertrophic cardiomyopathy. *Circ Heart Fail*. 2010;3:51–58.

84. Messroghli DR, Greiser A, Frohlich M, Dietz R, Schulz-Menger J. Optimization and validation of a fully-integrated pulse sequence for modified look-locker inversion-recovery (MOLLI) T1 mapping of the heart. *J Magn Reson Imaging*. 2007;26:1081–1086.

85. Kramer CM, Barkhausen J, Flamm SD, Kim RJ. Kramer: Society for Cardiovascular Magnetic Resonance... - Google Scholar. *J Cardiovasc Magn Reson*. 2008;

86. Scott PA, Morgan JM, Carroll N, Murday DC, Roberts PR, Peebles CR, Harden SP, Curzen NP. The extent of left ventricular scar quantified by late gadolinium enhancement MRI is associated with spontaneous ventricular arrhythmias in patients with coronary artery disease and implantable cardioverter-defibrillators. *Circ Arrhythm Electrophysiol*. 2011;4:324–330.

87. Amado LC, Gerber BL, Gupta SN, Rettmann DW, Szarf G, Schock R, Nasir K, Kraitchman DL, Lima JA. Accurate and objective infarct sizing by contrast-enhanced magnetic resonance imaging in a canine myocardial infarction model. *J Am Coll Cardiol*. 2004;44:2383–2389.

88. Messroghli DR, Radjenovic A, Kozerke S, Higgins DM, Sivananthan MU, Ridgway JP. Modified Look-Locker inversion recovery (MOLLI) for high-resolution T1 mapping of the heart. *Magn Reson Med*. 2004;52:141–146.

89. Mewton N, Liu CY, Croisille P, Bluemke D, Lima JAC. Assessment of

myocardial fibrosis with cardiovascular magnetic resonance. *J Am Coll Cardiol*. 2011;57:891–903.

90. Marijianowski MM, Teeling P, Becker AE. Remodeling after myocardial infarction in humans is not associated with interstitial fibrosis of noninfarcted myocardium. *J Am Coll Cardiol*. 1997;30:76–82.

91. Cleutjens JP, Kandala JC, Guarda E, Guntaka RV, Weber KT. Regulation of collagen degradation in the rat myocardium after infarction. *J Mol Cell Cardiol*. 1995;27:1281–1292.

92. Sun Y. Myocardial repair/remodelling following infarction: roles of local factors. *Cardiovasc Res*. 2009;81:482–490.

93. Iles L, Pfluger H, Phrommintikul A, Cherayath J, Aksit P, Gupta SN, Kaye DM, Taylor AJ. Evaluation of diffuse myocardial fibrosis in heart failure with cardiac magnetic resonance contrast-enhanced T1 mapping. *J Am Coll Cardiol*. 2008;52:1574–1580.

94. Broberg CS, Chugh SS, Conklin C, Sahn DJ, Jerosch-Herold M. Quantification of diffuse myocardial fibrosis and its association with myocardial dysfunction in congenital heart disease. *Circulation: Cardiovascular Imaging*. 2010;3:727–734.

95. Jerosch-Herold M, Sheridan DC, Kushner JD, Nauman D, Burgess D, Dutton D, Alharethi R, Li D, Hershberger RE. Cardiac magnetic resonance imaging of myocardial contrast uptake and blood flow in patients affected with idiopathic or familial dilated cardiomyopathy. *Am J Physiol Heart Circ Physiol*. 2008;295:H1234–H1242.

96. Schelbert EB, Testa SM, Meier CG, Ceyrolles WJ, Levenson JE, Blair AJ, Kellman P, Jones BL, Ludwig DR, Schwartzman D, Shroff SG, Wong TC. Myocardial extravascular extracellular volume fraction measurement by gadolinium cardiovascular magnetic resonance in humans: slow infusion versus bolus. *J Cardiovasc Magn Reson*. 2011;13:16.

97. Detsky JS, Paul G, Dick AJ, Wright GA. Reproducible classification of infarct heterogeneity using fuzzy clustering on multicontrast delayed enhancement magnetic resonance images. *IEEE Trans Med Imaging*. 2009;28:1606–1614.

98. Klein C, Nekolla SG, Balbach T, Schnackenburg B, Nagel E, Fleck E, Schwaiger M. The influence of myocardial blood flow and volume of distribution on late Gd-DTPA kinetics in ischemic heart failure. *J Magn Reson Imaging*. 2004;20:588–593.

99. Perez-David E, Arenal A, Rubio-Guivernau JL, Del Castillo R, Atea L, Arbelo E, Caballero E, Celorrio V, Datino T, Gonzalez-Torrecilla E, Atienza F, Ledesma-Carbayo MJ, Bermejo J, Medina A, Fernandez-Aviles F. Noninvasive identification of ventricular tachycardia-related conducting channels using contrast-enhanced magnetic resonance imaging in patients

with chronic myocardial infarction comparison of signal intensity scar mapping and endocardial voltage mapping. *J Am Coll Cardiol*. 2011;57:184–194.

100. Badger TJ, Daccarett M, Akoum NW, Adjei-Poku YA, Burgon NS, Haslam TS, Kalvaitis S, Kuppahally S, Vergara G, McMullen L, Anderson PA, Kholmovski E, MacLeod RS, Marrouche NF. Evaluation of left atrial lesions after initial and repeat atrial fibrillation ablation: lessons learned from delayed-enhancement MRI in repeat ablation procedures. *Circ Arrhythm Electrophysiol*. 2010;3:249–259.

101. Feld H, Priest S. A cyclic breathing pattern in patients with poor left ventricular function and compensated heart failure: a mild form of Cheyne-Stokes respiration? *J Am Coll Cardiol*. 1993;21:971–974.

102. Yajima T, Koike A, Sugimoto K, Miyahara Y, Marumo F, Hiroe M. Mechanism of periodic breathing in patients with cardiovascular disease. *Chest*. 1994;106:142–146.

103. Mortara A, Sleight P, Pinna GD, Maestri R, Prpa A, La Rovere MT, Cobelli F, Tavazzi L. Abnormal awake respiratory patterns are common in chronic heart failure and may prevent evaluation of autonomic tone by measures of heart rate variability. *Circulation*. 1997;96:246–252.

104. Jhooti P, Gatehouse PD, Keegan J, Bunce NH, Taylor AM, Firmin DN. Phase ordering with automatic window selection (PAWS): a novel motion-resistant technique for 3D coronary imaging. *Magn Reson Med*. 2000;43:470–480.

105. Kolbitsch C, Prieto C, Smink J, Schaeffter T. Highly efficient whole-heart imaging using radial phase encoding-phase ordering with automatic window selection. *Magn Reson Med*. 2011;66:1008–1018.

106. Look DC, Locker DR. Time Saving in Measurement of NMR and EPR Relaxation Times. *Review of Scientific Instruments*. 1970;41:250–251.

107. Stuber M, Botnar RM, Spuentrup E, Kissinger KV, Manning WJ. Three-dimensional high-resolution fast spin-echo coronary magnetic resonance angiography. *Magn Reson Med*. 2001;45:206–211.

108. White JA, Fine N, Gula LJ, Yee R, Al-Admawi M, Zhang Q, Krahn A, Skanes A, MacDonald A, Peters T, Drangova M. Fused whole-heart coronary and myocardial scar imaging using 3-T CMR. Implications for planning of cardiac resynchronization therapy and coronary revascularization. *JACC Cardiovasc Imaging*. 2010;3:921–930.

109. Andreu D, Berruezo A, Ortiz-Pérez JT, Silva E, Mont L, Borràs R, de Caralt TM, Perea RJ, Fernández-Armenta J, Zeljko H, Brugada J. Integration of 3D electroanatomic maps and magnetic resonance scar characterization into the navigation system to guide ventricular tachycardia ablation. *Circ Arrhythm Electrophysiol*. 2011;4:674–683.

110. Duckett SG, Ginks MR, Knowles BR, Ma Y, Shetty A, Bostock J, Cooklin M,

Gill JS, Carr-White GS, Razavi R, Schaeffter T, Rhode KS, Rinaldi CA. Advanced image fusion to overlay coronary sinus anatomy with real-time fluoroscopy to facilitate left ventricular lead implantation in CRT. *Pacing Clin Electro*. 2011;34:226–234.

111. Codreanu A, Odille F, Aliot E, Marie P-Y, Magnin-Poull I, Andronache M, Mandry D, Djaballah W, Régent D, Felblinger J, de Chillou C. Electroanatomic characterization of post-infarct scars comparison with 3-dimensional myocardial scar reconstruction based on magnetic resonance imaging. *J Am Coll Cardiol*. 2008;52:839–842.

112. Gulati A, Jabbour A, Ismail TF, Guha K, Khwaja J, Raza S, Morarji K, Brown TDH, Ismail NA, Dweck MR, Di Pietro E, Roughton M, Wage R, Daryani Y, O'Hanlon R, Sheppard MN, Alpendurada F, Lyon AR, Cook SA, Cowie MR, Assomull RG, Pennell DJ, Prasad SK. Association of fibrosis with mortality and sudden cardiac death in patients with nonischemic dilated cardiomyopathy. *JAMA*. 2013;309:896–908.

113. Neilan TG, Coelho-Filho OR, Danik SB, Shah RV, Dodson JA, Verdini DJ, Tokuda M, Daly CA, Tedrow UB, Stevenson WG, Jerosch-Herold M, Ghoshhajra BB, Kwong RY. CMR Quantification of Myocardial Scar Provides Additive Prognostic Information in Nonischemic Cardiomyopathy. *JACC Cardiovasc Imaging*. 2013;6:944–954.

114. van Rees JB, Borleffs CJW, de Bie MK, Stijnen T, van Erven L, Bax JJ, Schalij MJ. Inappropriate implantable cardioverter-defibrillator shocks: incidence, predictors, and impact on mortality. *J Am Coll Cardiol*. 2011;57:556–562.

115. Aliot EM, Stevenson WG, Almendral-Garrote JM, Bogun F, Calkins CH, Delacretaz E, Bella PD, Hindricks G, Jaïs P, Josephson ME, Kautzner J, Kay GN, Kuck K-H, Lerman BB, Marchlinski F, Reddy V, Schalij M-J, Schilling R, Soejima K, Wilber D, European Heart Rhythm Association, European Society of Cardiology, Heart Rhythm Society. EHRA/HRS Expert Consensus on Catheter Ablation of Ventricular Arrhythmias: developed in a partnership with the European Heart Rhythm Association (EHRA), a Registered Branch of the European Society of Cardiology (ESC), and the Heart Rhythm Society (HRS); in collaboration with the American College of Cardiology (ACC) and the American Heart Association (AHA). 2009. p. 771–817.

116. Ng J, Jacobson JT, Ng JK, Gordon D, Lee DC, Carr JC, Goldberger JJ. Virtual electrophysiological study in a 3-dimensional cardiac magnetic resonance imaging model of porcine myocardial infarction. *J Am Coll Cardiol*. 2012;60:423–430.

117. Yue AM, Paisey JR, Robinson S, Betts TR, Roberts PR, Morgan JM. Determination of human ventricular repolarization by noncontact mapping: validation with monophasic action potential recordings. *Circulation*. 2004;110:1343–1350.

118. Nash MP, Bradley CP, Sutton PM, Clayton RH, Kallis P, Hayward MP,

Paterson DJ, Taggart P. Whole heart action potential duration restitution properties in cardiac patients: a combined clinical and modelling study. *Exp Physiol*. 2006;91:339–354.

119. Wellens HJ, Brugada P, Stevenson WG. Programmed electrical stimulation of the heart in patients with life-threatening ventricular arrhythmias: what is the significance of induced arrhythmias and what is the correct stimulation protocol? *Circulation*. 1985;72:1–7.

120. Relan J, Chinchapatnam P, Sermesant M, Rhode K, Ginks M, Delingette H, Rinaldi CA, Razavi R, Ayache N. Coupled personalization of cardiac electrophysiology models for prediction of ischaemic ventricular tachycardia. *Interface Focus*. 2011;1:396–407.

121. Relan J, Pop M, Delingette H, Wright GA, Ayache N, Sermesant M. Personalization of a cardiac electrophysiology model using optical mapping and MRI for prediction of changes with pacing. *IEEE Trans Biomed Eng*. 2011;58:3339–3349.

122. Mitchell CC, Schaeffer DG. A two-current model for the dynamics of cardiac membrane. *Bull Math Biol*. 2003;65:767–793.

123. Ciaccio EJ, Ashikaga H, Kaba RA, Cervantes D, Hopenfeld B, Wit AL, Peters NS, McVeigh ER, Garan H, Coromilas J. Model of reentrant ventricular tachycardia based on infarct border zone geometry predicts reentrant circuit features as determined by activation mapping. *Heart Rhythm*. 2007;4:1034–1045.

124. Camelliti P, Borg TK, Kohl P. Structural and functional characterisation of cardiac fibroblasts. *Cardiovasc Res*. 2005;65:40–51.

125. Estner HL, Zviman MM, Herzka D, Miller F, Castro V, Nazarian S, Ashikaga H, Dori Y, Berger RD, Calkins H, Lardo AC, Halperin HR. The critical isthmus sites of ischemic ventricular tachycardia are in zones of tissue heterogeneity, visualized by magnetic resonance imaging. *Heart Rhythm*. 2011;8:1942–1949.

126. Gilmour RF, Chialvo DR. Electrical restitution, critical mass, and the riddle of fibrillation. *J Cardiovasc Electrophysiol*. 1999;10:1087–1089.

127. Clayton RH, Holden AV. A method to quantify the dynamics and complexity of re-entry in computational models of ventricular fibrillation. *Phys Med Biol*. 2002;47:225–238.

128. Nolasco JB, Dahlen RW. A graphic method for the study of alternation in cardiac action potentials. *J Appl Physiol*. 1968;25:191–196.

129. Guevara MR, Ward G, Shrier A, Glass L. http://scholar.google.com/scholar?q=related:_Lc3aAzg-DIJ:scholar.google.com/&hl=en&num=20&as_sdt=0,5. IEEE Comp. Cardiol; 1984.

130. Orini M, Taggart P, Srinivasan N, Hayward M, Lambiase PD. Interactions between Activation and Repolarization Restitution Properties in the Intact Human Heart: In-Vivo Whole-Heart Data and Mathematical Description. *PLoS ONE*. 2016;11:e0161765.

131. Arevalo H, Plank G, Helm P, Halperin H, Trayanova N. Tachycardia in post-infarction hearts: insights from 3D image-based ventricular models. *PLoS ONE*. 2013;8:e68872.

132. Child N, Bishop MJ, Hanson B, Coronel R, Opthof T, Boukens BJ, Walton RD, Efimov IR, Bostock J, Hill Y, Rinaldi CA, Razavi R, Gill J, Taggart P. An activation-repolarization time metric to predict localized regions of high susceptibility to reentry. *Heart Rhythm*. 2015;12:1644–1653.

133. Ashikaga H, Arevalo H, Vadakkumpadan F, Blake RC, Bayer JD, Nazarian S, Muz Zviman M, Tandri H, Berger RD, Calkins H, Herzka DA, Trayanova NA, Halperin HR. Feasibility of image-based simulation to estimate ablation target in human ventricular arrhythmia. *Heart Rhythm*. 2013;

134. Rudy Y. Noninvasive electrocardiographic imaging of arrhythmogenic substrates in humans. *Circ Res*. 2013;112:863–874.

135. Konukoglu E, Relan J, Cilingir U, Menze BH, Chinchapatnam P, Jadidi A, Cochet H, Hocini M, Delingette H, Ja ïs P, Ha ïssaguerre M, Ayache N, Sermesant M. Efficient probabilistic model personalization integrating uncertainty on data and parameters: Application to eikonal-diffusion models in cardiac electrophysiology. *Prog Biophys Mol Biol*. 2011;107:134–146.

136. Sermesant M, Coudi ère Y, Moreau-Vill èger V, Rhode KS, Hill DLG, Razavi RS. A fast-marching approach to cardiac electrophysiology simulation for XMR interventional imaging. *Med Image Comput Comput Assist Interv*. 2005;8:607–615.

137. Fenton F, Karma A. Vortex dynamics in three-dimensional continuous myocardium with fiber rotation: Filament instability and fibrillation. *Chaos*. 1998;8:20–47.

138. Chinchapatnam P, Rhode KS, Ginks M, Rinaldi CA, Lambiase P, Razavi R, Arridge S, Sermesant M. Model-based imaging of cardiac apparent conductivity and local conduction velocity for diagnosis and planning of therapy. *IEEE Trans Med Imaging*. 2008;27:1631–1642.

139. Keener J, Sneyd J. Mathematical Physiology. Springer Science & Business Media; 2009.

140. Decker KF, Rudy Y. Ionic mechanisms of electrophysiological heterogeneity and conduction block in the infarct border zone. *Am J Physiol Heart Circ Physiol*. 2010;299:H1588–97.

141. Epstein AE, DiMarco JP, Ellenbogen KA, Estes NAM, Freedman RA, Gettes LS, Gillinov AM, Gregoratos G, Hammill SC, Hayes DL, Hlatky MA, Newby LK, Page RL, Schoenfeld MH, Silka MJ, Stevenson LW, Sweeney

MO, American College of Cardiology Foundation, American Heart Association Task Force on Practice Guidelines, Heart Rhythm Society. 2012 ACCF/AHA/HRS focused update incorporated into the ACCF/AHA/HRS 2008 guidelines for device-based therapy of cardiac rhythm abnormalities: a report of the American College of Cardiology Foundation/American Heart Association Task Force on Practice Guidelines and the Heart Rhythm Society. Circulation. 2013;127:e283–352.

142. Scott PA, Roberts PR. Role of implantable cardioverter defibrillators in non-ischaemic dilated cardiomyopathy. *Postgrad Med J*. 2010;86:116–122.

143. Wu KC, Weiss RG, Thiemann DR, Kitagawa K, Schmidt A, Dalal D, Lai S, Bluemke DA, Gerstenblith G, Marbán E, Tomaselli GF, Lima JAC. Late gadolinium enhancement by cardiovascular magnetic resonance heralds an adverse prognosis in nonischemic cardiomyopathy. *J Am Coll Cardiol*. 2008;51:2414–2421.

144. Spach MS, Boineau JP. Microfibrosis produces electrical load variations due to loss of side-to-side cell connections: a major mechanism of structural heart disease arrhythmias. *Pacing Clin Electrophysiol*. 1997;20:397–413.

145. Massare J, Berry JM, Luo X, Rob F, Johnstone JL, Shelton JM, Bassel-Duby R, Hill JA, Naseem RH. Diminished cardiac fibrosis in heart failure is associated with altered ventricular arrhythmia phenotype. *J Cardiovasc Electrophysiol*. 2010;21:1031–1037.

146. Beltrami CA, Finato N, Rocco M, Feruglio GA, Puricelli C, Cigola E, Quaini F, Sonnenblick EH, Olivetti G, Anversa P. Structural basis of end-stage failure in ischemic cardiomyopathy in humans. *Circulation*. 1994;89:151–163.

147. Sibley CT, Noureldin RA, Gai N, Nacif MS, Liu S, Turkbey EB, Mudd JO, van der Geest RJ, Lima JAC, Halushka MK, Bluemke DA. T1 Mapping in cardiomyopathy at cardiac MR: comparison with endomyocardial biopsy. *Radiology*. 2012;265:724–732.

148. McMurray JJV, Adamopoulos S, Anker SD, Auricchio A, Böhm M, Dickstein K, Falk V, Filippatos G, Fonseca C, Gomez-Sanchez MA, Jaarsma T, Køber L, Lip GYH, Pietro Maggioni A, Parkhomenko A, Pieske BM, Popescu BA, Rønnevik PK, Rutten FH, Schwitter J, Seferovic P, Stepinska J, Trindade PT, Voors AA, Zannad F, Zeiher A, Bax JJ, Baumgartner H, Ceconi C, Dean V, Deaton C, Fagard R, Funck-Brentano C, Hasdai D, Hoes A, Kirchhof P, Knuuti J, Kolh P, McDonagh T, Moulin C, Popescu BA, Reiner Ž, Sechtem U, Sirnes PA, Tendera M, Torbicki A, Vahanian A, Windecker S, McDonagh T, Sechtem U, Bonet LA, Avraamides P, Ben Lamin HA, Brignole M, Coca A, Cowburn P, Dargie H, Elliott P, Flachskampf FA, Guida GF, Hardman S, Iung B, Merkely B, Mueller C, Nanas JN, Nielsen OW, Ørn S, Parissis JT, Ponikowski P. ESC Guidelines for the diagnosis and treatment of acute and chronic heart failure 2012. *European heart …*. 2012;

149. Brooks A, Schinde V, Bateman AC, Gallagher PJ. Interstitial fibrosis in the dilated non-ischaemic myocardium. *Heart*. 2003;89:1255–1256.

150. Pogwizd SM, McKenzie JP, Cain ME. Mechanisms underlying spontaneous and induced ventricular arrhythmias in patients with idiopathic dilated cardiomyopathy. *Circulation*. 1998;98:2404–2414.

151. Sugrue DD, Holmes DR, Gersh BJ, Edwards WD, McLaran CJ, Wood DL, Osborn MJ, Hammill SC. Cardiac histologic findings in patients with life-threatening ventricular arrhythmias of unknown origin. *J Am Coll Cardiol*. 1984;4:952–957.

152. Almaas VM, Haugaa KH, Strøm EH, Scott H, Dahl CP, Leren TP, Geiran OR, Endresen K, Edvardsen T, Aakhus S, Amlie JP. Increased amount of interstitial fibrosis predicts ventricular arrhythmias, and is associated with reduced myocardial septal function in patients with obstructive hypertrophic cardiomyopathy. *Europace*. 2013;15:1319–1327.

153. Dass S, Suttie JJ, Piechnik SK, Ferreira VM, Holloway CJ, Banerjee R, Mahmod M, Cochlin L, Karamitsos TD, Robson MD, Watkins H, Neubauer S. Myocardial Tissue Characterization Using Magnetic Resonance Noncontrast T1 Mapping in Hypertrophic and Dilated Cardiomyopathy. *Circulation: Cardiovascular Imaging*. 2012;5:726–733.

154. Puntmann VO, Voigt T, Chen Z, Mayr M, Karim R, Rhode K, Pastor A, Carr-White G, Razavi R, Schaeffter T, Nagel E. Native T1 Mapping in Differentiation of Normal Myocardium From Diffuse Disease in Hypertrophic and Dilated Cardiomyopathy. *J Am Coll Cardiol Img*. 2013;6:475–484.

155. Flett AS, Hasleton J, Cook C, Hausenloy D, Quarta G, Ariti C, Muthurangu V, Moon JC. Evaluation of techniques for the quantification of myocardial scar of differing etiology using cardiac magnetic resonance. *JACC Cardiovasc Imaging*. 2011;4:150–156.

156. Karamitsos TD, Piechnik SK, Banypersad SM, Fontana M, Ntusi NB, Ferreira VM, Whelan CJ, Myerson SG, Robson MD, Hawkins PN, Neubauer S, Moon JC. Noncontrast T1 mapping for the diagnosis of cardiac amyloidosis. *JACC Cardiovasc Imaging*. 2013;6:488–497.

157. Sado DM, Flett AS, Banypersad SM, White SK, Maestrini V, Quarta G, Lachmann RH, Murphy E, Mehta A, Hughes DA, McKenna WJ, Taylor AM, Hausenloy DJ, Hawkins PN, Elliott PM, Moon JC. Cardiovascular magnetic resonance measurement of myocardial extracellular volume in health and disease. *Heart*. 2012;98:1436–1441.

158. Wong TC, Piehler KM, Kang IA, Kadakkal A, Kellman P, Schwartzman DS, Mulukutla SR, Simon MA, Shroff SG, Kuller LH, Schelbert EB. Myocardial extracellular volume fraction quantified by cardiovascular magnetic resonance is increased in diabetes and associated with mortality and incident heart failure admission. *Eur Heart J*. 2014;35:657–664.

159. Moon JC, Messroghli DR, Kellman P, Piechnik SK, Robson MD, Ugander M, Gatehouse PD, Arai AE, Friedrich MG, Neubauer S, Schulz-Menger J,

Schelbert EB, Society for Cardiovascular Magnetic Resonance Imaging, Cardiovascular Magnetic Resonance Working Group of the European Society of Cardiology. Myocardial T1 mapping and extracellular volume quantification: a Society for Cardiovascular Magnetic Resonance (SCMR) and CMR Working Group of the European Society of Cardiology consensus statement. *J Cardiovasc Magn Reson*. 2013;15:92.

160. Mayer GA. Diurnal, postural and postprandial variations of hematocrit. *Can Med Assoc J*. 1965;93:1006–1008.

161. White SK, Sado DM, Fontana M, Banypersad SM, Maestrini V, Flett AS, Piechnik SK, Robson MD, Hausenloy DJ, Sheikh AM, Hawkins PN, Moon JC. T1 mapping for myocardial extracellular volume measurement by CMR: bolus only versus primed infusion technique. *JACC Cardiovasc Imaging*. 2013;6:955–962.

162. Dawson DK, Hawlisch K, Prescott G, Roussin I, Di Pietro E, Deac M, Wong J, Frenneaux MP, Pennell DJ, Prasad SK. Prognostic role of CMR in patients presenting with ventricular arrhythmias. *JACC Cardiovasc Imaging*. 2013;6:335–344.

163. Moss AJ, Schuger C, Beck CA, Brown MW, Cannom DS, Daubert JP, Estes NAM, Greenberg H, Hall WJ, Huang DT, Kautzner J, Klein H, McNitt S, Olshansky B, Shoda M, Wilber D, Zareba W, MADIT-RIT Trial Investigators. Reduction in inappropriate therapy and mortality through ICD programming. *N Engl J Med*. 2012;367:2275–2283.

164. Markowitz SM, Lewen JM, Wiggenhorn CJ, Abraham WT, Stein KM, Iwai S, Lerman BB. Relationship of reverse anatomical remodeling and ventricular arrhythmias after cardiac resynchronization. *J Cardiovasc Electrophysiol*. 2009;20:293–298.

165. Rickard J, Popovic Z, Verhaert D, Sraow D, Baranowski B, Martin DO, Lindsay BD, Varma N, Tchou P, Grimm RA, Wilkoff BL, Chung MK. The QRS narrowing index predicts reverse left ventricular remodeling following cardiac resynchronization therapy. *Pacing Clin Electrophysiol*. 2011;34:604–611.

166. Rickard J, Jackson G, Spragg DD, Cronin EM, Baranowski B, Tang WHW, Wilkoff BL, Varma N. QRS prolongation induced by cardiac resynchronization therapy correlates with deterioration in left ventricular function. *Heart Rhythm*. 2012;

167. Aiba T, Tomaselli G. Electrical remodeling in dyssynchrony and resynchronization. *J Cardiovasc Transl Res*. 2012;5:170–179.

168. Jeyaraj D, Wilson LD, Zhong J, Flask C, Saffitz JE, Deschenes I, Yu X, Rosenbaum DS. Mechanoelectrical feedback as novel mechanism of cardiac electrical remodeling. *Circulation*. 2007;115:3145–3155.

169. Medina-Ravell VA, Lankipalli RS, Yan G-X, Antzelevitch C, Medina-

Malpica NA, Medina-Malpica OA, Droogan C, Kowey PR. Effect of epicardial or biventricular pacing to prolong QT interval and increase transmural dispersion of repolarization: does resynchronization therapy pose a risk for patients predisposed to long QT or torsade de pointes? *Circulation*. 2003;107:740–746.

170. Fish JM, Di Diego JM, Nesterenko V, Antzelevitch C. Epicardial activation of left ventricular wall prolongs QT interval and transmural dispersion of repolarization: implications for biventricular pacing. *Circulation*. 2004;109:2136–2142.

171. Cutler MJ, Jeyaraj D, Rosenbaum DS. Cardiac electrical remodeling in health and disease. *Trends in pharmacological …*. 2011;

172. Ghosh S, Silva JNA, Canham RM, Bowman TM, Zhang J, Rhee EK, Woodard PK, Rudy Y. Electrophysiologic substrate and intraventricular left ventricular dyssynchrony in nonischemic heart failure patients undergoing cardiac resynchronization therapy. *Heart Rhythm*. 2011;8:692–699.

173. Aiba T, Hesketh GG, Barth AS, Liu T, Daya S, Chakir K, Dimaano VL, Abraham TP, O'Rourke B, Akar FG, Kass DA, Tomaselli GF. Electrophysiological consequences of dyssynchronous heart failure and its restoration by resynchronization therapy. *Circulation*. 2009;119:1220–1230.

174. Wecke L, van Deursen CJM, Bergfeldt L, Prinzen FW. Repolarization changes in patients with heart failure receiving cardiac resynchronization therapy-signs of cardiac memory. *J Electrocardiol*. 2011;44:590–598.

175. Braunschweig F, Pfizenmayer H, Rubulis A, Schoels W, Linde C, Bergfeldt L. Transient repolarization instability following the initiation of cardiac resynchronization therapy. *Europace*. 2011;13:1327–1334.

176. Lellouche N, De Diego C, Boyle NG, Wiener I, Akopyan G, Child JS, Shivkumar K. Relationship between mechanical and electrical remodelling in patients with cardiac resynchronization implanted defibrillators. *Europace*. 2011;13:1180–1187.

177. Kuijpers NHL, Hermeling E, Bovendeerd PHM, Delhaas T, Prinzen FW. Modeling cardiac electromechanics and mechanoelectrical coupling in dyssynchronous and failing hearts: insight from adaptive computer models. *J Cardiovasc Transl Res*. 2012;5:159–169.

178. Nattel S, Maguy A, Le Bouter S, Yeh Y-H. Arrhythmogenic ion-channel remodeling in the heart: heart failure, myocardial infarction, and atrial fibrillation. *Physiol Rev*. 2007;87:425–456.

179. Plotnikov AN, Yu H, Geller JC, Gainullin RZ, Chandra P, Patberg KW, Friezema S, Danilo P, Cohen IS, Feinmark SJ, Rosen MR. Role of L-type calcium channels in pacing-induced short-term and long-term cardiac memory in canine heart. *Circulation*. 2003;107:2844–2849.

180. Akar FG, Rosenbaum DS. Transmural electrophysiological heterogeneities

underlying arrhythmogenesis in heart failure. *Circ Res*. 2003;93:638–645.

181. Helm RH, Leclercq C, Faris OP, Ozturk C, McVeigh E, Lardo AC, Kass DA. Cardiac dyssynchrony analysis using circumferential versus longitudinal strain: implications for assessing cardiac resynchronization. *Circulation*. 2005;111:2760–2767.

182. Prinzen FW, Hunter WC, Wyman BT, McVeigh ER. Mapping of regional myocardial strain and work during ventricular pacing: experimental study using magnetic resonance imaging tagging. *J Am Coll Cardiol*. 1999;33:1735–1742.

183. Yano M, Kohno M, Konishi M, Takahashi T, Seki K, Matsuzaki M. Influence of left ventricular regional nonuniformity on afterload-dependent relaxation in intact dogs. *Am J Physiol*. 1994;267:H148–54.

184. Taggart P, Sutton PM. Cardiac mechano-electric feedback in man: clinical relevance. *Prog Biophys Mol Biol*. 1999;71:139–154.

185. Zabel M, Koller BS, Sachs F, Franz MR. Stretch-induced voltage changes in the isolated beating heart: importance of the timing of stretch and implications for stretch-activated ion channels. *Cardiovasc Res*. 1996;32:120–130.

186. Spragg DD, Akar FG, Helm RH, Tunin RS, Tomaselli GF, Kass DA. Abnormal conduction and repolarization in late-activated myocardium of dyssynchronously contracting hearts. *Cardiovasc Res*. 2005;67:77–86.

187. Martinac B. Mechanosensitive ion channels: molecules of mechanotransduction. *J Cell Sci*. 2004;117:2449–2460.

188. Trayanova NA, Constantino J, Gurev V. Models of stretch-activated ventricular arrhythmias. *J Electrocardiol*. 2010;43:479–485.

189. Alenghat FJ, Ingber DE. Mechanotransduction: all signals point to cytoskeleton, matrix, and integrins. *Sci STKE*. 2002;2002:pe6.

190. Sadoshima J, Izumo S. The cellular and molecular response of cardiac myocytes to mechanical stress. *Annu Rev Physiol*. 1997;59:551–571.

191. Jeyaraj D, Ashwath M, Rosenbaum DS. Pathophysiology and clinical implications of cardiac memory. *Pacing Clin Electrophysiol*. 2010;33:346–352.

192. Kroon W, Lumens J, Potse M, Suerder D, Klersy C, Regoli F, Murzilli R, Moccetti T, Delhaas T, Krause R, Prinzen FW, Auricchio A. In vivo electromechanical assessment of heart failure patients with prolonged QRS duration. *Heart Rhythm*. 2015;12:1259–1267.

193. Sohal M, Shetty A, Duckett S, Chen Z, Sammut E, Amraoui S, Carr-White G, Razavi R, Rinaldi CA. Noninvasive assessment of LV contraction patterns using CMR to identify responders to CRT. *JACC Cardiovasc Imaging*.

2013;6:864–873.

194. Kuijpers NHL, Hermeling E, Lumens J, Eikelder ten HMM, Delhaas T, Prinzen FW. Mechano-electrical coupling as framework for understanding functional remodeling during LBBB and CRT. *Am J Physiol Heart Circ Physiol*. 2014;306:H1644–59.

195. Hermeling E, Delhaas T, Prinzen FW. Mechano-electrical feedback explains T-wave morphology and optimizes cardiac pump function: Insight from a multi-scale model. *Progress in biophysics …*. 2012;

196. Pyle WG, Solaro RJ. At the crossroads of myocardial signaling: the role of Z-discs in intracellular signaling and cardiac function. *Circ Res*. 2004;94:296–305.

197. Akar FG, O'Rourke B. Mitochondria are sources of metabolic sink and arrhythmias. *Pharmacol Ther*. 2011;131:287–294.

198. Barth AS, Aiba T, Halperin V, DiSilvestre D, Chakir K, Colantuoni C, Tunin RS, Dimaano VL, Yu W, Abraham TP, Kass DA, Tomaselli GF. Cardiac resynchronization therapy corrects dyssynchrony-induced regional gene expression changes on a genomic level. *Circ Cardiovasc Genet*. 2009;2:371–378.

199. Thijssen J, Borleffs CJW, Delgado V, van Rees JB, Mooyaart EAQ, van Bommel RJ, van Erven L, Boersma E, Bax JJ, Schalij MJ. Implantable cardioverter-defibrillator patients who are upgraded and respond to cardiac resynchronization therapy have less ventricular arrhythmias compared with nonresponders. *J Am Coll Cardiol*. 2011;58:2282–2289.

200. Kurita T, Noda T, Aiba T, Nakajima I, Shimizu W, Motoki K, Yasuoka R, Miyazaki S, Kamakura S. Cardiac resynchronization therapy to prevent life-threatening arrhythmias in patients with congestive heart failure. *J Electrocardiol*. 2011;44:736–741.

201. Timóteo AT, Oliveira MM, Silva MN, Toste A, Ramos R, Feliciano J, Cunha PS, Soares R, Santos S, Ferreira RC. [Incidence of ventricular arrhythmias in patients with severe left ventricular systolic dysfunction: is there a benefit after cardiac resynchronization therapy?]. *Rev Port Cardiol*. 2011;30:823–828.

202. Tsvetkova AS, Kibler NA, Nuzhny VP, Shmakov DN, Azarov JE. Acute effects of pacing site on repolarization and haemodynamics of the canine ventricles. *Europace*. 2011;

203. Suzuki A, Shiga T, Nakai K, Futagawa K, Matsuyama Y, Shoda M, Kasanuki H, Hagiwara N. Interlead difference between T-peak to T-end intervals in resynchronization patients with an implantable cardioverter-defibrillator. *J Electrocardiol*. 2010;43:706–712.

204. Hsu JC, Solomon SD, Bourgoun M, McNitt S, Goldenberg I, Klein H, Moss AJ, Foster E, MADIT-CRT Executive Committee. Predictors of super-

response to cardiac resynchronization therapy and associated improvement in clinical outcome: the MADIT-CRT (multicenter automatic defibrillator implantation trial with cardiac resynchronization therapy) study. *J Am Coll Cardiol*. 2012;59:2366–2373.

205. Prinzen FW, Vernooy K, Auricchio A. Cardiac resynchronization therapy: state-of-the-art of current applications, guidelines, ongoing trials, and areas of controversy. *Circulation*. 2013;128:2407–2418.

206. Abraham WT, Hayes DL. Cardiac resynchronization therapy for heart failure. *Circulation*. 2003;108:2596–2603.

207. Cho H, Barth AS, Tomaselli GF. Basic science of cardiac resynchronization therapy: molecular and electrophysiological mechanisms. *Circ Arrhythm Electrophysiol*. 2012;5:594–603.

208. Kirk JA, Kass DA. Electromechanical dyssynchrony and resynchronization of the failing heart. *Circ Res*. 2013;113:765–776.

209. Chen Z, Hanson B, Sohal M, Sammut E, Child N, Shetty A, Boucher R, Bostock J, Gill J, Carr-White G, Rinaldi CA, Taggart P. Left ventricular epicardial electrograms show divergent changes in action potential duration in responders and nonresponders to cardiac resynchronization therapy. *Circ Arrhythm Electrophysiol*. 2013;6:265–271.

210. Bleeker GB, Mollema SA, Holman ER, Van de Veire N, Ypenburg C, Boersma E, van der Wall EE, Schalij MJ, Bax JJ. Left ventricular resynchronization is mandatory for response to cardiac resynchronization therapy: analysis in patients with echocardiographic evidence of left ventricular dyssynchrony at baseline. *Circulation*. 2007;116:1440–1448.

211. Chatterjee NA, Roka A, Lubitz SA, Gold MR, Daubert C, Linde C, Steffel J, Singh JP, Mela T. Reduced appropriate implantable cardioverter-defibrillator therapy after cardiac resynchronization therapy-induced left ventricular function recovery: a meta-analysis and systematic review. *Eur Heart J*. 2015;

212. Haugaa KH, Marek JJ, Ahmed M, Ryo K. Mechanical dyssynchrony after cardiac resynchronization therapy for severely symptomatic heart failure is associated with risk for ventricular arrhythmias. *Journal of the American …*. 2014;

213. Hasselberg NE, Haugaa KH, Bernard A, Ribe MP, Kongsgaard E, Donal E, Edvardsen T. Left ventricular markers of mortality and ventricular arrhythmias in heart failure patients with cardiac resynchronization therapy. *Eur Heart J Cardiovasc Imaging*. 2015;

214. Bernard A, Donal E, Leclercq C, Schnell F, Fournet M, Reynaud A, Thébault C, Mabo P, Daubert J-C, Hernandez A. Impact of Cardiac Resynchronization Therapy on Left Ventricular Mechanics: Understanding the Response through a New Quantitative Approach Based on Longitudinal Strain Integrals. *J Am Soc Echocardiogr*. 2015;28:700–708.

215. Ruschitzka F, Abraham WT, Singh JP, Bax JJ, Borer JS, Brugada J, Dickstein K, Ford I, Gorcsan J3, Gras D, Krum H, Sogaard P, Holzmeister J. Cardiac-resynchronization therapy in heart failure with a narrow QRS complex. *N Engl J Med*. 2013;369:1395–1405.

216. Khan FZ, Virdee MS, Palmer CR, Pugh PJ, O'Halloran D, Elsik M, Read PA, Begley D, Fynn SP, Dutka DP. Targeted left ventricular lead placement to guide cardiac resynchronization therapy: the TARGET study: a randomized, controlled trial. *J Am Coll Cardiol*. 2012;59:1509–1518.

217. Serdoz LV, Daleffe E, Merlo M, Zecchin M, Barbati G, Pecora D, Pinamonti B, Fantoni C, Lupo P, Di Lenarda A, Sinagra G, Cappato R. Predictors for restoration of normal left ventricular function in response to cardiac resynchronization therapy measured at time of implantation. *Am J Cardiol*. 2011;108:75–80.

218. Bonakdar HR, Jorat MV, Fazelifar AF, Alizadeh A, Givtaj N, Sameie N, Sadeghpour A, Haghjoo M. Prediction of response to cardiac resynchronization therapy using simple electrocardiographic and echocardiographic tools. *Europace*. 2009;11:1330–1337.

219. Park S-J, Miyazaki C, Bruce CJ, Ommen S, Miller FA, Oh JK. Left ventricular torsion by two-dimensional speckle tracking echocardiography in patients with diastolic dysfunction and normal ejection fraction. *J Am Soc Echocardiogr*. 2008;21:1129–1137.

220. Altiok E, Neizel M, Tiemann S, Krass V, Kuhr K, Becker M, Zwicker C, Koos R, Lehmacher W, Kelm M, Marx N, Hoffmann R. Quantitative analysis of endocardial and epicardial left ventricular myocardial deformation-comparison of strain-encoded cardiac magnetic resonance imaging with two-dimensional speckle-tracking echocardiography. *J Am Soc Echocardiogr*. 2012;25:1179–1188.

221. Knol MJ, Le Cessie S, Algra A, Vandenbroucke JP, Groenwold RHH. Overestimation of risk ratios by odds ratios in trials and cohort studies: alternatives to logistic regression. *CMAJ*. 2012;184:895–899.

222. Albertsen AE, Nielsen JC, Pedersen AK, Hansen PS, Jensen HK, Mortensen PT. Left ventricular lead performance in cardiac resynchronization therapy: impact of lead localization and complications. *Pacing Clin Electrophysiol*. 2005;28:483–488.

223. Ugander M, Oki AJ, Hsu L-Y, Kellman P, Greiser A, Aletras AH, Sibley CT, Chen MY, Bandettini WP, Arai AE. Extracellular volume imaging by magnetic resonance imaging provides insights into overt and sub-clinical myocardial pathology. *Eur Heart J*. 2012;33:1268–1278.

224. Bull S, White SK, Piechnik SK, Flett AS, Ferreira VM, Loudon M, Francis JM, Karamitsos TD, Prendergast BD, Robson MD, Neubauer S, Moon JC, Myerson SG. Human non-contrast T1 values and correlation with histology in diffuse fibrosis. *Heart*. 2013;99:932–937.

225. Leyva F, Taylor RJ, Foley PWX, Umar F, Mulligan LJ, Patel K, Stegemann B, Haddad T, Smith REA, Prasad SK. Left ventricular midwall fibrosis as a predictor of mortality and morbidity after cardiac resynchronization therapy in patients with nonischemic cardiomyopathy. *J Am Coll Cardiol*. 2012;60:1659–1667.

226. Miller CA, Naish JH, Bishop P, Coutts G, Clark D, Zhao S, Ray SG, Yonan N, Williams SG, Flett AS, Moon JC, Greiser A, Parker GJM, Schmitt M. Comprehensive validation of cardiovascular magnetic resonance techniques for the assessment of myocardial extracellular volume. *Circulation: Cardiovascular Imaging*. 2013;6:373–383.

227. Sparrow P, Messroghli DR, Reid S, Ridgway JP, Bainbridge G, Sivananthan MU. Myocardial T1 mapping for detection of left ventricular myocardial fibrosis in chronic aortic regurgitation: pilot study. *AJR Am J Roentgenol*. 2006;187:W630–5.

228. Maceira AM, Joshi J, Prasad SK, Moon JC, Perugini E, Harding I, Sheppard MN, Poole-Wilson PA, Hawkins PN, Pennell DJ. Cardiovascular magnetic resonance in cardiac amyloidosis. *Circulation*. 2005;111:186–193.

229. Puntmann VO, D'Cruz D, Smith Z, Pastor A, Choong P, Voigt T, Carr-White G, Sangle S, Schaeffter T, Nagel E. Native myocardial T1 mapping by cardiovascular magnetic resonance imaging in subclinical cardiomyopathy in patients with systemic lupus erythematosus. *Circulation: Cardiovascular Imaging*. 2013;6:295–301.

230. Dall'Armellina E, Piechnik SK, Ferreira VM, Si QL, Robson MD, Francis JM, Cuculi F, Kharbanda RK, Banning AP, Choudhury RP, Karamitsos TD, Neubauer S. Cardiovascular magnetic resonance by non contrast T1-mapping allows assessment of severity of injury in acute myocardial infarction. *J Cardiovasc Magn Reson*. 2012;14:15.

231. Ugander M, Bagi PS, Oki AJ, Chen B, Hsu L-Y, Aletras AH, Shah S, Greiser A, Kellman P, Arai AE. Myocardial edema as detected by pre-contrast T1 and T2 CMR delineates area at risk associated with acute myocardial infarction. *JACC Cardiovasc Imaging*. 2012;5:596–603.

232. Ferreira VM, Piechnik SK, Dall'Armellina E, Karamitsos TD, Francis JM, Choudhury RP, Friedrich MG, Robson MD, Neubauer S. Non-contrast T1-mapping detects acute myocardial edema with high diagnostic accuracy: a comparison to T2-weighted cardiovascular magnetic resonance. *J Cardiovasc Magn Reson*. 2012;14:42.

233. Piechnik SK, Ferreira VM, Lewandowski AJ, Ntusi NAB, Banerjee R, Holloway C, Hofman MBM, Sado DM, Maestrini V, White SK, Lazdam M, Karamitsos T, Moon JC, Neubauer S, Leeson P, Robson MD. Normal variation of magnetic resonance T1 relaxation times in the human population at 1.5 T using ShMOLLI. *J Cardiovasc Magn Reson*. 2013;15:13.

234. Scholz TD, Fleagle SR, Burns TL, Skorton DJ. Nuclear magnetic resonance

relaxometry of the normal heart: relationship between collagen content and relaxation times of the four chambers. *Magn Reson Imaging*. 1989;7:643–648.